A Biomimetic Approach to Lubricate Engineering Materials

Røn, Troels; Lee, Seunghwan

Publication date:
2014

Document Version
Peer reviewed version

A Biomimetic Approach to Lubricate Engineering Materials.

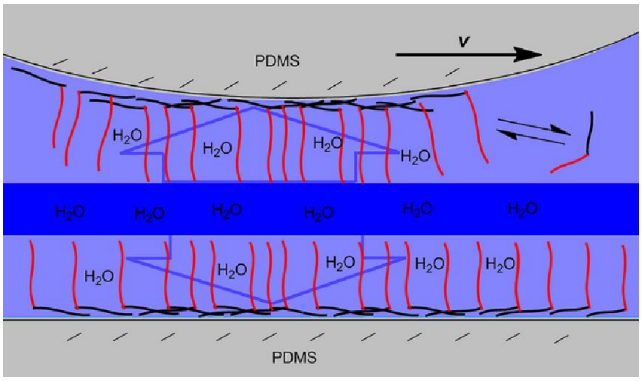

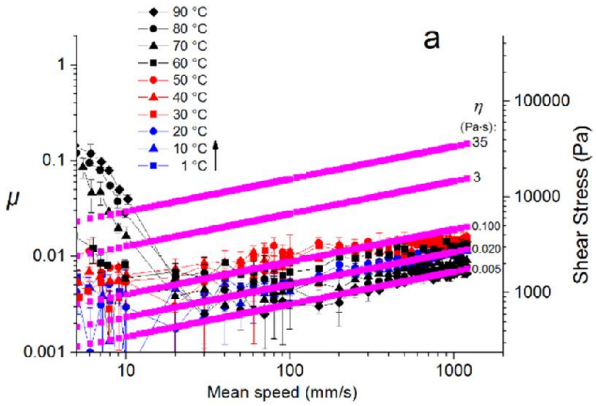

Ph.D. Thesis, June 2014

By

Troels Røn

Department of Mechanical Engineering

Technical University of Denmark (DTU)

DK-2800 Kgs. Lyngby, Denmark

"I would rather understand one cause than be the king of Persia"

Democritus

I. Preface

This thesis is submitted in candidacy for the Ph.D. degree from The Technical University of Denmark (DTU). The work has been carried out in the Department of Mechanical Engineering (MEK) under the supervision of Dr. Seunghwan Lee in the period April 2011 to June 2014.

The thesis is composed of Introduction sections to tribology and water based lubrication, whereas the Results are presented as either published articles or articles drafts which include the experimental and methods sections. The visual appearance of the articles are different from the article drafts due to the different requirements for either published or submission versions of the articles. Hence different formatting and typefaces apply in the Results section.

The project was funded by support from Technology and Production Sciences (FTP) (10-082707).

II. Acknowledgements

I would like to thank first of all my supervisor Seunghwan Lee for invaluable scientific support and guidance, and for giving me the opportunity to pursue a PhD degree. Additionally, I would like to thank him for believing in me despite my illness during the second year of my Ph.D.

I would also like to thank the other members of my group; Jan B. Madsen, Kirsi I. Pakkanen, Nikos Nikogeorgos and Petr Efler for good collaboration and inspiring conversations.

Furthermore, I have been very grateful for the technical support of the department's technicians John C. Troelsen and Lars Pedersen for making polymer samples and sample holders.

In relation to my external stay at ETH Zürich during the autumn of 2012, I would like to thank Rosa Espinoza-Marzal, Nicholas D. Spencer and many others for their supervision and help.

I would like to praise Marcels Somers for general guidance during my PhD and the people of IPU for technical assistance and advice. Finally I would like to thank the other PhD students and Post.docs at the MTU section of the Mechanical department for lots of good times and discussions.

III. Abstract in English

This PhD thesis consists of studies on biomimetic aqueous boundary lubrication by applying amphihilic copolymers and hydrophobin proteins as lubricant addtives. Studies on the temperature dependency of neat water and hydrogel lubrication were also conducted.

Amphiphilic diblock, triblock and graft copolymers were applied as synthetic boundary lubricant additives in water in relation to test the hypothesis that adsorbed polyelectrolyte brushes can displays the same superior lubricity over neutral brushes as has been observed for covalently anchored brushes. In the case of diblock copolymers, the diblocks consisted of a hydrophilic block of either neutral poly(ethylene glycol) (PEG) or negatively charged poly(acrylic acid) (PAA) and of a hydrophobic block of polystyrene (PS) or poly(2-methoxyethyl acrylate) (PMEA). Thus generating PEG-*b*-X or PAA-*b*-X, where X block was either PS or PMEA. Comparing the neutral PEG and charged PAA buoyant blocks, the neutral showed superior adsorption onto hydrophobic poly(dimethylsiloxane) (PDMS) surfaces from neutral aqueous conditions. Neutral PEG based copolymers showed substantial adsorption for both PS and PMEA as the anchoring block, whereas charged PAA-based copolymers showed effective adsorption only for PMEA anchoring block. PAA-*b*-PS diblock copolymer's poor lubricity for the PDMS–PDMS sliding contact was well correlated with poor adsorption. PAA-b-PMEA copolymers, despite their significant degree of adsorption, showed little lubricity. When adding NaCl to the aqueous solution or by lowering the pH, both the adsorption and lubricity of the PAA-b-PMEA diblock copolymer solutions improved. The poor adsorption and inferior aqueous lubricating properties of the polyelectrolyte based (PAA) diblock copolymers compared to their PEG-based counterparts was mainly attributed the electrostatic repulsion between charged PAA blocks, hindering the facile formation of the lubricating layer under cyclic tribological stress.

It is well known that graft copolymers anchor more efficiently to surfaces than their diblock counterparts, thus the synthesis and study on lubricating capabilities of this amphiphilic structure were conducted. The graft copolymers consisting of a backbone poly(2-hydroxyethyl methacrylate) (PHEMA) and polyelectrolyte graft chains of either anionic poly(methacrylic acid) or cationic poly((2-dimethylamino) ethyl methacrylate) (PDMEAMA) was synthesized, and neutral MEA repeating units were incorporated in the graft chain to provide dilution of the charges. Cationic based P(MEA-co-DMAEMA)-*graft*-PHEMA did not show any adsorption or lubricating properties at neutral (pH 7.0, 1 mM ionic strength) or 150 mM NaCl conditions. Graft copolymer of anionic P(MEA-co-MAA)-*graft*-PHEMA copolymers did not show

lubricating capabilities at neutral conditions either. However, the lubricity was significantly improved at saline conditions of 150 mM NaCl even at the slowest sliding speeds. Lubricity in this speed range was not observed for the PAA-*b*-PMEA diblocks in the diblock copolymer study. Graft copolymers were more successful than charged diblock copolymers in lubricating PDMS-PDMS sliding contact when charged moieties are present in the buoy chains.

The adsorption and aqueous lubricating properties of an amphiphilic triblock copolymers of PEG, PMEA and (PMAA) blocks, namely PEG-*b*-PMEA-*b*-PMAA was also studied. After adsorption onto a nonpolar hydrophobic surface from aqueous solution, an equal and homogeneous mixture of neutral PEG and charged PMAA chains is formed on the surface, with an adsorbed polymer mass comparable to its fully neutral counterpart, PEG-*b*-PMEA-*b*-PEG. The lubricity of PEG-*b*-PMEA-*b*-PMAA showed significant improvement compared to fully charged diblock of PAA-*b*-PMEA, which is attributed to dilution of charged moieties on the surface and subsequent improvement of the lubricating film stability in PDMS-PDMS sliding contact. However, no salt was needed to achieve the good lubricity in the sliding contact. The studies on amphiphilic block copolymers show that pure polyelectrolyte chains are not applicable as means of affording good lubricity as aqueous lubricant additives for boundary lubrication. Dilution or screening of the charges is necessary for obtaining good lubricity for amphiphilic block copolymers.

The influence of temperature on the lubricating properties of neat water for four tribopairs with different surface hydrophilicity and bulk elasticity moduli were investigated. The four contacts were soft and hard, and hydrophobic and hydrophilic. With increasing temperature, the coefficients of friction generally increased due to the decrease of water's viscosity. This change was more clearly observed at the soft interfaces due to easier lubricating film formation of water at the lower contact pressure. Nevertheless, dominant lubrication mechanism appeared to be boundary and mixed lubrication even for soft interfaces at all mean speeds (10-1200 mm/s) and temperatures (1 to 90 °C) investigated.

The temperature dependency on the lubricating properties of thermoresponsive F127 hydrogel was also studied in the same contacts. The high viscosity of gelation at certain temperatures (ca. 20-60 °C) was conjectured to tune the lubricity of the F127 hydrogels. However, due to significant shear thinning in the hard contacts, there was no or very little lubricity of the F127 hydrogel. In the soft contact good lubricity was observed, albeit the lubricating performance was ascribed (depending on the sliding speed) to viscosities which were still much lower than the bulk gel, and to boundary lubrication of the F127 polymer. Shear thinning was, however, assessed as a compelling property in the soft contact causing lower friction.

Amphiphilic proteins of hydrobins type II fungi hydrophobins, HFBI and FpHYD5, were studied as aqueous lubricant additives at PDMS tribopair interface. The two hydrophobins are featured as non-glycosylated and lighter (HFBI, m.w. ca. 7 kDa) vs glycosylated and heavier (FpHYD5, m.w. ca. 10 kDa) proteins. Their adsorption at PDMS-water interface were very similar. PDMS-PDMS sliding interface was effectively lubricated by the hydrophobin solutions, and showed a reduction in the coefficient of friction as much as by ca. two orders of magnitude. Better lubrication was provided at concentrations 1.0 mg/mL as compared to 0.1 mg/mL, espicially in low-speed regime, where boundary lubrication characteristic is dominant via 'self-healing' mechanism. The glycosylated FpHYD5 revealed a better lubrication than HFBI. Two type II hydrophobins function more favorably compared to synthetic amphiphilic copolymer, PEO-PPO-PEO, with a similar molecular weight. This is ascribed to higher amount of adsorption of the hydrophobins to hydrophobic surfaces from aqueous solution.

III. Resumé (Resume in Danish)

Denne Ph.D.-afhandling indeholder studiet af biomimetisk grænseflade smørring i vandig opløsning vha. amfifile copolymerer og hydrofobin-proteiner som lubrikant-additiver. Undersøgelser af temperatur-afhængigheden af smørring med rent vand og hydrogeler er også blevet udført.

Amfifile diblok, triblok og graft copolymerer blev anvendt som syntetiske smørringsadditiver ved grænseflader i vandig opløsning for at teste hypotesen om, at adsorberede polymer brushes (børster) med elektrisk ladning kan give lavere friktion, som det tidligere er vist for kovalent forankrede ladede polymer brushes, når disse sammenlignes med neutrale brushes. De undersøgte diblok copolymerer bestod af én hydrofil blok af enten neutral poly(ethylen glycol) (PEG) eller negativt ladet poly(akryl syre) (PAA) og af én hydrofob blok af polystyren (PS) eller poly(2-methoxyethyl akrylat) (PMEA) som forankringsblok på overfladen. Således var diblok copolymererne PEG-*b*-X eller PAA-*b*-X, hvor blok X var enten PS eller PMEA. Ved sammenligning af de neutrale PEG og ladede PAA baserede blokke, viste den neutrale sig bedre adsorption på den hydrofobe poly(dimethylsiloxane)-overflade (PDMS) ved pH 7.0 og lav saltkoncentration i vand. Neutrale PEG baserede copolymerer viste signifikant adsorption for både PS og PMEA som forankringsblok, hvor ladede PAA-baserede copolymerer kun viste effektiv adsorption med PMEA som forankringsblok. PAA-*b*-PS diblock copolymerens dårlige smørringsevne for PDMS–PDMS kontakten stemte overens med dens dårlige adsorption. Til trods for deres adsorption viste PAA-b-PMEA copolymererne lille smørringsevne. Ved tilførsel af NaCl til den vandige opløsning eller ved at sænke pH, blev både adsorptionen og smørringsevnen forbedret i tilfældet af PAA-b-PMEA. Den ringe smørringsevne og adsorption ifht. de ladede PAA diblok copolymerer i sammenligning med de neutrale PEG-baserede blev forklaret med den elektrostatiske frastødning mellem de ladede PAA blokke, som induceres under the cykliske tribologiske stress.

Det har længe været kendt, at graft copolymerer forankre bedre på overflader end diblok copolymerer gør. Ud fra dette udgangspunkt blev forskellige graft copolymerer syntetiseret og deres smørringsevne studeret. Graft copolymers af en backbone (rygrad) af poly(2-hydroxyethyl methakrylat) (PHEMA) og af polyelektrolyt graft kæder af enten anionisk poly(methakryl syre) eller kationisk poly((2-dimethylamino) ethyl methakrylat)) (PDMEAMA) blev syntetiseret, hvor neutrale MEA monomerer blev inkorporeret in graft sidekæderne for at mindske koncentrationen af ladninger. Den kationiske P(MEA-co-DMAEMA)-*graft*-PHEMA viste ingen adsorption eller smørring ved neutrale betingelser (pH 7.0, 1 mM ion styrke) eller

ved 150 mM NaCl. Graft copolymerer af anionisk P(MEA-co-MAA)-*graft*-PHEMA viste heller ikke nogen smørringsevne ved neutrale betingelser, men smørringsevnen blev kraftigt forbedret ved 150 mM NaCl, selv ved de laveste gnidningshastigheder. Smørringsevne ved disse lave gnidningshastigheder blev ikke observeret ved studiet af PAA-*b*-PMEA diblok copolymererne. Graft copolymererne var således bedre end de ladede diblok copolymererne til smørring af den gnidende PDMS-PDMS kontakt, når ladninger er tilstede.

Adsorptionen og smørringsevnen af amfifile triblok copolymerer bestående af PEG, PMEA og poly(methakryl syre) (PMAA) blokke, dvs. PEG-*b*-PMEA-*b*-PMAA blev også studeret. PEG-*b*-PMEA-*b*-PMAA viste same grad af adsorption ved en vand-PDMS-grænseflade som dens neutrale PEG-*b*-PMEA-*b*-PEG analog. Smørringsevnen af PEG-*b*-PMEA-*b*-PMAA viste signifikant forbedring ved sammenligning med de fuldt ladede PAA-*b*-PMEA diblok copolymerer. Denne egenskab blev korreleret med 'fortyndning' af ladninger på overflade vha. PEG blokken, hvorfor stabiliteten var markant bedre i den gidende PDMS-PDMS kontakt. Til forskel fra diblok copolymererne og graft copolymererne var det ikke nødvendigt at tilføje salt til opløsningen for at opnå god smørringsevne. Studierne af amfifile blok copolymerer viser, at ladede polyelektrolyte brushes (børster) ikke er anvendelige som smørringsadditiver ved grænsefladesmørring i vandige opløsninger med mindre at ladningerne er fortyndede eller salt er tilført for at skærme ladningerne fra elektrostatisk frastødning.

Smørringsevnen og dennes temperaturafhængighed i rent vand blev studeret i fire gnidningskontakter med forskellig hårdhed eller hydrofilicitet. De fire kontakter var enten hydrofob blød elastomer eller hård plast, og hydrofil elastomer og hydrofil stål mod glas kontakt. Ved stigende temperatur steg friktionskoefficienten generelt pga. af vands dalende viskositet ved højere temperaturer. Denne effekt blev tydeligt observeret ved de bløde kontakter, hvor filmdannelsen er lettere pga. det lavere normaltryk. Den dominante smørringmekanisme var dog ved grænsflade-kontakt (boundary regime) og blandet regime (mixed lubrication) selv for de bløde kontakter ved alle gennemsnitshastigheder (10-1200 mm/s) og temperaturer (1 til 90 °C).

Temperaturafhængigheden af smørringsevnen af den termo-responsive F127 hydrogel blev også studeret i samme kontakttyper som nævnt oven for. Pga. den høje viskositet ved geleringen af F127 ved specifikke temperaturer (ca. 20-60 °C) blev det formodet, at smørringsevnen af F127 hydrogel var temperaturafhængig. Studiet viste desværre, at viskositeten af F127 hydrogel blev kraftigt formindsket i tribointerfasen, specielt i de hårde kontakter. Således viste F127 hydrogel ingen eller lille smørringsevne i de hårde kontakter. Selvom god smørringsevne blev observeret for de bløde kontakter, så blev denne opførsel

tilskrevet meget lavere viskositet end selve hydrogelen. Denne viskositets-sænkende egenskab kan dog være fordelagtig for bløde kontakter, hvor friktionen bliver laverer pga. den lave viskositet, da den viskøse dissipative kraft sænkes.

Ampfifile proteiner af hydrofobiner type II (HFBI og FpHYD5) blev studeret som middel til grænsefladesmørring i vandige opløsninger ved et PDMS tribopar. De to hydrofobiner er non-glykosyleret og lettere (HFBI, m.w. ca. 7 kDa) og glykosyleret og tungere (FpHYD5, m.w. ca. 10 kDa) proteiner. Deres adsorption ved PDMS-vand interfasen var meget ens. PDMS-PDMS gnidningskontakten blev effektivt smurt af hydrofobin opløsningerne, og viste op til en faktor 100 reduktion af friktionskoefficienterne. Bedre smørringsevne blev observeret for koncentrationer af 1.0 mg/mL end 0.1 mg/mL, i særdeleshed ved lave gnidningshastigheder. Den glykosylerede FpHYD5 viste bedre smørringsevne end HFBI. Hydrofobinerne fungerede således bedre end syntetisk amfifil copolymer, PEO-PPO-PEO, med sammenlignelig molekylær vægt. Denne egenskab blev tildelt den højere adsorption af hydrofobiner til hydrofobe overflader i vandig opløsning.

Table of Contents

1.0 Aim

Petroleum derived oil and grease lubricants have for a more than a century been applied as effective means to afford low friction in metal-metal contacts of engineering entities such as engines and bearings. In biological systems, however, the only base lubricant available is water. Neat water is a poor lubricant from a conventional lubrication point of view due to its very low viscosity and low pressure coefficient of viscosity as compared to lubricant oils. Nevertheless, nature has effectively employed water as base lubricant, for example in contacts of synovial joints of mammals and mucus slime which assists the locomotion of slugs. This successful application of aqueous based lubrication of nature is generally based on the ability to retain water at the sliding interface. In the case of synovial joints the retention of water is partly due to the presence of incredibly hydrophilic macromolecules such as lubricin, aggrecan and hyaluronic acid thus affording a high osmotic pressure in the surface layers which can support very high loads. In synergy with the likewise hydrated cartilage synovial joint lubrication can afford coefficient of friction down to 0.001 even at very high loads and low sliding speeds.

One way of mimicking the lubricity of synovial joints is to apply water retaining hydrophilic polymer brushes (i.e. biomimicry). When opposing surface anchored polymer brushes are slid against each other in good solvent very low coefficient of friction can be afforded. Both neutral and charged hydrophilic polymer brushes can lubricate sliding contacts. In the case of covalently anchored hydrophilic brushes charged polyelectrolyte brushes have shown the best lubricity in water due to the higher osmotic pressure induced by the charges and low shear strength slip plane. Polymer brushes adsorbed via anchoring block have mostly been based on neutral poly(ethylene glycol) brushes where the anchoring was relatively weak and did not give the same low friction as covalently anchored polyelectrolyte brushes. Furthermore, adsorbed neutral polymer brushes from excess amphiphilic polymer in solution have displayed an attractive property of (re)adsorption even under cyclic tribostress i.e. 'self-healing' the contact, thus maintaining the long-term lubricity. However, no study exist where the desirable properties both of higher osmotic pressure of polyelectrolyte brushes and 'self-healing' by adsorption from excess solution are applied simultaneously.

The first main objective of this project is to develop surface-grafted polyelectrolyte chains and characterize the surface adsorption and aqueous lubricating properties as a biomimetic approach of lowering friction in water environments. To fully assess the lubricating properties of the polyelectrolyte chains, both macroscale and nanoscale tribological studies were be carried out by employing pin-on-disk tribometer and atomic force microscopy (AFM). Optical waveguide lightmode spectroscopy (OWLS) was employed to

investigate the surface adsorption of the polyelectrolyte polymers. It was chosen to apply non-polar substrates such as thermoplastics and elastomers to simplify the charge issues with polymer chains to adsorb onto the surface. Furthermore, they are free from corrosion problems in water and have a high potential to be fabricated as bearing materials in longer-term applications. In fact, various polymeric materials have already found some practical applications as bearing components in relation with aqueous lubrication, however, efforts to further improve aqueous lubricating properties are rare. Elastomers receive special attention for aqueous lubrication due to the possibility to form a fluid film (namely, soft Elastohydrodynamic lubrication (EHL) mechanism, see section 2.3), and to serve as excellent model systems for soft biological tissues. As means of forming polyelectrolyte brushes on surface adsorbed from solution we choose amphiphilic block copolymers. Block copolymerization is a most simple, yet powerful approach to graft polymer chains onto surface since anchoring block and buoyant block can be readily selected according to the characteristics of the solvent (lubricant) and the substrate surface (tribopairs).

Thus in the first main objective four main subjects are pursued:

(i) Synthesis of various amphiphilic block copolymers as an efficient means to graft polyelectrolyte chains onto non-polar surfaces in aqueous environment.
(ii) Characterization of the role of compositional parameters (chemical functional groups) and structural parameters (molecular weight, ratio of buoyant/anchoring blocks), of polyelectrolyte chains in their aqueous lubricating properties.
(iii) Characterization of the tribological properties of polyelectrolyte chains as a function of environmental parameters (pH, and ionic strength).
(iv) Comparison of the aqueous lubricating properties of polyelectrolyte chains with those of neutral PEG chains in brush conformation.

The second main objective of this project is to investigate the temperature dependency on neat water lubrication of soft and hard, hydrophobic and hydrophilic sliding engineering materials. Studies on temperature dependency in lubrication are not common, and for water they are very rare. This study is conducted by application of mini-traction-machine (MTM) and will cover the full range of sliding speeds thus affording investigations on all lubrication regimes (see section 2.3) in the temperature range 1-90 °C.

The study on temperature dependency in neat water lubrication will also act as a reference for an additional study on thermo-responsive hydrogel lubrication in the same types of contacts. Again the soft conformal contact may serve as excellent model systems in EHL regime for biological tissues. Applying thermoresponsive hydrogels of Pluronic F127 (PEG-*b*-PPO-*b*-PEG) in water solutions is an appealing approach to lubricate engineering materials due to the ability of tuning the viscosity (by gel formation) at specific temperatures, as bearing materials are often subjected to higher temperatures during service. The gelation of F127 occurs at human body temperature (37 °C) thus potentially acting as a biolubricant. Additionally, hydrogels are compelling as aqueous lubricant additives in areas where oil and grease based lubricants are avoided due to toxicity or flammability issues.

2.0 Introduction to Tribology, Friction and Lubrication

2.1 Tribology

The science field that studies the phenomena of friction, lubrication and wear is called 'tribology' and stems from the Greek word for rubbing 'τρίβω' '*tribo'* and 'λωγία' '*logos'* which means the 'study of' or 'knowledge of'. The word was coined by both David Tabor and Peter Jost in the 1960s to incorporate the science and engineering fields dealing with friction, lubrication, wear and corrosion into one term.[1,2] The word tribology is now used worldwide as the term describing the phenomena as stated above. Peter Jost and others published "The Jost Report" in 1966 and it constituted the first attempt to assess the importance of understanding and application of lowering friction and proper lubrication in the UK and the beneficial effect on the economy. Before the Jost Report, research on friction and lubrication was not neglected, however, the significance of embodying the field of tribology as a multidisciplinary science of mechanical engineering, material science, chemistry and physics was not recognized until then.[2]

2.2 Friction

Whenever two surfaces are rubbed or slid against each other energy is dissipated, this phenomenon or process is ascribed to friction forces. Non-destructive friction between sliding surfaces arises due to non-conservative forces when interfacial bonds are formed and broken. This form of energy dissipation is called adhesion hysteresis.[3] In many cases the friction is not proportional to how adhesive the contact is, however, depending more on the degree of adhesion hysteresis.[4,5] Dissipation occurs due to the energy difference between separating two surfaces and by bring the surfaces back together. Friction can also be ascribed to destructive wear due to e.g. plastic deformation and abrasion. Additionally, friction in lubricated sliding contacts can be caused by viscous dissipation of the lubricant film. The first efforts to systematize or study of surface friction were done by Leonardo da Vinci (1452-1519), who formulated two laws of dry friction. These laws were rediscovered or restated by Guillaume Amontons (1663-1705), which is the reason why they are called Amontons' laws of friction. Charles Augustin de Coulomb later added the third law. The three fundamental laws of dry friction are as follows:

No. 1	The friction force is directly proportional to the applied load.	Amontons' 1st law.
No. 2	The friction force is independent on the apparent area of contact.	Amontons' 2st law.
No. 3	Kinetic friction is independent of sliding speed	Coulomb's law of friction.

The friction force is always in the opposite direction of the movement, thus counteracting the movement of the sliding bodies or surface. This is illustrated in Figure 2.1 below:

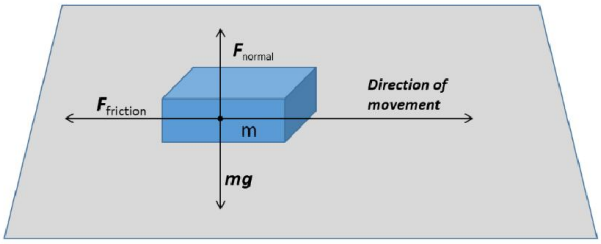

Figure 2.1: Diagram of the forces acting on a box sliding on a surface in dry contact.

The coefficient of friction is the ratio of friction force to the load (or resulting normal force). From the diagram of forces in Figure 2.1 it can be deduced that the coefficient of friction (μ) is then: $\mu = F_{friction}/F_{normal}$ which is the general formula due to the resulting normal force under load. When no external load is applied then on a horizontal plane, F_{normal} equals the mass of the sliding body multiplied with the gravitation thus $\mu = F_{friction}/mg$. How the friction increases as a function of load according to Amontons' 1st law of friction is illustrated in Figure 2.2 below:

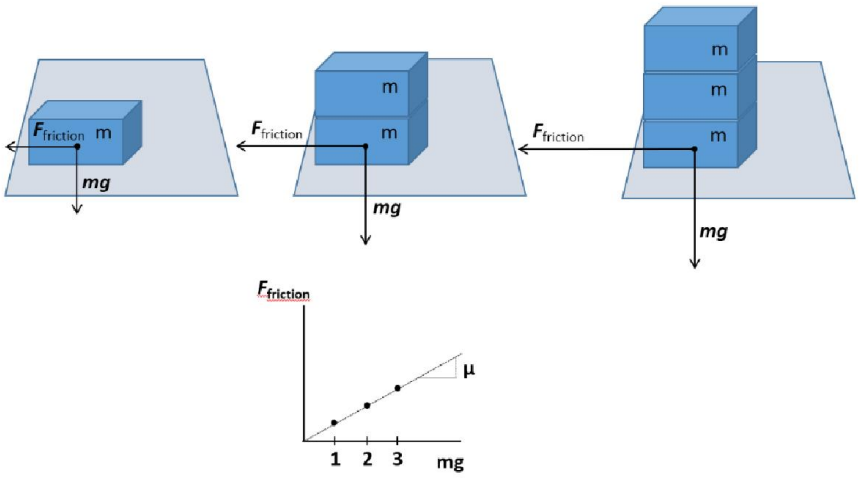

Figure 2.2: Force diagrams of friction forces proportionality to the load where $\mu = F_{friction}/F_{normal}$ at each load. For dry and rough multi-asperity contacts the friction force dependency on the applied load has typical linear behavior, thus in this case μ is slope of the plot friction force vs. load plot. However, in single asperity contacts the friction dependency on load is not always linear.

The coefficient of friction (μ) of two bodies sliding relatively to each other is the $F_{\text{friction}}/F_{\text{normal}}$ ratio at each load. Amontons' 1st law of friction is based on the fact that most surfaces are rough, and hence when two rough surfaces are in contact their real area of contact is quite small. Friction is proportional to the real area of contact. When the load is increased then the real area also increases and so does the friction. Figure 2.2 displays the typical dry and rough multi-asperity contact behavior where the friction force is linearly dependent on the applied load. However, in single asperity contacts the friction dependency on load is not always linear.

Amontons' 2nd law of friction is also based on the fact that most surfaces are rough. Hence when two rough surfaces are in contact their real area of contact is quite small and independent of the apparent area of contact. If for example a rectangular-shaped brick is slid against a surface, the friction force is the same whether the brick is placed horizontal or vertically on the surface because in both cases the real area of contact is the same.

Coulomb's law of friction stating that kinetic friction is independent of sliding speed is straightforward and suggests that the shear strength in dry friction is not influenced by sliding speed, albeit Coulomb could probably only measure friction forces at different sliding speeds within one order of magnitude.

By our modern knowledge of tribology and friction studies, we know that the three fundamental laws of friction do not corroborate with data in more extreme conditions such as adhesive contacts, single asperity contacts or very high or small sliding speeds, conditions at which da Vinci, Amontons and Coulomb were unable to measure at their times. Nevertheless, the three fundamental laws friction are today still applicable in many conditions under both dry and lubricated contacts.

2.3 Lubrication

In some applications like brakes high friction is desirable from the ability to rapidly convert kinetic energy of a car or bicycle into thermal energy. However, in most cases friction is avoided due to both wear and loss of kinetic energy. Efforts to reduce friction by lubricants have been known since ancient times e.g. in wall paintings from ancient Egypt and in the Hebrew Bible.[6,7] When two surfaces submerged in lubricant start to move relatively to each other the lubricant is entrained in the contact due to fluid dynamic forces, giving the lubricant film its load bearing ability. Higher sliding speed and viscosity afford thicker film thickness, whereas higher loads afford lower film thickness. One of the central methods of assessing the performance of a specific lubricant in a sliding contact under normal load is by plotting the coefficient of friction vs. the Stribeck

parameter (λ) thus giving the 'Stribeck curve' as shown in Figure 2.3. As mentioned above surfaces are rough and the Stribeck parameter is applied to evaluate the different regime of lubrication. The Stribeck parameter (λ) is the ratio of the lubricant film thickness (h) to the mean roughness (σ) of the two surfaces i.e. $\lambda = h/(\sigma)$.

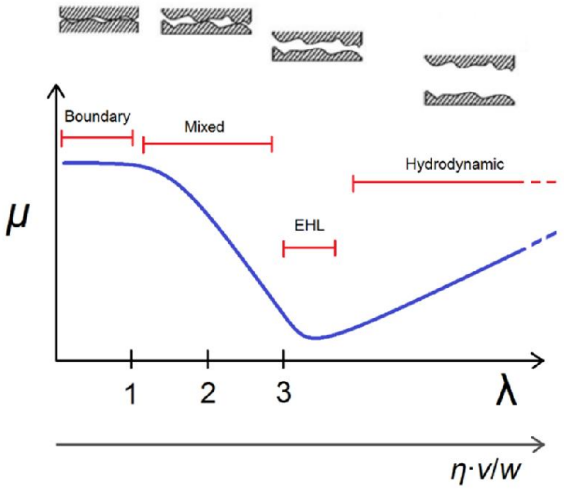

Figure 2.3: Stribeck curve (μ vs. λ) and Sommerfeld plot (μ vs. $\eta v/w$) in the different regimes of lubrication for two contacting surfaces under load. See text for definitions. Above the Stribeck curve are illustrations relative separation of the sliding contact in the different lubrication regimes.

When $0 < \lambda < 1$, the system is in *boundary lubrication* regime where the two surfaces are in close contact and no or very little fluid lubricant is entrained due to small sliding speed, thus the friction forces are similar or equal to unlubricated or dry contact. In oil lubrication engineering additives with surface affinity assist the base lubricant in lubrication at boundary regime condition. At $1 < \lambda < 3$ i.e. in the *mixed lubrication* regime, some of the load is supported by the formed film thickness resulting in lower friction than at the boundary condition, however, some of the surface asperities are still in contact causing friction. In the *elastohydrodynamic* regime (EHL) from $\lambda > 3$ and to the inception of the *hydrodynamic* regime (after the μ minimum) the surfaces are fully separated that surface roughness does not affect the friction. In EHL regime, the surfaces are elastically deformed by the high pressure and cause the lubricant's viscosity to change according to its pressure coefficient of viscosity. The *hydrodynamic* regime displays the behavior of full and extended separation of the sliding contacts, usually obtained at very high sliding speeds or at very high lubricant viscosity. The increasing trend of μ in the hydrodynamic regime is due to the viscous shear forces, where the friction or shear force is proportional to the shear rate ($\dot{\gamma}$) multiplied by the lubricant's viscosity and area of contact i.e.: $F_{\text{friction}} = \dot{\gamma}\,\eta A$, where the shear rate is proportional to the sliding speed.

If the horizontal axis of the Stribeck curve is replaced by the Sommerfeld number ($\eta v/w$) – where η, v and w is the viscosity, sliding speed and load, repectively – then the Sommerfeld plot is obtained. The Sommerfeld plot allows one to normalize the lubrication performance to the lubricant's viscosity, the sliding speeds and applied load. This affords easier comparison of lubricants measured under different conditions. With good engineering practice and calculations the EHL regime with minimum μ values can be obtained for a sliding contact of a bearing, if the right viscosity is applied and both the load and sliding speed are taken into account. For many bearings in service the sliding speed is constant and minimum μ values are afforded by proper design and choice of lubricant. However, for most tribological entities (like thrust bearings and synovial joints), the sliding speed is not constant and often goes to zero. This results in boundary lubrication regime and thus higher friction. In the Figure 2.3 the friction in the boundary lubrication regime is higher compared to the other regimes, because the mode of lubrication was caused entirely by entrainment of lubricant. Boundary lubrication by entrainment of lubricant is not possible due to the low sliding speed, disallowing load-bearing capacity of sufficient film thickness to lubricate the contact. However, if lubricant is retained at the interface thus preventing the rough (or adhesive) surfaces to come into contact – even at very low sliding speeds – then low friction can obtained even for small separation in the boundary regime. Boundary lubricants with high affinity to the sliding surfaces or surface modifications like polymer brushes and self-assembled monolayers (SAM) can significantly reduce the friction in the boundary regime. Boundary lubrication by application of polymer brushes is one of the topics of the next chapter on water based lubrication.

2.4 References

[1] Field. J.; *Biogr. Mems Fell. R. Soc.* **2008**, *54*, 427-459.

[2] Jost, P.; *Tribol Lubr Technol*, **2006**, *62*, 24-28.

[3] Klein, J.; *Friction*, **2013**, *1*, 1-23.

[4] Chen, Y. L.; Helm, C.; Israelachvili, J., *J. Phys. Chem.*, **1991**, *95*, 10736-10747.

[5] Yoshizawa, H.; Chen, Y. L.; Israelachvili, J., *J. Phys. Chem.*, **1993**, *97*, 4128-4140.

[6] Gohar, R.; Rahnejat, H.; Fundamentals of Tribology, 2nd edition, London, Imperial College Press, 2012.

[7] Nosonovsky, M., *Tribology Online*, **2007**, *2*, 44-49.

3.0 Water-based lubrication

3.1 Introduction

Water's poor lubricity as compared to oil lubricants is due to its very low viscosity and low pressure viscosity coefficient, causing low film thicknesses even at relatively high entrainment speeds. Water's viscosity is ca. 1 mPa·s, whereas oil lubricant usually have viscosities ranging from 100-800 mPa·s. However, aqueous based lubrication is possible if water is retained in the sliding interface under normal stress by means of 1) additives inducing an effective higher bulk viscosity, leading to higher film thickness upon sliding or high viscosity liquid hydrogel, preventing the water from dripping (for example personal lubricants or reversible hydrogels), 2) surface modification with hydrophilic proteins or polymers forming layers with high osmotic pressures and hydration sheet making it energetically unfavorable to approach the modified surfaces and afford low shear strength slip plane (e.g. polymer brush, mucin or hydrophobin type lubrication), or 3) hydrated bulk material which acts a water lubricant reservoir to provide a lubricating water film when deformed ('permanent'/'chemical' hydrogels).

The following sections will provide a description of the lubrication properties of the above mentioned entities. The major scope of this thesis is in the realm of amphiphilic adsorbing polymer brushes, thus most emphasis has been placed on this subjects, albeit lubrication by hydrophobins and hydrogel is also described. For more detailed descriptions of the lubrication mechanisms of chemical hydrogels, mucins and synovial joint and ocular lubrication the readers are directed towards more elaborate texts.[1,2]

3.2 Liquid and Solid Hydrogels

3.2.1 Liquid Hydrogels

Water solution based personal lubricants and hydrogels have long been used for sexual activity or lubrication of medical devices for endoscopic or gonioscopic examination or treatment. Aqueous personal lubricants and liquid hydrogels such as commercial 'K-Y Jelly' and 'Astroglide' are typically based on a mixture of water, cellulose and glycerin with viscosities in the range of 1-60 Pa·s.[3] Systematic investigation of liquid hydrogels lubrication are rare but the ability to retain the gel at the sliding contact can be rationalized by the higher viscosity of the jellies as compared to pure water should afford enough lubricity at the relatively soft tissue or endoscope-tissue contacts. Uyama et al.[4] performed a study of surface grafted hydrophilic N,N,-dimethyl acrylamide polymer vs. lidocaine liquid hydrogel on tubes poly(vinyl chloride) (PVC) and ethyl vinyl acetate

polymer (EVA) rubbed against PDMS sheets. The liquid hydrogel gave relatively low friction during the first rubbings, but was inferior to surface grafted hydrophilic polymers at more than 5 rubbings which gave friction values of $1/20^{th}$ to $1/40^{th}$ compared to the unlubricated case. Thus liquid hydrogel lubricant does not maintain lubricity for longer periods and must be reapplied during use due to the loss of hydrogel from the surface because of rubbing or dissolution.

3.2.2 Solid Hydrogels

Solid hydrogels are water swollen, non-flowing materials cross-linked by physical or chemical bond that generate a polymer or colloidal network affording a (semi)solid matrix (Figure 3.1) and are usually just referred to as 'hydrogels' if they are not liquid like.

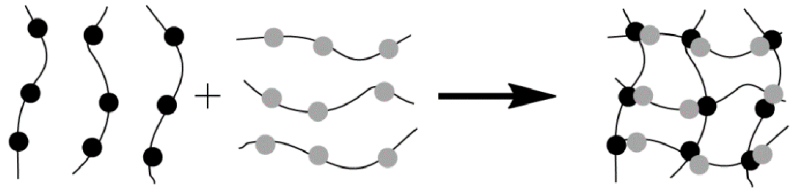

Figure 3.1: Schematic representation of crosslinking of a hydrogel.

Solid hydrogels can have water content up to 90% wt. but contrary to liquid hydrogels, solid hydrogels do not flow at steady-state.[5] When subjected to stress, hydrogels display both elastic (or plastic) behavior like solids and viscous dissipation and solute containing behavior like liquids. Hydrogels are often divided into two categories 'physical' (or 'reversible') and 'chemical' (or 'permanent') hydrogels.[5] For the 'chemical' (or 'permanent') hydrogels the network consists of chemical/covalent bonds, thus when the gel is formed it cannot go back to its original state of individual polymer chains or colloidal components.[5] Typical physical gels are chitosan (with various cross-linkers),[6] polyvinyl alcohol (PVA) hydrogels[7] subjected to several freezing and thawing cycles in aqueous solution and 'Pluronics' poly(ethylene oxide)-*b*-poly(propylene oxide)-*b*-poly(ethylene oxide) (PEO-*b*-PPO-*b*-PEO) thermo-responsive gels.[8] Examples of chemical hydrogels are PEO irradiated in water,[9] cross-linked PVA with chitosan[10] and crosslinked polyacrylamide gels.[11] The research group of Gong and Osada and their co-workers have studied the lubricity of physical, chemical and double networked hydrogels sliding against glass and polystyrene (PS), and observed remarkably low μ values down to 10^{-3}-10^{-4} sometimes even with negative load dependence on μ.[12,13] However,

in most of the cases the contact pressures were not higher than 0.1 MPa due to the hydrogels' low modulus of 2-600 kPa causing fracture stresses of 3.0 MPa or less.[14] Hydrogels with higher fracture stresses up to 21.0 MPa have been developed, but their frictional properties have not been reported yet.[14] Gong has also investigated the effect of polymer brush assisted lubrication by incorporating polymer chains into the hydrogel, which formed dangling chains on the surface, thus reducing the friction by one order of magnitude (from ca. $\mu = 0.1$ to $\mu = 0.01$) when sliding the hydrogel against a glass plate.[15] Ishikawa showed that 10 μm dimethylacrylamide (DMAA) hydrogel surface polymerized on a polyethylene (PE) head slid against PE cup artificial hip joint could reduce the friction from $\mu = 0.1$ down to 0.01 at contact loads 500 N, however, the contact pressure was not reported.[16] Contact lenses of hydrogels materials of poly(2-hydroxyethyl methacrylate) (PHEMA) and silicone have been applied for contact pressures of ca. 1-8 kPa in the eyelid epithelium.[17] Hydrogels are potential friction reducers for tissue engineering, albeit the lubricity have mostly been reported at lower contact pressures.

3.3 Polymer Brushes

3.3.1 Introduction

Colloidal dispersions of e.g. paints and inks have for many decades been known to be stabilized by polymers and proteins which separate the colloids' surfaces by inducing either steric or electrostatic repulsive forces, thus preventing the colloids from flocculating or precipitating.[18-20] Under normal loads surface anchored biomacromolecules and polymers on planar surfaces (or curved surfaces with a radius much larger than the brush thickness) also have the ability to keep the surfaces separated due to osmotic pressure in the brush and solvation sheet, thus when sheared e.g. polyelectrolyte brushes can afford friction coefficients down to $\mu = 0.0002$.[21,22] Polymer brush functionalized surfaces have also been reported to prevent fouling by bacteria.[23,24] These lubricious and antibacterial properties of polymer brushes are very compelling from a biomaterials perspective, where surfaces of artificial implants, catheters and endoscopes functionalized with friction reducing polymer brushes could benefit their service, thus reducing both pain and infections for patients.

3.3.2 Definition

There is no definition from the International Union of Pure and Applied Chemistry (IUPAC) of surface or interface tethered polymers or polymer brushes, but in the case of comb-like or graft copolymers macromolecule (i.e. polymers with a backbone and graft chains) IUPAC coins the term brush polymer as:

"A comb macromolecule in which branching points along a chain are separated by a few atoms only, typically by one atom, acquires the shape of a brush due to steric reasons and, therefore, it is usually referred to as a brush macromolecule. A polymer composed of such macromolecules is usually called a brush polymer." [25] Thus the chain-chain distance must be small enough in order to stretch the graft chains due to steric repulsion. Larger chain-chain distance inherently causes lower density on the backbone on comb-like polymers and surfaces, thus leading to a less stretched state of the brush chains. Brittain and Minko[26] attempted to discriminate between different polymer brush conformations by applying the following parameter:

$$\Sigma = \sigma \cdot \pi \cdot R_g \qquad \text{Eq. 3.1}$$

where σ is the chain density on surface and R_g is the radius of gyration at the specific solvent conditions. Depending on the value of the Σ parameter four different regimes apply: mushroom ($\Sigma < 1$), cross-over ($\Sigma \approx 1$) brush ($\Sigma > 1$) and 'true' brush ($\Sigma > 5$), see Figure 3.2.

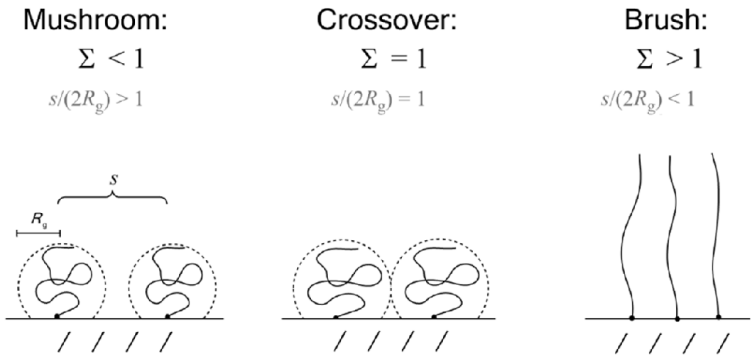

Figure 3.2: Regimes of tethered polymer chains on surfaces according to chain-chain distance and radius of gyration. See text for definitions of Σ and $s/(2R_g)$.

At low surface densities the distance between the polymer chains is too long to interfere with one another thus the extent of their radius of gyration is unperturbed and the conformation of the chains are like individual 'mushrooms' on the surface. In the crossover regime the surface density of the tethered chains is high enough for their R_g to begin to overlap hence inducing the chains to stretch. At brush regime the chain surface density is so high that the chains are forced to stretch away from the surface due to unfavorable excluded volume effects as in self-avoiding statistics of semidilute polymer solution.[27] Brittain and Minko argued that Σ has to

be larger than 5 in order to obtain the 'true' brush like configuration, thus either high surface densities and/or molecular weight of grafted chain are needed. The physical interpretation of Σ is the number of polymer chains that would occupy the same area as a none-overlapping chain would, under the same experimental conditions. The more popular $s/(2R_g)$ parameter for estimating polymer brush conformation is more straightforward. The $s/(2R_g)$ parameter simply states that when the pervaded volumes of grafted polymer chains start to overlap, chains begin to the stretch due to the excluded volume effect. This happens at $s/(2R_g) = 1$; at $s/(2R_g) > 1$ the mushroom regime applies, whereas at $s/(2R_g) < 1$ the grafted chains enter the brush regime. Figure 3.2 shows the $s/(2R_g)$ parameter values compared to Σ. For both $s/(2R_g)$ and Σ parameters conditions like solvent quality, curvature of surface, polydispersity and grafting inhomogeneity can greatly influence the conformation of the chains on the surface resulting in lower stretching. Hence one must be careful to assume brush or 'true' brush regime when applying the above mentioned parameters, as in real systems the transition from different regimes is gradual and less sharp.

3.3.3 Polymer brush formation

Polymer brushes can be synthesized or formed on surfaces in numerous ways, but the formations are commonly divided into three different approaches: *adsorption*, *grafting-to* and *grafting-from*. Adsorbed polymer chains on colloids' surfaces are known to stabilize colloid by the steric repulsion of the opposing polymer chains on other colloidal particles, thus preventing the colloids to flocculate and precipitate.[18] However, the steric repulsion of already adsorbed polymer chains impedes the adsorption of more chains onto the surface. Higher surface densities and stability are difficult to obtain when the interaction between surface and polymer is weak[28] as for homopolymer poly(ethylene glycol) adsorbed on mica.[29] Adsorption of block or graft copolymers with one or more blocks with affinity to the surface or due to selective solvent or selective surface of one of blocks affords higher surface densities and stability than homopolymers.[19] For block copolymer (diblock or triblock copolymers) one or more blocks can anchor to the surface whereas the remaining block(s) act as buoy thus stretching into the solvent.[30,31] Despite that graft copolymers have only one anchoring block, they have previously shown superior ability to stabilize colloids than their diblock copolymer analogues.[32] Figure 3.3 shows the different architectures of adsorbed polymer, i.e. weakly adsorbed homopolymer, diblock copolymer (adsorbed by one block) and graft copolymer. Nevertheless, the anchoring forces for adsorbed polymer brushes are mainly dispersion forces or hydrogen bonding origin, hence desorption diminishes the amount of polymer on the surface. However, for paints and colloidal disperions large amounts of polymer in the dispersion ensures long term stabilization.

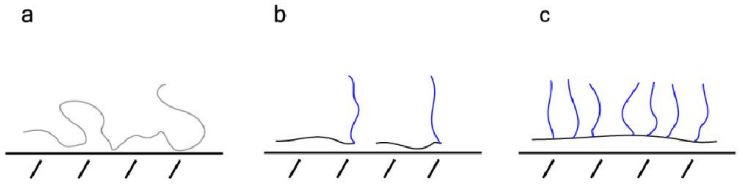

Figure 3.3: (a) Adsorbed homopolymer, (b) Adsorbed diblock copolymer with anchor block affinity to surface and selective solvent for the buoy block, (c) graft copolymer with backbone affinity to surface and selective solvent for the buoy blocks.

The *grafting-to* approach when forming polymer brushes on surface is commonly referred to when covalent anchoring is applied to polymers terminated with thiol, vinyl or azide functional groups to react with gold[33] or silicon[34], and also to react with alkyne functionalized surface by "click" chemistry.[35] Anchoring by means of annealing[36] and electrostatic forces[37] can also be considered as grafting-to due to the strong anchoring mechanism affording higher stability than adsorbed polymer brushes. As in the case for adsorbed polymer brushes, the grafting-to approach suffers from the steric repulsion of already anchored polymer chains causing lower surface densities. Here lower molecular self-assembled monolayers (SAM) are disregarded as polymer brushes. Although SAMs have some of the same structural characteristics on surfaces, SAMs do not have the distinct osmotic pressure and large gyration properties that polymer brushes have.

The *grafting-from* approach involves polymerization of the brush chains from initiator on the surface known as surface-initiated polymerization (SIP). It involves the supply of monomers to the propagation polymerization by e.g. atom-transfer-reaction-polymerization and reversible-addition fragmentation chain transfer (RAFT) initiated by an already grafted polymerization initiator. Monomers are usually of acrylic, vinyl or styrenic type.[38] Usually, the grafting-from approach supplies the highest chain densities on surfaces due to the lower degree of steric repulsion during the polymerization, hence forcing the conformation of the brushes to be very stretched and affording the 'true' brush conformation. Figure 3.4 shows the schematic formation of polymer brushes from the grafting to and grafting from approach.

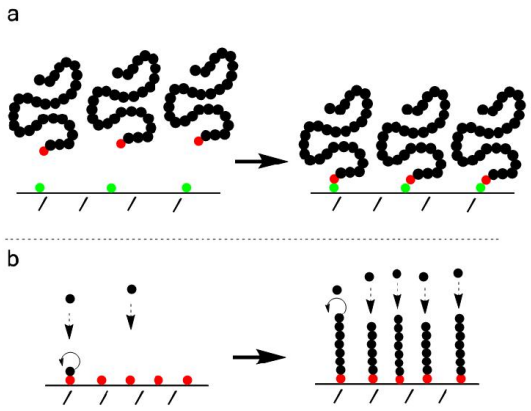

Figure 3.4: Schematic representation of (a) grafting to, and (b) grafting from (SIP) approaches for preparation of polymer brushes on surfaces.

3.3.4 Polymer brush lubrication in liquid media

When two opposing polymer brushes are compressed, the normal force associated with the compression can be described by the Alexander and de Gennes' scaling theory[39-41]:

$$f(D) \cong \frac{k_B T}{s^3} \cdot \left[\left(\frac{2L_0}{D} \right)^{9/4} - \left(\frac{D}{2L_0} \right)^{3/4} \right] \qquad \text{Eq. 3.2}$$

Eq. 3.2 applies for moderate compressions and higher density brushes in good solvents, where D, L_0, s, k_B and T are the distance between the grafted substrates, the length of the uncompressed or unperturbed polymer chain, the distance between grafted chains, the Boltzmann constant and the temperature (See Figure 3.5 for illustration).

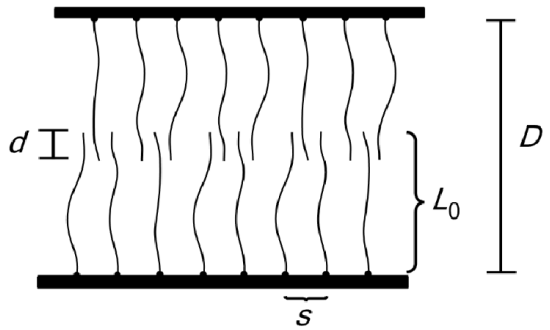

Figure 3.5: Schematic illustration of (uncompressed) opposing polymer brushes grafted on a surface.

As D decreases in Eq. 3.2, the first term in the square brackets increases and the second term decreases in absolute value. Thus as the polymer brushes are compressed ($D < L_0$) the normal force increases rapidly due to the exponent of the first term. The first term in Eq. 3.2 accounts for the osmotic repulsion when the brushes are compressed due to the solvation of the brushes in good solvent. The second term stems from elastic restoring force of the (over)stretched chains in good solvent. Eq. 3.2 can principally only describe the normal force of uniform brushes with sharp decrease of polymer volume fraction farther way from the surface than L_0, nevertheless, other expressions by Milner have been developed for lower surface density brushes and polymer volume fractions distributions.[42] When compressing two surfaces a hydrodynamic force opposing the compression is also present as first described by Reynolds. This hydrodynamic force is proportional to the rate of compression, however, since the scope of this thesis focuses on shearing polymer brushes where the separation is kept almost constant the readers are directed to other text on the effect.[43]

Together with normal force, the measurements of lateral shear force of polymers brushes have been pioneered by Jacob Klein and coworkers, where some of the earliest work was done by studying polystyrene brushes in toluene with surface force apparatus (SFA) which allows sub-nanometer control of separation and measurement of μN shear forces.[44] For realistic parabolic polymer volume fractions distributions the extent or depth of overlap (d) when compressing polymer brushes is described by the following equation:

$$d \approx s\left(\frac{2L}{D}\right)^{1/3} = s\beta^{1/3} \qquad \text{Eq. 3.3}$$

where L is the compressed brush height(Figure 3.5).[43] Thus $d \propto D^{-1/3}$ hence the penetration is small despite larger compressions, e.g. an 8 fold compression would only double the overlap of the polymer brushes due to the energetic unfavorable overlap.[45,46] Klein further extended Eq. 3.3 to estimate the shear force (τ) for compressed overlapping polymer brushes:

$$\tau = (\text{no. of chains / unit area}) \cdot (\text{no. of blobs per chain at the interpenetration zone } d) \cdot (\text{frictional drag per blob})$$

Eq. 3.4

where the blobs are 'Zimm blobs' thus modeling the segments of the polymer chains as spheres or blobs dragged in a medium of viscosity η_{eff}. Assuming that friction dissipation occurs in the interpenetration zone d, the expression for the frictional shear of the compressed polymer brushes is[27]:

$$\tau = \left(6 \cdot \pi \cdot \eta_{eff} \cdot v_s \cdot \beta^{7/4}\right) / s \qquad \text{Eq. 3.5}$$

v_s is the sliding or shear velocity. And hence the effective coefficient of friction is for the dissipative sliding:

$$\mu = \frac{\tau}{Load} = \frac{\left(6 \cdot \pi \cdot \eta_{eff} \cdot v_s \cdot \beta^{7/4}\right) / s}{Load} \qquad \text{Eq. 3.6}$$

where the load is given as Eq. 3.2.[43] Klein et al. studied polystyrene on mica surfaces in both the brush conformation and as free adsorbed chains. The friction force upon shear of the adsorbed polymer chains was more than 40 times higher than the brush configuration ($\mu < 0.005$).[44] The higher friction was attributed to the bridging of the adsorbed chains, however, the normal force during compression was very similar. In poor solvents the polymer chains are collapsed and the lubricity is typically retarded due to the lack of osmotic pressure.[47] For the above mentioned reasons the conformation of the polymer chains is thus imperative for obtaining good lubricity.

As stated by Eq. 3.6 the coefficient of friction is proportional to the sliding velocity and has been demonstrated experimentally by Tadmor et al. [48] and in simulations by Goujon,[49] both for sliding polymer brushes in good solvents. Tadmor's results stem from SFA experiments with shear rates on the order of 20 s^{-1}. In Tadmor's experiments, the dependence of friction on the sliding speed was attributed to the opposing polymer brushes' conformation and high penetration at the beginning of sliding, i.e. static friction; followed by kinetic friction due to the dissipation of energy in the overlap region as described in Eq. 3.6. Goujon applied macroscale shear rates up to 10^6 s^{-1} which is achievable in engineering bearings[50] and synovial joints.[22] In both cases the coefficient of friction (in the kinetic range) was on the order of $\mu \approx 0.03$-0.01 at very high compressions of $2L/D \approx 0.1$-0.2, thus displaying the lubricating performance of polymer brushes. Additionally, in his simulations Goujon also reasoned that a very fluidic hydration/solvent layer is formed at the interface between sheared polymer brushes imparting a low shear strength slip plane, thus further contributing to the lubricity. The lubrication mechanisms of hydration sheath have been shown experimentally by SFA, albeit for mica surfaces with very fluidic water bound to counter ions of the negatively

charged mica substrate. This afforded μ values down to 0.0002 at D = 1 nm i.e. only ca. 4 water molecules of separation.[51] At higher compressions $D << 2L$ or $D < R_g$ and low shear rates the overlap region is significant and the friction associated increases proportionally, however, hydration of the repeating units can retain a solvation shell around and consequently reduce the friction as the chains slide past each other.[22] Hence the lubricity of polymer brushes originates from the following properties 1) Osmotic pressure, causing the chains to swell and stretch rendering the brush structure, 2) energetically unfavorable overlap of opposing brushes at moderate compressions thus causing low overlap, 3) formation of low shear strength hydration sheet at shearing, and 4) hydration of the repeating units imparting hydration shells within the brushes that affords better lubricity at higher compressions.

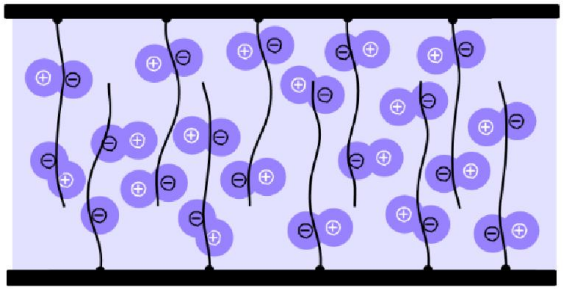

Figure 3.5: Schematic illustration of the hydration shells on the charges of a compressed anionic polyelectrolyte brush with counterions. Not to scale. Number of charges per graft chain is not to scale.

Property number 4) is mostly relevant to polyelectrolyte or zwitterionic polymer brushes in water. Charged repeating units are significantly hydrated giving the hydration or solvation shell (Figure 3.5) to afford low friction even at high compressions.[21,52] At molecular scale confinement carbon based lubricants tend to solidify, whereas water remains very fluidic, thus it is conjectured that the same mechanism of very fluidic water layers is present in the hydration shells.[22,50,51] Additionally, for polyelectrolytes the osmotic pressure is augmented by the counterions inside the brush giving higher load-carrying support. SFA studies of adsorbed poly(methylmethacrylate-*b*-sodium sulfonate glycidyl methacrylate) (PMMA-*b*-PSGMA) diblock copolymer brushes onto hydrophobized mica (s = 4 ± 0.7 nm, L_0 =13 ± 1.0 nm) have shown lubrication performance of μ values down to 0.0006 albeit only at pressures up to 0.3 MPa (where the PSGMA block is the hydrophilic brush buoy block and PMMA as anchor block).[21] However, grafting from brushes on mica of polyzwitterionic poly(2-(Methacryloyloxy)ethyl phosphocholine) (PMPC) (s = 3.5 ± 1 nm, L_0 = 37 ± 5.0 nm) has shown remarkable lubricity with μ = 0.001 at contact pressures up to 8 MPa.[52] The

lubricity of PMPC brushes has also been studied by Zheng et al.[53] by applying friction force (atomic force microscopy) AFM with contact pressures up to 7.5 MPa, however, the coefficients of frictions were somewhat higher $\mu \approx$ 0.03-0.05 depending on the brush thickness (s and L_0 not reported). Heeb et al.[54] investigated the lubricity of the of (SIP) grafted from poly(methacrylic acid) (PMAA) brushes in with different thicknesses (15-240 nm, dry thickness) on Si/SiO_2 surfaces where all brushes gave μ < 0.01 at contact pressures of 0.28 MPa. Neutral brushes of poly(ethylene glycol) (PEG) are not hydrated to the same extent due to lack of charges and this been used for explaining for the inferior lubricity of PEG on mica, compared to charged polymer brushes.[22] Raviv et al.[55] showed that PEG chains (s = 2.0 ± 0.3 nm, L_0 = 5.5 ± 0.5 nm) electrostatically grafted-to on mica gave μ = 0.03 measured by SFA at a contact pressure of 0.1 MPa. Lee et al.[56] has shown that neither covalently nor electrostatically grafting to PEG chains (5 kDa) on glass slides vs. steel pin in aqueous buffer with contact at a pressure of 0.51 GPa did provide long term lubricity. Due to the stronger covalently anchoring silane-PEG was not slid off so rapidly as the electrostatically grafted one, despite very similar grafting thickness. When the solution of poly(L-lysine)-*graft*-poly(ethylene glycol) (PLL-*g*-PEG) – which was electrostatically anchored via the cationic PLL backbone – was applied to the glass substrate by sliding in an aqueous solution of ample PLL-*g*-PEG (1 mg/mL), then the lubricity was retained. This afforded $\mu \approx$ 0.1 compared to the unlubricated contact of $\mu \approx$ 0.5. The lower friction coefficient provided by ample PLL-*g*-PEG was attributed to the ability of 'self-healing'. New PLL-*g*-PEG from solution re-adsorbed by rapid adsorption kinetics, to slid areas thus granting the longer term lubricity which was not observed for (pre)grafted PLL-*g*-PEG in aqueous buffer only.[56]

The most direct comparisons between the lubricity of neutral and polyelectrolyte brushes have probably been conducted by Raviv et al.[21] and Heeb et al.[54] Raviv compared the lubricity of PMMA-*b*-PSGMA in water to PS brushes in toluene (s = 9.4 ± 0.7 nm, L_0 = 29.6 ± 0.4 nm). The PMMA-*b*-PSGMA brush only marginally increased its μ values at very high compression whereas the PS brush system increased by orders of magnitude. Heeb et al. investigated a 15 nm thick grafted from PMAA brush and a 3 nm grafted to PEG brush (both dry thickness) on Si/SiO_2 surface, slid against oxidized PDMS pin. The μ values in aqueous buffer were ca. 0.001 for the PMAA brush and ca. 0.04-0.1 for the PEG brush, increasing with sliding speed. Thus neutral brushes are generally inferior to charged brushes, however, one might argue that in the case of PEG compared to polyelectrolyte brushes the thicknesses of the latter has always been higher than the compared PEG. The PEG brushes usually had a molecular weight usually 5 kDa or less as stated in the examples above. There are no studies to date of high thickness grafted-from PEG brushes on a surface and their lubricating properties. Nevertheless PEG based brushes have shown one area of successful lubricating

properties, namely as 'self-healing' polymer additives with ample polymer in solution to enable (re)adsorption during tribostress. As described above PLL-*g*-PEG has shown good lubricity by 'self-healing', [56] but also poly(ethylene oxide)-poly(propylene oxide)-poly(ethylene oxide) (PEO-PPO-PEO) block copolymers ("Pluronic") have shown low friction behavior at sliding hydrophobic interfaces by means of adsorption and supply of excess polymer additive in aqueous solution.[57,58] Polyelectrolytes brushes have never been successfully applied as aqueous lubricant additives to the best of our knowledge to provide friction lowering capabilities.

3.4 Biolubricants – Mucin and hydrophobins

3.4.1 Mucins

Figure 3.6(a) displays the schematic illustration of the amphiphilic mucins adsorbed onto hydrophobic surface with characteristic 'bottle brush' structure, where the anchoring to the hydrophobic surface proceeds via the hydrophobic moieties in the polypeptide backbone and hydrophilic glycosylated regions stretch to bulk water. Mucins are proteins excreted by the epithelial cells or glands in the gastrointestinal tract,[59] lungs,[60] and cervix[61] in humans and animals, and they constitute the major component of mucus gel, which are known to both lubricate and protect the epithelia. The molecular weights of mucins are very high in the range of 0.2-200 MDa, depending on the type.[62] Mucins readily adsorb onto and lubricate hydrophobic interfaces via their unglycosylated hydrophobic polypeptide backbone at the C- and N-termini. Their lubricity is attributed to the hydration of the carbohydrates inducing stretching of the hydrophilic glycosylates and increasing the osmotic pressure.[2,63,64] This reduces interpenetration of mucin layers between opposing surfaces under normal load, and lowers the interfacial friction forces, similarly to hydrophilic polymer brushes.[2] For soft PDMS-PDMS contacts $\mu \approx 0.01$-0.02 in aqueous solutions of bovine submaxillary mucin (BSM) were reported by Madsen,[64] where the contact pressure was ca. 0.3 MPa. Adsorption and lubrication by mucins are not restricted to hydrophobic surfaces, and have also been reported for hydrophilic surfaces. Pettersson et al.[65] have reported coefficient of friction of $\mu = 0.03 \pm 0.02$ for BSM adsorbed onto hydrophilic mica with contact pressures up to 40.0 MPa as measured by AFM colloidal probe technique.

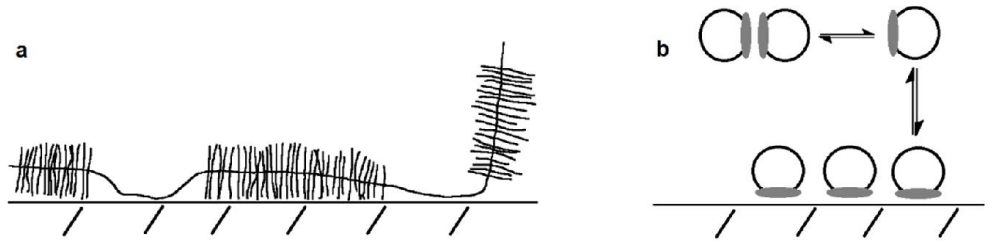

Figure 3.6: (a) Illustration of mucin protein, with hydrophilic 'bottle brush' structure, adsorbed onto a surface via its hydrophobic backbone moieties. (b) Schematic representation of the equilibrium between dimerized hydrophobins in solution, individual hydrophobins and adsorbed hydrophobins on hydrophobic surface. Both dimerization and adsorption are facilitated by the hydrophobic patch.

3.4.2 Hydrophobins

Another amphiphilic aqueous lubricant additive of biological origin is hydrophobins which stem from fungi. Hydrophobins can lower the surface tension of the water air interface from 72 to 24 mJ/m^2, thus allowing the fungi hyphae to escape their aqueous environment and spread and grow.[66] Hydrophobins also assist the fungi to spread on hydrophobic substrates by adhesion of excreted hydrophobins to new growth sites.[67] Unlike mucins, the molecular weights of proteinaceous hydrophobins are much lower, 7-10 kDa, and they consist of less than 100 amino acids.[67] Hydrophobins form dimers or tetramers depending on the concentration, which is facilitated via their hydrophobic face or patch.[68-70] Figure 3.6(b) shows the dimerization in equilibrium with unimer hydrophobin and adsorption onto hydrophobic surface via the hydrophobic patch. Due to the amphiphilic nature, hydrophobins can adsorb onto both hydrophobic and hydrophilic surfaces,[71] however, most tribological studies on hydrophobin mediated lubrication have been conducted on hydrophilic surfaces in aqueous environment to date. Hakala et al.[72] studied the friction and wear performance of 1.0 mg/mL HFBI and FpHYD5 types hydrophobins in 50 mM acetate buffer in self mated stainless steel sliding pin-on-disk contact. The coefficient of friction dropped to $\mu \approx 0.2$ in the hydrophobin solutions from $\mu \approx 0.6$ in pure water, likewise the wear was reduced in the hydrophobin solutions. However, the acetate buffer alone also contributed significantly to drop in both friction and wear compared to pure water. The contact pressure was between 4-22 MPa depending on the progress of wear. Similar results for HFBI at 1 mg/mL were observed by Ahlroos with the same tribopair and contact pressure. Additionally Ahlroos et al.[73] observed that further drop in friction did not occur when the concentration was increased to 5.0 mg/mL.

3.5 References

[1] Gong, J. P. *Soft Matter*, **2006**, *2*, 544-552.

[2] Dedinaite, A. *Soft Matter*, **2012**, *8*, 273-284.

[3] Dezzutti C.S.; Brown E. R.; Moncla B.; Russo J.; Cost M.; et al. (**2012**) Is Wetter Better? An Evaluation of Over-the-Counter Personal Lubricants for Safety and Anti-HIV-1 Activity. PLoS ONE 7(11): e48328. doi:10.1371/journal.pone.0048328.

[4] Uyama, Y; Tadokoro, H.; Ikada, Y. *Biomaterials*, **1991**, *12*, 71-75.

[5] Rimmer, S.; Biomedical Hydrogels, Woodhead Publishing Ltd., 2011, Cambridge, UK.

[6] Berger, J., Reist, M.; Mayer, J.M.; Felt, O.; Gurny, R.; *Eur. J. Pharm. Biopharm.*, **2004**, *57*, 35-52.

[7] Hassan, C.; Peppas, N.; *Macromolecules*, **2000**, 33, 2472-2479.

[8] Wanka, G.; Hoffmann, H; Ulbricht, W. *Macromolecules*, **1994**, *27*, 4145-4159.

[9] Hoffman, A.S. *Annals of the New York Academy of Sciences*, **2001**, *944*, 62-73.

[10] Wang, T.; Gunasekaran. S.; *J. Appl. Polym. Sci.* **2002**, 101, 3227-3232.

[11] Dunn, A. C.; Sawyer, W. G.; Angelini, T. E.; *Tribol Lett*, **2014**, *54*, 59-66.

[12] Gong, J. P. *Softmatter*, **2006**, *2*, 544-552.

[13] Gong, J. P., Kurokawa, T., Narita, T., Kagata, G.; Osada, Y.; Nishimura, G.; Kinjo, M.; *J. Am. Chem. Soc.* **2001**, *123*, 5582-5583.

[14] Gong, J. P., Katsuyama, Y.; Kurokawa, T.; Osada, Y., *Adv. Mater.*, **2003**, *15*, 1155-1158.

[15] Ohsedo, Y.; Takashina, R.; Gong, J. P., Osada, Y.; *Langmuir*, **2004**, 20, 6549-6555.

[16] Ishikawa, Y.; Sasada, T.; *Materials Transactions*, **2004**, *45*, 1041-1044.

[17] Dunn, A. C; Urueña, J. M.; Hou, Y.; Perry, S. S.; Angelini, T. E.; Sawyer, W. G. *Tribol Lett*, **2013**, *49*, 371-378.

[18] Hiemenz, P. C.; Rajagopalan, R.; Principles of Colloidal and Surface Chemistry, 1997, 3rd ed., Marcel Dekker Inc, New York, New York, USA.

[19] Vincent, B., *Adv. Colloid Interface Sci.*, **1974**, *4*, 193-277.

[20] van der Warden, M. *J. Colloid Sci.*, **1950**, *5*, 317-325.

[21] Raviv, U.; Giasson, S.; Kampf, N.; Gohy, J.; Jerôme, R.; Klein, J.; *Nature*, **2003**, *425*, 163-165.

[22] Klein, J. *Friction*, **2013**, *1*, 1-23.

[23] Kuang, J. H.; Messersmith, P. B. *Langmuir*, **2012**, *28*, 7258−7266.

[24] Liu, Q.; Singh, A.; Liu, L.; *Biomacromolecules*, **2013**, *14*, 226-231.

[25] Vohĺidal, J. *Pure Appl. Chem.*, **2009**, *81*, 1131-1186.

[26] Brittain, J. W.; Minko, S. *J. POLYM. SCI. PART A: POLYM. CHEM.*, **2007**, *45*, 3505-3512.

[27] Rubinstein, M.; Colby, R. H. Polymer Physics; Oxford University Press, Inc., Oxford, 2003.

[28] Zhao, B:; Brittain, W., *J. Prog. Polym. Sci.*, **2000**, *25*, 677-710.

[29] Raviv, U.; Tadmor, R.; Klein, J.; *J. Phys. Chem. B*, **2001**, *105*, 8125-8134.

[30] Dorgan, J. R.; Stamm, M.; Toprakcioglu., C.; *Polymer*, **1993**, *34*, 1554-1557.

[31] Nejadnik, M. R.; Olsson, A. L. J.; Sharma, P. K.; van der Mei, H. C.; Norde, W.; Busscher. H. J.; *Langmuir*, **2009**, *25*, 6245-6249.

[32] (a) Bijsterbosch, H. D.; Stuart, M. A.; Fleer, G. J. *J. Colloid Interface Sci.*, **1999**, *210*, 37−42. (b) Rieger, J.; Passirani, C.; Benoit, J.-P.; Van Butsele, K.; Jérôme, R.; Jérôme, C. *Adv. Funct. Mater.* **2006**, *16*, 1506−1514.

[33] Zhu, B.; Eurell, T.; Gunawan, R.; Leckband, D.; J. BIOMED. MATER. RES. PART B, **2001**, *56*, 406-416.

[34] Maas, J. H.; Stuart, M. A. C.; Sieval, A.B.; Zuilhof, H.; Sudhölter, E.J.R., *Thin Solid Films*, **2003**, *426*, 135-139.

[35] Ostaci, R.; Damiron, D.; Grohens, Y.; Léger, L.; Drockenmuller, E.; *Langmuir*, **2009**, *26*, 1304-1310.

[36] Librelle, B.; Giasson, S.; *Langmuir*, **2008**, *24*, 1550-1559.

[37] Müller, M.; Yan, X.; Lee, S.; Perry, S.; Spencer, N. D.; *Macromolecules*, **2005**, *38*, 5706-5713.

[38] Barbey, R. et al. *Chem. Rev.*, **2009**, *109*, 5437–5527.

[39] Alexander, S. *J. Phys. (France)*, **1977**, *38*, 983-987.

[40] de Gennes, P. G. *Macromolecules*, **1980**, *13*, 1069-1075.

[41] de Gennes, P. G. *Adv. Colloid Interface Sci.*, **1987**, 27, 189-209.

[42] Milner, S. T.; Witten, T. A.; Cates, M. E., *Macromolecules*, **1988**, *21*, 2610-2619.

[43] Klein, J.; *Annu. Rev. Mater. Sci.*, **1996**, *26*, 581-612.

[44] Klein, J.; Kumacheva, E.; Perahia, D.; Mahalu, D.; Warburg S. *Faraday Discuss.*, **1994**, *98*, 173-188.

[45] Witten, T. A.; Leibler, L.; Pincus, P. A., *Macromolecules*, **1990**, *23*, 824-829.

[46] Wijmans, C. M.; Zhulina, E. B.; Fleer, G. J., *Macromolecules*, **1994**, *27*, 3238-3248.

[47] Nalam, P. C.; Clasohm, J. N.; Mashaghi, A.; Spencer, N. D., *Tribol. Lett.*, **2010**, *37*, 541-552.

[48] Tadmor, R.; Janik, J.; Klein, J., *Phys. Rev. Lett.*, **2003**, 91, 115503-(1-4).

[49] Goujon, F:; Ghoufi, A.; Malfreyt, P.; Tildesley D. J.; *Soft Matter*, **2013**, *9*, 2966-2972.

[50] Stachowiak, G. W.; Batchelor, A. W.; Engineering Tribology, 3rd ed., Elsevier, Burlington, MA, USA, 2005.

[51] Raviv, U.; Klein, J.; *Science*, **2002**, *297*, 1540-1543.

[52] Chen, M.; Briscoe, W. H.; Armes, S. P.; Klein, J., *Science*, **2009**, *323*, 1698-1701.

[53] Zhang, Z.; Morse, A. J.; Armes, S. P.; Lewis, A. L.; Geoghegan, M.; Leggett. G. J., *Langmuir*, **2011**, *27*, 2514-2521.

[54] Heeb, R.; Bielecki, R. M.; Lee, S.; Spencer, N. D., *Macromolecules*, **2009**, *42*, 9124−9132.

[55] Raviv, U.; Frey, J.; Sak, R.; Laurat, P.; Tadmor, R.; Klein, J.; *Langmuir*, **2002**, *18*, 7482-7495.

[56] Lee, S.; Muller, M.; Heeb, R.; Zurcher, S.; Tosatti, S.; Heinrich, M.; Amstad, F.; Pechmann, S.; Spencer, N. D. *Tribol. Lett.*, **2006**, *24*, 217−223.

[57] Lee, S.; Iten, R.; Müller. M.; Spencer, N. D., *Macromolecules*, **2004**, *37*, 8349-8356.

[58] Lee, S.; Spencer, N. D. *Tribol. Lett.*, **2005**, *38*, 922-930.

[59] Schrager, J., *Gut*, **1970**, *11*, 450-456.

[60] Thornton, D. J.; Rousseau, K.; McGuckin, M. A., *Annu. Rev. Physiol.*, **2008**, *70*, 459-86.

[61] Daunter, B.; Counsilman, C., *Europ. J. Obstet. Gynec. reprod. Biol.*, **1980**, *10/3*, 141-161.

[62] McGuckin, M. A.; Thornton, D. J.; Mucins, Humana Press, 2012, New York, NY, USA.

[63] Yakubov. G. E.; McColl, J.; Bongaerts, J. H. H.; Ramsden, J. J., *Langmuir*, **2009**, *25*, 2313-2321.

[64] Madsen, J. B.; Pakkanen, K. I.; Lee, S.; *J. Colloid Interface Sci.*, **2014**, *424*, 113-119.

[65] Pettersson, T.; Dedinaite, A. *J. Colloid Interface Sci.*, **2008**, *324*, 246-256.

[66] Wösten, H. A. B.; van Wetter, M.; Lugones, L. G. et al. *Current Biology*, **1999**, *9*, 85-88.

[67] Wösten, H. A. B. *Annu. Rev. Microbiol.*, **2001**, *55*, 625-646.

[68] Kisko, K.; Szilvay, G. R.; Vainio, U.; Linder, M. B.; Serimaa, R., *Biophysical Journal*, **2008**, *97*, 198-206.

[69] Basheva, E. S.; Kralchecsky, P. A.; Christov, N. C. et al. Langmuir, 2011, 27, 2382-2392.

[70] Sarlin, T.; Kivioja, T.; Kalkkinen, N.; Linder, M. B.; Nakari-Setälä. T., *J. Basic Microb.*, **2012**, *52*, 184-194.

[71] Qin, M.; Wang, L.; Feng, X. et al., *Langmuir*, **2007**, *23*, 4465-4471.

[72] Hakala, T., Laaksonen, P.; Saikko, V. et al. *RSC Advances*, **2012**, *2*, 9867-9872.

[73] Ahlroos, T.; Hakala, T.; Helle, A.; Linder, M. B. et al., *Proc. IMechE Vol. 225 Part J: J. Engineering Tribology*, **2011**, *225*, 1013-1022.

4.0 Results

4.1 Introduction

This subsection is provided to the reader to grant understanding of the motivation and background behind the different chapters about aqueous lubrication additives, neat water lubrication or hydrogel lubrication. This is also done in order not just to provide the purpose of each chapter, but also to explain how the different chapters are related and connected to the overall aim of the thesis. The Result section chapters are:

Chapter	Title:	Status
4.2	Adsorption and Aqueous Lubricating Properties of Charged and Neutral Amphiphilic Diblock Copolymers at a Compliant, Hydrophobic Interface.	Published article in Langmuir, 2013.
4.3	Synthesis, Characterization, and Aqueous Lubricating Properties of Amphiphilic Graft Copolymers Comprising 2‑Methoxyethyl Acrylate.	Published article in Macromolecules, 2014.
4.4	Aqueous Lubricating Properties of Charged (ABC) and Neutral (ABA) Triblock Copolymer Chains.	Submitted article to the journal 'Polymer', 2014.
4.6	Influence of temperature on the frictional properties of water-lubricated surfaces.	Submitted article to the journal 'Lubricants', 2014.
4.6	Lubrication of Soft and Hard Interfaces with Thermoresponsive F127 Hydrogel.	Article draft.
4.7	Hydrophobins as aqueous lubricant additive for a soft sliding contact.	Article draft.

Adsorption and Aqueous Lubricating Properties of Charged and Neutral Amphiphilic Diblock Copolymers at a Compliant, Hydrophobic Interface.

The scope of this study was to investigate the boundary lubricating properties of neutral and charged diblock copolymers in aqueous environment at a soft hydrophobic sliding interface. Previously, grafted-from polyelectrolyte brushes have shown superior lubrication over neutral ones as described above.[1,2] In this context, it was hypothesized that similar superior lubrication capabilities would also be observed for polyelectrolyte brushes adsorbed from ample polymer solution i.e. 'self-healing'. Previous studies on 'self-healing' mechanism have been performed with triblock[3] and graft copolymers[4] with minimum one anchoring block. However, we chose the diblock copolymer architecture since we regard it as the simplest amphiphilic

copolymer. Hence the structural consideration consisted of applying diblock copolymers adsorbing to a hydrophobic surface via the hydrophobic block and the hydrophilic charged or neutral block would act as buoy, thus forming the polymer brush on the surface. Using ca. 5-10 kDa molecular weight blocks of PEG as buoy blocks for triblock and graft copolymer additives in aqueous conditions, it has earlier been shown to be effective at lubricating both hydrophobic (PDMS-PDMS) and negatively charged oxidized (oxPMDS-oxPDMS) sliding interfaces.[3,4] Thus a molecular weight of ca. 5 kDa was applied for the neutral PEG and charged poly(acrylic acid) (PAA) blocks. Similar molecular weights of 5 kDa of the hydrophobic anchoring blocks PS and poly(2-methoxyethyl acrylate) (PMEA) were employed. Using higher molecular weight hydrophobic blocks – in this case PS and PMEA blocks – might be assumed to facilitate better anchoring, however, this was avoided since it is known to induce low solubility or low critical micelle concentration (CMC) in aqueous environment.[5-7] Neutral diblock copolymers of PEG-*b*-PS and PEG-*b*-PMEA adsorbed at the sliding PDMS-PDMS interface in water and lubricated the contact very well. However, the PAA-*b*-PS and PAA-*b*-PMEA did not lubricate the sliding PDMS-PDMS contact, despite that PAA-*b*-PMEA diblocks showed significant adsorption. The inferior lubricating properties of the polyelectrolyte diblock copolymer additives were attributed to either no adsorption, in the case of PAA-*b*-PS, or electrostatic repulsion and desorption of the PAA-*b*-PMEA due to tribostress. The lubricity of the PAA-*b*-PS and PAA-*b*-PMEA diblock polymers was to some extent improved by employing 150 or 500 mM NaCl in the polymer solutions, or reducing the number of charges by lowering the pH. The study showed the significance of dilution or impedance on the charges of the diblock polyelectrolyte additives to obtain even a fair degree of lubricity.

Synthesis, Characterization, and Aqueous Lubricating Properties of Amphiphilic Graft Copolymers Comprising 2 -Methoxyethyl Acrylate.

The increased stabilization efficacy of colloidal dispersions by applying graft copolymers compared to diblock copolymer has been known for decades.[8] Furthermore, the polyelectrolyte based graft copolymers are known to stabilize colloidal dispersions better than their neutral counterparts due to stronger anchoring efficacy.[9,10] The study in this chapter/article explored these properties at soft PDMS-PDMS sliding contact for enhanced 'self-healing' boundary lubrication by applying graft copolymers consisting of a backbone poly(2-hydroxyethyl methacrylate) (PHEMA) and polyelectrolyte graft chains of either anionic poly(methacrylic acid) or cationic poly(2-dimethylamino) ethyl methacrylate (PDMEAMA). Additionally neutral MEA repeating units were incorporated in the graft chain to provide dilution of the charges. Thus the

structures of the graft copolymers were P(MEA-co-MAA)-*graft*-PHEMA or P(MEA-co-DMAEMA)-*graft*-PHEMA. The cationic based P(MEA-co-DMAEMA)-*graft*-PHEMA did not show any adsorption or lubricating properties at neutral (pH 7.0, 1 mM ionic strength) or 150 mM NaCl conditions. Anionic P(MEA-co-MAA)-*graft*-PHEMA copolymers did not show lubricating capabilities at neutral conditions either. However, the lubricity was significantly enhanced at 150 mM NaCl even at the slowest sliding speeds which was not observed for the PAA-*b*-PMEA diblocks in the previous study. 150 mM NaCl is close to physiological conditions which is interesting since lubrication in biological systems such as mucus and synovial joints occurs at physiological ion strength. Mucins (and similar lubricin in synovial joints) contain significant number of charges, and hence the physiological ionic strength may be required to afford lubricity of charged aqueous lubricant additives.[11,12] Applying graft copolymers was more successful than diblock copolymers in lubricating PDMS-PDMS sliding contact when charged moieties are present in the buoy chains.

Aqueous Lubricating Properties of Charged (ABC) and Neutral (ABA) Triblock Copolymer Chains.

Based on the observations of the two previous articles it was clear that dilution or screening of the charges in the buoy blocks was necessary in order to obtain lubricity when sliding at the hydrophobic PDMS-PDMS contact in the lubricant solution at boundary conditions. This article set out to investigate the effect of dilution of the charged buoy blocks by addition of neutral PEG block at the other end of the anchor block, i.e. a triblock copolymer composed of PEG-*b*-PMEA-*b*-PMAA, where the PMEA block is anchor block. The charged or partly charged triblock copolymer PEG-*b*-PMEA-*b*-PMAA was compared to the completely neutral PEG-*b*-PMEA-*b*-PEG triblock, where the molecular weights of the blocks were ca. 5kDa-*b*-7kDa-*b*-5kDa. The two polymers displayed good lubricity by both macro and microscale contact scales and showed none or minor differences in adsorption and opposition to normal force by compression. This coincides with the notion that 'dilution' of polyelectrolyte blocks by neutral PEG block is a feasible way of employing charged polymer brushes. Nevertheless, it is emphasized that the PEG-*b*-PMEA-*b*-PMAA triblock was not better than its entirely neutral counterpart. However, increasing the ionic strength was not needed in the lubricant solution of the charged PEG-*b*-PMEA-*b*-PMAA to obtain the same relatively good lubricity and adsorption as for PEG-*b*-PMEA-*b*-PEG. This again shows the necessity to dilute the charges in the brushes on the surface in order achieve stable lubricity under cyclic tribostress.

Influence of temperature on the frictional properties of water-lubricated surfaces.

Studies on the influence of temperature on the lubricating properties of oil lubricants are not uncommon. However, temperature dependency studies on neat water lubrication are rare. The aim of this article was to investigate the lubricating performance of neat water in different types of contact, by tuning the contacts' hydrophilicity and hardness, thus reflecting four different tribocontacts of engineering materials. The four types of contact were 1) soft hydrophobic PDMS-PDMS, 2) soft hydrophilic oxPDMS-oxPDMS, 3) hard hydrophobic poly(oxymethylene)-poly(oxymethylene) (POM-POM) and 4) hard hydrophilic steel-glass. Temperature dependency on the lubricity was characterized by measuring the friction in neat water at temperatures 1-90 °C. All tribocontacts were made in a mixed sliding/rolling regime where the friction response was measured by MTM (mini-traction-machine). A mean speed range of 10-1200 mm/s was applied to investigate not only boundary lubrication regime, but also to study the onset of hydrodynamic regime that occurs at high speeds in aqueous environment. The experimentally obtained friction response was compared to the theoretically predicted lubrication by employing the Stribeck parameter to estimate the onset of hydrodynamic regime and thus low friction of the different contacts. Whereas the theoretically predicted lubricity is only based on parameters such as sliding speed, load, viscosity of water, surface roughness and hardness/stiffness of the contact, the property of surface hydrophilicity and thereby ability to retain water at the interface are not taken into account by the Stribeck parameter. The lubricity of the hydrophobic contacts correlated reasonably well with the predicted theoretical lubricity. Nevertheless, the lubricity of the hydrophilic contacts was much better than theoretically predicted by the Stribeck parameter. Temperature effect on the bulk properties (Young's modulus and hardness) of the contacts was assessed to be small or negligible, hence change in bulk properties did not influence formed lubricating films. However, temperature's influence on the lubricity was apparent especially for the soft hydrophobic PDMS-PDMS and the hard hydrophilic steel-glass contacts, due to water's decrease in viscosity by increasing temperature. Thus providing smaller lubricant film thicknesses and less lubricity at higher temperatures. The study showed clear necessity of hydrophilic surface chemistry to induce favorable lubricity of sliding engineering contact in neat water. The study on the lubricity of neat water also provided a reference on future studies as investigations on the lubricity of thermoresponsive hydrogels in the same tribocontacts as described in the next chapter.

Lubrication of Soft and Hard Interfaces with Thermo-responsive F127 Hydrogel.

Thermo-responsive hydrogels are interesting candidates as aqueous lubricant since their gelation, and hence, viscosity can be tuned according to temperature. The purpose of this study was to investigate the lubricating properties of F127 gels in the same hard and soft, hydrophilic and hydrophobic contacts as mentioned in the previous section. F127 consists of PEO-*b*-PPO-*b*-PEO triblock copolymer, where PEO stands for poly(ethylene oxide) (equal to PEG) and PPO stands for poly(propylene oxide). It has been known for decades that aqueous solutions of F127 with 16 wt.% or higher transforms into a gel at temperatures between ca. 20-60 °C. Hence, it was conjectured that the higher viscosities would be reflected in lubricity when the F127 is in the gel state, inducing fluid film lubrication even at very low sliding speeds. However, due to severe shear thinning of the F127 gel the hard POM-POM and steel-glass contact showed high friction due to the low effective viscosities, which in the tribocontact, were calculated to be orders of magnitudes lower than in the bulk gel. POM-POM contact was negligibly lubricated at all temperatures as compared to neat water. The hydrophilic steel-glass contact was lubricated to some extent by the F127 solution as compared to neat water despite that the contact pressure was ten times higher than in POM-POM contact. This behavior was ascribed to better wetting of the F127 solution on the hydrophilic steel and glass substrates. The same shear thinning of the F127 gel behavior was observed for the soft hydrophobic PDMS-PDMS. Albeit in this case lower viscosity was assessed to provide lower friction due to the proportionality of the friction to the lubricants's viscosity when sliding contact is in full separation hydrodynamic regime. Temperature dependency on lubricity was observed to some extent for both soft hydrophobic PDMS-PDMS and hard hydrophilic steel-glass contacts. However, higher friction was mostly observed for higher temperatures but the origins of higher friction were different for the PDMS-PDMS and steel-glass contact due to different lubricating regimes. Hydrodynamic regime was dominant for PDMS-PDMS at most of the temperatures and mean speeds and boundary regime for steel-glass contact.

Hydrophobins as aqueous lubricant additive for a soft sliding contact.

Hydrophobins are amphiphilic proteins obtained from fungi and have previously displayed aqueous lubricating capabilities at self-mated sliding steel contacts and friction reducing properties by nanotribological studies in ambient conditions. As hydrophobins can lubricate such high pressure hard contacts, and have also previously shown to adsorb onto hydrophobic surfaces, it was hypothesized that hydrophobins can act as boundary aqueous lubricant additives in sliding hydrophobic PDMS-PDMS

contacts by 'self-healing'. In this study, two different hydrophobins were investigated – HFBI and FpHYD5 – where the latter was glycosylated and hence was expected to lubricate the sliding PDMS-PDMS contact better. Furthermore, the molecular weights of the hydrophobins ranged from 7-10 kDa, much lower than other biological lubricant aqueous additives such as mucins (Mw > 1 MDa), thus providing a comparison in molecular weight, to assess the importance of sheer mass on adsorption and lubricity. Both hydrophobin types displayed good adsorption and lubricity at the higher and medium sliding speed range, however, glycosylated FpHYD5 did provide better lubricity in the low speed range, which was not the case for HFBI. Thus hydrophobins act as efficient aqueous additives for boundary lubrication at sliding hydrophobic PDMS-PDMS interfaces.

4.1.2 References:

[1] Raviv, U.; Giasson, S.; Kampf, N.; Gohy, J.; Jerôme, R.; Klein, J.; *Nature*, **2003**, *425*, 163-165.

[2] Heeb, R.; Bielecki, R. M.; Lee, S.; Spencer, N. D., *Macromolecules*, **2009**, *42*, 9124−9132.

[3] Lee, S.; Iten, R.; Müller. M.; Spencer, N. D., *Macromolecules*, **2004**, *37*, 8349-8356.

[4] Lee, S.; Muller, M.; Heeb, R.; Zurcher, S.; Tosatti, S.; Heinrich, M.; Amstad, F.; Pechmann, S.; Spencer, N. D. *Tribol. Lett.*, **2006**, *24*, 217−223.

[5] Wilhelm, M.; Zhao, C. L.; Wang, Y. C.; Xu, R. L.; Winnik, M. A.; Mura, J. L.; Riess, G.; Croucher, M. D. *Macromolecules*, **1991**, *24*, 1033−1040.

[6] Astafieva, I.; Zhong, X. F.; Eisenberg, A. *Macromolecules*, **1993**, *26*, 7339−7352.

[7] Tanaka, M.; Motomura, T.; Ishii, N.; Shimura, K.; Onishi, M.; Mochizuki, A.; Hatakeyama, *Polym. Int.*, **2000**, *49*, 1709−1713.

[8] Vincent, B., *Adv. Colloid Interface Sci.*, **1974**, *4*, 193-277.

[9] Bijsterbosch, H. D.; Stuart, M. A.; Fleer, G. J. *J. Colloid Interface Sci.*, **1999**, *210*, 37−42.

[10] Rieger, J.; Passirani, C.; Benoit, J.-P.; Van Butsele, K.; Jérôme, R.; Jérôme, C. *Adv. Funct. Mater.*, **2006**, *16*, 1506−1514.

[11] Yakubov. G. E.; McColl, J.; Bongaerts, J. H. H.; Ramsden, J. J., *Langmuir*, **2009**, *25*, 2313-2321.

[12] Dedinaite, A. *Soft Matter*, **2012**, *8*, 273-284.

4.2 Adsorption and Aqueous Lubricating Properties of Charged and Neutral Amphiphilic Diblock Copolymers at a Compliant, Hydrophobic Interface.

Published in Langmuir, 2013. See next page.

Langmuir

Article

pubs.acs.org/Langmuir

Adsorption and Aqueous Lubricating Properties of Charged and Neutral Amphiphilic Diblock Copolymers at a Compliant, Hydrophobic Interface

Troels Røn,[†] Irakli Javakhishvili,[‡] Katja Jankova,[‡] Søren Hvilsted,[‡] and Seunghwan Lee*,[†]

[†]Department of Mechanical Engineering, Technical University of Denmark, DK-2800, Kgs. Lyngby, Denmark

[‡]Department of Chemical and Biochemical Engineering, Danish Polymer Centre, Technical University of Denmark, DK-2800, Kgs. Lyngby, Denmark

Supporting Information

ABSTRACT: We have investigated the adsorption and lubricating properties of neutral and charged amphiphilic diblock copolymers at a hydrophobic polydimethylsiloxane (PDMS) interface in an aqueous environment. The diblock copolymers consist of a hydrophilic block of either neutral poly(ethylene glycol) (PEG) or negatively charged poly(acrylic acid) (PAA) and of a hydrophobic block of polystyrene (PS) or poly(2-methoxyethyl acrylate) (PMEA), thus generating PEG-*b*-X or PAA-*b*-X, where X block is either PS or PMEA. The molecular weight ratios were roughly 1:1 with each block ca. 5 kDa. Comparing the neutral PEG and charged PAA buoyant blocks with all other conditions identical, the former showed superior adsorption onto nonpolar, hydrophobic PDMS surfaces from a neutral aqueous solution. PEG-based copolymers showed substantial adsorption for both PS and PMEA as the anchoring block, whereas PAA-based copolymers showed effective adsorption only when PMEA was employed as the anchoring block. For PAA-*b*-PS, the poor adsorption properties are chiefly attributed to micellization due to the high interfacial tension between the PS core and water. The poor lubricating properties of PAA-*b*-PS diblock copolymer for a PDMS−PDMS sliding contact was well correlated with the poor adsorption properties. PAA-*b*-PMEA copolymers, despite their sizable amount of adsorbed mass, showed insignificant lubricating effects. When the charges of the PAA-*b*-PMEA diblock copolymers were screened by either adding NaCl to the aqueous solution or by lowering the pH, both the adsorption and lubricity improved. We ascribe the poor adsorption and inferior aqueous lubricating properties of the PAA-based diblock copolymers compared to their PEG-based counterparts mainly to the electrostatic repulsion between charged PAA blocks, hindering the facile formation of the lubricating layer under cyclic tribological stress at the sliding PDMS−PDMS interface.

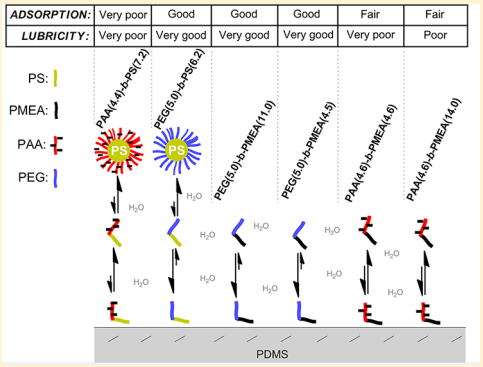

1. INTRODUCTION

Interest in aqueous lubrication has recently been growing due to its high relevance in biological tribosystems and potential biomedical applications such as knee and hip joint implants, catheters, and endoscopes, where traditional engineering lubricants (e.g., petroleum-based mineral oils and greases) are excluded because of biocompatibility issues.[1,2] Aqueous lubrication is very interesting also from an environmental and economic perspective, because water is nontoxic, abundant, and an effective coolant. One efficient approach to lubricate sliding contacts in aqueous environments is to functionalize the sliding surfaces with hydrophilic polymer brushes, affording retention of a water film at the interface.[3,4] While surface-grafted polymer brushes have long been studied in a broad range of science and engineering disciplines, including bioadhesive surfaces[5] and antifouling surfaces,[6] research on tribological applications, in particular for aqueous lubrication, is still relatively new,[7,8] and further understanding and improvements are required. The mechanisms behind the lubricity of sliding polymer brush contacts are mainly related to the formation of the highly solvated layers to oppose interpenetration[9] and to assist smooth lateral shear in theta or good solvents[7] (see Figure 1 for illustration).

To date, brush-forming polymer chains for aqueous lubrication have most actively been studied with neutral polymer brushes, especially PEG-based brushes.[8,10,11] In macroscale contacts using conventional tribometers, the friction coefficients of the sliding PEG brush interfaces have been reported to be as low as 0.03−0.006, even under the apparent contact pressure up to 0.50[12] or 0.70[13] GPa. Furthermore, employment of charged polymer chains[14−18] has shown even more enhanced lubricating performance with friction coefficients down to 0.0002 measured by SFA[14] and 0.001 by pin-on-disk tribometry,[18] in both cases at a contact pressure up to

Received: March 6, 2013
Revised: May 31, 2013
Published: May 31, 2013

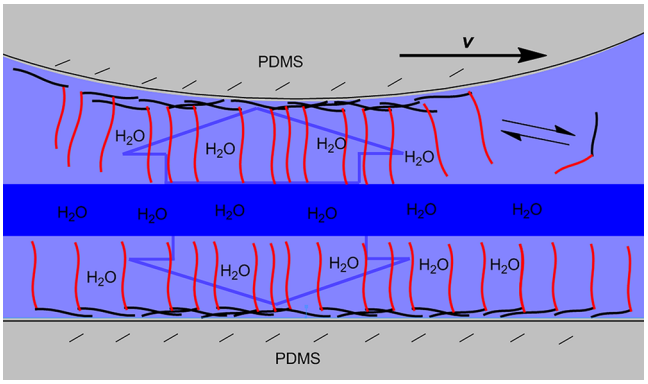

Figure 1. Illustration of opposing polymer brushes generated from physisorbed diblock copolymers, with osmotic pressure exerted by water and with the hydration film at a sliding PDMS−PDMS interface. The adsorbed diblock copolymers are in equilibrium with excess diblock copolymer unimers in solution. (The figure is not to scale).

≈0.3 MPa. The superior lubricating properties of polyelectrolyte brushes over neutral brushes are generally attributed to two factors: (1) The osmotic pressure within polyelectrolyte brushes in an aqueous environment is higher than that within neutral brushes due to the high concentration of counterions in the polyelectrolyte layer and hence reduced mutual penetration between opposing brush layers.[14,19] (2) Each of the charged segments within the sheared interpenetration zone is believed to comprise a tenaciously bound yet fluidic hydration sheath.[20] Overall, opposing polyelectrolyte brushes at the interface are better separated than neutral brushes in aqueous environment, resulting in smaller shear forces upon sliding.

Most of the tribological studies on charged polymer chains have been carried out by employing immobilized polyelectrolyte chains on the surface, either by preparing the film via the grafting-from approach[14,15,17,18] or chemically immobilizing free polymers on the surface.[16] A common problem of lubricating film as a coating is the risk of irreversible rupture from the underlying substrates, causing the subsequent impairment of the lubricating capabilities even at low contact pressures of ≈0.3 MPa.[18] On the contrary, grafting of polymer brushes via physical bonding to the surface, together with excess polymers in bulk solution, ensures that initially adsorbed polymers that are sheared off by tribostress can be readily replaced by excess polymers in solution, i.e., "self-healing"[21] tribologically stressed areas, thereby maintaining the lubricity, provided that the surface adsorption kinetics of the brush-forming polymers is sufficiently rapid (Figure 1). Despite the superiority of polyelectrolytes over neutral polymers for aqueous lubricating capabilities as mentioned above, "self-healing" behavior has only been observed for neutral brush chains to date.[21] In this context, one may conjecture that the combination of the superior lubricity of charged polymer brushes over neutral ones and the "self-healing" mechanism may offer a synergetic effect in aqueous lubrication.

To test this hypothesis, we have synthesized various amphiphilic diblock copolymers as lubricant additives for soft polydimethylsiloxane (PDMS) tribological sliding contacts in aqueous solution. The amphiphilic block copolymers consist of two blocks: (1) a hydrophilic block of either poly(ethylene glycol) (PEG) or poly(acrylic acid) (PAA); (2) a hydrophobic block of either polystyrene (PS) or poly(2-methoxyethyl acrylate) (PMEA). Thus, the block copolymers are PEG-*b*-X or PAA-*b*-X, where the X block is either PS or PMEA (see Scheme 1 for structures and Table 1 for properties). The hydrophobic block X is expected to act as a surface-anchoring block by interaction with hydrophobic PDMS substrate, whereas the hydrophilic, buoyant block (PEG or PAA) is expected to be hydrated and stretched toward bulk water (see Figure 1 for illustration). The polymers were designed to have number-average molecular weights (M_n) of each block of around 5 kDa; thus, the molecular weight ratio between hydrophilic and hydrophobic blocks is roughly 1:1. To test the influence of the size of the anchoring block, PAA-*b*-PMEA and PEG-*b*-PMEA with a higher molecular weight of hydrophobic anchoring block, e.g., 1:2 or 1:3 in molecular weight ratios, have also been employed. The full list of diblock copolymers is shown in Table 2.

The glassy state of PS vs the rubbery state of PMEA at room temperature and different interfacial tensions of PS and PMEA with water may influence the adsorption of the copolymers

Table 1. Structures and Bulk Properties of the Different Polymers Used

Polymer	PS	PMEA	PAA	PEG	PDMS
T_g (°C)	100[22]	-33[37]	106[22]	-66.4[22]	-123[22]
Surface energy (mJ/m²)	39.3[34]	36.7[37]	n/a	42.5[34]	20.4[22]
Structure	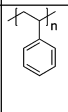	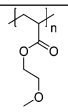	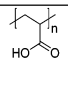	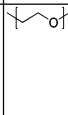	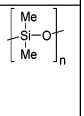

Scheme 1. Preparation of the Amphiphilic Diblock Copolymers

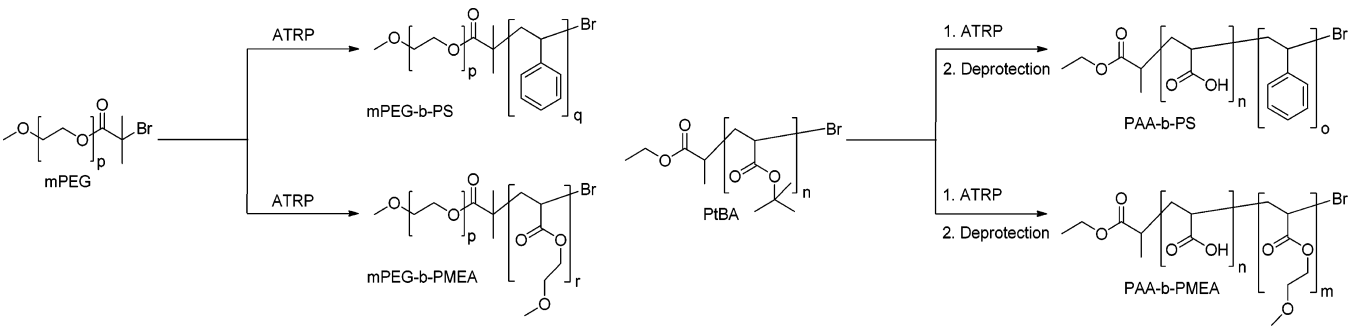

dx.doi.org/10.1021/la400827h | *Langmuir* 2013, 29, 7782−7792

Table 2. Adsorbed Mass on PDMS and Calculated Chain Surface Concentrations, Average Brush Chain−Chain Distance (L),[57] Radius of Gyration[58−60] (R_g, based on free polymers (hydrophilic blocks) in solution), and $L/2R_g$ ratios[a]

polymer (kDa)	polymer with repeating units	adsorbed mass, OWLS (mg/m^2) in HEPES, 1 mM, pH 7.0	+ 500 mM NaCl	chains (nm^2)	L (nm)	R_g (nm)	$L/2R_g$
PEG(5.0)-*b*-PS(6.2)	PEG_{110}-*b*-PS_{60}	1.31 ± 0.083	–	0.07	4.1	2.7	0.75
PEG(5.0)-*b*-PMEA(4.5)	PEG_{110}-*b*-$PMEA_{35}$	1.64 ± 0.131	–	0.1	3.4	2.7	0.63
PEG(5.0)-*b*-PMEA(11.0)	PEG_{110}-*b*-$PMEA_{85}$	2.097 ± 0.210	–	0.08	3.8	2.7	0.7
PAA(4.6)-*b*-PMEA(4.6)	PAA_{61}-*b*-$PMEA_{69}$	pH 7.0: 0.5 ± 0.071	0.84 ± 0.09	pH 7.0: 0.03	pH 7.0: 6.2	2.04	pH 7.0: 1.52
		pH 3.0: 1.73 ± 0.075		pH 3.0: 0.11	pH 3.0: 3.2		pH 3.0: 0.78
PAA(4.6)-*b*-PMEA(14.0)	PAA_{61}-*b*-$PMEA_{108}$	1.1 ± 0.212	–	0.04	5.4	2.04	1.32
PAA(4.4)-*b*-PS(7.2)	PAA_{59}-*b*-PS_{69}	pH 7.0: 0.072 ± 0.034	0.03 ± 0.04	pH 7.0: 0.004	pH 7.0: 17.0	2	pH 7.0: 4.25
		pH 3.0: 4.003 ± 0.049		pH 3.0: 0.22	pH 3.0: 2.3		pH 3.0: 0.58
PAA(5.1)	PAA_{71}	pH 7.0: 0[b]	–				
		pH 3.0: 0.28 ± 0.11					
PEG(5.0)	PEG_{113}	pH 7.0: 0[b]	–				
		pH 3.0: 0.15 ± 0.07					

[a]Polymer solution concentration was 0.50 mg/mL. If not stated otherwise, the adsorbed mass is reported at pH 7.0. For better overview, the number of repeating units of the block copolymers is also reported. The number average molecular weight was estimated by ^{1}H NMR spectroscopy. The number of repeating units was calculated from the blocks' average molecular weight without the macroinitiator. Adsorption of homopolymers PEG and PAA are stated for reference. [b]Below noise level.

onto a hydrophobic surface from aqueous solution and provide an interesting comparison between the two hydrophobic anchoring blocks (see Table 1 for comparison of the two anchoring blocks). PDMS was chosen as substrate for both surface adsorption and tribological studies due to its nonpolar nature, hydrophobicity (low surface energy), easy preparation, its compliance at room temperature (T_g (PDMS) = −123 °C[22]), and a Young's modulus of 1.80 MPa,[23] allowing facile lubrication of soft tribological contacts with aqueous solution via a soft elastohydrodynamic lubrication (soft EHL) mechanism.[24]

2. MATERIALS AND METHODS

HEPES Buffer. 4-(2-Hydroxyethyl)-1-piperazineethanesulfonic acid (HEPES 1 mM, pH 7.0) buffer solution was prepared by dissolution of HEPES salt (purchased from VWR BDH Prolabo) in Millipore water (18 MΩ) and subsequent adjustment of pH to 7.0 by adding 1.0 M NaOH (aq). HEPES buffer was employed as a base lubricant throughout this study.

Polymer Synthesis. All reagents and solvents were purified by conventional methods. The diblock copolymers were obtained by atom transfer radical polymerization (ATRP), employing the macroinitiator approach.[25,26] Thus, mPEG-OH (JenKem Technology, Allen, TX) was converted into an ATRP macroinitiator[27] and was subsequently chain-extended with styrene (St)[27] and 2-methoxyethyl acrylate (MEA).[28,29] Likewise, poly(*tert*-butyl acrylate) (P*t*BA) with active bromide at the chain end was synthesized with ATRP[30] and was chain-extended with St[31] and MEA.[29] Selective deprotection of the P*t*BA blocks afforded amphiphilic diblock copolymers PAA-*b*-PS and PAA-*b*-PMEA.[29] Molecular weight distributions of the diblock copolymers (except the polyanions) were estimated by size exclusion chromatography, employing tetrahydrofuran or *N*,*N*-dimethylformamide/LiCl as eluents: polydispersity indices (PDI) below 1.2 were obtained. The degrees of polymerization were determined by NMR spectroscopy. The molecular weight characteristics are summarized in Table 2.

PDMS Discs and Pins. PDMS discs and pins for tribological measurements were prepared with a two-component Sylgard 184 PDMS kit. Base and cross-linker were mixed at 10:1 wt ratio. Dispersed air bubbles generated during mixing were removed by vacuum using a mechanical oil pump. The mixture was then poured into molds and cured overnight at 70 °C. Disc (Ø = 30 mm) molds were home-machined aluminum, and Nunc U96 MicroWell plates (Thermo Scientific, Denmark) were used for pin (R = 3.0 mm) molds. The roughness of the PDMS discs and pins was measured by AFM tapping mode. The root-mean-square roughness (R_q) was measured to be 1.34 and 4.62 nm for discs and pins, respectively, over a 2 μm × 2 μm area. PDMS is hydrophobic with a contact angle of 105.6 ± 2.2° (tested with Millipore water, standard deviation from five measurements) and has a surface energy (γ) of 20 mJ/m^2.[22]

Polymer Solutions. Solutions of the diblock copolymers were prepared by initial dissolution in 2−3 mL of acetone and then adding ca. 10 mL of HEPES (1 mM) buffer solution. The acetone was subsequently removed by vacuum using a mechanical pump for 30 min. A negligible amount of ca. 2% vol. of the water was lost by evaporation by applying vacuum. One exception to this method was the dissolution of PEG(4.6)-*b*-PMEA(4.6), for which the polymer was dissolvable in water within ca. 20 min. The PAA-based diblock copolymer solutions pH was adjusted by addition of either 1.0 M NaOH (aq) or 1.0 M HCl (aq). HEPES buffer solution was added to the concentrated polymer solution after removal of acetone. The final concentrations of all diblock copolymer solutions were 0.50 mg/mL, except for the pH dependency experiments for PAA-*b*-PS where the concentration was 0.25 mg/mL (shown in Figure 7). All polymer solutions were visually clear except for PEG-*b*-PS (semitransparent). PAA blocks are regarded as 72% ionized at pH 7.0, and 2.5% ionized at pH 3.0.[32] Experiments with higher NaCl concentration were conducted by adding NaCl to the polymer solution and waiting 10 min for dissolution and equilibration of the solution with convection.

Surface Adsorption of Polymers. Adsorption of the diblock copolymers onto PDMS surfaces from aqueous solution has been characterized by means of optical waveguide lightmode spectroscopy (OWLS) (Microvacuum, OWLS model 210, running BioSense software version 2.6.10, Hungary). OWLS is based on the resonance phenomenon of the polarization modes of the electric and magnetic fields occurring when linearly polarized light (He−Ne laser) is coupled with a diffraction grating waveguide. When the laser beam is positioned at certain angles, total internal reflectance occurs. Theses angles depend on various parameters, such as the covering medium (solution) and adsorbate layer. A four-layer model consisting of glass substrate, waveguide layer, adsorbate layer, and covering medium can be applied to calculate the mass uptake on the surface of the waveguide by using the de Feijter equation:[33]

dx.doi.org/10.1021/la400827h | *Langmuir* 2013, 29, 7782−7792

$$\text{mass} = d_A \frac{(n_A - n_C)}{\frac{dn}{dc}} \quad (1)$$

where d_A designates the thickness of the adsorbate layer, n_A is the refractive index of the adsorbate layer, n_C is the refractive index of the covering medium, and dn/dc is an adsorbate-specific constant designating the change in refractive index relative to the change in concentration. The dn/dc constants for the diblock copolymers were estimated by assuming a linear relationship of the mass fraction of each block and its contribution to the diblock copolymers' total dn/dc value.[34] The dn/dc of PS, PMEA, PEG, PAA$^-$, and PAA are 0.250,[34] 0.060,[35] 0.132,[34] 0.231,[34] and 0.158,[34] respectively. Thus, for example, the dn/dc value of PEG(5.0)-*b*-PS(6.2) (5000-*b*-6200 Da) is calculated as dn/dc = (0.132 × 5000 Da + 0.250 × 6200 Da)/(5000 Da + 6200 Da) = 0.197. Specific dn/dc values for the various block copolymers are stated in ref [36]. n_A is calculated by the OWLS software.

To emulate the tribopair surface, the waveguides for OWLS adsorption experiments were coated with a thin layer of PDMS. To this end, waveguides were ultrasonicated in EtOH for 10 min and spin-coated with a Sylgard PDMS kit mixture (base component and cross-linker 3:1 wt ratio dissolved in heptane to give a spin coating solution of 0.5 wt %) at 2000 rpm for 60 s. After spin coating, the waveguides were cured overnight at 70 °C. The reference thickness of the spin-coated PDMS layer as measured on silicon wafers by ellipsometry was 16.4 ± 0.17 nm, assuming a native silicon oxide layer of 1.4 nm and a refractive index of 1.401 for the PDMS layer.

Adsorption measurements were performed by employing HEPES buffer (1 mM, pH 7) and a flow rate of 0.1 mL/min. A volume of 0.100 mL of block copolymer solution (concentration 0.50 mg/mL) was injected into the flow circuit with a microsyringe. The reported adsorbed masses were obtained after rinsing with HEPES buffer flow for a minimum of 5 min (see Figure 2 for examples). Two to three measurements were performed for each block copolymer solution to give a statistical average. Error bars in Figure 3 and Table 2 designate standard deviation. All surface adsorption measurements were performed at 20 °C.

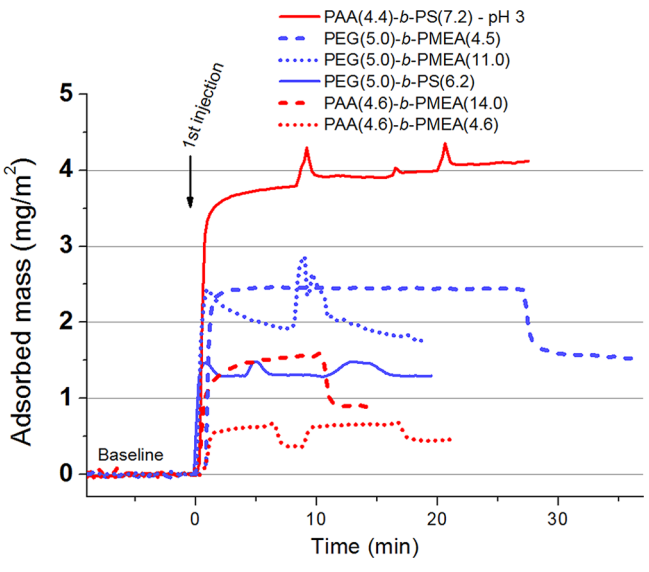

Figure 2. Examples of mass uptake measurements by OWLS with HEPES (1 mM, pH 7.0) buffer flow of 0.1 mL/min. A latency of 60 s from injection in valve for the polymer solution to flow to the OWLS sensor is typical. The surface of the OWLS sensor chip is coated with PDMS. The adsorption kinetics is fast for all block copolymers, with saturation within 1−2 min. Generally for all curves, a peak after first injection represents an additional injection. A drop in the curve is due to rinsing, thereby removing nonadsorbed copolymer in the proximity of the surface.

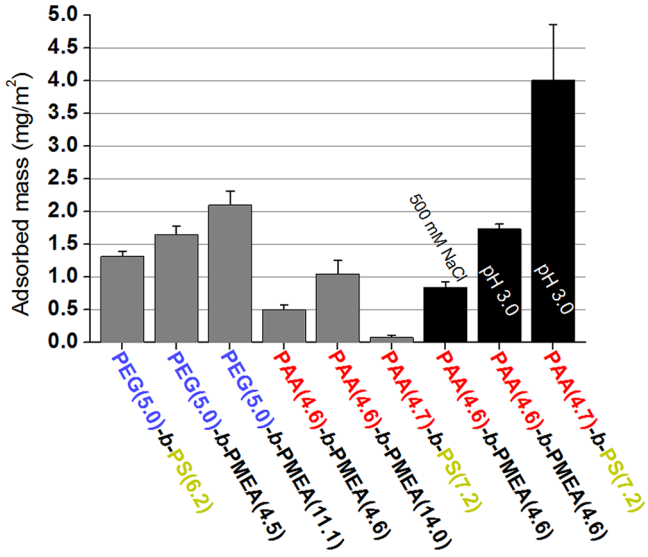

Figure 3. Adsorbed masses of the copolymers (mg/m^2) as measured by OWLS. The substrate was PDMS-coated OWLS waveguides. Gray bars designate standard measurements under the condition of HEPES buffer, 1 mM, pH 7, 0.50 mg/mL diblock copolymer concentration. Black bars represent experiments with increased salt concentration (screening the charges) or lower pH (i.e., deionized polyelectrolyte). For PAA(4.6)-*b*-PMEA, the adsorbed mass increased both by increasing the ionic strength and by lowering the pH to 3.0. For PAA(4.7)-*b*-PS(7.2), the adsorbed mass increased enormously by lowering the pH to 3.0; however, increasing the ionic strength to 500 mM did not lead to any noticeable increase in adsorbed mass (data not shown in graph).

Friction Experiments. Pin-on-disc tribometry was employed to assess the lubricating capabilities of the diblock copolymers in an aqueous environment. The tribopair was self-mated PDMS, and the range of sliding speed was from 100 to 0.25 mm/s. Friction experiments were conducted on a commercial tribometer (CSM Instruments, software version 4.4 M, Switzerland). The principal setup of the pin-on-disc tribometer consists of a rotating disc in contact with a stationary pin pressing down onto the disc's surface. The pin is connected to an arm with a strain gauge enabling measurement of the friction force laterally exerted onto the pin. The load was controlled by applying dead weights on the pin. The friction coefficient (μ) is calculated by the formula $\mu = F_{friction}/F_{load}$. The load in all experiments was 5 N, giving a contact pressure of 0.36 MPa (Hertzian contact, E' = 1.80 MPa,[23] Poisson's ratio of 0.5). A minimum of 20 laps was recorded for each speed measured. Error bars in μ vs sliding speed plots designate standard deviation. All friction experiments were performed at room temperature.

3. RESULTS AND DISCUSSION

3.1. Polymer Properties. PEG and PAA were employed to represent neutral or charged hydrophilic polymer chains, respectively, in neutral aqueous environment. For the hydrophobic blocks, PS and PMEA were chosen because of similar surface energies, 39.3 and 36.7 mJ/m^2, for PS[34] and PMEA,[37] respectively, yet a large difference in glass transition temperature, T_g(PS) = 100 °C[34] and T_g(PMEA) = −33 °C,[37] and interfacial energy with water, $\gamma_{PS/water}$ = 32 mJ/m^2,[38] and $\gamma_{PMEA/water}$ = −10.3 mJ/m^2.[39,40] Bulk PS is not dissolvable in water. Bulk PMEA with a molecular weight of 85 kDa has shown not to be dissolvable in water either;[41] however, PEG(4.6)-*b*-PMEA(4.6) block copolymer in this study is directly dissolvable in water within a relatively short time frame (20 min). Usually, if the interfacial tension between a

dx.doi.org/10.1021/la400827h | Langmuir 2013, 29, 7782−7792

polymer and a liquid is negative, then the two are completely miscible; nevertheless, in the cases of polymers with higher molecular weight some liquid/polymer systems may not be miscible.[42]

3.2. Polymer Synthesis. The reaction scheme for the synthesis of the amphiphilic diblock copolymers featuring neutral and anionic hydrophilic blocks is depicted in Scheme 1. mPEG-*b*-PS and mPEG-*b*-PMEA were prepared by copper-mediated ATRP. The same controlled radical polymerization technique coupled with protecting group chemistry was employed in the synthesis of the diblock copolymers bearing PAA as the hydrophilic block. Thus, P*t*BA-*b*-PS and P*t*BA-*b*-PMEA were synthesized first. Selective cleavage of the *tert*-butyl ester groups afforded the anionic diblock amphiphiles. Preparation of the PS-based diblock copolymers has been previously reported;[31,43] detailed synthetic protocols and exhaustive characterization data for the PMEA-based diblock copolymers are reported in the literature.[29]

Throughout the rest of this paper, PAA-based diblock copolymers are denoted as PAA(z)-*b*-X(y) with z and y designating the block's mass in kDa, and likewise mPEG-based diblock copolymers are denoted as PEG(z)-*b*-X(y).[44]

3.3. Surface Adsorption of the Diblock Copolymers. *3.3.1. Overall Trend.* From the adsorbed mass data (Figure 3 and Table 2), it is clear that neutral PEG-based diblock copolymers adsorb more efficiently onto the PDMS−water interface than charged PAA-based counterparts when all other parameters are held constant, e.g., PEG(5.0)-*b*-PS(6.2) (1.31 ± 0.083 mg/m^2) ≫ PAA(4.4)-*b*-PS-(7.2) (0.072 ± 0.034 mg/m^2), PEG(5.0)-*b*-PMEA(4.5) (1.647 ± 0.131 mg/m^2) > PAA(4.6)-*b*-PMEA(4.6) (0.500 ± 0.071 mg/m^2), and PEG(5.0)-*b*-PMEA(11.0) (2.097 ± 0.21 mg/m^2) > PAA(4.6)-*b*-PMEA(14.0) (1.100 ± 0.212 mg/m^2). This difference was more pronounced for the copolymers with a PS anchoring block, e.g., PEG(5.0)-*b*-PS(6.2) vs PAA(4.4)-*b*-PS-(7.2), than those with a PMEA anchoring block, e.g., PEG(5.0)-*b*-PMEA(4.5) vs PAA(4.6)-*b*-PMEA(4.6) and PEG(5.0)-*b*-PMEA(11.0) vs PAA(4.6)-*b*-PMEA(14.0). By changing the solvent from neutral HEPES buffer to an acidic one (pH 3), the adsorbed mass of PAA(4.4)-*b*-PS-(7.2) increased significantly, from 0.072 ± 0.034 mg/m^2 to 4.003 ± 0.849 mg/m^2, and in the case of PAA(4.6)-*b*-PMEA(4.6), from 0.500 ± 0.071 mg/m^2 to 1.730 ± 0.075 mg/m^2. Addition of 500 mM NaCl into neutral HEPES buffer solution did not improve the adsorption properties of PAA(4.4)-*b*-PS(7.2), but those of PAA(4.6)-*b*-PMEA(4.6) (from 0.500 ± 0.071 mg/m^2 to 0.837 ± 0.085 mg/m^2) were improved. Lastly, for the PMEA-based copolymers with a varying ratio of buoyant/anchoring blocks, both PEG-*b*-PMEA and PAA-*b*-PMEA showed higher adsorbed mass with longer anchoring blocks; for PEG-*b*-PMEA, the adsorbed mass increased by 27% on average by increasing the molecular weight of the PMEA block by 141%, and for PAA-*b*-PMEA, the adsorbed mass increased by 120% on average by increasing the molecular weight of the PMEA block by 204%. However, the density of buoyant block chains, PEG or PAA chains per unit area (nm^2), did not increase to the same extent; PAA-*b*-PMEA showed a slight increase from 0.03 to 0.04/nm^2 (increase by 33%), and PEG-*b*-PMEA showed rather a slight decrease from 0.1 to 0.08/nm^2 (decrease by 20%).

It is important to note that all the mass uptake profiles obtained by OWLS in this study showed a rapid saturation (within 1−2 min) upon exposing the PDMS surface to the copolymer solution as shown in Figure 2. Previous adsorption studies of amphiphilic moieties report that an onset of facile surface adsorption onto hydrophobic surfaces, either the air/water interface[45] or hydrophobic solids in water,[46] can be delayed as much as by a few hours. It should thus be kept in mind that some copolymers showing poor surface adsorption properties may show delayed onset of surface adsorption by extended exposure of the PDMS surface to copolymer solutions. This hypothesis was not examined in the current study, because the copolymers showing extremely slow surface kinetics are not expected to contribute to effective lubrication in the "self-healing" mechanism.[17]

3.3.2. Resources of Unimers for Surface Adsorption: Micelles vs Unimers. Amphiphilic moieties in an aqueous environment self-assemble into micelles and aggregate above a threshold concentration, i.e., critical micelle/aggregation concentration (CMC/CAC). The CMC/CAC reported in the literature for similar molecular weight PS-based diblock copolymers in water are around 1.6 × 10^{-3} mg/mL and 6 × 10^{-3} mg/mL for PEG-*b*-PS[47] and PAA-*b*-PS[48] diblock copolymers, respectively. The influence of the hydrophilic corona on the micellization in this study can be neglected.[49] The low CMCs of PS-based diblock copolymers are generally attributed to the high interfacial energy between PS and water $\gamma_{PS/water}$ = 32 mJ/m^2 and the glassy state[50] of bulk PS at room temperature.[45] In the case of PEG-*b*-PS in this study, at the concentration of 0.50 mg/mL (i.e., the concentration employed in this work), only ca. 0.3% are present as free unimers in bulk solution if the CMC is similar. Likewise, the CMC of the PAA-*b*-PS diblock copolymer is in the range of ca. 6 × 10^{-3} mg/mL as reported by Astafieva et al.;[48] thus, the amount of free unimers in a 0.50 mg/mL polymer solution would be only 1.2%. Given the abundance of the copolymers in the form of micelles, yet the paucity of free unimers in the bulk solution, it is of high importance to understand how adsorption of the copolymers onto surface takes place. In a study by Théodoly,[45] PAA-*b*-PS was shown not to adsorb directly onto an air/water interface in the form of micelles under neutral aqueous conditions due to the lack of affinity of the charged PAA corona toward the air/water interface. This tendency is considered to be applicable to all the copolymers studied in this study because neither PAA nor PEG has sufficient affinity to hydrophobic surfaces in a neutral aqueous environment. This does not mean though that adsorption of the copolymers onto the PDMS surface is chiefly governed by the initially available free unimers in equilibrium with micelles, because the fractions of free unimers at the concentration of 0.5 mg/mL are too small as mentioned above. This dilemma can be resolved by taking into account that unimers can be readily released from micelles, as long as the kinetics of release is fast enough and the ultimate energy gain is favorable by adsorption of the copolymers onto PDMS surfaces. In this process the hydrophobic core of the micelles plays a critical role, as discussed below in detail.

In contrast to the PS-based diblock copolymers, micellization/aggregation of the PMEA-based diblock copolymers appears to be nearly negligible. Micellization of amphiphilic block copolymers is inversely proportional to the interfacial tension between the solvent and the insoluble block, and the CMC can be modeled by the following equation:[51]

dx.doi.org/10.1021/la400827h | *Langmuir* 2013, 29, 7782−7792

$$\mathrm{CMC} \approx \frac{100M_{\mathrm{HB}}(X_{\mathrm{HB/HP}})}{\nu N_{\mathrm{A}}(1 + X_{\mathrm{HB/HP}})} \exp\left(-\frac{\pi^{1/3}\left(\frac{3n\nu}{4}\right)^{2/3}\gamma}{kT}\right) \quad (2)$$

The CMC is in wt % of sample HB-*b*-HP (hydrophobic-*b*-hydrophilic), M_{HB} is the molar mass of a monomer HB, $X_{\mathrm{HB/HP}}$ is the mass ratio of HB over HP in a hypothetical monodisperse diblock sample, N_{A} is Avogadro's number, ν is the molecular volume of a HB monomer, n is the polymerization number of the HB block, and γ is the interfacial tension between the hydrophobic insoluble core and the hydrophilic solvent (water). More generalized forms of calculated estimates of the CMC of amphiphiles are reported by Marques.[49] Given that the interfacial tension between PMEA and water is negative, $\gamma_{\mathrm{PMEA/water}} = -10.3 \pm 4.2$ mJ/m^2, the CMC of a PMEA diblock copolymer according to the eq 2 results in a positive exponent. This would afford a very high CMC. Thus, we argue that the degree of micellization of PEG-*b*-PMEA and PAA-*b*-PMEA diblock copolymers in the present experiments is very low or even nonexisting. Hence, micellization affects the adsorption of PMEA-based diblock copolymers very little or not at all.

3.3.3. Role of Anchoring Blocks: PS vs PMEA Blocks. Despite the general trend of superior adsorption of PEG-based copolymers over PAA-based copolymers, the magnitude in relative adsorbed masses between these two groups of copolymers was fairly different depending on the type of anchoring blocks employed. It is notable that the adsorption of aforementioned PAA-*b*-PS is substantially inferior to that of its PEG counterpart, whereas the adsorbed masses of PAA-*b*-PMEA copolymers are quite sizable despite being still lower than those of their PEG counterparts. This contrast is believed to arise first from the difference in the interfacial tension between the anchoring blocks (PS and PMEA) and water. As mentioned in the previous section, PMEA-based diblock copolymers are considered to not form micelles under the experimental conditions in this study, whereas PS-based diblock copolymers do.

The adsorption of PS-based diblock copolymer is thus governed by two coupled equilibria (see illustration in the abstract), where the first equilibrium is between micelle and unimers and the second equilibrium is between free unimers and adsorbed diblock copolymers. The adsorption of PMEA-based diblock copolymers is only dependent on the latter equilibrium. On the other hand, the adsorption of PS-based diblock copolymers must be preceded by one additional step of unimer exchange as compared to PMEA-based counterparts. Counterintuitively, copolymers with the less hydrophobic PMEA block adsorbs to a greater extent on the hydrophobic PDMS surface than on PS-based ones because of the lack of micellization of PMEA-based block copolymers. Improvement of adsorption behavior at an air/water interface by employing less hydrophobic anchoring blocks has been reported previously in the literature.[45] As mentioned in Introduction, the substantially different glass transition temperatures of PS and PMEA may also have an influence on the adsorption properties of the diblock copolymers, but this is valid in the sense that formation of frozen,[45] glassy PS-based micelles impedes the exchange of unimers significantly, i.e., the first equilibrium rather than the flexibility of the anchoring block affects the adsorption onto the surface in the second equilibrium, because a glassy or rubbery state of the polymers is meaningful in the bulk state, not in the form of unimers.

Noted that while the improvement in adsorption properties as a result of replacing PS with PMEA is more clearly visible from PAA-based copolymers, it is still observed for PEG-based copolymers as well. For instance, when comparing PEG(5.0)-*b*-PS(6.2) (1.31 ± 0.083 mg/m^2) with PEG(5.0)-*b*-PMEA(4.5) (1.647 ± 0.131 mg/m^2), the PEG chain density is increased from 0.07 to 0.10/nm^2 despite employing PMEA with an M_{n} somewhat lower than that of the PS block.

3.3.4. Role of Buoyant Block: Neutral (PEG) vs Charged (PAA) Blocks. As mentioned above, it is useful to consider the surface adsorption process of PS-based diblock copolymers in two steps: (1) exchange of unimers from micelles, and (2) diffusion and adsorption onto the PDMS surface, as schematically illustrated in the abstract. Thus, superior adsorption properties of PEG-*b*-PS copolymer over PAA-*b*-PS copolymers can be discussed by comparing their behavior in each step.

Among the copolymers employed in this study, PAA-*b*-PS has been most actively studied in terms of micelle formation and adsorption properties.[52,53] PAA-*b*-PS copolymers generally show "hampered" adsorption onto the hydrophobic surface from aqueous solution,[45] which concur with the observation in this study (Figure 3). This is ascribed to the extremely slow release kinetics of unimers from micelles with a PS core in aqueous solution. Because the micelles formed from PEG-*b*-PS have comparable CMCs, and the released unimers also have similar interfacial tension with water compared to those of PAA-*b*-PS for the common PS core, the kinetics of unimer release from micelles is not likely to be different for PAA-*b*-PS and PEG-*b*-PS. Instead, the second step, i.e., diffusion and adsorption process of the released copolymers onto the PDMS surface, should be significantly different depending on the presence/absence of charges along the hydrophilic blocks. It is well-known that electrostatic repulsion between initially adsorbed molecules and incoming molecules onto the surface is primarily responsible for the generally retarded adsorption of charged molecules onto nonpolar, hydrophobic surfaces.[54] While the adsorption of neutral brush-forming polymers onto the surface is limited by steric repulsion between initially adsorbed and incoming polymers, the repulsion between charged copolymers during the adsorption onto the nonpolar surface is augmented with electrostatic repulsion, and therefore the adsorption of PAA-*b*-X copolymers onto the PDMS surfaces is energetically more unfavorable than the PEG-*b*-X. This is most clearly evidenced by two experiments that screen the electrostatic repulsion between PAA-based copolymers, i.e., by either increasing salt concentration to 500 mM (NaCl) or by lowering pH from 7.0 to 3.0. The fraction (α) of PAA repeating units that are expected to be deprotonated (i.e., ionized) is 0.72 at pH 7.0, whereas it is expected to be only α = 0.025 at pH 3.0.[32] Thus, PAA-based copolymers at pH 3.0 are essentially neutral copolymers rather than charged ones.

Compared to PAA(4.4)-*b*-PS(7.2), both PAA-*b*-PMEA diblock copolymers showed significantly higher adsorption onto the PDMS surface. This is attributed to the fact that PAA-*b*-PMEA diblock copolymers are present mainly as unimers, and thus the adsorption is impeded only by the electrostatic repulsion. PAA(4.4)-*b*-PS(7.2) is limited by both electrostatic repulsion and slow exchange of unimers in two coupled equilibria (see illustration in the abstract).

3.3.5. Influence of Solvent Parameters. In this study, the control of solvent parameters, e.g., addition of 500 mM NaCl or lowering pH from 7 to 3, primarily serves to confirm the significance of electrostatic repulsion between PAA-based

dx.doi.org/10.1021/la400827h | Langmuir 2013, 29, 7782−7792

copolymers on the PDMS surface in determining their overall surface adsorption properties. Between the two approaches, the latter was observed to be more effective in removing the electrostatic repulsion. The significantly increased adsorbed mass of PAA(4.4)-*b*-PS(7.2) at pH 3 than at pH 7 highlights that the removal of electrostatic repulsion between PAA chains overwhelmingly enhances the driving force of the adsorption onto PDMS surfaces.

Apart from the fact that the adsorbed amount was increased to a larger extent by pH control than by salt addition, the two methods may yield a qualitatively different conformation of the adsorbed copolymer molecules on the surface. For instance, some portion of the enormously increased adsorbed mass of PAA(4.4)-*b*-PS(7.2) at pH 3 may be ascribed to the adsorption of micelles via the interaction between the PAA corona and PDMS surface. The facile adsorption of PAA chains onto the PDMS surface at pH 3, but not at pH 7, has been confirmed in a control experiment (Table 2).

3.3.6. Buoyant/Anchoring Block Ratio. Extending the molecular weight of PMEA anchoring block from 4.6 to 14.0 kDa improved the adsorption of the PAA-*b*-PMEA diblock copolymer (by 120% in the adsorbed mass on average), but the corresponding increase in surface chain density (Table 2) was not equally significant, i.e., from 0.03 to 0.04 chains/nm^2 (by 33%). This trend was even worse for PEG-*b*-PMEA diblock copolymer because the extension of the moleular weight of the anchoring block from 4.5 to 11 kDa increased the adsorbed mass by 27%, but the corresponding surface chain density of PEG rather decreased by 20%. This is because the increase in the molecular weight of anchoring block results in a concomitant increase in the spacing of the buoyant chains on the surface. Given that the chain density is roughly similar, whether the longer anchoring block can provide enhanced stability for the adsorbed copolymers can be tested by tribological studies, for instance (shown below).

3.4. Lubrication Properties. *3.4.1. Overall Trend.* Figure 4 presents the results of pin-on-disc experiments for all the diblock copolymers employed in this work in neutral buffer solution. All the PEG-*b*-X copolymers lubricate PDMS−PDMS sliding contacts very well over the entire sliding speed range with the coefficient of friction down to 0.02, except for PEG(5.0)-*b*-PMEA(4.5) at the slowest speed (0.25 mm/s). This data support the notion of amphiphilic PEG-based diblock copolymers as effective aqueous lubricant additives for soft sliding contacts. The insert in Figure 4 shows the "self-healing" ability of PEG(5.0)-*b*-PS(6.2) and PEG(5.0)-*b*-PMEA(11.0) over 300 laps. While the three PEG-based copolymers showed noticeable differences in the adsorbed mass and PEG chain density (Table 2), their lubricating capabilities at PDMS−PDMS sliding contact in neutral aqueous solution were nearly indistinguishable. On the other hand, all PAA-based copolymers showed negligible lubricating effects, except for a slight reduction in the friction coefficient in the high-speed regime. The poor lubrication performance of PAA(4.4)-*b*-PS(7.2), i.e., μ values being nearly indistinguishable from those of the reference buffer solution, was consistent with the very small extent of adsorption onto the PDMS−water interface observed by OWLS.

The inferior lubricating properties of PAA-*b*-PMEA compared to PEG-*b*-PMEA block copolymers may be related to the lower adsorbed mass of the former (section 3.3.1). Nevertheless, the insignificant lubrication by both PAA-*b*-PMEA copolymers cannot be fully explained by the relatively

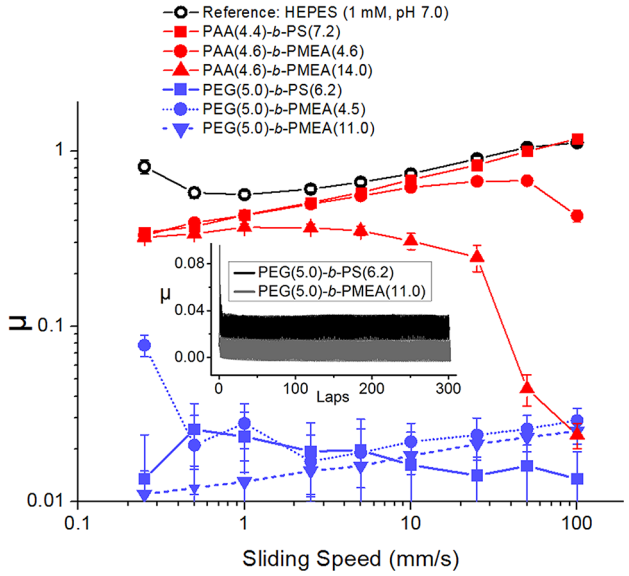

Figure 4. Friction coefficient (μ) vs sliding speed plots of the sliding contacts of PDMS−PDMS lubricated by the diblock copolymer solutions as characterized by pin-on-disc tribometry under a 5 N load: HEPES (1 mM, pH 7) buffer only [○]. All diblock copolymers were dissolved in HEPES buffer solution (1 mM, pH 7.0) at the concentration of 0.50 mg/mL. The lines connecting the points in the figures are a guide to the eye. The insert in the middle displays the self-healing ability of PEG(5.0)-*b*-PS(6.2) and PEG(5.0)-*b*-PMEA-(11.0) solution with maintained lubricity after sliding more than 300 laps (>2 h) at 0.50 mm/s.

low adsorbed masses alone, because the adsorbed masses, ranging from ca. 0.50 to 1.00 mg/m^2, are fairly sizable in an absolute sense. It should be, however, noted that the adsorbed mass of lubricating films cannot always be equated to their binding strength on the surface, which is proportional to the enthalpy of adsorption, and it is often more important to withstand the tribostress and provide effective lubrication. We propose that the binding strength of PAA-*b*-PMEA onto the PDMS surface can be divided into an attractive component of the PMEA−PDMS interaction and a repulsive component of packing the charged PAA blocks at the interface. The tribostress generated during sliding in this study (0.36 MPa) may be strong enough to shift the balance to detachment of the PAA-*b*-PMEA away from the PDMS surface and back into solution.

As discussed in section 3.3.6, increasing the molecular weight of PMEA anchoring blocks did not effectively improve the chain density of hydrophilic, buoyant block for both PAA-*b*-PMEA and PEG-*b*-PMEA copolymers. Nevertheless, lubricating properties of the copolymers were enhanced, especially for PAA(4.6)-*b*-PMEA(14.0), and this can be correlated to improving the anchoring strength by the longer anchoring blocks.

3.4.2. Influence of Solvent Parameters: Addition of Salt. As mentioned above, charged PAA(4.4)-*b*-PS(7.2) shows very ineffective lubricity in HEPES buffer with no additional NaCl, due to very little adsorbed mass. When a relatively high concentration of NaCl (500 mM) was added to the solution, improvement in lubricity was observed with the coefficient of friction of ca. 0.03 at higher speeds of 10−25 mm/s (Figure 5). It should be noted though that a large portion of the reduction in the coefficients of friction for the cases of PAA(4.4)-*b*-PS(7.2) with 500 mM is due to the lower coefficients of friction

dx.doi.org/10.1021/la400827h | *Langmuir* 2013, 29, 7782−7792

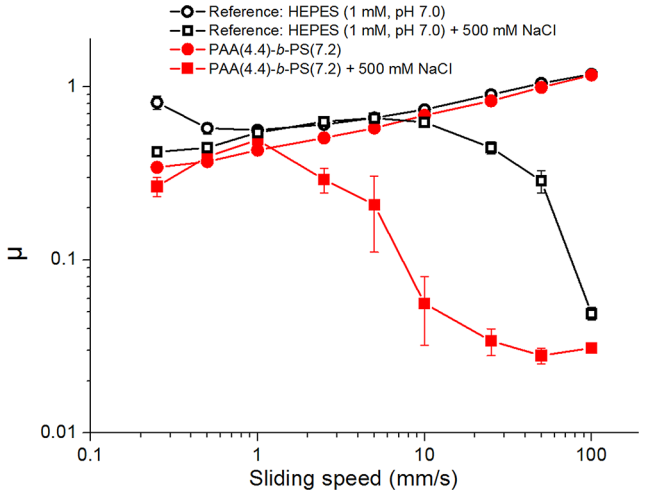

Figure 5. μ vs sliding speed plots of the sliding contacts between PDMS−PDMS lubricated with PAA(4.4)-*b*-PS(7.2) in varying aqueous solution conditions under 5 N load: HEPES (1 mM, pH 7) buffer only, HEPES buffer with 500 mM NaCl, 0.50 mg/mL of PAA(4.4)-*b*-PS(7.2) in HEPES (1 mM, pH 7) buffer, and 0.50 mg/mL of PAA(4.4)-*b*-PS(7.2) in HEPES (1 mM, pH 7) buffer with 500 mM NaCl.

of the corresponding buffer solutions without PAA(4.4)-*b*-PS(7.2). Thus, an insignificant change in the adsorbed mass by addition of 500 mM NaCl to the solution of PAA(4.4)-*b*-PS(7.2) (Table 2) is fairly well correlated with insignificant improvement of the lubricating properties.

Figure 6 presents the pin-on-disc tribometry results for the PAA(4.6)-*b*-PMEA(4.6) solution with varying ionic strength at neutral pH. In buffer solution with no added NaCl, the lubricating effect of PAA(4.6)-*b*-PMEA(4.6) for the PDMS vs

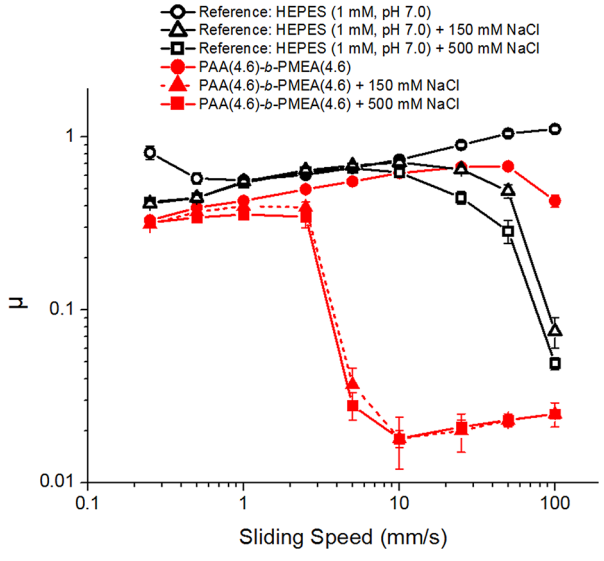

Figure 6. μ vs sliding speed plots of the sliding contacts between PDMS−PDMS lubricated with PAA(4.6)-*b*-PMEA(4.6) for varying aqueous solution conditions under a 5 N load: 0.50 mg/mL of PAA(4.6)-*b*-PMEA(4.6) in HEPES (1 mM, pH 7) buffer, 0.50 mg/mL of PAA(4.6)-*b*-PMEA(4.6) in HEPES (1 mM, pH 7) with 150 mM NaCl, 0.50 mg/mL of PMEA(4.6)-*b*-PAA(4.6) in HEPES (1 mM, pH 7) with 500 mM NaCl. HEPES (1 mM, pH 7) buffer only, with added 150 mM and 500 mM NaCl. The results of PAA(4.6)-*b*-PMEA(4.6) with 150 mM and 500 mM of added NaCl are almost the same.

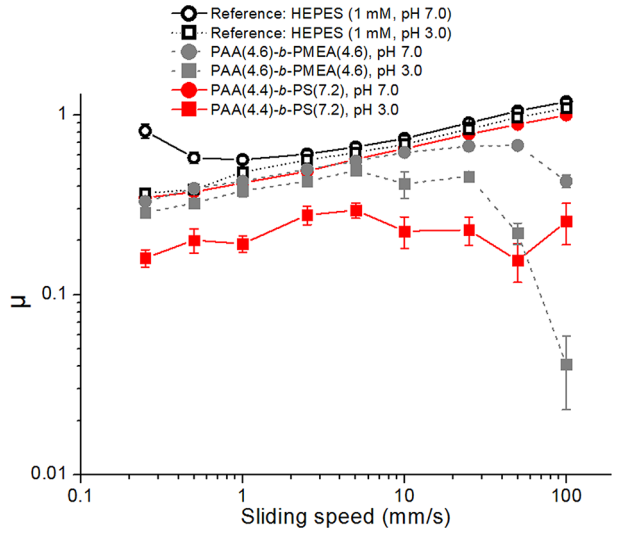

Figure 7. μ vs sliding speed plots of the sliding contacts between PDMS−PDMS lubricated with PAA(4.4)-*b*-PS(7.2) for varying pH conditions under a 5 N load: HEPES (1 mM, pH 7.0) buffer only, HEPES (1 mM, pH 3.0) buffer only, 0.25 mg/mL of PAA(4.4)-*b*-PS(7.2) in HEPES (1 mM, pH 7) buffer, 0.25 mg/mL of PAA(4.4)-*b*-PS(7.2) in HEPES (1 mM) buffer at pH 3.0, 0.50 mg/mL of PAA(4.6)-*b*-PMEA(4.6) in HEPES (1 mM) buffer at pH 7.0, 0.50 mg/mL of PAA(4.6)-*b*-PMEA(4.6) in HEPES (1 mM) buffer at pH 3.0.

PDMS sliding contact was negligible, even though the appreciable amount of PAA(4.6)-*b*-PMEA(4.6), 0.500 ± 0.071 mg/m^2, was observed to be adsorbed onto the PDMS surface. As mentioned above, this is attributed to the weak binding strength for the PAA(4.6)-*b*-PMEA(4.6) on PDMS surfaces to withstand the applied tribostress, consequently shearing off the copolymers from the surface. Compared to PAA(4.4)-*b*-PS(7.2), the lubricity of PAA(4.6)-*b*-PMEA(4.6) has more clearly improved by addition of 500 mM, in accordance with the clear increase of adsorbed mass (Table 2). In fact, the lubricity of PAA(4.6)-*b*-PMEA(4.6) was already improved when only 150 mM NaCl was added to the solution, whereas addition of 150 mM NaCl to the PAA(4.4)-*b*-PS(7.2) solution did not improve the lubricity (data not shown).

3.4.3. Influence of Solvent Parameters: pH. Change of the lubricating properties of PAA(4.4)-*b*-PS(7.2) by controlling the solution parameters have also been observed by lowering pH (Figure 7). As expected, μ values of PAA(4.4)-*b*-PS(7.2) at pH 3 are clearly lower than those of the polymer-free buffer solution at pH 3 in the entire speed regime. In particular, lowering the coefficients of friction at a low-speed regime was not readily observed by addition of excess salts (Figures 5 and 6). On the other hand, the absolute μ values are still fairly high even at pH 3, ranging from 0.1 to 0.3 over the entire sliding speed range, displaying much inferior lubricity compared to that of the neutral PEG-based copolymers at pH 7. This is puzzling when considering that the PAA(4.4)-*b*-PS(7.2) is not charged anymore at pH 3 and the adsorbed mass of PAA(4.4)-*b*-PS(7.2) is enormous, i.e., 4.003 ± 0.849 mg/m^2, and much higher than that of counterpart of PEG-based copolymers at pH 7. Several factors may contribute to this behavior. First, the hydration and swelling of the neutral, protonated PAA chains compared to that of charged PAA chains or neutral PEG chains may be weaker; therefore, the osmotic pressure between the opposing surfaces can be smaller. Second, the adhesive interaction between the two opposing surfaces carrying

dx.doi.org/10.1021/la400827h | *Langmuir* 2013, 29, 7782−7792

COOH groups by hydrogen bond formation can occur as reported previously in AFM studies of sliding COOH covalently functionalized surfaces.[56] Lastly, as previously mentioned (section 3.3.5), it is possible that not all the adsorbed PAA(4.4)-*b*-PS(7.2) copolymers on the PDMS surface are unimers in brush conformation, but some micelles may be directly "sitting" on the surface. The binding strength of those micelles onto the PDMS surface should be weaker than that of the unimers, and thus the contribution to lubrication should be weaker accordingly.

4. CONCLUSIONS

In this study, we have investigated the surface adsorption and aqueous lubricating properties of neutral vs charged amphiphilic diblock copolymers at a nonpolar, hydrophobic interface. The diblock copolymers are composed of either PEG or PAA block, representing neutral and charged buoyant chains, respectively, and PS or PMEA block, representing glassy/strongly hydrophobic and flexible/less hydrophobic anchoring chains, respectively. A primary motivation of this study was to test a hypothesis that the combination of superior lubricating properties of surface-grafted charged polymer chains over neutral ones and the "self-healing" mechanism for aqueous lubrication may give a synergistic effect. However, the experimental results in this study have clearly demonstrated that neutral diblock copolymers perform significantly better in surface adsorption compared to charged polyelectrolyte counterparts and consequently aqueous lubrication of the sliding contacts of PDMS−PDMS surfaces. While polyelectrolyte brushlike chains may have a potential for lubrication superior to that of neutral ones in an aqueous environment when firmly immobilized on surfaces,[14] to generate and maintain dense layers of charged brushlike chains via a physisorption and grafting-to approach encounters a high energetic barrier, especially under continuous tribostress. A fairly simple structure and systematic variation of the diblock copolymers in this study has clarified that this energy barrier is primarily due to the long-range repulsion between highly charged buoyant polymer chains formed on the nonpolar PDMS surface.

■ ASSOCIATED CONTENT

Ⓢ Supporting Information

AFM images of bare PDMS substrate and two diblock copolymers PAA(4.6)-*b*-PMEA(4.6) and PEG(5.0)-*b*-PMEA-(4.5) adsorbed on PDMS surfaces, experimental conditions, and detailed analysis of surface roughness. This material is available free of charge via the Internet at http://pubs.acs.org.

■ AUTHOR INFORMATION

Author Contributions

The manuscript was written through contributions of all authors. All authors have given approval to the final version of the manuscript.

Notes

The authors declare no competing financial interest.

■ ACKNOWLEDGMENTS

Authors appreciate greatly the Danish Council for Independent Research (DFF), Technology and Production Sciences (FTP) (10-082707), for the financial support.

■ REFERENCES

(1) Lee, S.; Spencer, N. D. *Achieving Ultra-low Friction by Aqueous, Brush-assisted Lubrication*, 1st ed.; Elsevier: Amsterdam, The Netherlands, 2007.
(2) Lee, S.; Spencer, N. D. Materials science - Sweet, hairy, soft, and slippery. *Science* **2008**, *319* (5863), 575−576.
(3) Dedinaite, A. Biomimetic lubrication. *Soft Matter* **2012**, *8* (2), 273−284.
(4) Chen, M.; Briscoe, W. H.; Armes, S. P.; Klein, J. Lubrication at physiological pressures by polyzwitterionic brushes. *Science* **2009**, *323* (5922), 1698−1701.
(5) Wang, X.; Gan, H.; Zhang, M. X.; Sun, T. L. Modulating cell behaviors on chiral polymer brush films with different hydrophobic side groups. *Langmuir* **2012**, *28* (5), 2791−2798.
(6) Kuang, J. H.; Messersmith, P. B. Universal surface-initiated polymerization of antifouling zwitterionic brushes using a mussel-mimetic peptide initiator. *Langmuir* **2012**, *28* (18), 7258−7266.
(7) Irfachsyad, D.; Tildesley, D.; Malfreyt, P. Dissipative particle dynamics simulation of grafted polymer brushes under shear. *Phys. Chem. Chem. Phys.* **2002**, *4* (13), 3008−3015.
(8) Raviv, U.; Frey, J.; Sak, R.; Laurat, P.; Tadmor, R.; Klein, J. Properties and interactions of physigrafted end-functionalized poly(ethylene glycol) layers. *Langmuir* **2002**, *18* (20), 7482−7495.
(9) de Gennes, P. G. Polymers at an interface - a simplified view. *Adv. Colloid Interface Sci.* **1987**, *27* (3−4), 189−209.
(10) Chawla, K.; Lee, S.; Lee, B. P.; Dalsin, J. L.; Messersmith, P. B.; Spencer, N. D. A novel low-friction surface for biomedical applications: modification of poly(dimethylsiloxane) (PDMS) with polyethylene glycol(PEG)-DOPA-lysine. *J. Biomed. Mater. Res., Part A* **2008**, *90* (3), 742−749.
(11) Perry, S. S.; Yan, X. P.; Limpoco, F. T.; Lee, S.; Muller, M.; Spencer, N. D. Tribological Properties of Poly(L-lysine)-graft-poly(ethylene glycol) Films: Influence of Polymer Architecture and Adsorbed Conformation. *ACS Appl. Mater. Interfaces* **2009**, *1* (6), 1224−1230.
(12) Nalam, P. C.; Clasohm, J. N.; Mashaghi, A.; Spencer, N. D. Macrotribological Studies of Poly(L-lysine)-graft-Poly(ethylene glycol) in Aqueous Glycerol Mixtures. *Tribol. Lett.* **2010**, *37* (3), 541−552.
(13) Muller, M.; Lee, S.; Spikes, H. A.; Spencer, N. D. The influence of molecular architecture on the macroscopic lubrication properties of the brush-like co-polyelectrolyte poly(L-lysine)-g-poly(ethylene glycol) (PLL-g-PEG) adsorbed on oxide surfaces. *Tribol. Lett.* **2003**, *15* (4), 395−405.
(14) Raviv, U.; Giasson, S.; Kampf, N.; Gohy, J. F.; Jerome, R.; Klein, J. Lubrication by charged polymers. *Nature* **2003**, *425* (6954), 163−165.
(15) Kobayashi, M.; Terayama, Y.; Hosaka, N.; Kaido, M.; Suzuki, A.; Yamada, N.; Torikai, N.; Ishihara, K.; Takahara, A. Friction behavior of high-density poly(2-methacryloyloxyethyl phosphorylcholine) brush in aqueous media. *Soft Matter* **2007**, *3* (6), 740−746.
(16) Liberelle, B.; Giasson, S. Friction and normal interaction forces between irreversibly attached weakly charged polymer brushes. *Langmuir* **2008**, *24* (4), 1550−1559.
(17) Duner, G.; Thormann, E.; Ramstrom, O.; Dedinaite, A. Letter to the editor: Friction between surfaces polyacrylic acid brush and silica mediated by calcium ions. *J. Dispersion Sci. Technol.* **2010**, *31* (10), 1285−1287.
(18) Heeb, R.; Bielecki, R. M.; Lee, S.; Spencer, N. D. Room-temperature, aqueous-phase fabrication of poly(methacrylic acid) brushes by UV-LED-induced, controlled radical polymerization with high selectivity for surface-bound species. *Macromolecules* **2009**, *42* (22), 9124−9132.
(19) Pincus, P. Colloid stabilization with grafted polyelectrolytes. *Macromolecules* **1991**, *24* (10), 2912−2919.
(20) Raviv, U.; Klein, J. Fluidity of bound hydration layers. *Science* **2002**, *297* (5586), 1540−1543.
(21) Lee, S.; Muller, M.; Heeb, R.; Zurcher, S.; Tosatti, S.; Heinrich, M.; Amstad, F.; Pechmann, S.; Spencer, N. D. Self-healing behavior of

a polyelectrolyte-based lubricant additive for aqueous lubrication of oxide materials. *Tribol. Lett.* **2006**, *24* (3), 217−223.
(22) Mark, J. E. *Polymer Data Handbook*; Oxford University Press, Inc.: New York, 1999.
(23) Choi, K. M.; Rogers, J. A. A photocurable poly-(dimethylsiloxane) chemistry designed for soft lithographic molding and printing in the nanometer regime. *J. Am. Chem. Soc.* **2003**, *125* (14), 4060−4061.
(24) Esfahanian, M.; Hamrock, B. J. Fluid-film lubrication regimes revisited. *Tribol. Trans.* **1991**, *34* (4), 628−632.
(25) Braunecker, W. A.; Matyjaszewski, K. Controlled/living radical polymerization: Features, developments, and perspectives. *Prog. Polym. Sci.* **2007**, *32* (1), 93−146.
(26) Matyjaszewski, K.; Tsarevsky, N. V. Nanostructured functional materials prepared by atom transfer radical polymerization. *Nature Chem.* **2009**, *1* (4), 276−288.
(27) Jankova, K.; Chen, X. Y.; Kops, J.; Batsberg, W. Synthesis of amphiphilic PS-b-PEG-b-PS by atom transfer radical polymerization. *Macromolecules* **1998**, *31* (2), 538−541.
(28) Bednarek, M.; Jankova, K.; Hvilsted, S. Novel polymers based on atom transfer radical polymerization of 2-methoxyethyl acrylate. *J. Polym. Sci. Part A: Polym. Chem* **2007**, *45* (3), 333−340.
(29) Javakhishvili, I.; Jankova, K.; Hvilsted, S. Neutral, anionic, cationic, and zwitterionic diblock copolymers featuring poly(2-methoxyethyl acrylate) "hydrophobic" segments. *Polym. Chem.* **2013**, *4*, 662−668.
(30) Ma, Q. G.; Wooley, K. L. The preparation of t-butyl acrylate, methyl acrylate, and styrene block copolymers by atom transfer radical polymerization: Precursors to amphiphilic and hydrophilic block copolymers and conversion to complex nanostructured materials. *J. Polym. Sci., Part A: Polym. Chem.* **2000**, *38*, 4805−4820.
(31) Davis, K. A.; Matyjaszewski, K. Atom transfer radical polymerization of *tert*-butyl acrylate and preparation of block copolymers. *Macromolecules* **2000**, *33* (11), 4039−4047.
(32) Electrostatic intrarepulsion between adjacent ionized PAA units increases the pK_{app}, thus resulting in lower acidity of the PAA units in the chain as the ionization goes up. The degree of ionization (α) of PAA was calculated according to Katchalsky (see ref 55): $pH = 6.17 - 2 \times \log(1-\alpha)/\alpha$. By inserting pH = 7 and pH = 3 in the equation gives $\alpha = 0.72$ and $\alpha = 0.03$.
(33) de Feijter, J. A.; Benjamins, J.; Veer, F. A. Ellipsometry as a Tool to Study Adsorption Behavior of Synthetic and Biopolymers at Air-Water-Interface. *Biopolymers* **1978**, *17* (7), 1759−1772.
(34) Brandrup, J.; Immergut, E. H.; Grulke, E. A. *Polymer Handbook*, 4th ed.; John Wiley & Sons, Inc.: New York, 1999.
(35) Coelho, J. F. J.; Gois, J.; Fonseca, A. C.; Carvalho, R. A.; Popov, A. V.; Percec, V.; Gil, M. H. Synthesis of Poly(2-methoxyethyl acrylate) by Single Electron Transfer-Degenerative Transfer Living Radical Polymerization Catalyzed by $Na_2S_2O_4$ in Water. *J. Polym. Sci., Part A: Polym. Chem.* **2009**, *47* (17), 4454−4463.
(36) dn/dc values. PEG(5.0)-*b*-PS(6.2): 0.197, PEG(5.0)-*b*-PMEA(4.5): 0.098, PAA(4.4)-*b*-PS(7.2): 0.252 at pH 7.0, PAA(4.4)-*b*-PS(7.2): 0.211 at pH 3.0, PAA(4.6)-*b*-PMEA(4.6): 0.135 at pH 7.0, PAA(4.6)-*b*-PMEA(4.6): 0.135 at pH 3.0, PAA(4.6)-*b*-PMEA(14.0): 0.096, PEG(4.6)-*b*-PMEA(11.0): 0.082.
(37) Hirata, T.; Matsuno, H.; Tanaka, M.; Tanaka, K. Surface segregation of poly(2-methoxyethyl acrylate) in a mixture with poly(methyl methacrylate). *Phys. Chem. Chem. Phys.* **2011**, *13* (11), 4928−4934.
(38) Sasaki, T.; Shimizu, A.; Mourey, T. H.; Thurau, C. T.; Ediger, M. D. Glass transition of small polystyrene spheres in aqueous suspensions. *J. Chem. Phys.* **2003**, *119* (16), 8730−8735.
(39) The interfacial tension is calculated by Young's equation: $\gamma_{SL} = \gamma_{SV} - \gamma_{SL}\cos(\theta) = \gamma_{PMEA/air} - \gamma_{air/water}\cos(\theta) = 36.7\ mJ/m^2 - 72.8\ mJ/m^2 \cos(49.8° \pm 4.3°) = -10.3 \pm 4.2\ mJ/m^2$. 49.8° ± 4.3° is the contact angle of water on PMEA.
(40) Tanaka, M.; Motomura, T.; Kawada, M.; Anzai, T.; Kasori, Y.; Shiroya, T.; Shimura, K.; Onishi, M.; Mochizuki, A. Blood compatible aspects of poly(2-methoxyethylacrylate) (PMEA) - relationship between protein adsorption and platelet adhesion on PMEA surface. *Biomaterials* **2000**, *21* (14), 1471−1481.
(41) Tanaka, M.; Motomura, T.; Ishii, N.; Shimura, K.; Onishi, M.; Mochizuki, A.; Hatakeyama, T. Cold crystallization of water in hydrated poly(2-methoxyethyl acrylate) (PMEA). *Polym. Int.* **2000**, *49* (12), 1709−1713.
(42) van Oss, C. J.; Chaudhury, M. K.; Good, R. J. Interfacial Lifshitz−Vanderwaals and polar interactions in macroscopic systems. *Chem. Rev.* **1988**, *88* (6), 927−941.
(43) Guo, F.; Jankova, K.; Schulte, L.; Vigild, M. E.; Ndoni, S. One-step routes from di- and triblock copolymer precursors to hydrophilic nanoporous poly(acrylic acid)-*b*-polystyrene. *Macromolecules* **2008**, *41* (4), 1486−1493.
(44) We argue that the terminal end-group of OH or OMe for the PEG chain can be disregarded in terms of a hydrophilic brush nature of $a > 100$ repeating unit PEG chain; thus, we write PEG instead of mPEG for simplicity.
(45) Theodoly, O.; Jacquin, M.; Muller, P.; Chhun, S. Adsorption kinetics of amphiphilic diblock copolymers: From kinetically frozen colloids to macrosurfactants. *Langmuir* **2009**, *25* (2), 781−793.
(46) Abraham, T.; Giasson, S.; Gohy, J. F.; Jerome, R.; Muller, B.; Stamm, M. Adsorption kinetics of a hydrophobic-hydrophilic diblock polyelectrolyte at the solid−aqueous solution interface: A slow birth and fast growth process. *Macromolecules* **2000**, *33* (16), 6051−6059.
(47) Wilhelm, M.; Zhao, C. L.; Wang, Y. C.; Xu, R. L.; Winnik, M. A.; Mura, J. L.; Riess, G.; Croucher, M. D. Poly(styrene-ethylene oxide) block copolymer micelle formation in water: A fluorescence probe study. *Macromolecules* **1991**, *24* (5), 1033−1040 [sample DB40]..
(48) Astafieva, I.; Zhong, X. F.; Eisenberg, A. Critical micellization phenomena in block polyelectrolyte solutions. *Macromolecules* **1993**, *26* (26), 7339−7352 (polymer: 86-*b*-390 in repeat units)..
(49) Marques, C.; Joanny, J. F.; Leibler, L. Adsorption of block copolymers in selective solvents. *Macromolecules* **1988**, *21* (4), 1051−1059.
(50) Forrest, J. A.; Mattsson, J. Reductions of the glass transition temperature in thin polymer films: Probing the length scale of cooperative dynamics. *Phys. Rev. E* **2000**, *61* (1), R53−R56.
(51) Jacquin, M.; Muller, P.; Cottet, H.; Crooks, R.; Theodoly, O. Controlling the melting of kinetically frozen poly(butyl acrylate-*b*-acrylic acid) micelles via addition of surfactant. *Langmuir* **2007**, *23* (20), 9939−9948.
(52) Joncheray, T. J.; Bernard, S. A.; Matmour, R.; Lepoittevin, B.; El-Khouri, R. J.; Taton, D.; Gnanou, Y.; Duran, R. S. Polystyrene-*b*-poly(*tert*-butyl acrylate) and polystyrene-*b*-poly(acrylic acid) dendrimer-like copolymers: Two-dimensional self-assembly at the air−water interface. *Langmuir* **2007**, *23* (5), 2531−2538.
(53) Wang, X. L.; Ma, X. Y.; Zang, D. Y. Aggregation behavior of polystyrene-b-poly(acrylic acid) at the air-water interface. *Soft Matter* **2013**, *9* (2), 443−453.
(54) Stuart, M. A. C.; Hoogendam, C. W.; deKeizer, A. Kinetics of polyelectrolyte adsorption. *J. Phys.: Condens. Matter* **1997**, *9* (37), 7767−7783.
(55) Katchalsky, A.; Spitnik, P. Potentiometric Titrations of Polymethacrylic Acid. *J. Polym. Sci.* **1947**, *2* (4), 432−446.
(56) van der Vegte, E. W.; Hadziioannou, G. Scanning force microscopy with chemical specificity: An extensive study of chemically specific tip−surface interactions and the chemical imaging of surface functional groups. *Langmuir* **1997**, *13* (16), 4357−4368.
(57) The average chain−chain distance (L) on the surface was calculated by assuming a two-dimensional hexagonal packing with 1 chain + 6 × (1/3 chain) = 3 chains per unit hexagon. L was isolated from the relation $[(x\ \text{chains})/1\ nm^2] = [(3\ \text{chains})/(\text{area of unit hexagon})] = [(3\ \text{chains})/(3 \times 3^{1/2} \times 2^{-1} \times L^2)]$; thus, $L = \{[2 \times (3 \times \text{chains})]/[3 \times 3^{1/2} \times (x\ \text{chains/nm}^2)]\}^{1/2}$.
(58) R_g of the PEG block was calculated by the formula: $R_g = (Nb^2/6)^{1/2}$ for an ideal chain, where b is the Kuhn length and N the number of Kuhn segments. The Kuhn length of PEG is 1.1 nm.[60] The number of Kuhn segments were calculated by first estimating a repeating unit length of 0.36 nm by ChemBio3D Ultra 12.0. The totally stretched

length of the chain (R_{max}) was then calculated by multiplying the number of repeating units with the repeat unit length; thus, for a PEG chain of mass 5000 Da: R_{max} = 110 × 0.36 nm = 39.6 nm. The number of Kuhn segments (N) was then calculated by the formula: $N = R_{max}/b$, where a 5000 Da PEG chain has N = (39.6 nm)/(1.1 nm) = 36.0 Kuhn segments. Hence, the radius of gyration would be: $R_g = (36.0 \times (1.1\ \text{nm})^2/6)^{1/2}$ = 2.7 nm. R_g of the PAA block was calculated by the formula: $R_g = (Nb^2/6)^{1/2}$ for an ideal chain. PAA (charged) has a Kuhn length (b) of 1.57 nm,[60] giving ≈ 10.3 Kuhn segments for a PAA chain of mass 4400 Da. The radius of gyration for the protonated polyelectrolytes (PAA-*b*-PS at pH 3.0) was also modeled as an ideal chain. For all R_g, the number of Kuhn segments (N) were calculated by $N = R_{max}/b$ = [(no. repeat units) × (repeat unit length)]/b, where the repeating unit length of PAA was estimated to 0.26 nm by ChemBio3D Ultra v. 12.0.

(59) Miquelard-Garnier, G.; Creton, C.; Hourdet, D. Strain induced clustering in polyelectrolyte hydrogels. *Soft Matter* **2008**, *4* (5), 1011−1023.

(60) Rubinstein, M.; Colby, R. H. *Polymer Physics*; Oxford University Press, Inc.: Oxford, 2003.

4.3 Synthesis, Characterization, and Aqueous Lubricating Properties of Amphiphilic Graft Copolymers Comprising 2‑Methoxyethyl Acrylate.

Published in Macromolecules 2014. See next pages.

Macromolecules

Article

pubs.acs.org/Macromolecules

Synthesis, Characterization, and Aqueous Lubricating Properties of Amphiphilic Graft Copolymers Comprising 2-Methoxyethyl Acrylate

Irakli Javakhishvili,[‡,†] Troels Røn,[‡,§] Katja Jankova,[†] Søren Hvilsted,*[,†] and Seunghwan Lee*[,§]

[†]Department of Chemical and Biochemical Engineering, Danish Polymer Centre, and [§]Department of Mechanical Engineering, Technical University of Denmark, DK-2800, Kongens Lyngby, Denmark

Supporting Information

ABSTRACT: Amphiphilic anionic and cationic graft copolymers possessing poly(2-hydroxyethyl methacrylate) (PHEMA) backbone and poly(methacrylic acid), poly(2-methoxyethyl acrylate-*co*-methacrylic acid), and poly(2-methoxyethyl acrylate-*co*-2-(dimethylamino)ethyl methacrylate) grafts are constructed by merging reversible addition−fragmentation chain transfer (RAFT) polymerization, copper-mediated atom transfer radical polymerization (ATRP), and a selective deprotection reaction. Initially, multifunctional ATRP macroinitiators based on PHEMA backbone are prepared by RAFT polymerization. Then ATRP of the corresponding monomers followed by deblocking reaction leads to well-defined amphiphiles with narrow molecular weight distributions (PDI ≤ 1.29) and varying content of methacrylic acid. The graft copolymers showed effective surface adsorption and lubrication for self-mated poly(dimethylsiloxane) (PDMS) contacts in physiological salt concentration. This is indebted from "dilution" of the charges along the grafted chains by balancing neutral/charged repeating units to minimize the accumulated charge repulsion on neutral surface. Improved lubricating properties of the graft copolymers compared to the block copolymer counterparts further support superior stability of graft copolymers on surfaces.

INTRODUCTION

The advance of controlled polymerization methods such as atom transfer radical polymerization (ATRP)[1] and reversible addition−fragmentation chain transfer (RAFT) polymerization[2] allows preparation of a vast and exceedingly diverse pool of macromolecules with distinct composition and topology. Almost innumerable permutations of monomers, initiators, catalysts, and chain transfer agents (CTA) as well as relative ease and fairly high degree of control over the target macromolecular architecture, cement ATRP and RAFT polymerization as rather robust and resourceful techniques.[1,2]

One of the vivid examples is the preparation of amphiphilic random,[3] block,[4] and graft[5] copolymers incorporating 2-methoxyethyl acrylate (MEA) repeating units. The presence of the freezing bound water warrants excellent blood compatibility of the intermediately hydrophilic poly(2-methoxyethyl acrylate) (PMEA),[6] which has been approved by FDA for medical purposes.[6b] These findings have been fuelling our interest in building a library of MEA-based materials, and expanding their biomedical applications.

In this study, of particular interest is the aqueous lubrication with brush-like polymers chains. Water has gained significant interest as lubricant for its environmental friendliness as well as the potential in the biomedical applications where the biocompatibility is of utmost importance.[7−14] However, due to its relatively low bulk viscosity and its low pressure viscosity coefficient, water alone is a poor lubricant, and is easily squeezed out of sliding interfaces even at low contact pressures. One promising approach to improve the lubricating performance of water is to functionalize the sliding surfaces with strongly hydrating and "brush-forming" polymer chains, which can formulate repulsive and slippery interface, due to osmotic pressure and retainment of fluidic layer at the interface.[8] Examples of the polymer chains that showed excellent lubricating effects include neutral,[9] ionic,[10] and zwitterionic[11] hydrophilic polymer brushes. In terms of surface grafting strategy, noncovalent "grafting-to" approach based on free polymer chains provides a facile means to lubricate cyclic tribological contacts, as the polymeric lubricant layers that might shear off from the sliding surfaces can be readily replenished by excess free polymers in solution, i.e., "self-healed".[12]

This is particularly important when a long-term lubrication performance is expected, such as in bearings. In a previous study,[13] it was hypothesized that the lubricating efficacy of free polymers may be further improved by incorporating charged moieties along the chains, since polyelectrolyte brushes immobilized on the surface were reported to display superior load-bearing and lubricating properties compared to neutral ones.[8c] A systematic study with diblock copolymers composed of hydrophobic anchoring blocks such as polystyrene (PS) or PMEA and hydrophilic buoyant blocks such as neutral

Received: December 3, 2013
Revised: February 27, 2014
Published: March 10, 2014

Scheme 1. Synthetic Sequence Leading to the Anionic and Cationic Graft Copolymers[a]

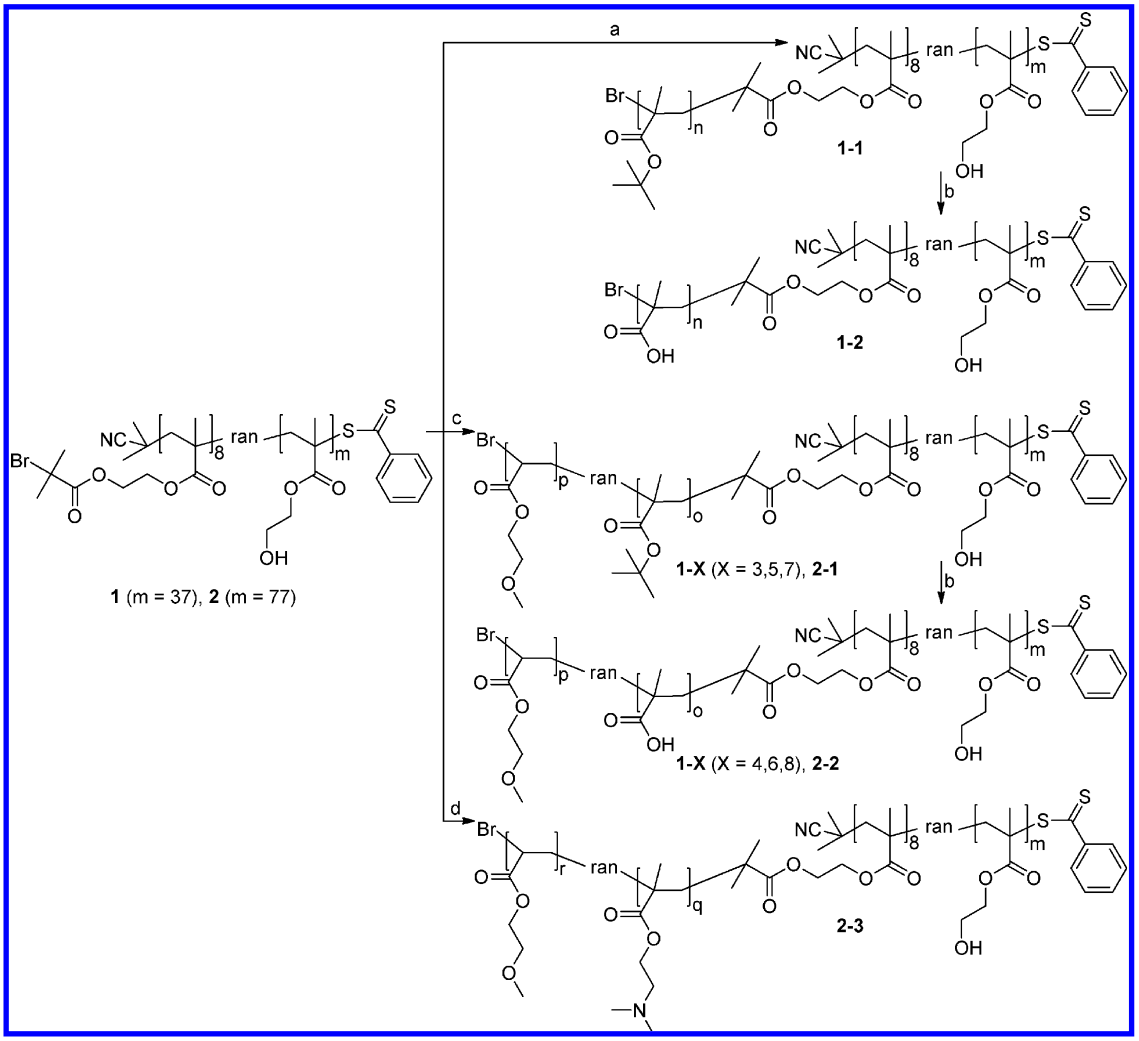

[a]Reagents and conditions: (a) *t*BMA, CuBr/PMDETA, 1:1:1 (v/v) monomer:DMF:anisole, 70 °C; (b) TFA, TES, CH_2Cl_2; (c) MEA, *t*BMA, CuBr/PMDETA, 1:1:1 (v/v) monomer:DMF:anisole, 70 °C; (d) MEA, DMAEMA, CuCl/HMTETA, 1:1:1 (v/v) monomer:DMF:anisole, 70 °C.

poly(ethylene glycol) monomethyl ether (mPEG) or charged poly(acrylic acid) has shown that the diblock copolymers with neutral buoyant block are far superior to their charged counterparts in lubricating a sliding PDMS−PDMS interface;[13] excessive charge density along the polyelectrolyte chains induces the electrostatic repulsion between neighboring polymers on the same surface prior to the repulsion between the opposing surfaces, and thus the formation of polymer lubricant layer is impeded under tribological stress.

Alongside block copolymers, aqueous lubricating properties of graft copolymers have also been studied extensively; several features of graft copolymers, including facile control of side chains' density along the backbone by polymer synthesis, multiple binding of anchoring groups onto the surface, and fast surface adsorption kinetics, render them the most effective "self-healing"-based aqueous lubricant additive, although previous studies have been focused on grafting neutral mPEG chains on surface.[12,14,15]

In this study, it is hypothesized that two structural parameters may improve the aqueous lubricating properties of free charged polymer chains. First, "dilution" of charge density of brush-forming polymer may reduce the electrostatic repulsion among the neighboring polyelectrolytes on the same surface, and yet promote the repulsion between the opposing surfaces. This can be readily achieved by random copolymerization of charged and neutral monomer units. Second, grafting of the charged brush-forming polymers onto an anchoring backbone may also enhance the aqueous lubricating capabilities due to enhanced adsorption stability on surfaces as mentioned above. It has long been known that graft copolymers are superior to diblock copolymers in stable anchoring onto surface for the reasons mentioned above.[16] Particular attention was paid to the aqueous lubricating properties of these copolymers at physiological ionic strength by employing 150 mM NaCl at neutral pH as an aqueous buffer.

In this context, a series of amphiphilic graft copolymers based on MEA have been synthesized and their surface adsorption and aqueous lubricating properties have been investigated in this work. Methacrylic acid (MAA), 2-(dimethylamino)ethyl methacrylate (DMAEMA), and MEA were selected as charged and neutral monomeric units, whereas 2-hydroxyethyl methacrylate (HEMA) was utilized to build the backbone. These novel and multivalent graft copolymers, which comprise poly(2-hydroxyethyl methacrylate) (PHEMA) backbone and poly(methacrylic acid) (PMAA), poly(2-methoxyethyl acrylate-*co*-methacrylic acid) (P(MEA-*co*-MAA)), and poly(2-methox-

dx.doi.org/10.1021/ma4024747 | *Macromolecules* 2014, 47, 2019−2029

yethyl acrylate-*co*-2-(dimethylamino)ethyl methacrylate) (P(MEA-*co*-DMAEMA)) grafts were constructed by combination of the RAFT polymerization, ATRP, and postpolymerization modifications. PDMS was chosen as a nonpolar substrate for adsorption and aqueous lubrication studies.[9,10,13]

EXPERIMENTAL SECTION

Materials. 2-Methoxyethyl acrylate (MEA; Aldrich, 98%), *tert*-butyl methacrylate (*t*BMA; Aldrich 98%), 2-(dimethylamino)ethyl methacrylate (DMAEMA; Aldrich, 98%), and 2-hydroxyethyl methacrylate (HEMA; Aldrich, 99% +) were passed through short aluminum oxide columns (Sigma-Aldrich, activated, basic, Brockmann I, standard grade, ~150 mesh, 58 Å) before use. Ethyl 2-bromoisobutyrate (EBr^{i}Bu; Aldrich, 98%), CuBr (Sigma-Aldrich, 98%), 1,1,4,7,7-pentamethyldiethylenetriamine (PMDETA; Aldrich, 99%), CuCl (Sigma-Aldrich, 99% +), 1,1,4,7,10,10-hexamethyltriethylenetetramine (HMTETA; Aldrich, 97%), *N*,*N*-dimethylformamide (DMF; Sigma-Aldrich, ≥99.9%), anisole (Sigma-Aldrich, 99%), tetrahydrofuran (THF; Sigma-Aldrich, 99.9%), heptane (Sigma-Aldrich, 99%), diethyl ether (Sigma-Aldrich, ≥99.8%), trifuoroacetic acid (TFA; Sigma-Aldrich, ≥98%), triethylsilane (TES; Aldrich, 99%), $CDCl_3$ (Aldrich, 99.8 atom % D), and dimethyl sulfoxide-d_6 (DMSO-d_6) (Aldrich, 99.9 atom % D) were used as received.

4-(2-Hydroxyethyl) piperazine-1-ethanesulfonic acid (HEPES 1 mM, pH 7.0) buffer solution was prepared by dissolving the HEPES salt (VWR BDH Prolabo) in Millipore water (18 MΩ), and adjusting the pH to 7.0 by adding 1.0 M NaOH (aq). HEPES buffer was employed as a base lubricant throughout this study.

PDMS disks and pins for tribological measurements were prepared with a two-component Sylgard 184 PDMS kit. Base and cross-linker were mixed at 10:1 wt. ratio. The air bubbles generated during mixing were removed by applying vacuum. The mixture was then poured into molds, and cured at 70 °C overnight. Disk (o.d. = 30 mm) molds were home-machined aluminum, and Nunc U96 MicroWell plates (Thermo Scientific, Denmark) were used for pin (R = 3.0 mm) molds. The roughness of the PDMS disks and pins was assessed by the tapping mode atomic force microscopy (AFM). The root-mean-square roughness (R_q) was measured to be 1.34 and 4.62 nm for disks and pins, respectively, over a 2 μm × 2 μm area. PDMS is hydrophobic with a contact angle of 105.6 ± 2.2° (tested with Millipore water, standard deviation from five measurements) and has a surface tension (γ) of 20 mJ/m^2.[17]

The polymer solutions were prepared as follows. Initially, the graft and diblock copolymers were dissolved in 2−3 mL of acetone, and then ca. 15 mL of HEPES (1 mM) buffer solution was added. Acetone was removed by applying vacuum for 30 min; a negligible amount of water—ca. 2% vol.—was lost in the process. The polymer concentration was adjusted to 0.50 mg·mL^{-1} by addition of HEPES buffer solution. The graft copolymers **1**−**6** and **2**−**3** (Scheme 1) were dissolved directly in HEPES buffer solution. When necessary, pH was tuned by adding either 1.0 M NaOH (aq) or 1.0 M HCl (aq). The polymer solutions were visually clear except for **1**−**8** (Scheme 1), which contained small white aggregates that precipitated within 30 min. Electrostatic intrarepulsion between adjacent ionized MAA units increases the pK_{app}, thus resulting in lower acidity as the ionization increases. The degree of ionization (α) of PMAA chains in the graft copolymer **1**−**2** (Scheme 1) was calculated according to Katchalsky assuming same degree of ionization as in case of the PMAA homopolymer in solution:[18] inserting pH = 7.0 and pH = 3.0 in the following equation: pH = 6.50−2 log$((1-\alpha)/\alpha)$—gives α = 0.64 and α = 0.017. Experiments with higher NaCl concentration were conducted by adding solid NaCl to the polymer solution and waiting 10 min for dissolution and equilibration of the solution with convection.

Analytical Techniques. NMR spectroscopy experiments were carried out on a Bruker Avance 300 MHz spectrometer. Chemical shifts are given in ppm. Molecular weights and polydispersity indices were estimated by size exclusion chromatography (SEC) using the following instruments: (1) A Viscotek GPCmax VE-2001 equipped with a Viscotek TriSEC Model 302 triple detector array (TDA) (refractive index (RI) detector, viscometer detector, and laser light scattering detector with the light wavelength of 670 nm, and measuring angles of 90° and 7°) and a Knauer K-2501 UV detector using two PLgel mixed-D columns from Polymer Laboratories (PL). The samples were run in THF at 30 °C (1 mL·min^{-1}). Molecular weights were calculated using PS standards from PL. (2) A HLC-8320GPC from Tosoh Corporation Bioscience Division equipped with RI and UV detectors employing three PFG micro columns (100, 1000, and 4000 Å) from Polymer Standards Service (PSS). The samples were run in DMF (5 mM LiCl) at 50 °C (0.3 mL·min^{-1}). Molecular weights were calculated using WinGPC Unity 7.4.0 software and PMMA standards from PSS. Thermogravimetric analysis (TGA) was performed on a Q500 from TA Instruments from 20 to 800 °C with a heating rate of 20 °C·min^{-1} under nitrogen flow.

The copolymer composition was estimated by NMR spectroscopy and TGA, and was then used to determine the molecular weights. ^{1}H NMR experiments allowed calculation of the molar fractions of the monomers in the grafted chains. The contribution of the PHEMA backbone was disregarded because the corresponding resonance signals were dramatically diminished due to the severe shielding. The weight fractions of *t*BMA were independently obtained by TGA, and converted to the corresponding molar fractions. PHEMA backbone was not taken into account again. The refractive index increments of the copolymers were calculated to be dn/dc = 0.06 since dn/dc (PMEA) = 0.06[19] and dn/dc (P*t*BMA) = 0.06 (determined by injecting 60, 80, and 100 μL of the sample in the SEC system with the TDA). These values were then employed for the estimation of the molecular weights by SEC with the TDA in THF. Finally, the degree of polymerization (DP) of randomly incorporated MEA and *t*BMA were calculated for every graft copolymer utilizing the $\bar{M}_n$ obtained by SEC and the molar fractions obtained by ^{1}H NMR experiments or TGA.

The random copolymer of MEA and *t*BMA was analyzed in a similar manner. DP of PHEMA in the diblock copolymer was estimated by NMR spectroscopy.

The molecular weights of the graft and block copolymers after deprotection were determined by taking into account molecular weights of the precursor polymers and employing NMR spectroscopy—quantitative cleavage of the *tert*-butyl ester groups was assumed. In case of the graft copolymer with P(MEA-*co*-DMAEMA) grafts, contribution from the PHEMA backbone was taken into consideration when calculating the molecular weight by NMR spectroscopy.

This information together with some of the experimental details is summarized in Table 1.

Adsorption of the copolymers from aqueous solutions on PDMS surfaces were characterized by optical waveguide lightmode spectroscopy (OWLS) employing OWLS 210 from MicroVacuum Ltd. and BioSense 2.6.10 software. A four-layer model consisting of the glass substrate, waveguide layer, adsorbate layer, and covering medium was utilized to calculate the mass uptake on the surface of the waveguide by applying the de Feijter equation:[20]

$$m = d_A \frac{(n_A - n_C)}{\mathrm{d}n/\mathrm{d}c}$$

where d_A designates the thickness of the adsorbate layer, n_A is the refractive index of the adsorbate layer, n_C is the refractive index of the covering medium, and dn/dc is the refractive index increment of the adsorbate. The dn/dc of PHEMA, PMEA, PMAA$^-$ and PMAA are 0.1349,[17,21] 0.060,[19] 0.260,[17] and 0.175,[17] respectively. The dn/dc of the graft and block copolymers were calculated by assuming a linear relationship between the weight fraction of each constituent and its contribution to the total dn/dc value, and are given in the note.[22] n_A was calculated by the OWLS software.

In order to emulate the tribopair surface, the waveguides for the OWLS adsorption experiments were coated with a layer of PDMS on top of a layer of PS. To this end, waveguides were ultrasonicated in EtOH for 10 min and spin-coated first with the toluene solution (6.0 g·L^{-1}) of the broad molecular weight distribution PS at 2 500 rpm for

dx.doi.org/10.1021/ma4024747 | *Macromolecules* 2014, 47, 2019−2029

Table 1. Molecular Weight Characteristic of the Graft and Block Copolymers

entry	graft and block copolymer	$[M_1]_0$:$[M_2]_0$:$[I]_0$: $[CuBr]_0$:$[ligand]_0$[a]	time [min]	$\bar{M}_n$[d] [Da]	$\bar{M}_w$[d]/$\bar{M}_n$	$\bar{M}_n$[e] [Da]	$\bar{M}_w$[e]/$\bar{M}_n$	($\bar{M}_n$(PMEA))/($\bar{M}_n$(PMAA))
1–1	P(Br^{i}BuEMA$_8$-*co*-HEMA$_{37}$)-*g*-P*t*BMA$_{553}$	390:1:1.7:1.3	7	85 900	1.29			
1–2	P(Br^{i}BuEMA$_8$-*co*-HEMA$_{37}$)-*g*-PMAA$_{553}$					——	——	0/(47600)
1–3	P(Br^{i}BuEMA$_8$-*co*-HEMA$_{37}$)-*g*-P(MEA$_{488}$ -*co*-*t*BMA$_{756}$)	250:180:1:1.6:1.2	11	171 000	1.07			
1–4	P(Br^{i}BuEMA$_8$-*co*-HEMA$_{37}$)-*g*-P(MEA$_{488}$ -*co*-MAA$_{756}$)					112 000	1.17	(63100)/(65300)
1–5	P(Br^{i}BuEMA$_8$-*co*-HEMA$_{37}$)-*g*-P(MEA$_{347}$ -*co*-*t*BMA$_{319}$)	350:130:1:1.7:1.3	11	90 600	1.12			
1–6	P(Br^{i}BuEMA$_8$-*co*-HEMA$_{37}$)-*g*-P(MEA$_{347}$ -*co*-MAA$_{319}$)					81 900	1.15	(45100)/(27500)
1–7	P(Br^{i}BuEMA$_8$-*co*-HEMA$_{37}$)-*g*-P(MEA$_{321}$ -*co*-*t*BMA$_{131}$)	410:65:1:1.8:1.3	11	60 500	1.16			
1–8	P(Br^{i}BuEMA$_8$-*co*-HEMA$_{37}$)-*g*-P(MEA$_{321}$ -*co*-MAA$_{131}$)					64 500	1.21	(41800)/(11300)
2–1	P(Br^{i}BuEMA$_8$-*co*-HEMA$_{77}$)-*g*-P(MEA$_{508}$ -*co*-*t*BMA$_{509}$)	350:135:1:1.7:1.3	20	138 400	1.11			
2–2	P(Br^{i}BuEMA$_8$-*co*-HEMA$_{77}$)-*g*-P(MEA$_{508}$ -*co*-MAA$_{509}$)					109 000	1.25	(66100)/(43800)
2–3	P(Br^{i}BuEMA$_8$-*co*-HEMA$_{77}$)-*g*-P(MEA$_{131}$-*co*-DMAEMA$_{92}$)	350:130:1:1.6:1.5[b]	20	42 700		69 800	1.25	(17000[f])/(13200)
3–1	P(MEA$_{143}$-*co*-*t*BMA$_{92}$)-*b*-PHEMA$_{194}$	660:1:7.1:6.6[c]	50	56 900		108 000	2.01	
3–2	P(MEA$_{143}$-*co*-MAA$_{92}$)-*b*-PHEMA$_{194}$			51 700		113 000	1.29	(18600)/(7900)

[a]The ratios are derived from the total initial initiator concentrations. PMDETA was used as the ligand. [b]CuCl/HMTETA was used as the catalytic complex. [c]The reaction was mediated by CuCl/PMDETA. [d]The number-average molecular weights were obtained by combination of ^{1}H NMR experiments, TGA, and SEC employing THF as an eluent and a TDA. PDI were estimated by SEC employing THF as an eluent and a TDA. [e]The number-average molecular weights and PDI were determined by SEC employing DMF (5 mM LiCl) as an eluent. [f]$\bar{M}_n$(PMEA)/$\bar{M}_n$(PDMAEMA).

15 s with subsequent annealing at 100 °C for 1 h. This afforded a 24.3 ± 3.1 nm thick PS film as measured with AFM by scratch removal of a PS layer on a similarly spin-coated glass slide. The PS-modified waveguides were then spin-coated with a Sylgard 184 PDMS kit mixture (the base component and cross-linker with the 3:1 wt. ratio were dissolved in heptane (0.5 wt %)) at 2 000 rpm for 60 s. After spin-coating, the waveguides were cured at 70 °C overnight. The reference thickness of the spin-coated PDMS layer as measured on silicon wafers by ellipsometry was 16.4 ± 0.17 nm, assuming a native silicon oxide layer of 1.4 nm and the refractive index of 1.401 of the PDMS layer. The PS sandwich layer was applied for easier recycling of the waveguides by exfoliation of the cross-linked PDMS layer when ultrasonicated in toluene. OWLS measurements showed no statistical difference between adsorption on pure PDMS spin-coated waveguides and PS + PDMS spin-coated ones.

Adsorption measurements were performed employing the HEPES buffer (1 mM, pH 7) at a flow rate of 0.1 mL·min^{-1} at 20 °C. After stabilization, the polymer solution was flown through the waveguide until the saturation in the mass uptake was attained. For all polymer solutions maximum adsorption was observed within ca. 3 min, indicating rapid adsorption kinetics. The flow was then stopped for 10 min, and switched back to the pure HEPES buffer. The reported adsorbed masses were obtained after rinsing the waveguide with the HEPES buffer for a minimum of 10 min. 2–3 measurements were performed for each copolymer solution to give a statistical average. The reported adsorbed masses and derived surface densities are shown in Table 2, where the surface densities are calculated by dividing the adsorbed mass with the molar mass of the copolymer (i.e., the sum of the weights of the grafted chains in Table 1 and backbone) and multiplying with (10^{-3} g·mg^{-1} × N_A × 10^{-18} m^2·nm^{-2}), where N_A is the Avogadro constant. The adsorbed masses are also displayed in Figure 5. Error bars in Figure 5 and uncertainties in Table 2 designate standard deviation.

The lubricating capabilities of the graft and block copolymers in an aqueous environment were assessed by a pin-on-disk tribometer from CSM Instruments with the 4.4 M software. The tribopair was self-mated PDMS, and the range of sliding speed was from 100 to 0.25 mm·s^{-1}. The load was controlled by applying dead weights on the pin. The friction coefficient (μ) was calculated from the following expression: $\mu = F_{friction}/F_{load}$. The load in all experiments was 5 N, giving a contact pressure of 0.38 MPa (Hertzian contact, E = 2.00 MPa, Poisson's ratio of 0.5).[23] The experiments were conducted at room temperature recording a minimum of 20 laps for each speed measured. Error bars in μ vs sliding speed plots designate standard deviation.

Synthetic Procedures. All reactions were carried out under nitrogen atmosphere.

1: Synthesis as well as structural analysis of P(Br^{i}BuEMA$_8$-*co*-HEMA$_{37}$) has been reported before (Br^{i}BuEMA = 2-(bromoisobutyryloxy)ethyl methacrylate).[5] SEC (DMF + 5 mM LiCl): $\bar{M}_n$ = 34 900 Da, $\bar{M}_w$ = 42 700 Da, $\bar{M}_w/\bar{M}_n$ = 1.22. $\bar{M}_n$ (^{1}H NMR) = 7300 Da, DP of Br^{i}BuEMA was 8, DP of HEMA was 37.

2: The random copolymer **2** was obtained in a similar fashion as **1**, except that the monomer ratio in the feed was $[HEMA]_0$:$[Br^iBuEMA]_0$ = 8.6. SEC (DMF + 5 mM LiCl): $\bar{M}_n$ = 55 000 Da, $\bar{M}_w$ = 64 700 Da, $\bar{M}_w/\bar{M}_n$ = 1.18. $\bar{M}_n$ (^{1}H NMR) = 12 500 Da, DP of Br^{i}BuEMA was 8, DP of HEMA was 77.

Preparation of the Graft Copolymers. *General Procedure for ATRP.* The macroinitiator **1** or **2**, *t*BMA or MEA and *t*BMA or MEA and DMAEMA, CuBr or CuCl, DMF, and anisole were introduced into a Schlenk tube. Prior to the injection of the ligand – PMDETA or HMTETA – two freeze–pump–thaw cycles were performed. Afterward, two additional freeze–pump–thaw cycles were carried out. The polymerization was conducted at 70 °C. The graft copolymers were precipitated in heptane or a heptane–Et_2O mixture, and dried in the vacuum oven at room temperature.

Preparation of the graft copolymers from the macroinitiator **2** is elaborated below as an example.

2–1: **2** (86 mg, 0.055 mmol of the initiating sites), MEA (2.5 mL, 19.4 mmol), *t*BMA (1.2 mL, 7.4 mmol), CuBr (13.5 mg, 0.094 mmol),

Table 2. Adsorption Characteristics of the Copolymers[a]

copolymer	adsorbed mass [mg·m^{-2}]	density of entire copolymer on surface [chains·nm^{-2}][b]	average copolymer distance on surface[c] [nm]	average spacing between the grafted chains[d] [nm]	R_g of an individual grafted chain[e] [nm]
1−**2**	0.22 ± 0.12	0.002	24.0	8.5	2.5
	pH 3.0: 2.35 ± 0.33	pH 3.0: 0.026	pH 3.0: 6.7	pH 3.0: 2.4	
	150 mM NaCl: 0.03 ± 0.04	0.0004	55.1	19.5	
1−**4**	0		——	——	3.7
	150 mM NaCl: 0.49 ± 0.01	0.002	24.0	8.5	
1−**6**	2.76 ± 0.82	0.021	7.4	2.6	2.7
	150 mM NaCl: 0.56 ± 0.03	0.004	17.0	6.0	
1−**8**	0.39 ± 0.20	0.004	17.0	6.0	2.2
2−**2**	1.14 ± 0.06	0.005	15.2	5.4	3.4
	150 mM NaCl: 0.57 ± 0.04	0.003	19.6	6.9	
2−**3**	0	——	——	——	1.6
	pH 9.0: 0.68 ± 0.04	pH 9.0: 0.01	pH 9.0: 11.0	pH 9.0: 3.8	
3−**2**	1.48 ± 0.17	0.017	8.2	n/a	1.6
	150 mM NaCl: 1.25 ± 0.07	0.015	8.8	n/a	
3−**3**	0.36 ± 0.06	0.008	12.0	n/a	1.6[f]

[a]Measurement conditions: 0.50 mg·mL^{-1} of the copolymer in HEPES buffer (1 mM) at pH 7.0 and PDMS surface. The copolymers **1**−**2** and **2**−**3** were also investigated at pH 3.0 and pH 9.0, respectively. [b]Calculated by dividing the adsorbed mass with the molar mass of the copolymer, i.e. the sum of the weights of the grafted chains (in Table 1) and backbone, and multiplying with (10^{-3} g·mg^{-1} × N_A × 10^{-18} m^2·nm^{-2}). [c]Assuming hexagonal packing on the surface.[25] [d]Assuming average spacing of all adsorbed copolymers in a hexagonal packing and equal spacing between the grafted chains on the PHEMA backbone. [e]Modeled as ideal chains in the Θ solvent: $R_g = (N/6)^{1/2} \times l$, where N is the number of the repeating units (both MEA and MAA) and l = 0.258 nm (estimated with ChemBio3D Ultra 12.0 assuming staggered backbone) is the effective bond length.[26] [f]R_g of the entire chain.

PMDETA (15 μL, 0.072 mmol), DMF (3.6 mL), and anisole (3.6 mL) were taken. The polymerization was quenched in 20 min. ^{1}H NMR (300 MHz, $CDCl_3$, δ): 3.80−4.60 (*b*, C(O)OC*H*$_2$CH$_2$OH, C-(CH$_3$)$_2$C(O)OC*H*$_2$CH$_2$, and HCC(O)OC*H*$_2$), 3.45−3.70 (*b*, C*H*$_2$OH, CH$_3$OC*H*$_2$), 3.25−3.45 (*b*, C*H*$_3$O), 0.80−2.60 (*b*, CH$_2$C-(C*H*$_3$)C(O)O, CH$_2$C(CH$_3$)C(O)O, OC(C*H*$_3$)$_3$, CH$_2$C*H*C(O)O and C*H*$_2$CHC(O)O). Resonance signals at 0.87 ppm (*t*, 6.8 Hz, C*H*$_3$) and 1.25 ppm (*b*, C*H*$_2$) correspond to the residual heptane.

Selective cleavage of *tert*-butyl esters was carried out as reported before.[4]

2−**2**: **2**−**1** (0.39 g, approximately 1.43 mmol of *tert*-butyl ester groups) was dissolved in CH_2Cl_2 (10 mL). TFA (1.0 mL, 13.1 mmol) and TES (0.5 mL, 3.1 mmol) were employed. ^{1}H NMR (300 MHz, DMSO-d_6, δ): 11.90−12.70 (*b*, C(O)O*H*), 4.43−4.77 (*b*, CH$_2$O*H*), 3.65−4.38 (*b*, C(O)OC*H*$_2$CH$_2$OH, C(CH$_3$)$_2$C(O)OC*H*$_2$CH$_2$, and HCC(O)OC*H*$_2$), 3.37−3.65 (*b*, C*H*$_2$OH, CH$_3$OC*H*$_2$), 3.10−3.37 (*b*, C*H*$_3$O), 2.09−2.42 (*b*, CH$_2$C*H*C(O)O), 0.45−2.08 (*b*, CH$_2$C(C*H*$_3$)-C(O)O, C*H*$_2$C(CH$_3$)C(O)O, and C*H*$_2$CHC(O)O).

2−**3**: **2** (86 mg, 0.055 mmol of the initiating sites), MEA (2.5 mL, 19.4 mmol), DMAEMA (1.2 mL, 7.1 mmol), CuCl (8.7 mg, 0.089 mmol), HMTETA (22.5 μL, 0.083 mmol), DMF (3.6 mL), and anisole (3.6 mL) were used. The polymerization was quenched in 20 min. ^{1}H NMR (300 MHz, DMSO-d_6, δ): 4.65−5.05 (*b*, CH$_2$O*H*), 3.70−4.40 (*b*, C(O)OC*H*$_2$CH$_2$OH, C(CH$_3$)$_2$C(O)OC*H*$_2$CH$_2$, C(O)-OC*H*$_2$CH$_2$N, and HCC(O)OC*H*$_2$), 3.34−3.70 (*b*, C*H*$_2$OH, CH$_3$OC*H*$_2$), 3.15−3.34 (*b*, C*H*$_3$O), 2.40−2.65 (DMSO, C(O)-OCH$_2$C*H*$_2$N), 2.05−2.40 (CH$_2$C*H*C(O), CH$_2$N(C*H*$_3$)$_2$) 0.50−2.05 (*b*, CH$_2$C(C*H*$_3$)C(O)O, C*H*$_2$C(CH$_3$)C(O)O, and C*H*$_2$CHC(O)O).

Preparation of the Block Copolymers. 3: The Schlenk tube equipped with a magnetic stirring bar and a rubber septum was charged with MEA (2.5 mL, 19.4 mmol), *t*BMA (1.2 mL, 7.4 mmol), and CuBr (10.2 mg, 0.071 mmol), and two freeze−pump−thaw cycles were performed. PMDETA (15 μL, 0.072 mmol) was introduced, and one freeze−pump−thaw cycle was carried out. Then EBr^{i}Bu (10 μL, 0.068 mmol) was injected followed by another freeze−pump−thaw cycle. The polymerization was conducted at 70 °C for 130 min. The reaction mixture was diluted with THF, precipitated in heptane, and dried in the vacuum oven at room temperature. SEC (THF) with a TDA: $\bar{M}_n$ = 31 700 Da, $\bar{M}_w$ = 35 000 Da, $\bar{M}_w/\bar{M}_n$ = 1.11. DP of 143 and 92 for PMEA and P*t*BMA, respectively, were estimated by ^{1}H NMR spectroscopy.

3−**1**: **3** (0.25 g, 0.008 mmol), HEMA (0.64 mL, 5.3 mmol), CuCl (5.6 mg, 0.057 mmol), DMF (0.64 mL), and anisole (0.64 mL) were introduced into a Schlenk tube. A total of four freeze−pump−thaw cycles were performed: two prior to the addition of PMDETA (11 μL, 0.053 mmol). The polymerization was carried out at 60 °C for 50 min. The reaction mixture was diluted with DMF, precipitated in a heptane−Et$_2$O (1:1) mixture, and dried in the vacuum oven at room temperature.

3−**2**: **3**−**1** (95 mg) was dissolved in TFA (1.0 mL), and stirred at room temperature for 2 h. The polymer was precipitated in Et$_2$O. The solvent was decanted; the product was washed with Et$_2$O, and dried in the vacuum oven at room temperature.

RESULTS AND DISCUSSION

Synthesis. Synthetic routes to the anionic and cationic graft copolymers are depicted in Scheme 1.

While backbones of these graft copolymers comprise HEMA and Br^{i}BuEMA repeating units, the grafted chains are composed of MAA (**1**−**2**), MEA and MAA (**1**−***X***, *X* = 4, 6, 8; and **2**−**2**), and MEA and DMAEMA (**2**−**3**).

Copolymers **1** and **2** that feature eight ATRP initiating sites apiece were prepared by RAFT copolymerization as reported before.[5] Due to employing higher monomer feed ratio than in the synthesis of **1**, [HEMA]$_0$:[Br^{i}BuEMA]$_0$ = 8.6, **2** incorporates approximately twice as many HEMA repeating units. Both of these macroinitiators exhibit monomodal SEC traces, and narrow molecular weight distributions (MWD) (PDI ≤ 1.22). The difference in their number-average molecular weights—7300 Da for **1** and 12 500 Da for **2**—

dx.doi.org/10.1021/ma4024747 | *Macromolecules* 2014, 47, 2019−2029

serves as one of the parameters while investigating the lubricating properties of the corresponding graft copolymers.

Graft copolymer **1−2** was obtained by treating the precursor—P(Br^{i}BuEMA$_8$-*co*-HEMA$_{37}$)-*g*-P*t*BMA (**1−1**)—with a combination of TFA/TES in CH_2Cl_2.[4] Selective and near to quantitative cleavage of the *tert*-butyl esters was verified by ^{1}H NMR spectroscopy. However, **1−2** displayed poor lubricating properties, which were ascribed to the presence of the dominant repulsive forces among the fully anionic grafted chains. To diminish the adverse impact of these repulsive forces, the graft copolymers **1−*X*** (*X* = 4, 6, 8) were constructed (Scheme 1). The charge across the grafted chains was "diluted" by incorporating MEA repeating units together with MAA ones in a random fashion. The content of MAA units was manipulated by changing the initial monomer feed ratio of MEA to *t*BMA when building the corresponding precursors (Scheme 1). The structure and composition of these graft copolymers were elucidated by the combination of NMR spectroscopy, TGA, and SEC (Table 1). The TGA results for the graft copolymers **1−3**, **1−5**, and **1−7** with the decreasing *t*BMA content are shown in Figure 1.

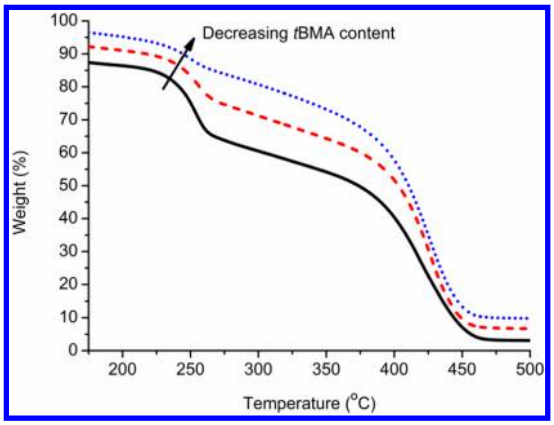

Figure 1. Overlay of the TGA thermograms of the graft copolymers **1−3** (solid line), **1−5** (dashed line), and **1−7** (dotted line).

The weight loss in the range of 190−280 °C corresponds to the loss of isobutylene, and can be correlated to the amount of *t*BMA repeating units. Thus, **1−3**, **1−5**, and **1−7** comprise 74, 49, and 31 wt % of *t*BMA units, respectively.

2−2 was synthesized in a similar manner. Initially, MEA and *t*BMA were polymerized from the macroinitiator **2** by ATRP making use of CuBr/PMDETA catalytic complex to afford the precursor **2−1**. Fairly high $[M]_0$:$[I]_0$ was taken to avoid interchain coupling reactions (Table 1).[5] The SEC analysis with a TDA revealed a monomodal trace with a narrow MWD (PDI = 1.11). The SEC analysis employing DMF (5 mM LiCl) as an eluent confirmed high macroinitiator efficiency: the chromatogram was shifted to the lower elution volume with no evidence of the unreacted macroinitiator (Figure 2).

The structure of the graft copolymer **2−1** was substantiated by a ^{1}H NMR experiment. While the resonance signals originating from the backbones overlap in the range of 0.80−2.60 ppm, the peak **g** corresponds to the *tert*-butyl group, and **j**, **k**, and **l** are ascribed to the methyl ethylene glycol ester fragment (Figure 3).

The monomer ratio was determined by comparing the area of **l** with that of the overlying resonances in the range of 0.80−2.60 ppm. The contribution from P(Br^{i}BuEMA$_8$-*co*-HEMA$_{77}$)

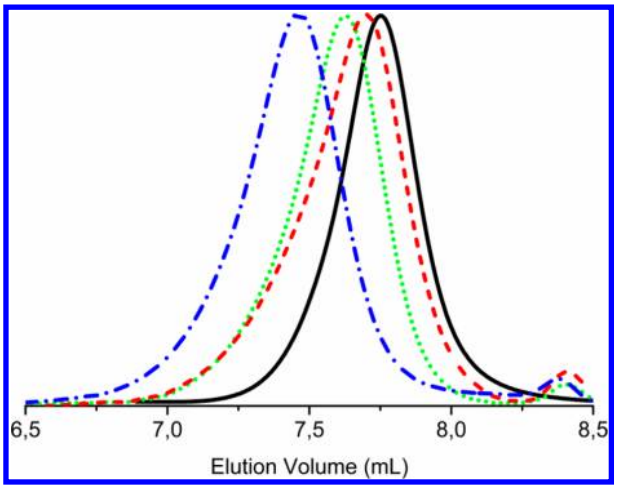

Figure 2. Overlay of the SEC (DMF + 5 mM LiCl) traces of **2** (solid line) and the graft copolymers **2−1** (dotted line), **2−2** (dash-dotted line), and **2−3** (dashed line).

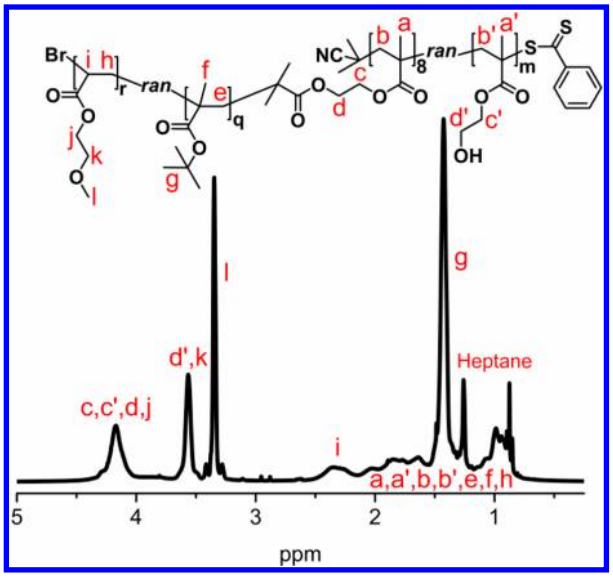

Figure 3. ^{1}H NMR spectrum of the graft copolymer **2−1** acquired in $CDCl_3$.

could not be taken into consideration due to extensive shielding of the backbone. Thus, MEA and *t*BMA contents in the graft copolymer **2−1** add up to 66 100 Da and 72 300 Da, respectively (Table 1).

This is in agreement with the result obtained from the TGA: 51 wt % of *t*BMA. Deblocking of the methacrylic acid units was conducted with TFA/TES. The resonance signal at 11.90−12.70 ppm attributed to the methacrylic acid carboxyl group and the resonance signal at 4.43−4.77 ppm assigned to the HEMA hydroxyl group emerge, while the peak **g** almost disappears in the ^{1}H NMR spectrum acquired in DMSO-d_6. The SEC trace of the graft copolymer **2−2** is fairly symmetrical (PDI = 1.25), but it is shifted further to the lower elution volume perhaps due to its amphiphilic nature and resulting ambivalent solubility in DMF (5 mM LiCl) (Figure 2).

Graft copolymer **2−3**—P(Br^{i}BuEMA$_8$-*co*-HEMA$_{77}$)-*g*-P(MEA-*co*-DMAEMA)—was synthesized as a cationic counterpart (Scheme 1). Copolymerization of MEA and DMAEMA by ATRP was carried out in the DMF/anisole 1:1 (v/v) mixture at 70 °C employing CuCl/HMTETA catalytic complex and

dx.doi.org/10.1021/ma4024747 | *Macromolecules* 2014, 47, 2019−2029

$[MEA]_0$:$[DMAEMA]_0$ = 2.7. The SEC trace is monomodal, and the MWD is quite narrow (PDI = 1.25) (Figure 2). The structure and composition of the graft copolymer was examined by ^{1}H NMR spectroscopy. Peaks **d″**, **g‴**, and **l** can be assigned unequivocally to the hydroxyl group of the HEMA repeating unit, the methyl groups neighboring the nitrogen atom in the DMAEMA repeating unit, and the methyl group adjacent to the oxygen atom in the MEA repeating unit, respectively (Figure 4).

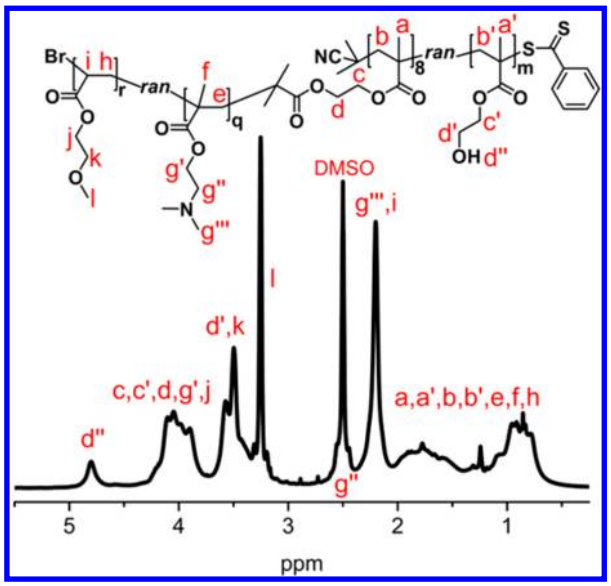

Figure 4. ^{1}H NMR spectrum of the graft copolymer **2−3** acquired in DMSO-d_6.

Most of the other resonance signals overlap though exhibit characteristic chemical shifts. The monomer ratio of [MEA]:[DMAEMA] = 1.6 was estimated by comparing the areas of the resonance signals **l** and **g‴** + **i**.

The diblock copolymer comprising P(MEA-*co*-MAA) and PHEMA blocks was synthesized in order to compare its lubricating properties with those of the graft copolymer with similar composition. Thus, bulk copolymerization of MEA and *t*BMA by ATRP, which was initiated by EBr^{i}Bu and mediated by CuBr/PMDETA, afforded the random copolymer with narrow MWD (PDI = 1.11) (Scheme 2, **3**).

Number of repeating units of MEA and *t*BMA were 143 and 92, respectively, as judged from the NMR spectroscopy and SEC data. The copolymer **3** was chain-extended with HEMA resulting in the diblock copolymer with the DP (PHEMA) = 194 as estimated by ^{1}H NMR experiment. However, the SEC trace acquired in DMF (5 mM LiCl) was not symmetrical, and exhibited a rather high PDI = 2.01. This was attributed to the association of the polymer chains and ineffectual initiation by the macroinitiator, which manifested itself as a small shoulder on the lower molecular weight side. Nevertheless, P(MEA-*co*-*t*BMA)-*b*-PHEMA was treated by neat TFA to deprotect the methacrylic acid repeating units. The structure of **3−2** (Scheme 2) was confirmed by NMR spectroscopy. SEC analysis in DMF (5 mM LiCl) revealed the trace that was much more symmetrical than that of the precursor diblock copolymer, and the MWD was quite narrow (PDI = 1.28). This result somewhat enhances the conjecture that the SEC analysis of the diblock copolymer **3−1** was obstructed by the undesirable interactions.

Finally, the copolymer **3** was deprotected with TFA/TES to obtain the copolymer **3−3** (Scheme 2) with the same ratio of $\bar{M}_n$(PMEA)/$\bar{M}_n$(PMAA) = 18600/7900 as the diblock copolymer **3−2**. This amphiphilic random copolymer, rich in hydrophobic content, would provide some understanding whether the individual grafted chains—P(MEA-*co*-MAA) interacted with the PDMS surface and played a significant role in the graft copolymer adsorption.

Adsorption of the Copolymers on PDMS surface. In the series of graft copolymers based on P(Br^{i}BuEMA$_8$-*co*-HEMA$_{37}$) backbone, **1−8** exhibited significant aggregation followed by precipitation upon standing, as was mentioned in the Experimental Section. This is well correlated with the relatively small amount of adsorbed mass 0.39 ± 0.20 mg·m^{-2} (Figure 5). The majority of the copolymer is present in the form of aggregates and there are simply too few free unimers available to dynamically interact with the PDMS surface.[24] This is ascribed to the high content of the hydrophobic PMEA in **1−8** (($\bar{M}_n$(PMEA))/($\bar{M}_n$(PMAA)) = 3.69 is the highest in the series), which results in low water solubility. The graft copolymer **1−2** also showed little adsorption at pH 7.0 (0.22 ± 0.12 mg·m^{-2} corresponding to a polymer density of 0.002 nm^{-2} polymers on the PDMS surface, Table 2), yet for different reason compared to **1−8**. In case of **1−2**, the grafted chains are composed of MAA only, and ca. 64% of the PMAA repeating units are expected to be deprotonated.[18] Thus, high solubility rather than aggregation is expected in aqueous solution. The retarded adsorption of **1−2** onto nonpolar PDMS surface is therefore due to the repulsion against charge accumulation on

Scheme 2. Synthetic Sequence Leading to the Anionic Block and Random Copolymers[a]

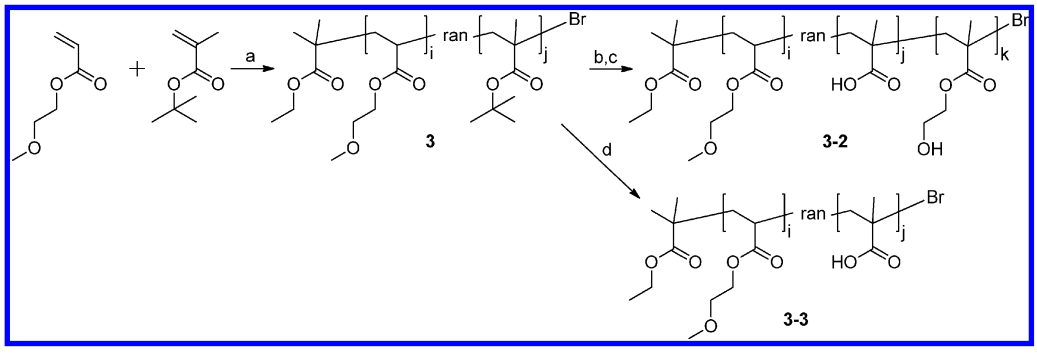

[a]Reagents and conditions: (a) EBr^{i}Bu, CuBr/PMDETA, 70 °C; (b) HEMA, CuCl/PMDETA, 1:1:1 (v/v) monomer:DMF:anisole, 60 °C; (c) TFA; (d) TFA, TES, CH_2Cl_2.

dx.doi.org/10.1021/ma4024747 | *Macromolecules* 2014, 47, 2019−2029

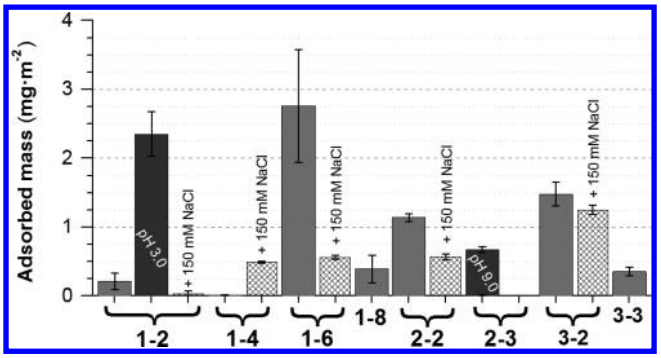

Figure 5. Adsorbed masses of the copolymers as measured by OWLS. (Light Gray) Measurement conditions : substrate, PDMS-coated OWLS waveguide, 0.50 mg·mL^{-1} of the copolymer in HEPES buffer (1 mM) at pH 7.0. The error bars designate standard deviation. (Dark Gray) pH-dependent condition in HEPES buffer (1 mM). (Shaded) Measuement in HEPES buffer + 150 mM NaCl.

the surface, which is common for the adsorption of charged species from aqueous solutions onto nonpolar surfaces.[13,27] Significant increase of the adsorbed mass of the same copolymer at pH 3.0 (2.35 ± 0.33 mg·m^{-2}) supports this argument; the PMAA chains are almost fully protonated at pH 3.0, and the surface adsorption is boosted by approximately 10 times.

Addition of 150 mM NaCl, close to physiological ionic strength, appeared to display contradicting effects for the surface adsorption of the other copolymers (Figure 5). For example, the adsorption of **1**−**4** was improved from zero to 0.49 ± 0.01 mg·m^{-2}, whereas the adsorption of **1**−**6** and **2**−**2** was significantly hampered by addition of 150 mM NaCl; the adsorbed mass decreased from 2.76 ± 0.82 mg·m^{-2} to 0.56 ± 0.03 mg·m^{-2} for **1**−**6** and from 1.14 ± 0.06 mg·m^{-2} to 0.57 ± 0.04 mg·m^{-2} for **2**−**2**, respectively. A closer look at the adsorption profiles shows that not only the adsorbed amount, but also surface adsorption kinetics was significantly altered by addition of 150 mM NaCl. As an example, the adsorption profiles of **1**−**6** are presented in the Figure 6.

In the absence of 150 mM NaCl, a rapid increase of the adsorbed mass upon exposure of PDMS surface to the polymer solution (in the first 1 min or less), was followed by a gradual

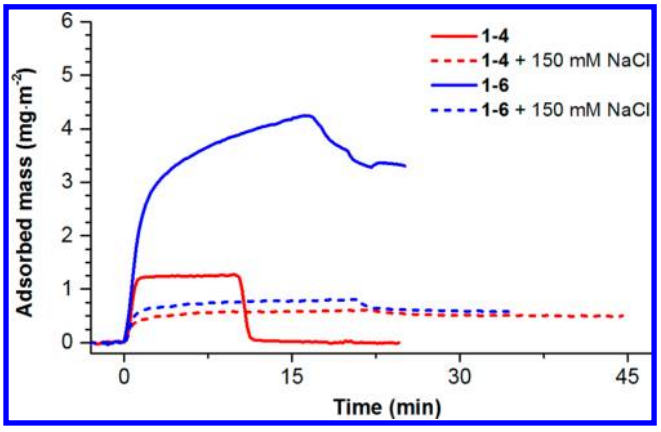

Figure 6. Representative surface adsorption profiles of **1**−**6** (blue) and **1**−**4** (red) as measured by OWLS, both in the absence (dotted lines) and presence (solid lines) of 150 mM NaCl. Measurement conditions: substrate, PDMS-coated OWLS waveguide, 0.50 mg·mL^{-1} of the copolymer in HEPES buffer (1 mM) at pH 7.0.

and continuing increase in the adsorbed mass. This behavior was commonly observed for most of the graft copolymers under the condition of pH 7 and 1 mM HEPES buffer (The surface adsorption profiles of all the copolymers are shown in Figure S1 in the Supporting Information). In contrast, in the presence of 150 mM NaCl, all the graft copolymers showed an immediate completion of surface adsorption within 1−2 min. We propose that slow adsorption kinetics of the graft copolymers in near salt-free condition indicates the formation of multilayers and/or rearrangement on the surface. In this condition, grafted P(MEA-*co*-MAA) chains along PHEMA backbone are expected to be so highly extended that it is difficult for hydrophobic PHEMA backbone to anchor on the PDMS surface, especially because the molecular weights of the P(MEA-*co*-MAA) side chains are mostly much larger than those of the PHEMA backbone. It is also possible that the side chains can directly interact with PDMS due to the presence of PMEA moieties, as shown by the finite adsorbed mass of copolymer **3**−**3**, 0.36 ± 0.06 mg·m^{-2}, onto PDMS surfaces. Consequently, the stability of the adsorbed copolymers on PDMS surface is expected to be weak. An exceptional and extreme case is **1**−**4**; a rapid completion of adsorption even in the absence of 150 mM NaCl, is due to extremely high molecular weight of the side chains (128 400 Da on average). Nevertheless, all adsorbates were completely rinsed away by rinsing with buffer, reflecting the weak adsorption strength of the **1**−**4** copolymer (Figure 6). If the Debye length (κ^{-1}) is larger than the R_g of the polymer chain, then the charges on the polymer chain are not affected by the added salt.[28] At pH 7.0 1 mM HEPES buffer κ^{-1} = 19.6 nm whereas at 150 mM NaCl κ^{-1} = 0.8 nm, thus the charge repulsion is significantly reduced at the physiological conditions. By addition of 150 mM NaCl, the charged side chains are expected to be shrunk or coiled due to the screening of electrostatic repulsion between them;[29] this, effectively, may boost the access of the anchoring units of PHEMA backbone to the surface and leads to the immediate and stable surface adsorption. In this sense, quantitative comparison of the adsorbed masses of the copolymers as a result of 150 mM NaCl, as shown in Figure 5, is not too meaningful since there is a substantial difference in the adsorption mechanism and stability. Rather, a qualitative, yet general effect by addition of 150 mM NaCl is to strengthen the stability of the adsorbed copolymers on PDMS surfaces. This will be further confirmed in tribological studies below.

The series **2**−***X*** of graft copolymers with P(Br^{i}BuEMA$_8$-*co*-HEMA$_{77}$) backbone is designed in such a way that HEMA content in the backbone is doubled while the number of the ATRP initiating sites is still eight. This may provide higher stability in anchoring on the surface, whereas the spacing between the side chains tends to be larger, both in bulk solution and on surface. However, at neutral conditions the density of the grafted side chains of **2**−**2** on the surface, 0.040 nm^{-2}, is smaller than that of **1**−**6**, 0.168 nm^{-2} (in 1 mM HEPES buffer). This is ascribed first to a larger spacing between P(MEA-*co*-MAA) graft chains along the backbone. Additionally, higher molecular weight of **2**−**2**'s graft chains (109 000 Da), which is closer to that of **1**−**4** (128 400 Da) than **1**−**6** (79 900 Da), may have also contributed to impeding the surface adsorption due to the graft chains' large gyration. Nevertheless, the adsorbed mass of **2**−**2** in the presence of 150 mM NaCl was comparable to those of **1**−**4** and **1**−**6**, as shown in Figure 5.

The cationic graft copolymer **2**−**3** did not show any adsorption after rinsing with buffer at pH 7.0. However,

dx.doi.org/10.1021/ma4024747 | *Macromolecules* 2014, 47, 2019−2029

when the pH was raised to 9.0, the adsorption increased to 0.68 ± 0.04 mg·m^{-2}. This indicates that the unfavorable adsorption of **2**−**3** onto neutral PDMS surface at neutral pH is also a result of electrostatic repulsion, similarly with the anionic copolymers; pK_a of PDMAEMA has been reported to be 7.4−7.5.[30] No other analogues of **2**−**3** were further synthetically elaborated with dilution of the graft chains' cationic charges with MEA moieties.

The diblock copolymer **3**−**2** displayed good adsorption with a mass uptake of 1.48 ± 0.17 mg·m^{-2}. The corresponding surface density of 0.017 chains·nm^{-2} and average polymer distance of 8.2 nm are comparable with those of the graft copolymer **1**−**6**.

Lubricating Properties. Figure 7 depicts the measured coefficients of friction (μ) of the PDMS−PDMS sliding

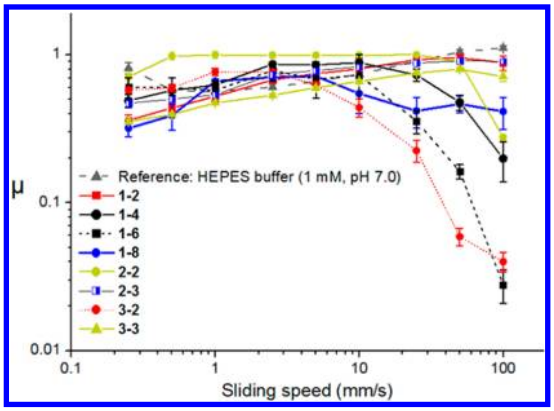

Figure 7. Pin-on-disk friction experiments of the graft and block copolymer solutions at a PDMS−PDMS sliding interface. Measurement conditions: 0.50 mg·mL^{-1} of the copolymer in HEPES buffer (1 mM) at pH 7.0 and 5 N load. The lines connecting to points are a guide to the eye.

contacts against the sliding speed in the neutral copolymer solutions (0.5 mg·mL^{-1} in 1 mM HEPES buffer). None of the copolymers showed effective lubricating properties when compared to the PDMS−PDMS sliding in reference buffer solution. Even though the graft copolymer **1**−**6** and the diblock copolymer **3**−**2** displayed some magnitude of reduction in friction coefficient in high-speed regime (>25 mm·s^{-1}), it is related to the entrainment of the copolymer solutions at high speeds, not modification of shear strength between PDMS−PDMS contacts based on strong adsorption of the copolymers on the surface. While the poor lubricating capacity of **1**−**2**, **1**−**4**, **1**−**8**, and **2**−**3** is expected from their poor surface adsorption properties (Figure 5), similarly poor lubricity of **1**−**6**, **2**−**2**, and **3**−**2** with fairly high adsorbed mass is somewhat difficult to comprehend.

However, this discrepancy between the adsorbed mass and lubricating properties rather indicates that the adsorption strength and/or conformation of **1**−**6**, **2**−**2**, and **3**−**2** on PDMS surface is not optimal enough to withstand the exerted tribological stress.

Poor lubricating capacity of the "surface adsorbing" copolymers can be ascribed to the repulsion between the neighboring copolymers as well as opposing MAA$^-$ repeating units upon compression and shear. This factor has already been considered as a reason for retarding the adsorption of other copolymers with high charge content such as **1**−**2** and **1**−**4**. Even for **1**−**6**, **2**−**2**, and **3**−**2,** initially adsorbed copolymers are likely to be sheared off from the surface upon initiation of lateral shear in tribological contacts. Even if these copolymers may display low friction forces at this stage, they have to reform the lubricating layers immediately and continuously in order to maintain the lubricating interface under cyclic tribostress exerted on the PDMS surfaces.[12,31] Continuous readsorption onto the surface following tribostress-induced desorption may encounter higher energy barrier than the adsorption in the absence of tribostress. This barrier is particularly high in the case of the experiments shown in Figure 7, since the HEPES buffer in this test has very low salinity (ionic strength =1 mM), where electrostatic screening between charged moieties, MAA$^-$, cannot be expected.

2−**3** did not improve its lubricity even at pH 9.0, although adsorbed mass was somewhat increased. **1**−**2** improved its lubricity at pH 3.0 only in the higher sliding speed regime ≥25 mm/s (data not shown), similarly with neutral-anionic diblock copolymers in a previous study.[13] We attribute this to poor solvency, in turn poor hydration of graft chains at pH 9.0 and pH 3.0 for **2**−**3** and **1**−**2**, respectively.

As mentioned in the Introduction, one of the major goals of this study is to test the feasibility of the lubricating efficacy of the copolymers in physiological condition. In order to emulate the physiological salt concentration, the same tribological tests were repeated in HEPES buffer solution with additional 150 mM NaCl. As shown in Figure 8, the lubricity of all copolymers except for **2**−**3** significantly improved in high-speed regime (>25 mm·s^{-1}).

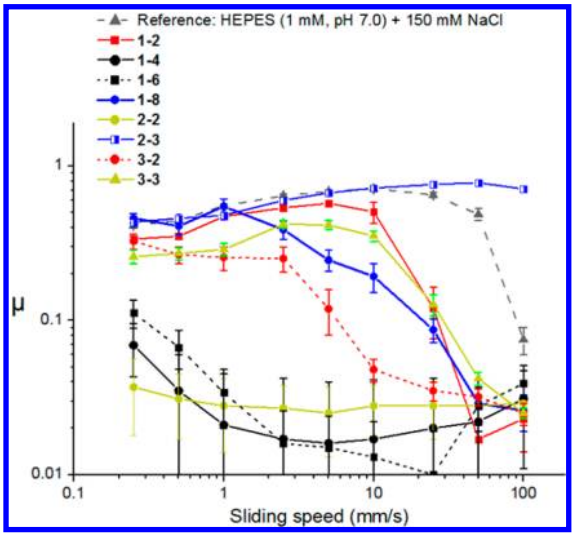

Figure 8. Pin-on-disk friction experiments of graft and block copolymer solutions at a PDMS−PDMS sliding interface. Measurement conditions: 0.50 mg·mL^{-1} of the copolymer in HEPES buffer (1 mM) + 150 mM NaCl at pH 7.0 and 5 N load.

Among them, **1**−**4**, **1**−**6**, and **2**−**2** have shown most substantial improvement in boundary lubricating properties in low-speed regime. Common to all these copolymers is a rapid saturation in the surface adsorption profiles in the presence of additional 150 mM NaCl in buffer (Figure 6 for **1**−**4** and **1**−**6**, and Figure 1S for the rest). A few points are worthy of comments. First, a significant improvement in surface adsorption and the lubricating capabilities of **1**−**4** in HEPES with physiological ionic strength is particularly notable since the molecular weight of P(MEA-*co*-MAA) side chains, 128 400 Da,

dx.doi.org/10.1021/ma4024747 | *Macromolecules* 2014, 47, 2019−2029

is the highest among the graft copolymers, and thus it should be most challenging for the PHEMA backbone to reach and anchor on the PDMS substrates. Thus, charge screening effect by additional salts is activated not only via reducing the intermolecular electrostatic repulsion between neighboring copolymers, but also via intramolecular shrinking or coiling of P(MEA-*co*-MAA) side chains, which promotes the interaction of anchoring units of PHEMA backbone with the PDMS surface. As seen from the case of **1−2**, which is composed of ionic PMAA only, 150 mM NaCl is not sufficient to improve the lubricating (Figure 8) properties. On the other hand, the lubricating properties of a polymer composed of nonionic monomer units only would not be influenced by 150 mM NaCl either. Thus, ca. 1:1 $(\bar{M}_n(\mathrm{PMEA}))/(\bar{M}_n(\mathrm{PMAA}))$ ratio between MEA and MAA repeating units for **1−4** may be optimal to induce the charge screening effect by additional 150 mM NaCl. Second, despite that the adsorbed mass of **1−6** and **2−2** decreased in HEPES by addition of 150 mM NaCl, their boundary lubricating properties have shown a significant improvement. This is also ascribed to that the adsorption stability of the layer of **1−6**, **2−2**, and **1−4** is enhanced in the presence of 150 mM NaCl due to the reduced electrostatic repulsion between neighboring copolymers, especially under tribostress; this observation again confirms that the most important parameter in determining the efficacy of boundary lubrication is the adsorption stability rather than adsorbed amount.[32] Third, in contrast, the diblock copolymer **3−2**, which has a comparable composition and displayed comparable adsorption behavior with the two graft copolymers **1−6** and **2−2** in HEPES with low ionic strength, did not improve its lubricating behavior at 150 mM NaCl as effectively as the two graft copolymers. A simple comparison with the graft copolymers (**1−6** and **2−2**) is not valid due to somewhat different $(\bar{M}_n(\mathrm{PMEA}))/(\bar{M}_n(\mathrm{PMAA}))$ ratio and the molecular weights. Nevertheless, it is very likely that the anchoring mechanism of a graft copolymer is superior to that of a diblock copolymer, as was mentioned in the Introduction, and could be a significant contributing factor to better lubricating properties of the grafts **1−6** and **2−2** than the diblock **3−2** in HEPES buffer at the same physiological salt concentration.

CONCLUSIONS

In summary, we have presented the synthetic routes for the preparation of amphiphilic anionic and cationic graft copolymers. This library of multifunctional amphiphiles was built by combination of controlled polymerization methods—RAFT polymerization and ATRP—and the subsequent mild deprotection reaction. Thus, RAFT copolymerization of HEMA and Br^{i}BuEMA afforded well-defined ATRP macroinitiators, from which *t*BMA, MEA and *t*BMA, and MEA and DMAEMA were grafted by ATRP. Fairly good control over the composition of the graft copolymers was attained allowing synthesis of the similar architectures with varying hydrophilic/hydrophobic content. Fine-tuning of the comonomer ratios facilitated systematic investigation of the influence of the macromolecular topology and composition on surface adsorption and lubricating properties. The anionic **1−2**, **1−4**, **1−8**, and cationic **2−3** graft copolymers, P(Br^{i}BuEMA$_8$-*co*-HEMA$_{37}$)-*g*-P(MEA$_x$-*co*-MAA$_y$) and P(Br^{i}BuEMA$_8$-*co*-HEMA$_{77}$)-*g*-P(MEA-*co*-DMAEMA), respectively, did not exhibit significant adsorption on the PDMS surface at neutral conditions, which was reflected in poor lubricity at the PDMS−PDMS sliding interface. Despite the significant adsorption of the anionic graft copolymers **1−6**, **2−2**, and block copolymer **3−2**, their lubricating performance was not good enough at low-salt conditions. For the three graft copolymers, **1−4**, **1−6**, and **2−2**, the lubricity improved by addition of 150 mM NaCl due to the reduced intra- and intermolecular electrostatic repulsion between P(MEA-*co*-MAA) side chains. The lubricating efficacy of three graft copolymers were far better than those of diblock **3−2**, P(MEA-*co*-MAA)-*b*-PHEMA, suggesting superior anchoring and stability of the anionic graft copolymers on a hydrophobic PDMS surface over that of comparable diblock copolymer counterpart at physiological ion strength. Furthermore, "dilution" of the charges across the grafted chains by balancing neutral/charged repeating units also plays a pivotal role in improving the aqueous lubrication properties of free charged copolymers at physiological ionic strength.

ASSOCIATED CONTENT

Supporting Information

Surface adsorption profiles. This material is available free of charge via the Internet at http://pubs.acs.org.

AUTHOR INFORMATION

Corresponding Authors

*(S.H.) E-mail: sh@kt.dtu.dk.
*(S.L.) E-mail: seele@mek.dtu.dk.

Author Contributions

‡These authors contributed equally.

The manuscript was written through contributions of all authors. All authors have given approval to the final version of the manuscript.

Notes

The authors declare no competing financial interest.

ACKNOWLEDGMENTS

Authors appreciate greatly the Danish Council for Independent Research (DFF), Technology and Production Sciences (FTP) (10-082707), for the financial support.

REFERENCES

(1) (a) Braunecker, W. A.; Matyjaszewski, K. *Prog. Polym. Sci.* **2007**, *32*, 93−146. (b) Matyjaszewski, K.; Tsarevsky, N. V. *Nat. Chem.* **2009**, *1*, 276−288. (c) Matyjaszewski, K. *Macromolecules* **2012**, *45*, 4015−4039.

(2) (a) Moad, G.; Rizzardo, E.; Thang, S. H. *Aust. J. Chem.* **2012**, *65*, 985−1076. (b) Barner, L.; Davis, T. P.; Stenzel, M. H.; Barner-Kowollik, C. *Macromol. Rapid Commun.* **2007**, *28*, 539−559.

(3) Javakhishvili, I.; Kasama, T.; Jankova, K.; Hvilsted, S. *Chem. Commun.* **2013**, *49*, 4803−4805.

(4) Javakhishvili, I.; Jankova, K.; Hvilsted, S. *Polym. Chem.* **2013**, *4*, 662−668.

(5) Javakhishvili, I.; Tanaka, M.; Ogura, K.; Jankova, K.; Hvilsted, S. *Macromol. Rapid Commun.* **2012**, *33*, 319−325.

(6) (a) Tanaka, M.; Mochizuki, A.; Ishii, N.; Motomura, T.; Hatakeyama, T. *Biomacromolecules* **2002**, *3*, 36−41. (b) Tanaka, M. *Bio-Med. Mater. Eng.* **2004**, *14*, 427−438.

(7) Lee, S.; Spencer, N. D. *Science* **2008**, *319*, 575−576.

(8) (a) Raviv, U.; Frey, J.; Sak, R.; Laurat, P.; Tadmor, R.; Klein, J. *Langmuir* **2002**, *18*, 7482−7495. (b) Klein, J. *Friction 1* **2013**, 1−23. (c) Raviv, U.; Giasson, S.; Kampf, N.; Gohy, J. F.; Jérôme, R.; Klein, J. *Nature* **2003**, *425*, 163−165.

(9) Chawla, K.; Lee, S.; Lee, B. P.; Dalsin, J. L.; Messersmith, P. B.; Spencer, N. D. *J. Biomed. Mater. Res. A* **2008**, *90*, 742−749.

(10) Heeb, R.; Bielecki, R. M.; Lee, S.; Spencer, N. D. *Macromolecules* **2009**, *42*, 9124−9132.

(11) Chen, M.; Briscoe, W. H.; Armes, S. P.; Klein, J. *Science* **2009**, *323*, 1698−1701.
(12) Lee, S.; Muller, M.; Heeb, R.; Zurcher, S.; Tosatti, S.; Heinrich, M.; Amstad, F.; Pechmann, S.; Spencer, N. D. *Tribol. Lett.* **2006**, *24*, 217−223.
(13) Røn, T.; Javakhishvili, I.; Jankova, K.; Hvilsted, S.; Lee, S. *Langmuir* **2013**, *29*, 7782−7792.
(14) Lee, S.; Spencer, N. D. *Langmuir* **2008**, *24*, 9479−9488.
(15) (a) Perrino, C.; Lee, S.; Choi, S. W.; Maruyama, A.; Spencer, N. D. *Langmuir* **2008**, *24*, 8850−8856. (b) Muller, M.; Lee, S.; Spikes, H. A.; Spencer, N. D. *Tribol. Lett.* **2003**, *15*, 395−405. (c) Naderi, A.; Iruthayaraj, J.; Vareikis, A.; Makuska, R.; Claesson, P. M. *Langmuir* **2007**, *23*, 12222−12232.
(16) (a) Bijsterbosch, H. D.; Stuart, M. A.; Fleer, G. J. *J. Colloid Interface Sci.* **1999**, *210*, 37−42. (b) Rieger, J.; Passirani, C.; Benoit, J.-P.; Van Butsele, K.; Jérôme, R.; Jérôme, C. *Adv. Funct. Mater.* **2006**, *16*, 1506−1514.
(17) Brandrup, J.; Immergut, E. H.; Grulke, E. A. *Polymer Handbook*, 4th ed.; John Wiley & Sons, Inc.: New York, 1999.
(18) Katchalsky, A.; Spitnik, P. *J. Polym. Sci.* **1947**, *2*, 432−446.
(19) Coelho, J. F. J.; Gois, J.; Fonseca, A. C.; Carvalho, R. A.; Popov, A. V.; Percec, V.; Gil, M. H. *J. Polym. Sci., Part A: Polym. Chem.* **2009**, *47*, 4454−4463.
(20) de Feijter, J. A.; Benjamins, J.; Veer, F. A. *Biopolymers* **1978**, *17*, 1759−1772.
(21) Refractive index increment of PHEMA is estimated by extrapolating from the dioxane-water mixtures.
(22) **1**−**2**: 0.217. **1**−**4**: 0.146. **1**−**6**: 0.125. **1**−**8**: 0.101. **2**−**2**: 0.150. **2**−**3**: 0.118. **3**−**2**: 0.119. **3**−**3**: 0.119.
(23) Schmid, H.; Michel, B. *Macromolecules* **2000**, *33*, 3042−3049.
(24) Theodoly, O.; Jacquin, M.; Muller, P.; Chhun, S. *Langmuir* **2009**, *25*, 781−793.
(25) The average chain-chain distance (L) on the surface was calculated by assuming a 2-dimensional hexagonal packing with 1 chain + 6 × (1/3 chain) = 3 chains per unit hexagon. L was isolated from the relation $[(X \text{ chains})/1 \text{ nm}^2] = [(3 \text{ chains})/(\text{area of unit hexagon})] = [(3 \text{ chains})/(3 \times 3^{1/2} \times 2^{-1}L^2)]$, thus $L = \{[2 \times (3 \text{ chains})]/[3 \times 3^{1/2} \times (X \text{ chains/nm}^2)]\}^{1/2}$.
(26) Rubinstein, M.; Colby, R. H. *Polymer Physics*: Oxford University Press, Inc.: Oxford, U.K., 2003.
(27) Abrahams, T.; Giasson, S.; Gohy, J. F.; Jérôme, R.; Müller, B.; Stamm, M. *Macromolecules* **2000**, *33*, 6051−6059.
(28) Dobrynin, A. V.; Rubinstein, M. *Prog. Polym. Sci.* **2005**, *30*, 1049−1118.
(29) Ragnetti, M.; Oberthür, R. C. *Colloid Polym. Sci.* **1986**, *264*, 32−45.
(30) Alhoranta, A. M.; Lehtinen, J. K.; Urtti, A. O.; Butcher, S. J.; Aseyev, V. O.; Tenhu, H. J. *Biomacromolecules* **2011**, *12*, 3213−3222.
(31) Nalam, P. C.; Clasohm, J. N.; Mashaghi, A.; Spencer, N. D. *Tribol. Lett.* **2010**, *37*, 541−552.
(32) Lee, S.; Müller, M.; Rezwan, K.; Spencer, N. D. *Langmuir* **2005**, *21*, 8344−8353.

4.4 Aqueous Lubricating Properties of Charged (ABC) and Neutral (ABA) Triblock Copolymer Chains.

Submitted to the journal Polymer, 2014. See next pages.

Aqueous Lubricating Properties of Charged (ABC) and Neutral (ABA) Triblock Copolymer Chains

Troels Røn,[a] Irakli Javakhishvili,[b] Navin J. Patil,[c] Katja Jankova,[b] Bruno Zappone,[d] Søren Hvilsted[b]

and Seunghwan Lee[a]

[a]Department of Mechanical Engineering, and

[b]Department of Chemical and Biochemical Engineering, Danish Polymer Centre, Technical University of Denmark, DK-2800, Kongens Lyngby, Denmark,

[c]Dipartimento di Fisica, Università della Calabria, Cubo 33/B, 87036 Rende (CS), Italy,

[d]CNR-IPCF and LICRYL, c/o Università della Calabria, Cubo 33/B, 87036 Rende (CS), Italy

Keywords: Lubrication, Triblock Copolymer, Amphiphilic, ATRP, “Click” Chemistry, Polymer Brushes, Interface.

Abstract

Application of charged polymer chains as additives for lubricating neutral surfaces in aqueous environment, especially via polymer physisorption, is generally impeded by the electrostatic repulsion between adjacent polymers on the surface. In this study, we have investigated the adsorption and aqueous lubricating properties of an amphiphilic triblock copolymer, comprised of a neutral poly(ethylene glycol) (PEG) block, a hydrophobic poly(2-methoxyethyl acrylate) (PMEA) block, and a charged poly(methacrylic acid) (PMAA) block, namely PEG-*b*-PMEA-*b*-PMAA. After adsorption onto a nonpolar hydrophobic surface from aqueous solution, an equal and homogeneous mixture of neutral PEG and charged PMAA chains is formed on the surface, with an adsorbed polymer mass comparable to its fully neutral counterpart, PEG-*b*-PMEA-*b*-PEG. The lubricity of PEG-*b*-PMEA-*b*-PMAA showed significant improvement compared to fully charged polymer chains, e.g. poly(acrylic acid)-*block*-poly(2-methoxyethyl acrylate) (PAA-*b*-PMEA), which is attributed to dilution of charged moieties on the surface and subsequent improvement of the lubricating film stability.

1. Introduction

Functionalization of surfaces with polymer brushes has previously shown to afford desirable low friction/low shear strength interfaces when the polymer brushes are fully stretched in good or θ solvent as, for example, hydrophilic brushes in water.[1,2] Water-based lubrication is desirable from an environmental and biocompatibility perspective as compared to mineral oils or greases. Among hydrophilic polymer chains in aqueous environment, surface-anchored polyelectrolyte brushes showed superior[3,4] lubricity over neutral ones[5,6] primarily due to the incorporation of a large amount of counterions within polymer brush layers, which contributes to the improved osmotic pressure at the opposing interface. However, since covalently-immobilized polymer chains are exposed to a risk of irreversible rupture from the underlying substrates by shear stress, its practical application is limited to low-pressure contacts only. In this context, it is a tempting idea to introduce 'self-healing', physisorbed grafting-to approach,[7] which ensures a persistent recovery of the lubricating film as long as excess polymers are present in bulk solution. As shown in our previous study,[8] however, application of amphiphilic diblock copolymers composed of neutral-*b*-polyelectrolyte blocks, such as poly(acrylic acid)-*block*-polystyrene (PAA-*b*-PS) and poly(acrylic acid)-*block*-poly(2-methoxyethyl acrylate) (PAA-*b*-PMEA), revealed lubricating capabilities inferior to the entirely neutral counterparts, such as poly(ethylene glycol)-*block*-polystyrene (PEG-*b*-PS) or poly(ethylene glycol)-*block*-poly(2-methoxyethyl acrylate) (PEG-*b*-PMEA) at a non-polar shearing interface.[8] This was primarily attributed to the retarded adsorption of polyelectrolyte-based diblock copolymers onto non-polar surfaces or fast desorption due to compressive tribostress, arising from the electrostatic repulsion between neighboring copolymers on the same surface. Nevertheless, the importance of charged moieties for aqueous lubrication is evident from biological tribosystems where water is employed as a base lubricant; many biological tribosystems employ charged macromolecules to reduce friction during movement, e.g. in synovial joints.[9] This study sets out under a hypothesis that

the major reason for the ineffective aqueous lubricating capabilities of the diblock copolymers mentioned above is too high concentration of charged moieties accumulating on the substrate surface. Thus, "dilution" of the charged polyelectrolyte brush buoyant block may improve the lubricity of physisorbed "self-healing" polymer in aqueous conditions.

While various approaches can be exploited to dilute the charged moieties along polyelectrolytes, in this study, we have devised an amphiphilic, triblock copolymer comprised of a hydrophobic PMEA anchoring block in the middle and charged poly(methacrylic acid) (PMAA) and neutral PEG chains as two buoyant blocks (Scheme 1). Thus, adsorption of the triblock copolymer, PEG-*b*-PMEA-*b*-PMAA, facilitates the grafting of charged and neutral polymer chains at a 1:1 ratio on surface, effectively diluting the charged moieties into a half compared to diblock copolymers, such as PAA-*b*-PMEA. As a reference, fully neutral PEG-*b*-PMEA-*b*-PEG triblock copolymer was also synthesized and compared (Scheme 1). The molecular weights of the copolymers were roughly 5kDa-*b*-7kDa-*b*-5kDa for both triblock copolymers. We envision that the "dilution" of charged buoyant blocks with PEG blocks will reduce the electrostatic repulsion between polyelectrolyte brushes anchored on the same substrate, hence improve film stability and lubricity, yet without losing the characteristics of polyelectrolytes. The surface forces and lubricating properties of the two triblock copolymers have been studied in both micro- and macro-contact scales by means of surface force apparatus (SFA), colloidal probe atomic force microscopy (AFM), and pin-on-disk tribometry, respectively. Surface adsorption was studied by optical waveguide lightmode spectroscopy (OWLS).

2. Materials and Methods

Polymer synthesis. All reagents and solvents were purified by conventional methods. Alkyne end-tagged PMAA was prepared in two steps: first the atom transfer radical polymerization (ATRP)[10] of

tert-butyl methacrylate (*t*BMA) initiated by 3-(trimethylsilyl)propargyl bromide[11,12] resulted in a well-defined P*t*BMA, and then trimethylsilyl as well as *tert*-butyl protecting groups were removed simultaneously[12,13,14] to obtain alkynyl-PMAA. In parallel, mPEG-alkyne was synthesized by coupling mPEG-OH with pentynoic acid in the presence of *N*,*N*′-dicyclohexylcarbodiimide (DCC)/4-(dimethylamino)pyridine (DMAP) catalytic system.[15] The diblock copolymer mPEG-*b*-PMEA was obtained by ATRP as reported before.[13,16] Terminal bromide was replaced by azide in a nucleophilic substitution reaction employing 3 equivalents of NaN_3.[15] The resulting mPEG-*b*-PMEA-N_3 was coupled with either alkynyl-PMAA or mPEG-alkyne in a Cu (I)-mediated "click" reaction.[15,17] 1 – 1.05 equivalents of the alkyne were taken, and the reaction products were used for further analysis after being isolated by precipitation without rigorous purification from the excess reagent. Structural characterization of the intermediate and final products was carried out by FTIR and NMR spectroscopy. Degrees of polymerization were determined by NMR spectroscopy. The polydispersity indices (PDI) were estimated by size exclusion chromatography (SEC) employing tetrahydrofuran (THF) or *N*,*N*′-dimethylformamide (DMF)/LiCl as eluents. The molecular weight characteristics of the triblock copolymers obtained by NMR spectroscopy are 5.0kDa-*b*-7.2kDa-*b*-4.3kDa for PEG-*b*-PMEA-*b*-PMAA and 5.0kDa-*b*-7.2kDa-*b*-5.0kDa for PEG-*b*-PMEA-*b*-PEG.

HEPES buffer. 4-(2-Hydroxyethyl)-1-piperazineethanesulfonic acid (HEPES 1 mM, pH 7.0) buffer solution was prepared by dissolution of HEPES salt (purchased from VWR BDH Prolabo) in Millipore water (resistivity >18 M·Ω) and subsequent adjustment of pH to 7.0 by adding 1.0 M NaOH (aq). HEPES buffer was employed as a base lubricant solution throughout this study.

Polymer solution preparation. The polymers were dissolved in HEPES buffer at a concentration of 0.50 mg·mL^{-1}. pH of the PEG-*b*-PMEA-*b*-PMAA[18] copolymer solutions was adjusted to pH 7 by

addition of 1.0 M NaOH (aq.). The degree of ionization (α) of PMAA block was calculated according to Katchalsky assuming same degree of ionization as of the PMAA homopolymer in solution:[19] inserting pH = 7.0 in the following equation – $pH = 6.50 - 2 \cdot \log((1- \alpha)/\alpha)$ – gives $\alpha = 0.64$.

Surface Adsorption. Adsorption properties of the copolymers from aqueous solutions onto polydimethylsiloxane (PDMS) surfaces were characterized with OWLS by employing OWLS 210 from MicroVacuum Ltd and BioSense 2.6.10 software. A four-layer model consisting of the glass substrate, waveguide layer, adsorbate layer, and covering medium was utilized to calculate the mass uptake on the surface of the waveguide by applying the de Feijter equation:[20]

$$m = d_A \cdot \frac{(n_A - n_C)}{\frac{dn}{dc}} \quad \text{eq. 1}$$

where m designates the mass per unit area, d_A the thickness of the adsorbate layer, n_A the refractive index of the adsorbate layer, n_C the refractive index of the covering medium, and dn/dc the refractive index increment of the adsorbate as a function of the mass density c. The dn/dc of PEG, PMEA, $PMAA^-$ and PMAA is 0.132cm^3/g,[21] 0.060 cm^3/g,[22] 0.260 cm^3/g,[21] and 0.175 cm^3/g,[21] respectively. The dn/dc values of the triblock copolymers were calculated by assuming a linear relationship between the weight fraction of each constituent and its contribution to the total dn/dc value. The dn/dc is 0.102 and 0.127 for PEG-*b*-PMEA-*b*-PEG and PEG-*b*-PMEA-*b*-PMAA, respectively. n_A was calculated by the OWLS software.

In order to emulate the tribopair surface, the OWLS waveguides were coated with a layer of polystyrene (PS), followed by a layer of PDMS. This procedure has previously been described in detail elsewhere.[14] Briefly, waveguides were ultrasonicated in EtOH for 10 min and spin-coated first

with a toluene solution (6.0 $g \cdot L^{-1}$) of a PS with a broad molecular weight distribution at 2500 rpm for 15 sec, and subsequently annealed at 100 °C for 1 h. The PS-modified waveguides were then spin-coated with a Sylgard® 184 PDMS kit mixture (the base component and cross-linker with the 3:1 wt. ratio were dissolved in heptane (0.5 wt. %)) at 2000 rpm for 60 sec. After spin-coating, the waveguides were cured at 70 °C overnight.

Adsorption measurements were performed by employing HEPES buffer (1 mM, pH 7) at a flow rate of 0.1 $mL \cdot min^{-1}$ at 20 °C. The buffer solution was passed through the flow cell until the baseline was stabilized. Then, the polymer solution was flown through the flow cell until a sudden increase in the mass uptake signal was observed, which indicates the onset of surface adsorption of the polymers. The flow of polymer solution was then stopped for ca. 15 min, and the flow was switched back to the polymer-free HEPES buffer. The adsorbed masses were obtained after rinsing the waveguide with the HEPES buffer for a minimum of 10 min. 2-3 measurements were performed for each copolymer solution to give a statistical average. The adsorbed masses and surface densities are shown in Table 1, where the surface densities (σ) are calculated by dividing the adsorbed mass per m^2 with the molar mass of the copolymer and multiplying with $2 \cdot N_A \cdot 10^{-18} \cdot nm^{-2}$, where the factor 2 accounts for the 2 buoyant chains per polymer and N_A is the Avogadro constant. The adsorbed masses are also displayed in Fig. 4.

Surface Force Apparatus (SFA). SFA (Mark III by Surforce LLC, Santa Barbara, CA) was used to measure the normal forces between two curved macroscopic surfaces bearing layers of triblock copolymer adsorbed on hydrophobic surface and interacting across HEPES buffer. Details about the SFA technique can be found in reference.[23] Briefly, two atomically smooth sheets of mica were glued onto cylindrical glass supports with radius $R \approx 2$ cm, facing each other in crossed-cylinder configuration. The geometry around the point of closest approach (contact position) was equivalent

to that of a plane and a sphere of radius R. A multiple-beam optical interferometry technique allowed the measurement of the surface separation distance D at the contact position with a resolution better than 1 nm. A set of cantilever springs and microactuators was used to control the surface movement and measure the normal force F with an accuracy of about 1 μN. The zero distance (D = 0) was determined by measuring the interference fringes obtained for direct contact between bare (uncoated) mica surfaces in clean nitrogen. To create hydrophobic mica surfaces, silanol groups (Si-OH) were activated first by exposing the mica surfaces to UV plasma for 5 min in low vacuum. Activated surfaces were immersed and sonicated in 0.1 % v/v solution in decalin of dichlorodimethyl-siloxane (DCDMS), then rinsed with an abundant amount of EtOH, sonicated again in EtOH for 5 min and dried with clean nitrogen. DCDMS polymerizes and reacts with silanol groups (-SiOH) at the surface in the presence of trace amount of water, creating surface layers similar to PDMS. The contact angle of water on DCDMS-treated mica surfaces was 105 ± 1°. After the treatment, the mica-mica distance at DCDMS-DCDMS contact was found to be $D = 2T_s \approx 6.0$ - 11.0 nm corresponding to twice the thickness T_s = 3.0 - 5.5 nm of a single DCDMS layer (see also Table 2). AFM images showed that DCDMS-coated mica surfaces had RMS roughness between 0.4 and 0.6 nm, with overall height variation less than 7 nm over an area of a few μm² (AFM image of DCDMS coated mica in provided in the Supporting Information Fig. S3). The triblock copolymers were left adsorbing on the surfaces for 2 h from an 80 μL droplet of polymer solution. Force measurements were started after rinsing the surfaces with protein-free HEPES solution, unless otherwise specified.

For each SFA experiment, at least two distant contact positions were selected. For each of them, the force measurements were repeated at least twice by approaching, bringing in contact and separating the polymer-coated surfaces. To characterize the force curves (F *vs.* D) in the presence of hysteresis, three layer thicknesses were defined (Table 2). Firstly, $T_{max} = (D_{max} - T_s) / 2$ was calculated as half the distance D_{max} - T_s between DCDMS coatings below which the repulsive force due to

polymer coating overlap increased above the noise level (F/R >0.05 mN/m) during surface approach. Table 2 shows the maximum value of T_{max}, measured during the first approach at a given contact position, and corresponds to the polymer layer thickness before compression. Secondly, $T_{min} < T_{max}$ was calculated as half the DCDMS-DCDMS distance above which the force decreased below the noise level upon retraction. Table 2 shows the value of T_{min} measured after completing a few runs at the same contact position. Finally, T_h, was the hard-wall thickness, defined as the DCDMS-DCDMS distance below which large variations of the applied force produced negligible variation of the layer thickness. T_h was the same upon approaching and retracting the surfaces, and was measured at a load level F/R = 8 - 10 mN·m^{-1}.

Atomic Force Microscopy (AFM). Microscale friction force measurements were conducted using a Vecco Nano Scope IIIa AFM running v. 5.30r3.sr3 software. A silicon AFM probe with rectangular cantilever was employed ('NCHV', Bruker, CA). The cantilever's normal spring constant was determined by thermal tune measurements of the resonance by fitting the resonance peak with Mathematica software to obtain the frequency and quality factor. This data along with the cantilever width and length was applied in Sader's method[24] to calculate the normal spring constant (k_{norm}) of 47.0 ± 1.7 N·m^{-1} from the average of 3 different cantilevers without colloidal spheres. The effective normal spring constants with colloidal spheres were ca. 150 N·m^{-1} due to the position of the sphere on the cantilever. The torsional deflection sensitivity was obtained by bumping a cantilever attached with a 52.5 μm diameter colloidal polyethylene (PE) sphere against a vertical 'wall' made by an AFM probe chip glued onto a glass slide. The torsional spring constant was deduced by 1) isolating the thickness (t) from the following expression[25] for rectangular cantilevers, $k_{norm} = Et^3w/(4L)$, where E, w and L are the Young's modulus of the material, and width and length of the cantilever; this gave a thickness of 4.33 ± 0.04 μm. 2) shear modulus and thickness of the cantilever were applied in the

approximated formula of Sader[26] stipulated by Álvarez-Asencio et al.;[27] a torsional spring constant of $4.68 \cdot 10^{-7}$ Nm was obtained for a cantilever with width of 40.4 μm and length of 122.1 μm. 112.4 GPa and 43.9 GPa were employed for Young's and shear moduli of silicon in the calculations.[28] PE colloidal spheres (Cospheric, CPMS-0.96, Santa Barbara, CA) were glued onto the cantilever by using a micromanipulator, etch-sharpened tungsten thread, and epoxy glue (DANA LIM, Epoxy Universal 335, Denmark). An optical microscope image of the glued sphere on cantilever is provided in the Supporting Information (Fig. S1). PE spheres were used as colloidal counter surface to PDMS due to the commercial availability and hydrophobic nature with a surface tension of 35.7 $mJ \cdot m^{-2}$.[21] Prior to friction measurements, topography and friction images over 20 μm × 20 μm area were obtained first, and very smooth morphology and homogeneous frictional properties in this area were confirmed. Then, friction forces were characterized by scanning the colloidal tip/cantilever assembly on the sample surface in *x*-axis direction over 20 μm (90° with respect to the cantilever) by disabling *y*-axis scanning. Friction values were defined from a half of the difference between trace and retrace scans in a friction loop. For an average friction value, 5 random readings were obtained at each load. The load was varied at 0.25 V increments up to 3 V (corresponding to ca. 12 ± 0.5 μN) and then decreased until pull off was observed. Prior to the start of friction measurements, the PE sphere was rubbed against the PDMS substrate in order to run-in the contact. The sliding speed was 12 $\mu m \cdot s^{-1}$. Error bars in friction vs. load plots designate standard deviation from the average of multiple friction force measurements. The applied polymer solutions were filtered through a 5 μm pore size filter (cellulose acetate) before measurement. The friction measurements were performed in polymer solution without rinsing. Silica spheres (KOBO, MSS-500, Labège, France) were glued onto the cantilevers and UV treated 10 min before measurements. For rinsing control experiment (section 3.4), the tribopair was PDMS slab vs. PE sphere (Ø = 34 μm) glued onto a NCHV cantilever. The same cantilever with PE sphere was used in all experiments shown in Fig. 8. A fixed load of 1.2 μN was

applied and two macroscopically distant scanning lines were selected to confirm statistical validity. The sliding speed was 12 μm·s^{-1} over a scan distance of 20 μm. In this experiment, the tribopair was first subjected to the polymer solution for 15 min and continuously slid against each other during which the frictional responses were recorded every 5 min. Then, the substrates were rinsed gently with HEPES buffer, thus leaving a layer of strongly bound polymers only on the PDMS surface. With a restart of the sliding contacts of the tribopair in HEPES buffer, the frictional responses were recorded at 5 min intervals for another 15 min. Prior to the measurements with polymer solution, the frictional response of the tribopair in HEPES buffer were recorded as a reference.

Pin-on-disk tribometry. The macroscale lubricating capabilities of the triblock copolymers in an aqueous environment were assessed by a pin-on-disc tribometer (CSM Instruments with 4.4M software, Peseux, Switzerland). The range of sliding speed was from 100 to 0.25 mm·s^{-1}. The load was controlled by applying dead weights on the pin. The friction coefficient (μ) was calculated as $\mu = F_{\text{Friction}}/F_{\text{Load}}$. The tribopair in low contact pressure regime was self-mated PDMS, where the load in all experiments was 5 N on PDMS pin (R = 3 mm), giving a contact pressure of 0.38 MPa (Hertzian contact, E= 2.00 MPa, Poisson's ratio of 0.5).[29] Oxidized PDMS (oxPDMS) pins were obtained by air plasma treatment of PDMS pins for 2 min at 29 W in a plasma cleaner/sterilizer (Harrick Plasma, Ithaca, NY), and used for pin-on-disk experiment with oxPDMS pin against PDMS disc. The tribopair in high contact pressure regime was composed of DCDMS-functionalized Si_3N_4 ball (R = 3 mm) and PDMS-spin-coated glass slides, giving a Hertizan contact pressure of 4.94 MPa at 1 N load.[30] All the tribological experiments were conducted at room temperature (RT). The number of laps was 20 for each speed measured. Error bars in μ *vs*. sliding speed plot designate standard deviation from the average over 20 laps of measurements of μ values in the same track.

PDMS discs and pins for low-pressure regime tribological measurements were prepared with a two-component Sylgard® 184 PDMS kit. Base and cross-linker were mixed at 10:1 wt. ratio. The foams generated during mixing were removed by applying vacuum. The mixture was then poured into molds, and cured at 70 °C overnight. Disc (Ø = 30 mm) molds were home-machined aluminum, and Nunc U96 MicroWell plates (Thermo Scientific, Denmark) were used for pin (R = 3.0 mm) molds. For high-pressure regime tribological contacts, a tribopair composed of hydrophobized silicon nitride (Si_3N_4) ball (R = 3.0 mm, Boca Bearing Company, Boynton Beach, FL) and PDMS spin coated glass slide was employed. The Si_3N_4 ball was first ultrasonicated in EtOH, treated in plasma cleaner for 5 min and ultrasonicated in a solution of 5 drops of DCDMS (ca. 100 μL in total) and 25 mL decalin. The hydrophobized Si_3N_4 ball displayed water contact angle of > 90°. Glass slides were first plasma-treated to improve the adhesion, then coated with PDMS mixture in a two-step spin coating of 10 sec at 1000 rpm, followed by 15 sec at 2500 rpm, and cured overnight at 70 °C. The thickness of PDMS films was 38 μm as measured with AFM. The roughness of the PDMS discs (pristine) and pins was assessed by the tapping mode atomic force microscopy (AFM). The root-mean-square roughness (R_q) was measured to be 1.34 and 4.62 nm for discs and pins, respectively, over a 2 μm × 2 μm area. PDMS is hydrophobic with a contact angle of 105.6 ± 2.2° (tested with Millipore water, standard deviation from five measurements) and has a surface tension (γ) of 20 mJ/m^2.[31] In order to remove uncross-linked monomer species, the PDMS substrates used for AFM friction experiments were immersed in toluene for 2 days, then subsequently ultrasonicated in acetone for 30 min, and dried prior to measurements.

3. Results & Discussion

3.1 Polymer Properties and Synthesis

PEG and PMAA were employed to represent neutral and charged hydrophilic polymer chains, respectively, in aqueous conditions. Both polymers are highly hydrophilic and soluble in water.[31] PMEA was chosen as the central anchoring block for its hydrophobicity (surface tension of 36.7 $mJ \cdot m^{-2}$), yet excellent water solubility at low molecular mass.[32,33]

The sequence of reactions leading to the triblock copolymers PEG-*b*-PMEA-*b*-PEG and PEG-*b*-PMEA-*b*-PMAA is depicted in Scheme 1.

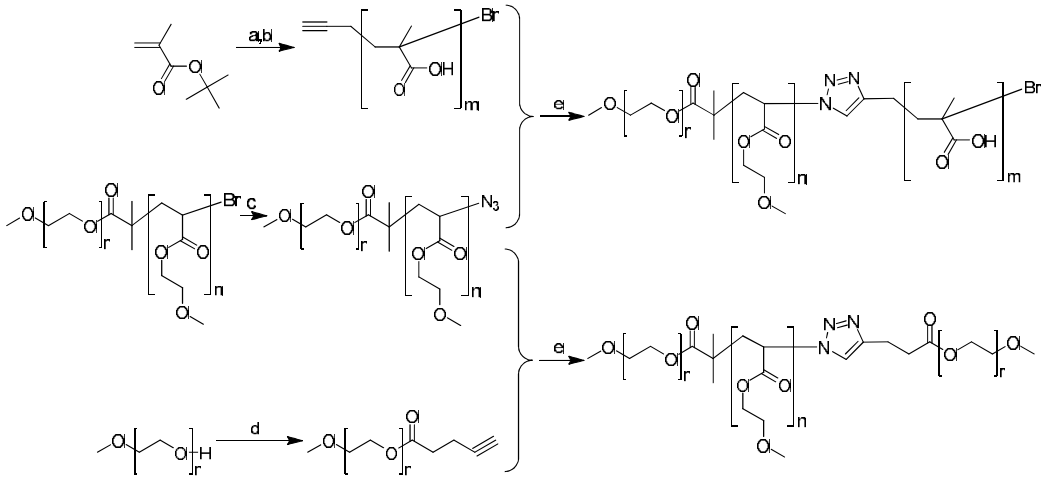

Scheme 1. *Reagents and conditions*: (a) $(CH_3)_3SiC{\equiv}CCH_2Br$, $CuBr/CuBr_2$/4,4′-di(5-nonyl)-2,2′-bipyridine, 60 °C; (b) CF_3COOH, CH_2Cl_2, RT; (c) NaN_3, DMF, 45 °C; (d) $HC{\equiv}C(CH_2)_2COOH$, DCC/DMAP, CH_2Cl_2, RT; (e) CuI, $(C_2H_5)_3N$, THF (or THF/DMF), 35 °C.

Although ^1H NMR experiments were inconclusive in corroborating the triblock copolymer formation in either case, both SEC and FT IR spectroscopy verified successful synthesis of the target macromolecular architectures. While the resonance peaks characteristic to all three blocks are present in the ^1H NMR spectra, the absence of the resonance signal attributed to the triazole proton undermines the argument in favor of the "click" coupling of the diblock copolymer with either PMAA or PEG blocks, but FT IR spectroscopy provides evidence for the near to quantitative consumption

of the azide functional group, which must have reacted to the alkyne counterpart in both cases (Fig. 1).

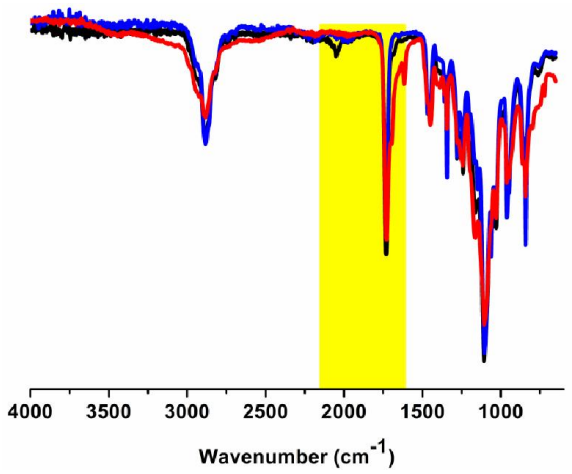

Fig. 1. Overlay of the FT IR spectra of the diblock copolymer PEG-*b*-PMEA-N_3 (black), the triblock copolymer PEG-*b*-PMEA-*b*-PEG (blue), and the triblock copolymer PEG-*b*-PMEA-*b*-PMAA (red).

Thus, the band at about 2050 cm^{-1} that is ascribed to the stretching vibration of the azide group disappears after the "click" reactions. Moreover, a new band corresponding to the stretching vibration of the carboxylic acid C=O in PMAA emerges at around 1700 cm^{-1} as a shoulder of the band attributed to the ester C=O in PMEA at around 1726 cm^{-1} (Fig. 1, red).

Furthermore, SEC trace of PEG-*b*-PMEA-*b*-PEG is shifted to lower elution volume compared to the trace of PEG-*b*-PMEA with a small amount of residual mPEG still present. Due to the difficulties associated with the SEC of polyelectrolytes, no significant shift of the PEG-*b*-PMEA-*b*-PMAA trace is observed when using DMF/LiCl as eluent. However, when the SEC system with THF as eluent is employed, the trace of PEG-*b*-PMEA-*b*-PMAA substantially differs from that of the diblock – it is shifted to the higher elution volume with the PDI = 1.23 being still fairly low (Fig. 2). This counterintuitive shift may be ascribed to the interaction of the PMAA block with the SEC system's columns, and thus indirectly supports the argument favoring the triblock formation.

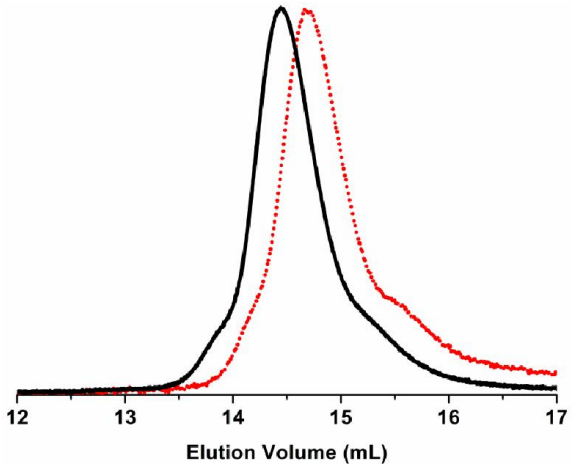

Fig. 2. Overlay of the SEC traces of the diblock copolymer PEG-*b*-PMEA-N_3 (solid) and the triblock copolymer PEG-*b*-PMEA-*b*-PMAA (dotted). THF was employed as the eluent.

3.2 Surface adsorption

Fig. 3 shows representative surface adsorption profiles of the two different triblock copolymers as characterized by OWLS. Both polymers display fast adsorption kinetics with ca. 80% of the adsorption completed after only a few minutes.

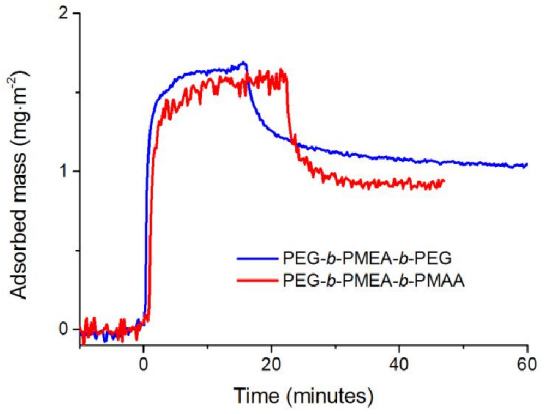

Fig. 3. Examples of mass uptake measurements of the triblock copolymers (0.50 mg·mL^{-1} in HEPES buffer (1 mM, pH 7.0)) by OWLS. The surface of the OWLS sensor chip is coated with an ultrathin layer of PS + PDMS. The adsorption kinetics is fast for both copolymers, with 80% of the maximum adsorption reached within ca. 2 min and with plateau after ca. 15-20 min. The drop in the curves is due to rinsing with the buffer solution, thereby removing non-adsorbed copolymer at the proximity of the water-PDMS interface.

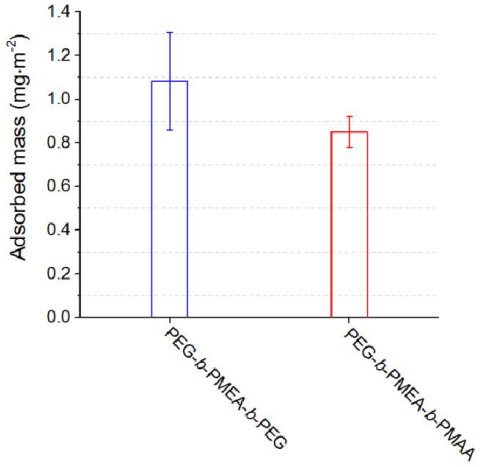

Fig. 4. Adsorbed masses per unit area of the copolymers (mg·m^{-2}) as measured by OWLS. The substrate was PS + PDMS-coated OWLS waveguide. The concentration of the triblock copolymers was 0.50 mg·mL^{-1} in HEPES buffer (1 mM, pH 7). Error bars designate standard deviation from the average values.

Table 1: Adsorbed masses of PEG-*b*-PMEA-*b*-PEG and PEG-*b*-PMEA-*b*-PMAA with calculated buoyant block density, lateral spacing, packing ratio, brush height, and radius of gyration.

Polymer	Adsorbed mass m (mg·m^{-2})	Buoyant block surface density σ (nm^{-2})	Radius of gyration R_F (nm)	Lateral spacing S (nm)	Packing ratio $S/2R_F$	Brush height H (nm)
PEG-*b*-PMEA-*b*-PEG	1.08 ± 0.22	0.076 ± 0.016	9.6	3.9 ± 0.5	0.20 ± 0.03	18.5
PEG-*b*-PMEA-*b*-PMAA	0.85 ± 0.07	0.062 ± 0.006	7.5	4.3 ± 0.2	0.29 ± 0.01	12.0

The adsorbed masses of the two polymers were statistically indistinguishable, 1.08 ± 0.22 and 0.85 ± 0.07 mg·m^{-2} for PEG-*b*-PMEA-*b*-PEG and PEG-*b*-PMEA-*b*-PMAA, respectively (Fig. 4). Under the assumption of the formation of a monolayer, the surface densities of buoyant polymer chains (σ) of the two copolymers are calculated to be 0.076 ± 0.016 nm^{-2} and 0.062 ± 0.006 nm^{-2} (Table 1). The

similar adsorbed masses from the two copolymers show that the adsorption of PEG-*b*-PMEA-*b*-PMAA onto PDMS substrate is apparently not impeded by the electrostatic repulsion between charged PMAA chains on nonpolar PDMS substrate, as in the case of its entirely neutral counterpart. The lateral spacing (*S*) between the buoyant polymer chains on surface is calculated by the following equation under an assumption of hexagonal packing:

$$S = \left\{ \frac{6}{3^{3/2} \cdot \mathrm{x}} \right\}^{1/2} \qquad \text{eq. 2}$$

where x is the number of buoyant blocks per nm^{-2}. For PEG-*b*-PMEA-*b*-PEG, $S = 3.9 \pm 0.5$ nm and for PEG-*b*-PMEA-*b*-PMAA, $S = 4.3 \pm 0.2$ nm. In good solvent for both PEG and PMAA, such as water, the Flory radius of gyration (R_F) of the buoyant blocks was calculated by assuming a Kuhn-length of 1.1 nm and 1.57 nm for PEG[34] and PMAA,[35] thus giving $R_F = 9.6$ nm for PEG and $R_F = 5.5$ nm for PMAA, respectively, by using the following formula:[34]

$$R_F \approx b \cdot N^{3/5} \qquad \text{eq. 3}$$

The R_F for PEG-*b*-PMEA-*b*-PMAA reported in Table 1, i.e. 7.5 nm, is the average R_F of one PEG chain and one PMAA chain. The degree of polymerization of PEG and PMAA are 114 and 50, respectively, explaining the relative difference in R_F. The ratios of $S/2R_F$ for PEG-*b*-PMEA-*b*-PEG and PEG-*b*-PMEA-*b*-PMAA are 0.20 ± 0.03 and 0.29 ± 0.01, respectively.[36] Despite the similar adsorbed masses for the two copolymers, somewhat lower $S/2R_F$ ratio for PEG-*b*-PMEA-*b*-PEG compared to that of PEG-*b*-PMEA-*b*-PMAA is observed. In other words, relatively more stretched neutral PEG chains are expected to form from PEG-*b*-PMEA-*b*-PEG compared to the mixture of PEG

and PMAA chains from PEG-*b*-PMEA-*b*-PMAA on the PDMS surface. $S/2R_F$ ratio much lower than 1 suggests that the surface adsorption of PEG-*b*-PMEA-*b*-PEG is strong enough to pack the buoyant blocks so close that their pervaded volumes in solution overlap, thus forming a stretched brush on the PDMS surface.

The scaled height (H) of the brushes in good solvent can be estimated by the following formula:[34]

$$H \approx N \cdot \sigma^{1/3} \cdot b^{5/3}$$

where σ designates the grafting density of the buoyant blocks; $H \approx 18.5$ nm in the case of PEG-*b*-PMEA-*b*-PEG with a grafting density of 0.076 nm^{-2}, and $H \approx 12.0$ nm for and PEG-*b*-PMEA-*b*-PMAA (assuming an average of the brush height for PEG chains of 17.3 nm and the for PMAA chains of 6.7 nm when the grafting density is 0.062 nm^{-2}). Hence, for both triblock copolymers, the brush heights are a bit less than twice the R_F. It is noted that due to the longer PEG chains, PEG chains are expected to be somewhat more protruded than PMAA chains for the PEG-*b*-PMEA-*b*-PMAA film.

3.3 SFA force measurements

The force measured for polymer layers adsorbed on DCDMS-coated mica and interacting across HEPES solution were mainly repulsive and showed a large degree of hysteresis during a cycle of approach/retraction of the surfaces, with a larger thickness measured during approach, T_{max}, than upon retraction, T_{min} (Fig. 5).

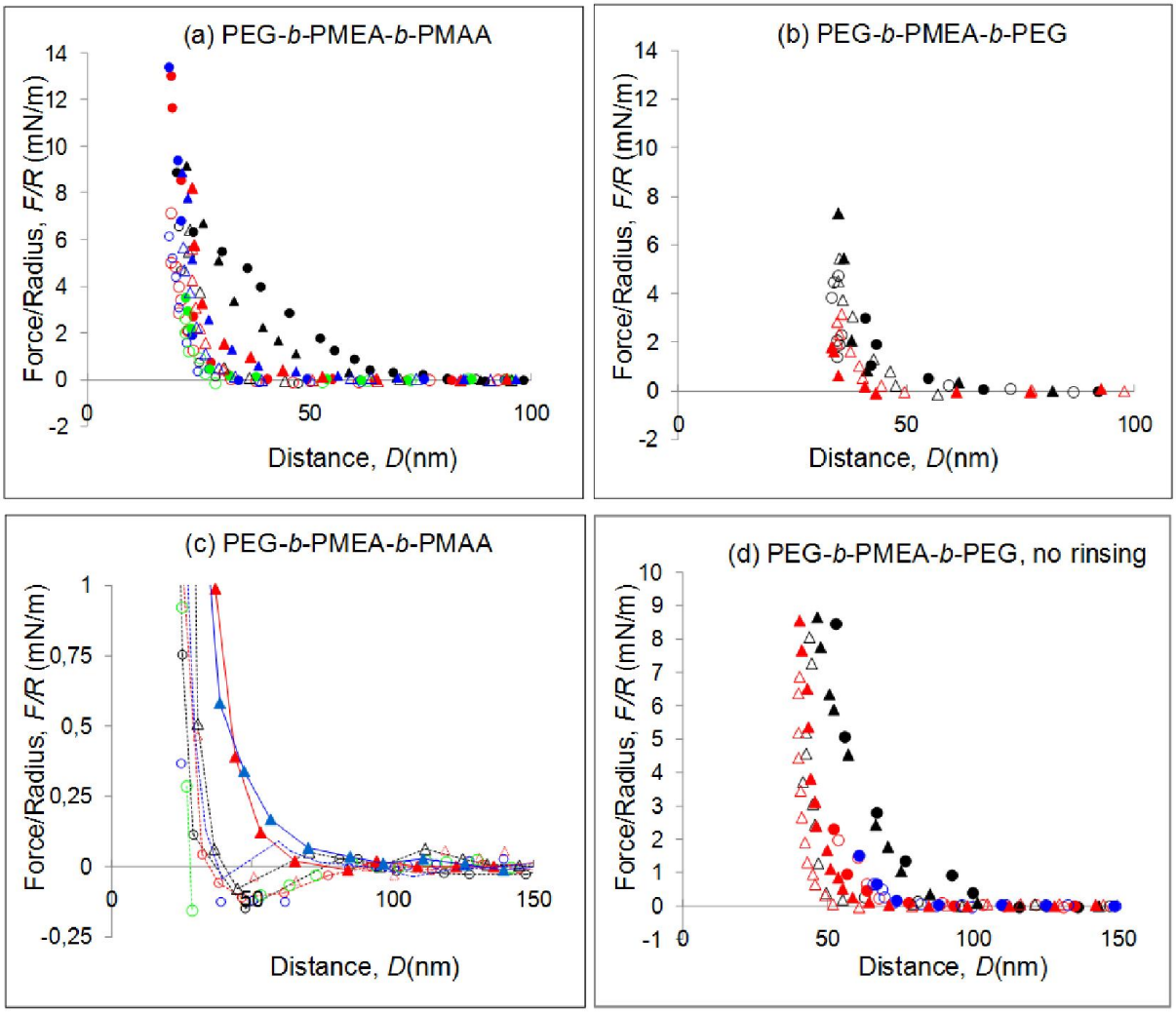

Fig. 5. Normal forces F measured with the SFA between two hydrophobic DCDMS-coated mica surfaces bearing adsorbed polymer layers and interacting across HEPES solution. F is plotted as function of the mica-mica separation distance D and normalized by the surface radius R. Symbols ● and ▲ indicate respectively the first and second contact position considered for a pair of surfaces. Black, red, blue and green colours indicate successive measurements (in chronological order) at the same contact position. Filled and open symbols indicate surface approach and retraction, respectively. (a) PEG-*b*-PMEA-*b*-PMAA. (b) PEG-*b*-PMEA-*b*-PEG. (c) Detail showing a weak adhesion after contact between PEG-*b*-PMEA-*b*-PMAA layers. (d) Large hysteresis observed in the interaction between unrinsed PEG-*b*-PMEA-*b*-PEG layers (polymer in solution).

The repulsive force between PEG-*b*-PMEA-*b*-PMAA layers had a shorter range than between fully neutral PEG-*b*-PMEA-*b*-PEG layers (Fig. 5(a-b) and Table 2), despite the fact that electrostatic repulsions between charged PMAA blocks should increase the repulsion and apparent layer thickness (T_{max}, T_{min}) compared to neutral PEG-*b*-PMEA-*b*-PEG layers.

Table 2: Thickness of a polymer layer as measured with the SFA under different conditions. See text for definitions. All values are in nm.

	T_{max}	T_{min}	T_h	T_s
PEG-*b*-PMEA-*b*-PEG, no rinsing	50	25	20	5.5
PEG-*b*-PMEA-*b*-PEG, after rinsing	39	25	18	3.0
PEG-*b*-PMEA-*b*-PMAA, after rinsing	38	14	10	3.0

The shorter repulsion range observed for PEG-*b*-PMEA-*b*-PMAA reveals the formation of less densely packed and thinner layers than for PEG-*b*-PMEA-*b*-PEG, in line with the OWLS results obtained from PDMS surfaces (Table 1). Moreover, the interaction between PEG-*b*-PMEA-*b*-PEG layers was purely repulsive (Fig. 5(b)), whereas a weak adhesion was observed after contact between PEG-*b*-PMEA-*b*-PMAA layers (Fig. 5(c)). In the former case, the repulsion was due to steric and osmotic interactions during the overlap and confinement of polymer chains adsorbed on opposite surfaces. In the latter case, the surface coverage of PEG-*b*-PMEA-*b*-PMAA was not dense enough to prevent the formation of sparse and/or weak adhesive bonds, either due to polymer interdigitation or attractive hydrophobic interactions between incompletely covered DCDMS substrates. The presence of hysteresis indicates the formation of a multilayer on DCDMS-coated mica, where weakly adsorbed polymers at the outer layer interface could be squeezed out by compression. For PEG-*b*-PMEA-*b*-PEG, we noticed that T_{max} was larger when the surfaces were not rinsed and the polymer molecules could continue adsorbing during the experiment (cf. Figs 5(b) and (d)), whereas T_{min} remained constant (Table 2). Therefore, rinsing removed part of the weakly adsorbed molecules, leaving a layer of molecules strongly adsorbed to the hydrophobic substrate, with thickness T_{min}. For both PEG-*b*-PMEA-*b*-PEG and PEG-*b*-PMEA-*b*-PMAA, the thicknesses T_{min} (Table 2) was much larger than the

calculated radii of gyration, R_F (Table 1). Therefore, the buoyant block were significantly stretched along the surface normal due to their dense packing inside the layers, in agreement with the results obtained for PDMS surfaces ($S/2R_g < 1$, Table 1).

3.4 AFM: Microscale friction experiments

Fig. 6 shows the frictional behavior of the microscale contact of PE sphere (Ø = 29.6 µm) on PDMS substrate in HEPES buffer. The friction force vs. load plots display the typical behavior of hydrophobic contacts with adhesive friction at zero applied load and pull-off occurring at a significantly negative load.

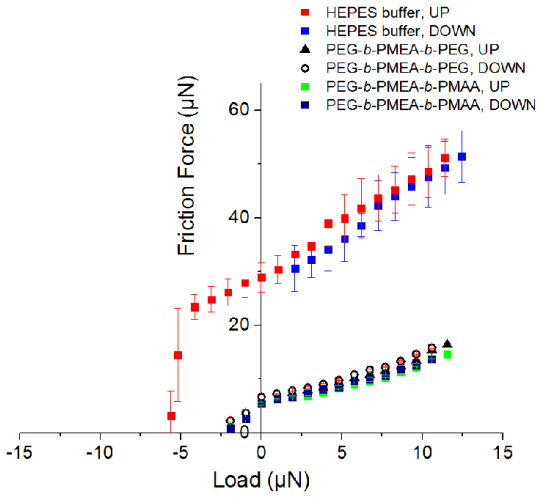

Fig. 6. Friction force vs. load of the sliding contacts of PE sphere (Ø = 29.6 µm) vs. PDMS in the copolymer solutions or HEPES buffer (1 mM, pH 7). Polymer concentration was 0.50 mg·mL^{-1}. Two macroscopically distant spots were studied for each contact. 'UP' designates the friction forces obtained during increasing load and 'DOWN' during decreasing load. The last data point of DOWN series is the last recorded friction loop before pull off.

The soft PDMS contact was modeled according to the Johnson-Kendall-Roberts (JKR) theory[37,38] and by assuming that the last data point before 'pull-off' or critical negative load (L_c) at negative loads to be equivalent to the minimum force needed to separate the PE sphere from the PDMS surface. The average of L_c value from the measurements at two spots in HEPES buffer is 5.6 µN (Fig. 6). The

following three equations describe L_c, contact radius a_0 at zero load, and contact radius a depending on load in the JKR model:[39,40]

$$L_c = -\frac{3}{2}\cdot\pi\cdot\gamma\cdot R \qquad \text{eq. 4}$$

$$a_0 = \left(\frac{6\cdot\pi\cdot\gamma\cdot R^2}{K}\right)^{1/3} \qquad \text{eq. 5}$$

$$a = \left(\frac{R}{K}\cdot\left(\sqrt{L_c} + \sqrt{L_n + L_c}\right)^2\right)^{1/3} \qquad \text{eq. 6}$$

where γ, R, and K represent the work of adhesion, radius of sphere, and the combined elastic modulus of tip and sample as given by $K = 4/3\cdot((1-\nu_1^2)/E_1+(1-\nu_2^2)/E_2)^{-1}$ where ν_x and E_x are respective Poisson's ratios and Young's moduli of the sample and tip. The Young's modulus and Poisson's ratio of PE were 1 GPa and 0.47.[41] The interfacial tension deduced from eq. 4 was γ = 80.3 mN·m^{-1} for the PE sphere vs. PDMS surface contact. This value is in a good agreement with a theoretically predicted work of adhesion between the PDMS and PE surfaces in water: $\gamma = \gamma_{PDMS/water} + \gamma_{PE/water} - \gamma_{PDMS/PE}$ = (43.1 + 43.6 – 5.3) mN·m^{-1} = 81.4 mN·m^{-1}.[31,42] Inserting γ of 80.3 mN·m^{-1} in eq. 5 gives a contact radius of 4.54 μm at zero load. In turn, this gives the contact pressure (P) of 86.4 kPa at zero applied load from $P = L_c/(\pi a_0^2)$. The interfacial shear strength (τ) of the PE vs. PDMS contact was calculated by $\tau = F/A$ by applying the friction force and contact radius at zero load, thus giving 0.45 MPa.

Table 3 shows the calculated (τ) of the PE sphere vs. PDMS slab and PDMS vs. PDMS for pin-on-disk experiments. It is evident that the interfacial shear strengths of the PE vs. PDMS contacts obtained in the triblock copolymer solutions at zero load, $\tau \approx$ 0.08-0.1, are lower compared to the reference values obtained in pure HEPES buffer, τ = 0.45, hence confirming that the triblock copolymers do lubricate the sliding contact of PE sphere vs. PDMS slab.

Table 3: Pull off forces (L_c) and shear strengths (τ) obtained from AFM and pin-on-disk experiments in the copolymer solutions. See text for definitions.

	AFM PE sphere vs. PDMS			**Pin-on-disk** PDMS vs. PDMS	
Polymer/Solution	L_c (μN)	τ, at zero load (MPa)	τ, *at* L_{max} (MPa)	τ, at 50 mm/s (MPa)	τ, at 0.25 mm/s (MPa)
HEPES (1 mM, pH 7.0)	5.6	0.45	0.51	0.40	0.31
PEG-*b*-PMEA-*b*-PEG	1.9	0.10	0.17	0.01	0.01
PEG-*b*-PMEA-*b*-PMAA	1.9	0.08	0.15	0.01	0.02

The lubricity of the polymer solution is also clear at the highest load (L_{max}) with $\tau \approx 0.15$-0.17 in the polymer solutions compared to the reference in pure HEPES buffer, $\tau = 0.51$. Furthermore, the critical negative load needed for pull out of the contact is also smaller in the triblock copolymer solutions, suggesting that the adsorbed polymers help keep the surfaces separated. However, when comparing the two triblock copolymers, the friction response was very similar, although PEG-*b*-PMEA-*b*-PMAA displayed slightly lower shear strength than its entirely neutral counterpart (Table 3). Another set of experiments with another cantilever with PE sphere showed similar results, confirming the reproducibility of the frictional properties as summarized in Table 3. Hence, the AFM friction force data is in good agreement with the data obtained by pin-on-disk tribometry (section 3.5 below), where a small or negligible difference in lubricity between the two triblock copolymers was observed. Nevertheless, the τ values obtained in the triblock copolymer solutions were ca. one order of magnitude higher than those obtained from pin-on-disk tribometry experiments (Table 3). The higher interfacial shear strength observed from PE sphere vs. PDMS contact in AFM experiment could to some extent be attributed to the high surface roughness of the PE sphere, R_q = 76 nm (Fig. S2),[43] possibly causing the asperities of the PE sphere to come into a direct contact with the PDMS substrate. The rough surface of the PE sphere will cause significantly higher local contact pressures, thus

affording easier shearing off of adsorbed polymer at the interface and increasing interfacial friction forces. However, the roughness of the PE sphere does not necessarily decrease the real area of contact judging from the experimentally determined work of adhesion being close to the theoretical value as described above. Furthermore, the sliding speed in the AFM friction experiments is much lower (12 μm/s) than those in the pin-on-disk measurements, hence the formation of slip plane formed by the opposing polymer brushes at higher sliding speeds is retarded, driving the polymer chains to interdigitate at very low sliding speeds and thereby increasing the friction.[44,45] Lastly, the adsorption of the triblock copolymers could be lower onto PE sphere than PDMS surface, which could contribute to lower brush chain density and higher friction forces at the interface as well.

One of the effects expected from the sliding contacts between charged brush-brush layers is improved osmotic pressure arising from the incorporation of a large amount of counterions within the brush layers. Due to the poorly defined adsorption behavior of the copolymers onto PE surface, and additionally due to high surface roughness of PE sphere, this effect may not be realized in the experiment conducted between PE sphere and PDMS surface in the copolymer solution (Fig. 6). In order to provide a negatively charged counter surface against surface-grafted PMAA brushes, the friction vs. load plots employing a silica sphere attached at the end of cantilever were also obtained. The results are shown in Fig. 7. While slightly lower friction forces were observed from PEG-*b*-PMEA-*b*-PMAA compared to PEG-*b*-PMEA-*b*-PEG layers in low load regime (< 5 μN), this difference disappeared completely at higher load regime. A slightly decreased, yet still clearly visible adhesive force in the negative load regime indicates that the adhesion between silica particle and PDMS surface is not completely suppressed by either of the triblock copolymers.

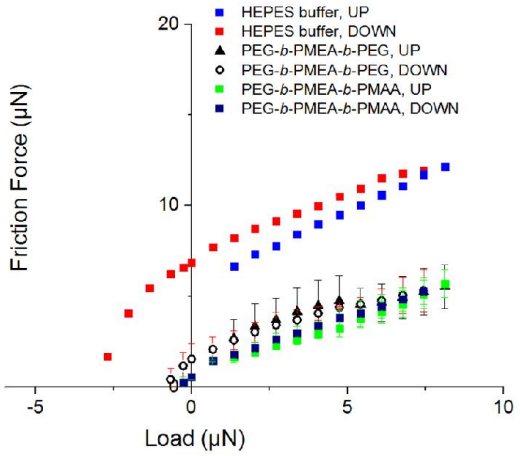

Fig. 7. Friction force vs. load of the sliding contacts of silica sphere (Ø = 20.6 μm) vs. PDMS in the copolymer solutions or HEPES buffer (1 mM, pH 7). Polymer concentration was 0.50 mg·mL^{-1}. Two macroscopically distant spots were studied for each contact. 'UP' designates the friction forces obtained during increasing load and 'DOWN' during decreasing load. The last data point of DOWN series is the last recorded friction loop before pull off.

Lastly, the role of excess polymers in bulk solution in determining the lubricating properties at microscale contacts by AFM was assessed by comparing the frictional forces in the polymer solutions and the repeated measurements after rinsing the excess polymers with HEPES buffer. The contribution of excess polymers for macroscale, cyclic tribological contacts, such as with pin-on-disk tribometry, is generally manifested in helping the reformation of lubricating films, or "self-heal" the contact area as the films are rubbed away from the substrate due to tribostress.[46] The results are presented in Fig. 8. For both copolymers, PEG-*b*-PMEA-*b*-PEG and PEG-*b*-PMEA-*b*-PMAA, the relative frictional responses are in the order of HEPES buffer > copolymer layer after rinsing > copolymer solution in HEPES buffer. Thus, the contribution by excess polymers in bulk solution to enhance the lubricity at the microscale contact between PE sphere and PDMS surface is evident. Higher frictional responses after rinsing suggest that "self-healing" mechanism by excess copolymers may occur on this scale as well. However, persistent frictional responses from the contact obtained after rinsing, which is higher than those in polymer solution, yet lower than those in reference buffer,

suggest that the removal of the lubricating films from the substrate is not significant, presumably due to the low contact pressure.

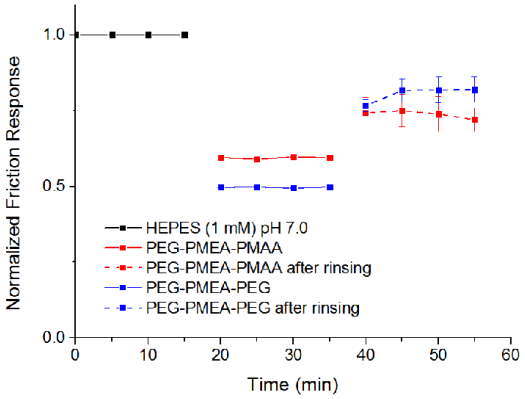

Fig. 8. Comparison of the friction measurements of PEG-*b*-PMEA-*b*-PMAA and PEG-*b*-PMEA-*b*-PEG layers in the respective copolymer solution (0.50 mg·mL^{-1} in HEPES (1 mM, pH 7.0)) vs. in HEPES buffer. Tribopair: PE sphere (Ø = 34 µm) vs. PDMS slab. 20 min of rubbing in polymer solution was followed by rinsing with HEPES buffer and additional 20 min of rubbing. The measured friction response is normalized to lateral friction loop signal when sliding in pure HEPES buffer.

3.5 Pin-on-disc: macroscale friction experiments

Fig. 9 presents the μ vs. speed plots as characterized by pin-on-disc tribometry both in the low (0.38 MPa) and high (4.94 MPa) contact pressure regimes. At the lower contact pressure, the two triblock copolymers showed similar lubricity over the entire speed range. The coefficients of friction were very low, ca. 0.01-0.02, in the entire sliding speed regime with the exception of ca. 0.03 and 0.05 for PEG-*b*-PMEA-*b*-PEG and PEG-*b*-PMEA-*b*-PMAA, respectively, at the slowest speed, 0.25 mm·s^{-1}. At the higher contact pressure, the coefficients of friction were generally higher than at the low contact pressure, namely from $\mu \approx 0.02$ at the highest sliding speeds to $\mu \approx 0.05$ at the lowest sliding speeds. Nevertheless, the coefficients of friction were significantly lower than that of the 1 mM HEPES reference solution with $\mu \approx 0.18$-0.19, and were not distinguishable for the two copolymers. Overall, the lubricating capabilities of the two copolymers were very similar on macroscale contact.

This is significant because the lubrication mechanism in the pin-on-disk tribometry (Fig. 9) is based on repeating cycles of the disruption and reformation of the adsorbed copolymers on tribopairs, and the efficacy of persistent lubricating film formation primarily determines the overall lubricating efficacy in this condition.[7] Thus, comparable lubricating capabilities of the two triblock copolymers imply that the kinetics for the continuous (re)formation of lubricating film for PEG-*b*-PMEA-*b*-PMAA is comparable to that of PEG-*b*-PMEA-*b*-PEG. This is a strong contrast to the polyelectrolyte-hydrophobic diblock copolymers in a previous study,[8] where the copolymers are either not adsorbing or sheared off from the surface too easily. While rapid adsorption kinetics is a requirement for the 'self-healing' behavior of lubricious physisorbed polymer brushes,[7] it is not necessarily a sufficient condition for effective lubrication. As expected, dilution of charged polymer chains into a half in PEG-*b*-PMEA-*b*-PMAA enabled the stability of the lubricating films, compared to its diblock copolymer analogue such as PMEA-*b*-PAA.[8]

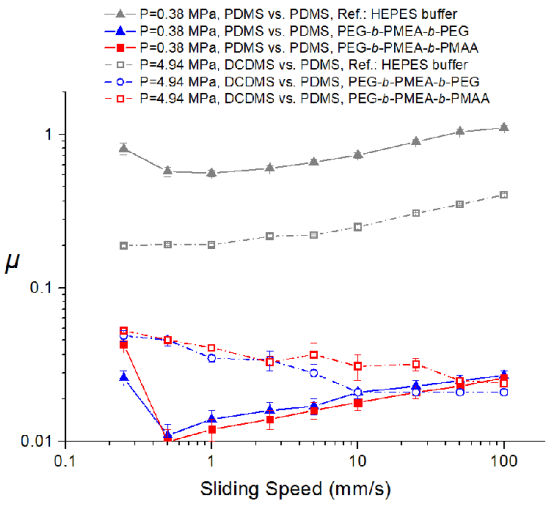

Fig. 9. Friction coefficient (μ) vs. sliding speed plots of the sliding contacts of PDMS vs. PDMS and DCDMS-functionalized Si_3N_4 vs. PDMS lubricated by the triblock copolymer solutions as characterized by pin-on-disc tribometry under a 5 and 1 N load, respectively. The measurements in HEPES buffer (1 mM, pH 7) solution are included as reference. Both triblock copolymers were dissolved in HEPES buffer solution (1 mM, pH 7.0) at the concentration of 0.50 mg·mL^{-1}. The lines connecting the points in the figures are a guide to the eye.

Similarly with the AFM studies (Fig. 7), negatively charged surface was employed as counter-surface for the copolymer layers in pin-on-disk tribometry experiments, in order to investigate if any difference in relative lubricating capabilities of the two triblock copolymers is observed. To this end, plasma-treated PDMS pin was employed since the surface is known to be coated with a thin silica layer due to the oxidation.[47] In Fig. 10, the μ vs. speed plots obtained from the sliding contacts of oxPDMS pin vs. PDMS disc in the copolymer and HEPES buffer solutions are displayed. Due to the strong hydrophilic nature of oxPDMS pin, the μ values in HEPES buffer in high speed regime were nearly indistinguishable even from those in the polymer solutions. With lowering speed, the μ values obtained for the triblock copolymers solutions were clearly lower than for the HEPES reference. While the μ values of PEG-*b*-PMEA-*b*-PMAA is substantially lower than those of PEG-*b*-PMEA-*b*-PEG at 0.5 mm/s in the data presented in Fig. 10, further testing at this speed for more than 20 laps showed no statistical difference.

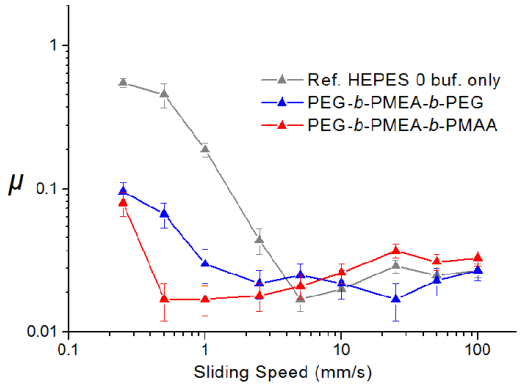

Fig. 10. Friction coefficient (μ) vs. sliding speed plots of the sliding contacts of oxPDMS pin vs. PDMS disc at 5 N load as measured by pin-on-disk tribometer. Both triblock copolymers were dissolved in HEPES buffer solution (1 mM, pH 7.0) at the concentration of 0.50 mg·mL^{-1}.

4. Conclusions

Charged moieties along polyelectrolyte chains display ambivalent effects in terms of lubricating properties in aqueous environment. As long as the stable formation of the lubricating films by polymer chains on non-polar surface is warranted, enhanced lubrication is expected. On the other hand formation of lubricating film by polyelectrolyte-based chains is impeded in the first place, due to the electrostatic repulsion between adjacent polyelectrolyte chains. It is particularly challenging to generate polymer chain-based lubricating films without irreversible anchoring onto the substrates, such as covalent bonding, due to easy removal of the films under cyclic shear stress. In this study, employing the amphiphilic triblock architecture (PEG-*b*-PMEA-*b*-PMAA) in order to "dilute" the charged moieties in the surface-anchored polymer films turned out to be an efficient strategy to enhance the stability of polyelectrolyte-based lubricating films. The surface coverage of PEG-*b*-PMEA-*b*-PMAA was statistically comparable to that of PEG-*b*-PMEA-*b*-PEG onto PDMS surface as studied by OWLS. Moreover, both films showed highly stretched, "brush-like" conformation on PDMS surfaces. Although SFA studies revealed a slightly less repulsive interaction between the two opposing surfaces bearing PEG-*b*-PMEA-*b*-PMAA triblock copolymer compared to its fully neutral counterpart, PEG-*b*-PMEA-*b*-PEG, both films showed comparable lubricating properties, coefficient of friction down to ca. 0.01-0.02, by pin-on-disk tribometry as well as by colloidal friction AFM studies. These results support the idea that too high charge density on the substrate surface from polyelectrolyte-based chains generates more negative effects than positive ones by weakening the stability of physisorbed polyelectrolyte films. Moreover, the strategy of manipulation of charged moieties by synthetic control on the same copolymer as shown in this study offers a significant improvement in the stability and efficacy of the lubricating films due to enforced dilution of charged moieties on the tribopair surfaces. However, it should also be pointed out that the lubricating

capabilities of PEG-*b*-PMEA-*b*-PMAA were not necessarily superior to those of PEG-*b*-PMEA-*b*-PEG. Presumably "halving" the number of charged polymer chains does not provide an optimal charge density on the surface. Further manipulation of the density of charged moieties along polymer chains and/or on the surface may possibly provide more effective lubricating performance than fully neutral ones.

5. References and notes

[1] Chen, M.; Briscoe, W. H.; Armes, S. P.; Klein, J. *Science*, **2009**, *323*, 1698-1701.
[2] Lee, S.; Spencer, N. D. Achieving Ultra-low Friction by Aqueous, Brush-assisted Lubrication, 1st ed.; Elsevier: Amsterdam, The Netherlands, 2007.
[3] Raviv, U.; Giasson, S.; Kampf, N.; Gohy, J. F.; Jerome, R.; Klein, J. *Nature*, **2003**, *425*, 163-165.
[4] Heeb, R.; Bielecki, R. M.; Lee, S.; Spencer, N. D. *Macromolecules*, **2009**, *42*, 9124-9132.
[5] Nalam, P. C.; Clasohm, J. N.; Mashaghi, A.; Spencer, N. D. *Tribol. Lett.* **2010**, *37*, 541-552.
[6] Muller, M.; Lee, S.; Spikes, H. A.; Spencer, N. D. *Tribol. Lett.*, **2003**, *15*, 395-405.
[7] Lee, S.; Muller, M.; Heeb, R.; Zurcher, S.; Tosatti, S.; Heinrich,M.; Amstad, F.; Pechmann, S.; Spencer, N. D. *Tribol. Lett.*, **2006**, *24*, 217-223.
[8] Røn, T.; Javakhishvili, I.; Jankova, K.; Hvilsted, S.; Lee, S. *Langmuir*, **2013**, *29*, 7782-7792.
[9] (a) Dedinaite, A. *Soft Matter*, **2012**, *8* (2), 273-284.(b) Zappone, B.; Ruths, M,; Greene, G. W.; Jay, G. D.; Israelachvili,; J. N., *Biophysical J*, **2007**, *92*, 1693-1708. (c) Das, S.; Banquy, X,; Zappone, B.; Greene, G. W.; Jay, G. D.; Israelachvili, J. N. *Biomacromolecules*, 2013, *14*, 1669-1677.
[10] (a) Braunecker, W. A. and Matyjaszewski, K. *Prog. Polym. Sci.* **2007**, *32*, 93-146; (b) Matyjaszewski, K. and Tsarevsky, N. V. *Nat. Chem.* **2009**, *1*, 276-288; (c) Matyjaszewski, K. *Macromolecules*, **2012**, *45*, 4015-4039
[11] 2. Qin, S.; Saget, J.; Pyun, J.; Jia, S.; Kowalewski, T.; Matyjaszewski, K. *Macromolecules*, **2003**, *36*, 8969-8977.
[12] (a) Berges, C.; Javakhishvili, I.; Hvilsted, S.; Sánchez, C.; Alcalá, R. *Macromol. Chem. Phys.*, **2012**, *213*, 2299-2310; (b) Dimitrov, I.; Takamuku, S.; Jankova, K.; Jannasch, P.; Hvilsted, S. *Macromol. Rapid Commun.* **2012**, *33*, 1368-1374.
[13] Javakhishvili, I.; Jankova, K.; Hvilsted, S. *Polym. Chem.* **2013**, *4*, 662-668.
[14] Javakhishvili, I.; Røn, T.; Jankova, K.; Hvilsted, S.; Lee, S. *Macromolecules*, 2014, *47*, 2019–2029.
[15] Javakhishvili, I.; Binder, W. H.; Tanner, S.; Hvilsted, S. *Polym. Chem.* **2010**, *1*, 506-513.
[16] Jankova, K.; Chen, X.; Kops, J.; Batsberg, W. *Macromolecules,* **1998**, *31*, 538-541.
[17] (a) Rostovtsev, V. V.; Green, L. G.; Fokin, V. V.; Sharpless, K. B. *Angew. Chem. Int. Ed.* **2002**, *41*, 2596-2599; (b) Tornøe, C. W.; Christensen, C.; Meldal, M. *J. Org. Chem.* **2002**, *67*, 3057-3064; (c) Binder, W. H. and Sachsenhofer, R. *Macromol. Rapid Commun.* **2008**, *29*, 952-981; (d) Lutz, J.-F. and Schlaad, H. *Polymer* **2008**, *49*, 817-824; (e) Billiet, L; Fournier, D.; Du Prez, F. *Polymer* **2009**, *50*, 3877-3886.
[18] We argue that the terminal end-group of OH or OMe for the PEG chain can be disregarded in terms of a hydrophilic brush nature of degree of polymerization of PEG chain larger than 100.
[19] Katchalsky, A.; Spitnik, P. *J. Polym. Sci.*, **1947**, *2*, 432-446.

[20] de Feijter, J. A.; Benjamins, J.; Veer, F. A. *Biopolymers*, **1978**, *17*, 1759-1772.
[21] Brandrup, J.; Immergut, E. H.;Grulke, E. A. Polymer Handbook, 4th ed.; John Wiley & Sons, Inc.: New York, 1999.
[22] Coelho, J. F. J.; Gois, J.; Fonseca, A. C.; Carvalho, R. A.; Popov,A. V.; Percec, V.; Gil, M. H. *J. Polym. Sci.,Part A: Polym. Chem.,* **2009**, *47*, 4454-4463.
[23] Israelachvili, J.; McGuiggan, P. *J. Mater. Res.* **1990**, *5*, 2223-2231.
[24] Sader, J; *Rev. Sci. Instrum.* **2012**, *83*, 103705, (1-16).
[25] Cannara, R. J.; Eglin, M.; Carpick, R. W., *Rev. Sci. Instrum.*, **2006**, *77*, 053701, (1-11).
[26] Sader, J. *Rev. Sci. Instrum.*, **2003**, *74*, 2438-2443.
[27] Álvarez-Asencio, R.; Thormann, E.; Rutland M. W. *Rev. Sci. Instrum.,* **2013**, *84*, 096102.
[29] Wong, Eehern J., Modeling and control of rapid cure in polydimethylsiloxane (PDMS) for microfluidic device applications, Modeling and control of rapid cure in PDMS for microfluidic device applications, Ph.D. Thesis, MIT, 2010.
[30] The effective Young's modulus of composite layers in the antiparallel direction of the layers is calculated from the relation: $E = (f_1/E_1+f_2/E_2)^{-1}$, where f_x is volume fraction the material and E_x is the bulk Young's modulus. For the case of 38 μm PDMS layer on a 2 mm thick glass slide the effective Young's modulus is: $((0.038/2.038)/2\ \text{MPa} + (2.0/2.038)/73\ \text{GPa}))^{-1} = 107.1$ MPa. The Young's moduli of glass and Si_3N_4 were 73 GPa and 304 GPa. See other reference by Callister.
[31] Mark, J. E. Polymer Data Handbook; Oxford University Press, Inc.: New York, 1999.
[32] Hirata, T.; Matsuno, H.; Tanaka, M.; Tanaka, K. *Phys. Chem. Chem. Phys.*, **2011**, *13*, 4928-4934.
[33] Tanaka, M.; Motomura, T.; Kawada, M.; Anzai, T.; Kasori, Y.; Shiroya, T.; Shimura, K.; Onishi, M.; Mochizuki, A. *Biomaterials*, **2000**, *21*, 1471-1481.
[34] Rubinstein, M.; Colby, R. H. Polymer Physics ; Oxford University, Press, Inc.: Oxford, 2003.
[35] Assuming same Kuhn length for PMAA as for PAA.Miquelard-Garnier, G.; Creton, C.; Hourdet, D. *Soft Matter*, **2008**, *4*, 1011-1023.
[36] R_F of PEG-b-PMEA-b-PMAA was calculated as the average of the two buoyant blocks.
[37] Song, J.; Tranchida, D.; Vancso, G. J. *Macromolecules*, **2008**, *41*, 6757-6762.
[38] Vaenkatesan, V.; Li, Z.; Vellinga, W.; de Jeu, W. H.; *Polymer*, **2006**, *47*, 8317-8325.
[39] Carpick, R. W.; Ogletree, D. F.; Salmeron, M. *J. Colloid Interface Sci.*, **1999**, *211*, 395-400.
[40] Piétrement, O.; Troyon, M. *J. Colloid Interface Sci.*, **2000**, *266*, 166-171.
[41] van Krevelen, D. W.; te Nijenhuis, K, Properties of Polymers, Elsevier, Amsterdam, 4th ed. 2009.
[42] : $\gamma_{PE/water}$was calculated by applying the Young's equation and a water contact angle of 96° obtained from www.accudynetest.com/polytable_03.html?sortby=contact_angle.
[43] Obtained after 2nd order flattening of the image.
[44] Brochard, F.; de Gennes, P. G. *Langmuir*, **1992**, *8*, 3033-3037.
[45] Tadmor, R.; Janik, J.; Klein, J.; Fetters, L. J. *Phys. Rev. Lett.*, **2003**, *91*, 115503-(1-4).
[46] Lee, S.; Müller, M.; Heeb, R.; Zürcher, S.; Tosatti, S.; Heinrich, M.; Amstad, F.; Pechman, S.; Spencer, N. D. *Tribology Letters*, **2006**, *24*, 217-223.
[47] Béfahy, S.; Lipnik, P.; Pardoen, T.; Nascimento, C.; Patris, B.; Bertrand, P.; Yunus, S. *Langmuir*, *26*, **2009**, 3372-3375.
[48] Callister WDJ. Material Science and Engineering, an Introduction. 7th ed. John Wiley & Sons, Inc., New York; 2007.

6. Acknowledgements

Authors appreciate greatly the Danish Council for Independent Research (DFF), Technology and Production Sciences (FTP) (10-082707) for the financial support.

7. Miscellaneous

Author Contributions
The manuscript was written through contributions of all authors. All authors have given approval to the final version of the manuscript.

Notes
The authors declare no competing financial interest.

Author Information:

Seunghwan Lee, Department of Mechanical Engineering, Technical University of Denmark, DK-2800, Kongens Lyngby, Denmark, Telephone: +45 4525 2193. Email: seele@mek.dtu.dk

Søren Hvilsted, Department of Chemical and Biochemical Engineering, Danish Polymer Centre, Technical University of Denmark, DK-2800, Kongens Lyngby, Denmark, Telephone: +45 4525 2965. Email: sh@kt.dtu.dk

Bruno Zappone, CNR-IPCF and LICRYL, c/o Università della Calabria, Cubo 33/B, 87036 Rende (CS), Italy. Telephone: +39 0984 496120. Email: Bruno.zappone@cnr.it

4.6 Influence of temperature on the frictional properties of water-lubricated surfaces.

This article was submitted to the journal lubricant, 2014. See next pages.

Lubricants **2014**, *2*, 1-x manuscripts; doi:10.3390/lubricants20x000x

OPEN ACCESS

lubricants

ISSN 2075-4442

www.mdpi.com/journal/lubricants

Article

Influence of temperature on the frictional properties of water-lubricated surfaces

Troels Røn [1] and Seunghwan Lee [1,*]

[1] Department of Mechanical Engineering, Technical University of Denmark, DK-2800 Kgs. Lyngby, Denmark: tror@mek.dtu.dk; seele@mek.dtu.dk

***** Author to whom correspondence should be addressed; E-Mail: seele@mek.dtu.dk; Tel.: +45-4525-2193; Fax: +45-4525-6213.

Received: / Accepted: / Published:

Abstract: The influence of temperature on the lubricating properties of neat water for tribopairs with varying bulk elasticity moduli and surface hydrophilicity, namely hard-hydrophobic interface (*h*-**HB**), hard-hydrophilic interface (*h*-**HL**), soft-hydrophobic interface (*s*-**HB**), and soft-hydrophilic interface (*s*-**HL**), has been investigated. With increasing temperature, the coefficients of friction generally increased due to the decreasing viscosity of water. This change was more clearly manifested from soft interfaces for more feasible formation of lubricating films. Nevertheless, dominant lubrication mechanism appears to be boundary and mixed lubrication even for soft interfaces at all speeds (up to 1 200 mm/s) and temperatures (1 to 90 °C) investigated. The results from this study are expected to provide a reference to explore the temperature-dependent tribological behavior of more complex aqueous lubricants, e.g. those involving various additives, for a variety of tribosystems.

Keywords: aqueous lubrication; temperature; soft; hard; hydrophilic; hydrophobic

1. Introduction

Biomimetics has been drawing increasing attention in modern science and technology as various interesting and useful inspirations can be acquired from biological systems in order to solve the problems in engineering systems. Lubrication is not an exception; extensive efforts to utilize the principles of biological lubrication for man-made, engineering tribosystems have been put forth in the past a couple of decades [1–3]. One of the instrumental approaches in this endeavor is to use water as base lubricant [1–5], mimicking, for example, life-long maintenance of synovial joints of human and animals [6,7]. Industrial application of water-based lubricants is desirable from economic and environmental standpoints as well since water is abundant, non-toxic, and an effective coolant. Moreover, water is practically the only viable base stock in biomedical applications due to the requirement of biocompatibility.

Beyond biomedical engineering, however, practical use of water as base lubricant is presently limited [8,9]. This is mainly due to that viscosity, and more importantly pressure coefficient of viscosity of water, is too low, resulting in, even at relatively high entrainment speeds, insufficient fluid film formation, which hampers activation of elastohydrodynamic lubrication (EHL) [10,11]. In order to broaden the scope of industrial applications of aqueous lubrication, several subjects must be further understood. One of them is the influence of temperature. Most bearing systems operate at higher temperatures than room temperature. While a number of previous studies have investigated the lubricating properties of various materials with water, absolute majority of them were studied at room temperature [4,10–13], whereas those at other temperatures than ambient are rare to date [14]. At elevated temperatures, many parameters affecting aqueous lubrication may change. Most apparently, the viscosity of base lubricant, water, would be decreasing with increasing temperature. Generally, the relationship between temperature and viscosity of organic liquids is expressed similarly with chemical reactions, such as

$$\eta = \eta_0 \cdot e^{\frac{\Delta E_a}{kT}} \qquad (1)$$

where η and η_0 are viscosities at elevated and ambient temperatures [15,16]. The influence of temperature on the viscosity of water is empirically well established, and also shows exponentially decreasing trend with increasing temperature: from 1.793 mPa·s to 0.282 mPa·s from 0 °C to 100 °C [17]. A general expectation of reduced viscosity of lubricants in fluid-film lubrication is decreasing film thickness with increasing temperature [18,19]. However, its influence in boundary or mixed lubrication regimes, in which aqueous lubrication typically occurs, is much more complex, since it is dependent on various surface properties of interacting tribopairs [20–22]. As aqueous lubricants can include a variety of additives, which may exhibit additional complexity in response to temperature

change, it is important to establish the impact of temperature on the lubricating properties of base lubricant, neat water, first.

In this context, we have investigated the lubricating properties of neat water for various tribological contacts with varying temperature, therefore to formulate a reference for further complex aqueous lubricant systems involving a variety of additives. Since the efficacy of water-based lubrication is known to be greatly influenced by bulk elasticity moduli [20,21] as well as surface hydrophilicity [22] of tribopairs, these two parameters have been systematically varied, and four tribopairs have been employed: hard-hydrophobic interface (*h*-**HB**, self-mated polyoxymethylene (POM)), hard-hydrophilic interface (*h*-**HL**, steel-glass), soft-hydrophobic interface (*s*-**HB**, self-mated poly(dimethylsiloxane (PDMS)), and soft-hydrophilic interface (*s*-**HL**, self-mated oxidized PDMS).

2. Results and Discussion

2.1. Theoretically predicted lubricating properties: lubricating film thickness

A numerical model proposed by Hamrock and Dowson [20], which was later revised by Esfahanian and Hamrock [21], provides a useful first guideline to estimate the lubricant film thickness as a function of materials parameters, including tribopairs' elasticity moduli and lubricant's viscosity, as well as operating parameters, such as load and entrainment speed. In order to identify the EHL regime to which the tribological contacts in this study belong, i.e. among isoviscous-rigid (IR), piezoviscous-rigid (VR), isoviscous-elastic (IE), and piezoviscous-elastic (VE) regimes, dimensionless viscosity parameter, g_E, and dimensionless elasticity parameter, g_V, must be evaluated first [20,21]. It was confirmed that all the tribological contacts under the experimental conditions in this study belong to isoviscous-elastic (IE) regime (or as known as "soft EHL" regime). The results of the calculations are shown in Supplementary Data (SD1). Then, the *minimum* lubricating film thickness ("lubricating film thickness", hereafter) for circular contacts can be estimated according to the equation,

$$h = 3.28\left(w^{-0.21}E'^{-0.45}\eta_0^{0.66}u^{0.66}R_x^{0.76}\right) \qquad (2)$$

where η_0 is lubricant's viscosity at atmospheric pressure, u is mean speed, E' is reduced Young's modulus, w is applied load, R_x is radius in the x direction, which is equal to R_y in circular contact. It is noted that pressure viscosity coefficient is not included as a parameter to influence the lubricating film thickness in soft EHL regime.

The calculated film thicknesses according to the Hamrock and Dowson equation 1 are presented in Figure 1 for (a) POM-POM, (b) steel-glass, and (c) PDMS-PDMS.

Figure 1. Plots of minimum film thickness (*h*) as a function of speed, (**a**) *h*-**HB** interface (POM-POM), (**b**) *h*-**HL** interface (steel-glass), and (**c**) *s*-**HB** and *s*-**HL** interfaces (PDMS-PDMS and *ox*PDMS-*ox*PDMS).

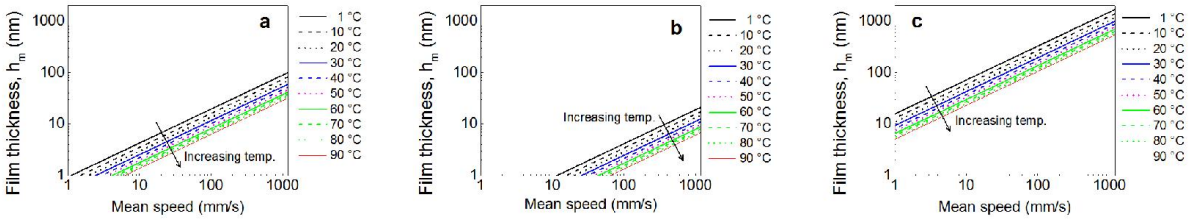

For all cases, the lubricating film thickness was expected to be increasing with increasing speed. The expected film thickness was in the order of PDMS-PDMS > POM-POM > steel-glass at all temperatures. Temperature is not included as an explicit parameter affecting the thickness of lubricating film in equation 2, but has, in fact, a significant influence as the viscosity of lubricant (water), η_0, is expected to change with varying temperature. The change of elasticity moduli of hard materials (*E'*) in this study, e.g. glass, steel, POM, within 1–90 °C is not expected [23,24]. Corresponding change for PDMS is un-ignorable [25], but its ultimate influence on the calculated film thickness is of little significance; for instance, the decrease of lubricating film thickness solely due to the increase of elasticity modulus of PDMS at the highest temperature, 90 °C, compared to that at 1 °C is expected to be 12% only. Further details on the calculations are provided in SD2 in Supplementary Data.

2.2. Theoretically predicted lubricating properties: consideration of surface properties

The estimation of lubricating film thickness according to the equation 1, however, does not take into account surface parameters such as surface roughness and surface hydrophilicity of the tribopairs. Among them, the influence of surface roughness on the lubrication regime can be readily quantified by obtaining Stribeck parameter or lambda (λ) parameter: λ = (film thickness)/(mean surface roughness), where λ parameter is defined as $\lambda = h/(\sigma_{ball}^2 + \sigma_{disc}^2)^{½}$, where σ_x are the root-mean-square roughness of ball and disc substrates. The calculated λ parameters are in the order of POM-POM < steel-glass < PDMS-PDMS as a function of speed (not shown). λ parameters were plotted as a function of temperature in Figure 2 from 1 °C to 90 °C by the increment of 10 °C at 10, 100, and 1 000 mm/s: (a) POM-POM, (b) steel-glass, and (c) PDMS-PDMS tribopairs.

Figure 2. Plots of lambda parameter (λ) vs as a function of temperature for the three tribopairs: (**a**) *h*-**HB** interface (POM-POM), (**b**) *h*-**HL** interface (steel-glass), and (**c**) *s*-**HB** and *s*-**HL** interfaces (PDMS-PDMS and *ox*PDMS-*ox*PDMS).

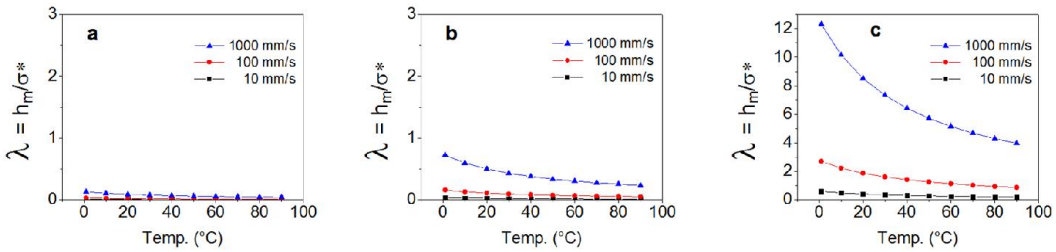

For all tribopairs, λ parameters were estimated to be decreasing with increasing temperature, as a result of decreasing viscosity, i.e. $h \propto \eta_0^{0.66}$. According to a conventional view, λ has to be 3 or higher for full-fluid lubricating films to be formulated [26,27]. However, the threshold λ value for the activation of fluid-film has been reported to be highly variant, and somewhat larger values are proposed for deformable surfaces as elastomers [28,29]. Nevertheless, it is clear that both hard tribopairs showed extremely low λ values; for example, λ ≈ 0.25 even at 1 °C for steel-glass pair, where the film thickness should be highest. Thus, elastohydrodynamic lubrication is hardly expected at any temperature. Due to very high surface roughness of POM ball and disc (see Table 1), the λ parameters of POM-POM pair were calculated to be lowest at all conditions. For PDMS-PDMS pair, as well as *ox*PDMS-*ox*PDMS pair, PDMS disc was extremely smooth on surface, but PDMS ball showed fairly high surface roughness, replicating the surface roughness of the aluminum mold (Table 1). Thus, in high-speed regime (1 000 mm/s), λ parameter of ca. 12 to 4 is expected from 1–90 °C. But in the medium- (100 mm/s) and low-speed (10 mm/s) regimes, λ parameters were estimated to be lower than 3 at all temperatures.

2.3. Experimentally determined friction forces

Lubricating film thickness can be experimentally determined by means of interferometry [30−32]. But, this technique is applicable to a limited range of materials as tribopair, and cannot cover all the materials in this study. Thus, the experimental assessment of the predicted lubricating film thickness was carried out by measuring and comparing with coefficients of friction, as will be shown below in detail. Since the relationship between lubricating film thickness and friction forces is non-trivial, it should be noted that friction forces cannot be a direct probe of the lubricating film thickness. The influence of temperature on the frictional properties of the four tribopairs lubricated with water was investigated by acquiring μ vs mean speed with MTM, and plotting μ vs Sommerfeld number (speed × viscosity × load^{-1}) as a function of temperature.

2.3.1 Hard interfaces

As shown in Figure 3, for *h*-**HB** interface, the μ values were very weakly dependent on the speed, and only a slight decreasing trend of μ was observed with increasing speed at all temperatures.

Figure 3. (**a**) μ vs mean speed (b) μ vs Sommerfeld number (mean speed × viscosity × load^{-1}) plots for *h*-**HB** interface (POM-POM) lubricated with water as characterized by MTM. All experiments were performed in water at 50% SRR. Temperature was increased from low (1 °C) to high (90 °C). Each point in the plots consists of averaging three measurements. Error bars designate standard deviation from the average values.

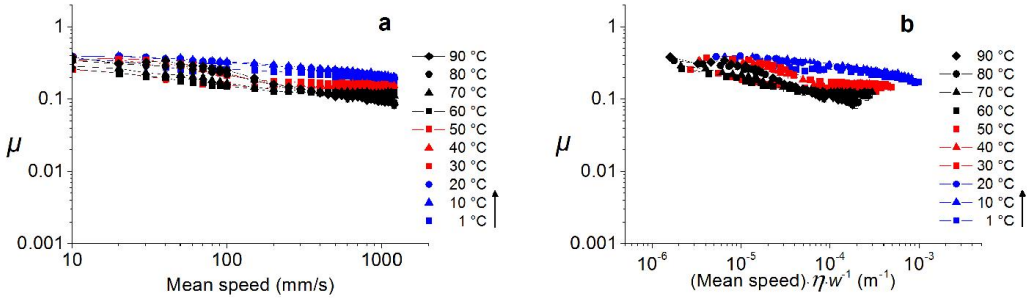

The μ values remained within 0.1–0.4 over the entire range of speed at all temperatures. The conversion of the μ vs speed plots to μ vs Sommerfeld number plots (Figure 3(b)) did not change somewhat scattered data points, and in fact, they appear to scatter slightly more by the conversion. This is closely related to the fact that POM surface is hydrophobic, hard, and rough, thus resulting in harsh asperity contacts. Consequently, water is mostly expelled from the interface. In fact, the μ vs speed plots obtained from dry sliding contacts of POM-POM at 20 °C (data not shown) were not distinguishable from those obtained in water. Thus, POM-POM sliding in water has essentially the characteristics of dry sliding contact, and insignificant changes of μ over the entire range of temperature are also resulted from it even in water. A previous study has also reported stable and consistent μ values from the self-mated contact of POM in air up to ca. 150 °C [14].

Figure 4 shows μ vs speed plots and μ vs Sommerfeld number plots for *h*-**HL** interface (steel vs glass) at various temperatures.

Figure 4. (**a**) μ vs mean speed (**b**) μ vs Sommerfeld number (mean speed × viscosity × load^{-1}) plots for *h*-**HL** interface (steel-glass) lubricated with water as characterized by MTM. All experiments were performed at 50% SRR. Temperature was increased from low (1 °C) to high (90 °C). Each point in the plots consists of averaging of three measurements. Error bars designate standard deviation.

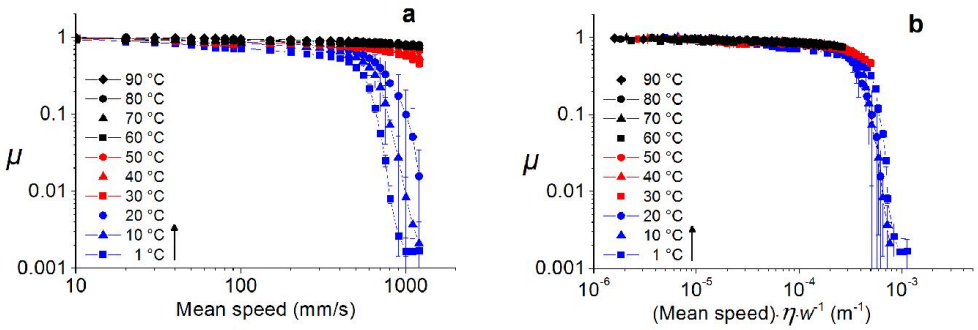

Although much higher μ values compared to *h*-**HB** pair were observed in low- and medium-speed regimes (10 – 100 mm/s), μ being close to 1, a rapid decrease in μ values with increasing speed was observed at low temperatures (20 °C or lower). Based on the elasticity moduli, it is expected to be more difficult for steel-glass pair to form lubricating film than POM-POM interface (Figure 1(b)). By taking the surface roughness into account, however, λ parameters of the former are slightly higher than those of the latter (Figure 2(b)). Nevertheless, λ parameters of both hard tribopairs are very small (maximum ca. 0.72 for steel-glass and ca. 0.13 for POM-POM at 1 °C, 1 000 mm/s) that the difference in λ parameters cannot solely account for a large difference in μ values in high-speed regime. This lubricating effect is attributed to superior water wettability of the steel-glass tribopair compared to POM-POM. The conversion of the μ vs speed plots to the μ vs Sommerfeld number (Figure 4(b)) plots has revealed an overlap of the data points on a master curve. With increase of Sommerfeld number, activation of mixed lubrication is apparent.

Overall, the influence of temperature on the lubrication with water is generally weak for both hard interfaces. This is firstly because the thickness of aqueous lubricating film is small due to high bulk elasticity for hard materials according to soft EHL model ($h \propto E'^{-0.45}$). Additionally, hard engineering materials, especially those that are polished or cast, tend to display high surface roughness, and thus the formation of lubricating film becomes further hampered. A related problem is that despite the selection of low applied load, 2 N, to facilitate the formation of lubricating films, apparent contact pressure reaches ca. 16 MPa and 160 MPa for *h*-**HB** and *h*-**HL** (Table 2), respectively. Furthermore, as local asperity contact pressures of hard materials are much higher, plastic deformation and/or wear process are inevitably involved even in lubricated contacts. Judging from Tresca yield criterion [33], bulk plastic deformation is not likely to occur for any of the tribopairs in this study [34]. However,

plastic shear of the surface asperities is fairly probable for the two hard tribopairs, POM-POM and steel-glass. According to Greenwood and Williamson [35], for an exponential asperity distribution,

$$\Psi = \frac{E'}{H} \cdot \left(\frac{\sigma}{R_{asp}} \right)^{1/2} \quad (3)$$

where E', σ, H and R_{asp} is the reduced Young's modulus, the roughness, the hardness and the average asperity radius of tribopair (for dissimilar material tribocontact, σ, H and R_{asp} of the softer material from the two materials in contact are used in the equation), a dimensionless plasticity index (ψ) can be introduced as a guideline for plastic shear of surface asperities; the contact will be elastic if $\psi <$ ~0.69 and plastic (or fracture for brittle materials) if $\psi >$ ~0.69. It is noted that ψ is independent of load. The ψ values of POM-POM and steel-glass pairs are 1.9 and 5.80, respectively, and thus plastic deformation of asperities for these hard pairs is expected. This is in accordance with wear tracks observed on POM, glass, and steel surfaces (data not shown). For POM-POM, the surface roughness along the sliding track was observed to decrease from ca. 223 nm to 133 nm (R_q) after MTM experiments (see Table 1). This could be attributed to lapping of the surfaces where the surface asperities deform plastically and thereby flattening the surface. On the other hand, for steel-glass pair, the surface roughness along the sliding track on glass increased from ca. 3 nm to 24 nm (R_q) after MTM experiments (see Table 1). This is also an indication of plastic deformation or fracture. In contrast, for all PDMS interfaces, ψ is much lower than 0.69 (Table 2) and no wear track was observed after the tribological contacts.

2.3.2 Soft interfaces

Figure 5 shows μ vs speed plots and μ vs Sommerfeld number plots for *s*-**HB** interface (PDMS-PDMS) at various temperatures.

Figure 5. (**a**) μ vs mean speed (**b**) μ vs Sommerfeld number (mean speed × viscosity × load-1) plots for *s*-**HB** interface (PDMS-PDMS) lubricated with water as characterized by MTM. All experiments were performed at 50% SRR. Temperature was increased from low (1 °C) to high (90 °C). Each point in the plots consists of averaging of three measurements. Error bars designate standard deviation

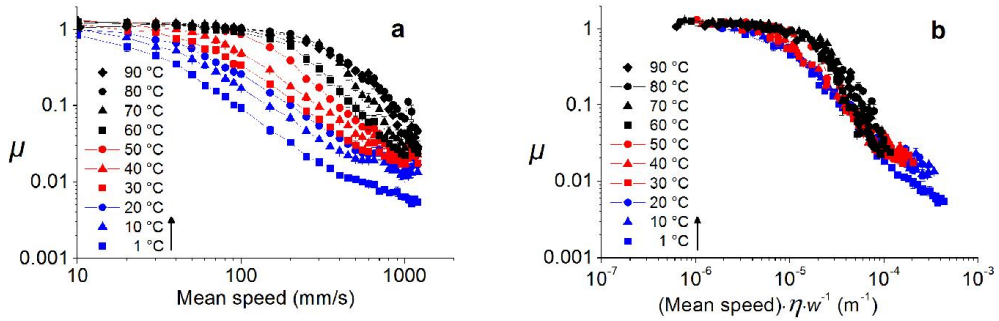

For this tribopair, large changes in μ values are observed as a function of speed at all temperatures, from μ being close to 1 down to 0.01. This trend is similar to that of *h*-**HL** interface (Figure 4), but effective lubricating properties in high-speed regime are not indebted from hydrophilicity of the interface, but from the softness of the tribopair. In fact, according to the theoretical prediction by soft-EHL model, where the bulk mechanical properties of the tribopair only is considered, *s*-**HB** interface is expected to form a large film thickness, for example as high as ca. 1 µm at 1 000 mm/s, at room temperature (20 °C). As with *h*-**HL** interface, μ vs Sommerfeld number plot (Figure 5(b)) shows a convergence of the data points on a master curve. μ vs Sommerfeld number plots in Figure 5(b) suggest that the type of lubrication in high Sommerfeld number regime is mixed lubrication than full fluid-film lubrication judging from the lack of EHL transition in μ.

Figure 6 shows μ vs speed plots and μ vs Sommerfeld number plots for *s*-**HL** interface (*ox*PDMS-*ox*PDMS), which is different only in surface hydrophilicity compared to *s*-**HB** interface, at various temperatures.

Figure 6. (**a**) μ vs mean speed (**b**) μ vs Sommerfeld number (mean speed × viscosity × load^{-1}) plots for s-HL interface (*ox*PDMS-*ox*PDMS) lubricated with water as characterized by MTM. All experiments were performed at 50% SRR. Temperature was increased from low (1 °C) to high (90 °C). Each point in the plots consists of averaging of three measurements. Error bars designate standard deviation.

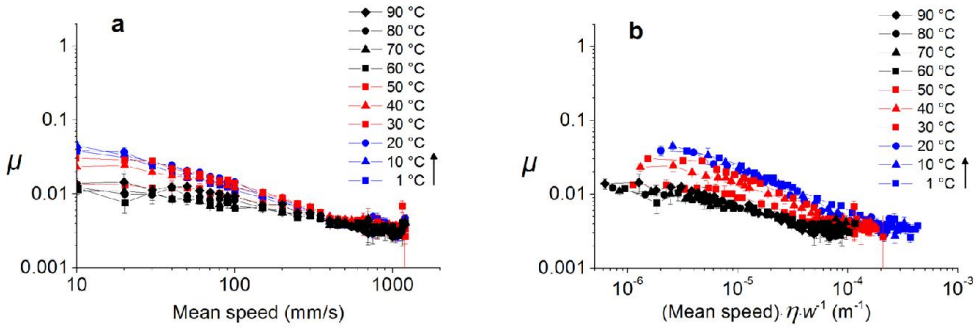

As a function of speed, a slight decrease of μ with increasing speed is also observed at all temperatures (Figure 6(a)). The data points over the universal line for the μ vs Sommerfeld number plots (Figure 6(b)) appear to be somewhat scattered, however, the magnitude of scatter is very small, μ of ±0.02 (note that the Figure 6 is in log-log scale). Compared to *s*-**HB** interface, very low μ values, 0.01 or below, were reached from much lower Sommerfeld numbers. Highly enhanced lubricating properties of water for *s*-**HL** interface compared to *s*-**HB** interface were apparently due to higher hydrophilicity of *ox*PDMS surfaces.

Collectively, the influence of temperature on the lubrication with water was much more significant for soft contacts, apparently because of more feasible formation of lubricating films. When both bulk mechanical properties and surface roughness are considered, PDMS-PDMS contacts in this study are expected to provide λ parameters that are higher than 4 in the high-speed regime (1 000 mm/s) at all temperatures (Figure 2 (c)). Nevertheless, no transition to increasing trend in μ values in the highest

Sommerfeld number was observed, even for *s*-**HL** interface where surface wetting and entrainment of water into the contact area is substantially facilitated. This may suggest that λ parameters within the temperature range of 1 to 90 °C, i.e. ca. 12 to 4, are still not sufficient to activate fluid-film lubrication. Previous studies of aqueous lubrication of soft contacts involving PDMS showed clear transition of μ to increasing trend with increasing speed in high-speed regime [29,36−38]. But, the base fluids in those studies were mixtures of water and corn syrup [36,37] or glycerol [38], and the viscosities of the fluids were a few orders of magnitude higher than that of water. Even with fluids with much higher viscosity, the transition to fluid-film lubrication was reported to occur from λ is ca. 10 [29]. With neat water, it appears that characteristic transition to increasing trend of μ for EHL is not feasible under the experimental conditions in this study. In turn, this is resulting from that distilled water is a representative Newtonian fluid and the increase of friction shear forces due to viscous shear is too small to be detected by MTM (discussed in detail in SD3, Supplementary Data).

2.4. Temperature dependence of water-lubricated tribocontacts

As an overview for the influence of temperature on the lubricating properties of water, the plots for μ values obtained from the four tribopairs, (a) *h*-**HB**, (b) *h*-**HL**, (c) *s*-**HB**, and (d) *s*-**HL**, are displayed as a function of temperature in Figure 7. In this plot, the μ values at 10, 100 and 1 000 mm/s are presented.

Figure 7. μ vs temperature plots for (**a**) *h*-**HB** (POM-POM), (**b**) *h*-**HL** (steel-glass), (**c**) *s*-**HB** (PDMS-PDMS), (**d**) *s*-**HL** (*ox*PDMS-*ox*PDMS) interfaces lubricated with water. All experiments were performed at 50% SRR.

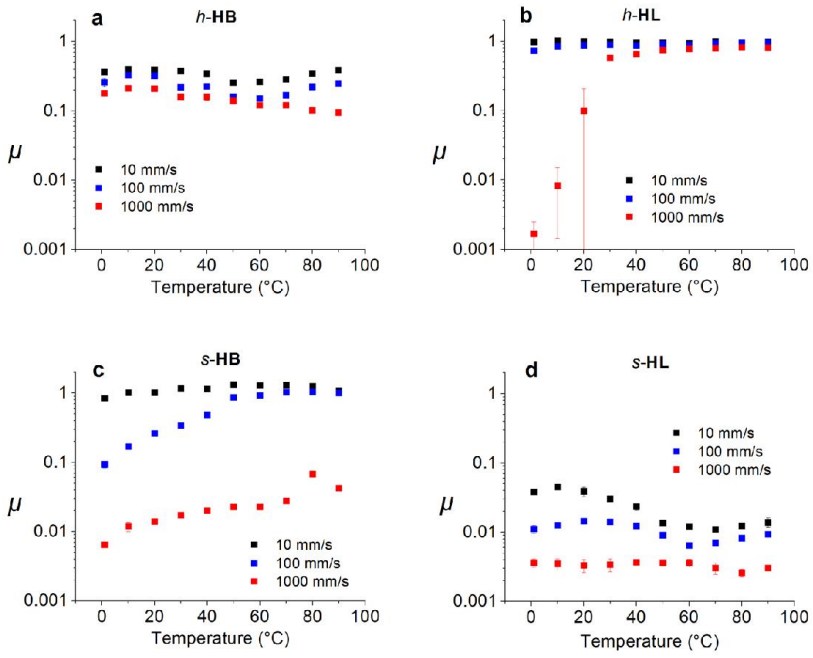

Figure 7 clearly shows that the influence of temperature on the lubricating properties of water is different for different tribopairs. For *h*-**HB** interface, nearly ignorable temperature dependence of μ is observed at all temperatures, due to hydrophobic, rough, as well as hard characteristics of the interface. For both *h*-**HL** and *s*-**HB** interfaces, a gradual increase of μ with increasing temperature is visible in high-speed regimes, due to the gradually decreasing viscosity of water with increasing temperature; however, this trend is much clearer for *s*-**HB** interface, and generally much lower μ values are observed from this interface. Even though a generalization is not possible at this stage, this observation suggests that mechanical properties of the tribopair may be more important than surface hydrophilicity in determination of the efficacy of lubrication with water. Lastly, for *s*-**HL** interface, weak temperature dependence of the lubricating properties is also observed. However, the μ values are maintained low at all conditions, suggesting that sufficient lubricating films might be sustained despite the changes in speed and temperature. Nevertheless, even at the highest speed (1 200 mm/s), dominant lubricating mechanism for this interface appears to be boundary or mixed lubrication, judging from the lack of changes in μ values with increasing temperature. If a full-fluid film is formed between the two rubbing surfaces and the applied loads are entirely taken up by the fluid, decrease of fluid viscosity should lead to decreased friction as a result of reduced viscous drag. The lack of increasing trend of μ with increasing speed (Figure 5) and the lack of decrease in μ with increasing temperature (Figure 6(d)) collectively suggest that the full-fluid lubrication is still not achieved in this condition. Alternatively, the magnitude of change in μ from the formed fluid film is too small to be detected by MTM (SD3 in Supplementary Information).

3. Experimental Section

3.1. Tribopairs

Four different tribopairs have been employed (ball-disc): (a) polyoxymethylene-polyoxymethylene (POM-POM) to represent *h*-**HB** interface, (b) steel-glass to represent *h*-**HL** interface, (c) poly(dimethylsiloxane)-poly(dimethylsiloxane) (PDMS-PDMS) to represent *s*-**HB** interface, (d) oxidized poly(dimethylsiloxane)-oxidized poly(dimethylsiloxane) (*ox*PDMS-*ox*PDMS) to represent *s*-**HL** interface. POM discs were prepared by cutting from commercially available rods (Rias A/S, Roskilde, Denmark). Commercially available POM balls (¾ inch (19.05 mm) in diameter) were used as received (Precision Plastic Ball Company, Franklin Park, IL). Commercially available bearing steel balls (AISI 52100) and glass discs were employed (PCS Instruments, London, UK). PDMS balls and discs were fabricated from a two-component kit (SYLGARD® 184, Dow Corning, Midland, MI) consisting of base PDMS and crosslinker. The PDMS base and crosslinker were mixed at 10:1 wt. ratio, and dispersed air bubbles formed during mixing were removed by a vacuum using an oil pump. For PDMS disc, the mixture fluid was poured on top of the steel disc in a plastic mold with nearly same diameter and cured overnight at 70 °C. PDMS-coated disc was obtained by removing the mold. The thickness of PDMS disc on top of the steel disc was 2 mm. PDMS balls with ¾ inch (19.05 mm) in diameter were cast in a home-machined aluminum mold.

Surface roughness of the discs and balls was characterized by acquiring root-mean-square roughness (R_q) from topographic images over a 100 µm × 100 µm area with tapping-mode AFM. Three different spots were characterized for statistical evaluation. In order to obtain the average asperity radius of the tribopairs, surface topographic images of 1 µm × 1 µm area were obtained. The full list of the surface roughness and asperity radii of the tribopairs is shown in Table 1. A Bruker AFM model Dimension® Edge™ and NanoScope 8.02 software were used for AFM imaging, with NanoScope Analysis software (ver. 1.40) for calculating roughness and asperity radii.

Table 1. Bulk mechanical and surface properties of the tribopair materials.

Substrate	**Young's modulus (MPa)**	**Poisson's Ratio**	**Hardness (MPa)**	**Roughness, R_q, (nm)**		**Asperity diameter average (nm)**		**Static water contact angle (°)**
				Disc	Ball	Disc	Ball	
PDMS	2.0[39] (7.0)[a,40]	0.5 [39]	2.2[f]	1.6 ± 0.3 2.9 ± 0.7 (plasma tr.)	HB: 121.4 ± 36.4 HL: 116.9 ± 50.6	No asperities	HB: 1448 ± 300 HL: 2189 ± 246	pristine: 105.6 ± 2.2[e] plasma tr.: < 2
POM	3100[41]	0.35[41]	354[41,h]	223 ± 51 Wear track: 133 ± 44	659 ± 179 414 ± 180	5086 ± 504	4743 ± 1419	pristine: 84.8 ± 2.9[c]
Steel (AISI E 52100)	210000[41]	0.3[41]	8319[41]	-	26.1 ± 5.5 Wear track:		116 ± 17	pristine: 57.5 ± 0.7[b] plasma tr.: < 2
Glass	73000[42]	0.17[42]	7848[41]	2.9 ± 0.3 Wear track:	-	73 ± 49		pristine: 32.9 ± 3.3 plasma tr.: < 2

3.2 Hydrophilization of substrates

The static water contact angles on POM and PDMS surfaces were 84.8 ± 2.9 ° and 105.6 ± 2.2 °, respectively. In order to hydrophilize balls and discs, including PDMS, steel, and glass, a plasma cleaner/sterilizer (Harrick Plasma, model PDC-002, New York, NY) was employed. Air plasma treatment for 3 minutes lowered the water contact angles of the substrates significantly. For *ox*PDMS and glass, the contact angles were less than 2 °. See Table 1 for contact angle values of pristine and hydrophilized substrates.

Table 2. Contact characteristics of the tribopairs: load, Hertzian contact pressure, reduced Young's modulus (*E'*), mean surface roughness (σ*), and plasticity index: ($\psi = (E'/H)\cdot(\sigma/R_{asp})^{.1/2}$

	Hydrophobic	**Hydrophilic**
Soft	**PDMS†-PDMS†**	**PDMS-PDMS**
Load	5 N	5 N
E'	2.07	2.07
Pressure	0.24 MPa	0.24 MPa
σ*	121.4 nm	116.9 nm
ψ	0.22	0.27
Hard	**Steel†-glass†**	**POM-POM**
Load	2 N	2 N
E'	56 700 MPa	1 766 MPa
Pressure	160 MPa	16 MPa
σ*	26.3 nm	695 nm
ψ	5.8	1.9

†Plasma-treated

3.3 Lubricant

Millipore water (resistivity higher than 18 MΩ·cm) was employed as lubricant, if not stated otherwise. The viscosity of water within the temperature range from 0 °C to 100 °C is shown in Table 3 [17].

Table 3. Viscosity of water as a function of temperature.[17] (* = estimated value).

T, Temperature (°C)	η, Viscosity (mPa·s)
0	1.793
*1	*1.750
10	1.307
20	1.002
30	0.798
40	0.653
50	0.547
60	0.467
70	0.404
80	0.354
90	0.315
100	0.282

3.4 MTM (Mini-traction Machine)

A mini-traction machine (MTM) (MTM2, PCS Instruments, London, UK) with software version 3.2.3.0 was employed to investigate the frictional properties of tribopairs lubricated with water. The principal setup of MTM consists of independently rotating ball and disc immersed in fluid lubricant with the possibility to control load and temperature. The friction forces are measured with a strain gauge connected to ball shaft arm. Coefficient of friction, μ, is defined from the relationship, $\mu = F_{\text{friction}}/F_{\text{load}}$. Independent control of disc and ball speeds allows for the variation of the degree of slide/roll ratio. The mean speed is defined as $[|\text{speed}_{\text{ball}} - \text{speed}_{\text{disc}}|/2]$. The slide/roll ratio, SRR (%), is defined as $\text{SRR}(\%) = (|\text{speed}_{\text{ball}} - \text{speed}_{\text{disc}}|)/[(\text{speed}_{\text{ball}} + \text{speed}_{\text{disc}})/2] \times 100\%$, where 0% SRR represents pure rolling and 200% SRR represents pure sliding. The SRR in this study was 50% unless otherwise stated. A pair of measurements is performed to yield a mean μ at each mean speed; in one measurement, the speed of disc is higher and in the other one, the speed of ball is higher. The mean speed was changed from 10 mm/s to 1 200 mm/s for all cases. The data points in Figure 2 – 5 are

average values of three measurements, and the error bars represent the standard deviation. The applied load was 2 N for hard contacts (POM-POM and steel-glass) and 5 N soft contacts (PDMS-PDMS and *ox*PDMS-*ox*PDMS), respectively. Apparent contact pressures for each tribopair are shown in Table 2.

Since MTM operates with an enclosed pot inside which a lubricated tribocontact is formed, it is feasible to control the temperature. Higher temperatures than ambient were obtained by heating the pot with a built-in thermistor, whereas lower temperatures than ambient were obtained by circulating a coolant surrounding the pot. The lowest temperature at which the friction measurements were conducted was 1 °C. From 10 °C to 90 °C, the coefficients of friction were measured at 10 °C increments. The temperature was automatically regulated by the MTM control units with an accuracy of ±1 °C, with thermocouple inside the pot. The order of measurements was from the lowest to highest temperature, where three consecutive measurements series at each temperature were performed to give a statistical average.

4. Conclusions

In this study, the influence of temperature on the lubrication properties of water has been explored by employing tribopairs with distinctively different mechanical properties and surface hydrophilicity, namely *h*-**HB** (POM-POM), *h*-**HL** (steel-glass), *s*-**HB** (PDMS-PDMS), and *s*-**HL** (*ox*PDMS-*ox*PDMS) interfaces. The temperature was varied from 1 to 90 °C. The theoretically predicted lubricating film thicknesses, and in turn, λ parameter estimates by further taking the surface roughness into account, were compared with the coefficients of friction obtained by MTM experiments. It was shown that soft EHL model considering mechanical properties of the tribopair only was not sufficiently accurate to predict the feasibility of fluid film formation. While λ parameters were estimated as high as ca. 12 for *s*-**HL** interface at an optimum condition, no clear indication of transition to fluid-film lubrication was observed or the change in the coefficient of friction was too small to be detected by MTM. For hard tribopairs, *h*-**HB** (POM-POM) and *h*-**HL** (steel-glass) interfaces, the influence of temperature on the frictional properties was weak due to high elasticity moduli and high surface roughness, and consequently hampered formation of aqueous lubricating films. *h*-**HL** interface (steel-glass) displayed some degree of lubricity at the highest entrainment speeds and low temperatures due to surface hydrophilicity. For soft contacts, the influence of temperature on the frictional properties was more apparent and drastic, reflecting the feasible formation of aqueous lubricating films. But, the lack of characteristic transition to increasing μ trend, even for *s*-**HL** interface (*ox*PDMS-*ox*PDMS) in the highest speed regime, together with the lack of changes in μ with increasing temperature (decreasing viscosity) at the highest speed, implies that the soft EHL films were not generated with neat water as sole lubricant. Alternatively, the magnitude of μ change in this condition may be too small to be sensed by MTM. Establishment of the influence of temperature on the tribocontacts lubricated with water in this study is expected to provide a useful reference in understanding the respective role of base fluid (water) and additives for more complex aqueous lubricants under the variation of temperature for a variety of tribopairs.

Acknowledgments

The authors acknowledge the financial supports from the Danish Council for Independent Research (DFF), Technology and Production Sciences (FTP) (10-082707) and European Research Council (ERC) (Funding Scheme: ERC Starting Grant, 2010, Project Number 261152) for this study.

Conflicts of Interest

The authors declare no conflict of interest.

References and Notes

1. Dedinaite, A.; Pettersson, T.; Mohanty, B.; Claesson, P.M. Lubrication by organized soft matter. *Soft Matter* **2010***, 6*, 520–1526.
2. Dai, Z.; Tong, J.; Ren, L. Researches and developments of biomimetics in tribology. *Chinese Science Bulletin* **2006**, 51, 2681–2689.
3. Ahlroos, T.; Hakala, T.J.; Helle, A.; Linder, M.B.; Holmberg, K.; Mahlberg, R.; Laaksonen, P.; Varjus, S. Biomimetic approach to water lubrication with biomolecular additives. *Proc. IMechE. Part J: J. Eng. Tribol.* **2011**, *225*, 1013–1022.
4. Lee, S.; Spencer, N.D. Achieving ultra-low friction by aqueous, brush-assisted lubrication. In: *Superlubricity*; Erdemir, A., Martin, J.-M. Eds; Elsevier: Amsterdam, The Netherlands, 2007; pp. 365–396.
5. Klein, J. Hydration lubrication. *Friction* **2013**, *1*, 1–23.
6. Neville, A.; Morina, A.; Liskiewicz, T.; Yan, Y. Synovial joint lubrication – does nature teach more effective engineering lubrication strategies? *Proc. IMechE Part C: J. Mech. Eng. Sci*. **2007**, *221*, 1223–1230.
7. Crockett, R. Tribology of natural articular joints. In: *Aqueous lubrication: Natural and Biomimetic Approaches*; Spencer, N.D. Ed; Elsevier: World Scientific, IISc Press, 2014; pp. 1–32.
8. Wang, B.; Sun, J.; Wu, Y. Lubricating performances of nano organic-molybdenum as additives in water-based liquid during cold rolling. *Adv. Mater. Res.* **2011**, *337*, 550–555.
9. Wang, Z.; Gao, D. Comparative investigation on the tribological behavior of reinforced plastic composite under natural seawater lubrication. *Materials & Design* **2013**, *51*, 983–988.
10. Lee, S.; Müller, M.; Vörös, J.; Pasche, S.; de Paul, S.; Textor, M.; Ratoi, M.; Spikes, H.A.; Spencer, N.D. Boundary lubrication of oxide surfaces by poly(L-lysine)-*g*-poly(ethylene glycol) (PLL-*g*-PEG) in aqueous media. *Tribo. Lett.*, **2003**, *15*, 231–239.
11. Ratoi, M.; Spikes, H.A. Lubricating properties of aqueous surfactant solutions. *Tribol. Trans*. **1999**, *42*, 479–486.

12. Chinas-Castillo, F.; Lara-Romero, J.; Alonso-Nunez, G.; Lopez-Velazquez, A. Tribology of aqueous thiomolybdate and thiotungstate additives in low-pressure contacts. *Tribol. Trans*. **2013**, *56*, 366–373.
13. Penga, Y.; Hua, Y.; Wang, H. Tribological behaviors of surfactant-functionalized carbon nanotubes as lubricant additive in water. *Tribol. Lett*. **2007**, *25*, 247-253.
14. Mens, J.W.M.; de Gee, A.W. Friction and wear behavior of 18 polymers in contact with steel in environments of air and water. *Wear* **1991**, *149*, 255–268.
15. Hsu, J.-P.; Lin, S.-H. Temperature dependence of the viscosity of nonpolymeric liquids. *J. Chem. Phys*. **2003**, *118*, 172–178.
16. Bair, S.; Jarzynski, J.; Winer, W.O. The temperature, pressure and time dependence of lubricant viscosity. *Tribol. Int.* **2001**, *34*, 461–468.
17. CRC Handbook of Chemistry and Physics. 89 ed.; Taylor and Francis Group LLC: 2009.
18. Tripaldi, G.; Vettor, A.; Spikes, H.A. Friction behavior of ZDDP films in the mixed, boundary/EHD regime. *SAE Trans*. **1996**, *105*, 1819–1830.
19. Dardin, A.; Hedrich, K.; Müller, M.; Ksenija, T.-M., Spikes, H.A. Influence of polyalkylmethacrylate viscosity index improvers on the efficiency of lubricants. *SAE Technical paper* **2003**, 2003-01-1967.
20. Hamrock, B.J.; Dowson, D. Minimum film thickness in elliptical contacts for different regimes of fluid-film lubrication. *Proceedings of the 5th Leeds-Lyon symposium on tribology. Bury St Edmunds, Suffolk: Mechanical Engineering Publication* **1979**, pp. 22–27.
21. Esfahanian, M. Hamrock, B.J. Fluid-film lubrication regimes revisited. *Tribol. Trans*. **1991**, *34*, 628–632.
22. Lee, S.; Spencer, N.D. Aqueous lubrication of polymers: Influence of surface modification. *Tribol. Int.* **2005**, *38*, 922–930.
23. Kumikov, V.K.; Khokonov, Kh.B. On the measurement of surface free energy and surface tension of solid metals. *J. Appl. Phys*. **1983**, *54*, 1346–1350.
24. Wu, S. Surface and interfacial tensions of polymer melts II. *J. Phys. Chem*. **1970**, *74*, 632–638.
25. Lui, M.; Sun, J.; Chen, Q. Influences of heating temperature on mechanical properties of polydimethylsiloxane. *Sensors and Actuators A* **2009**, *151*, 42–45.
26. Hutchings, I.M. Tribology: Friction and Wear of Engineering Materials, Elsevier, 1992
27. Stachowiak, G.; Batchelor, A.W. Engineering Tribology, 3rd ed. Butterworth-Heinemann, 2005.
28. Cassin,G.; Heinrich, E.; Spikes, H.A. The influence of surface roughness on the lubrication properties of adsorbing and non-adsorbing biopolymers. *Tribol. Lett*. **2001**, *11*, 95–102.
29. Bongaerts, J.H.H.; Fourtouni, K.; Stokes, J.R. Soft-tribology: Lubrication in a compliant PDMS–PDMS contact. *Tribol. Int.* **2007**, *40*, 1531–1542.
30. Glovnea, R.P.; Forrest, A.K.; Olver, A.V.; Spikes, H.A. Measurement of sub-nanometer lubricant films using ultra-thin film interferometry. *Tribol. Lett*. 2003, *15*, 217–230.

31. Guo, F.; Wong, P.L.; Fu, Z.; Ma, C. Interferometry measurement of lubricating films in slider-on-disc contacts. *Tribol. Lett*. **2010**, *39*, 71–79.
32. Bongaerts, J.H.H.; Day, J.P.R.; Marriott, C.; Pudney, P.D.A.; Willamson, A-.M. In situ confocal Raman spectroscopy of lubricants in a soft elastohydrodynamic tribological contact. *J. App. Phys*. **2008**, *104*, 014913.
33. Gohar, R.; Rahnejat, H. Fundamentals of Tribology. Imperial College Press, 2012.
34. Onset of plastic bulk deformation due to shear stress under normal load can be judged by Tresca yield criterion (sphere on plane with ideal smoothness), $\frac{3}{2}(p_m)_Y = 1.60\,Y \approx 0.6\,H \Rightarrow (p_m)_Y \approx 0.4\,H$, where p_m is the mean pressure, Y is the elastic limit and H is the hardness of the softer of the two materials in contact. The thresholds for PDMS-PDMS, POM-POM, and steel-glass are 0.8, 142 and 3140 MPa, respectively, that the contact pressures in this study are sufficiently lower than these thresholds.
35. Greenwood, J.A.; Williamson, J.B.P. Contact of nominally flat surfaces. *Proc. Roy. Soc. London Series A-Mathematical and Physical Sciences* **1966**, *295*, 300–319.
36. de Vicente, J.; Stokes, J.R.; Spikes, H.A. The frictional properties of Newtonian fluids in rolling-sliding soft-EHL contact. *Tribol. Lett*. **2005**, *20*, 273–286.
37. de Vicente, J.; Stokes, J.R.; Spikes, H.A. Soft lubrication of model hydrocolloids. *Food Hydrocolloids* **2006**, *20*, 483–491.
38. Nalam, P.C.; Clasohm, J.N.; Mashaghi, A.; Spencer, N.D. Macrotribological studies of Poly(L-lysine)-*graft*-poly(ethylene glycol) in aqueous glycerol mixtures. *Tribol. Lett*. **2010**, *37*, 541–552.
39. Mark, J.E. Polymer Data Handbook. Oxford University Press, Inc., New York, 1999.
40. The effective Young's modulus of composite layers in the antiparallel direction of the layers is calculated from the relation: $E = (f_1/E_1+f_2/E_2)^{-1}$, where f_x is volume fraction the material and E_x is the bulk Young's modulus. For the case of 2 mm PDMS layer on a 5 mm thick steel disc the effective Young's modulus is: $((0.2/0.7)/2\text{ MPa} + (0.5/0.7)/207\text{ GPa}))^{-1} = 7.0$ MPa.
41. www.matweb.com.
42. Callister, W.D.J. Material Science and Engineering, an Introduction. 7th ed. John Wiley & Sons, Inc., New York, 2007.
43. Mata, A.; Fleischman, A.J.; Roy, S. Characterization of polydimethylsiloxane (PDMS) properties for biomedical micro/nanosystems. *Biomed*. *Microdev*. **2005**, *7*, 281–293.

Supplementary Data (SD).

SD 1: Fluid film lubrication regime

To identify the regime to which a specific tribological contact belongs, two dimensionless viscosity and elasticity parameters must be evaluated by the parameters g_V and g_E:

Dimensionless viscosity parameter, $$g_V = \frac{GW^3}{U^2} \quad (1)$$

Dimensionless elasticity parameter, $$g_E = \frac{W^{\frac{8}{3}}}{U^2} \quad (2)$$

where U, G and W are the respective dimensionless parameters for speed, material, and load:

Dimensionless speed parameter $$U = \frac{\eta_0 u}{E' R_x} \quad (3)$$

Dimensionless material parameter $$G = \xi E' \quad (4)$$

Dimensionless load parameter $$W = \frac{w}{E' R_x^2} \quad (5)$$

Ellipticity parameter $$k = \frac{2}{\pi}\left(\frac{R_y}{R_x}\right)^{2\pi} \quad (6)$$

In these equations, η_0 is the lubricant's viscosity at atmospheric pressure, u is the mean speed, E' is the reduced Young's modulus, w is the applied load, R_x is the radius in the x direction, R_y is the radius in the y direction, and ξ designates the pressure viscosity coefficient. For circular contacts, the ellipticity parameter (k) is approximated to 1.The Figure S1 below shows that all three different types of contacts in this study belong to isoviscous-elastic (IE) regime for all speeds at 20 °C:

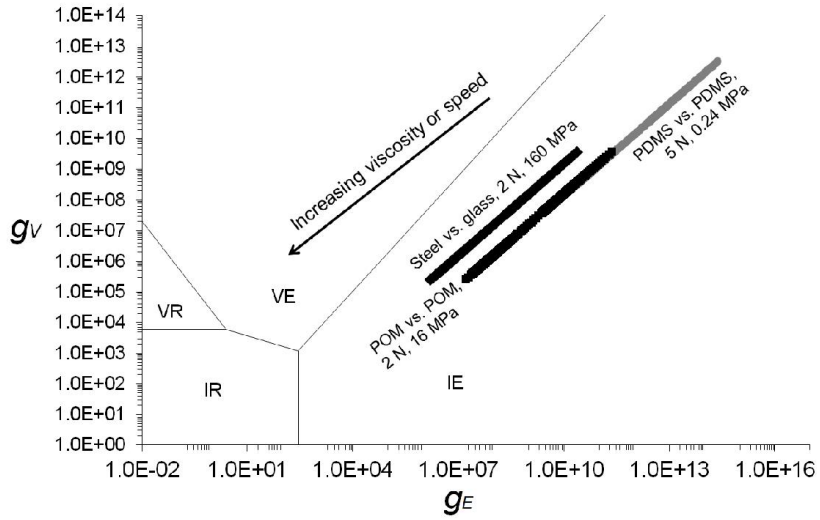

Figure S1: Fluid film lubrication regime, for the three types of contacts, Steel vs. glass (*h*-**HL**), POM vs. POM (*h*-**HB**) and PDMS vs. PDMS (*s*-**HB**/*s*-**HL**). The shown plots are for all speeds (10-1200 mm/s) at 20 °C. However, all the three types of contacts lie in the isoviscous-elastic (IE) regime in the plot even temperature is varied from 1 °C to 90 °C (not shown).

SD 2: Temperature dependence of PDMS's Young's modulus.

For elastomers, the influence of temperature on the Young's modulus (E) can be modeled by the following equation[X1]:

$$E = 3 \cdot G = 3 \cdot n_c \cdot k_B \cdot T \qquad (8)$$

where G, n_c, k_B and T is shear modulus, number of crosslinks per unit volume of an elastomer, Boltzmann's constant, and absolute temperature. In cured PDMS from Sylgard 184® at 10:1 base: crosslinker wt. ratio, the number of crosslinks is $1.6 \cdot 10^{26}/m^3$.[X2] In Figure SD2-A, E vs. temperature is plotted.

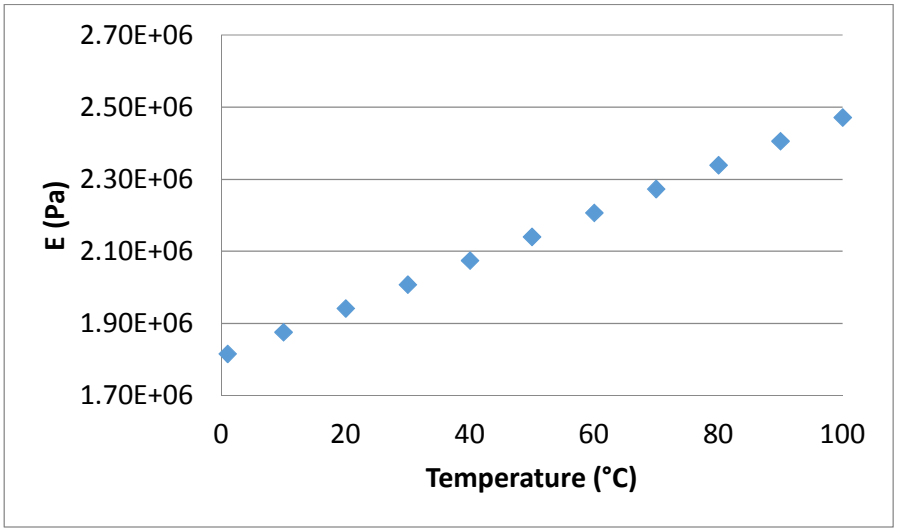

Figure SD2-A: *E* vs. temperature from 1-100 °C.

At the lowest temperature, 1 °C, E = 1.82 MPa, and the highest temperature, 90 °C, E = 2.41 MPa. The resulting effective Young's modulus of the 2 mm PDMS on the 5 mm steel disc substrate is then 6.37 and 8.43 MPa, at 1 and 90 °C, respectively. The difference in film thickness due to the change in Young's modulus as a result of temperature change is $E \propto (E_2/E_1)^{-0.45}$ = (8.43 MPa/6.37 MPa)$^{-0.45}$ = 0.88, thus only a 12 % difference in film thickness. The contact pressure change due to the difference in Young's modulus at difference temperature goes from 0.235 MPa to 0.245 MPa. Figure SD2-B below shows the calculated Stribeck parameter (λ) vs. mean speed at the different temperatures, compensated and non-compensated for the changes in Young's modulus. The difference is ignorable.

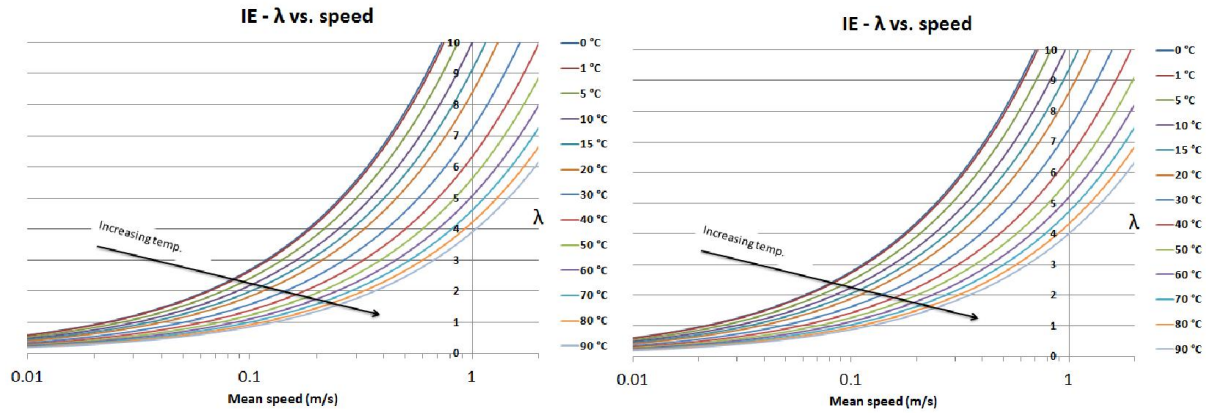

Figure SD2-B: Left plot: Calculated Stribeck parameter (λ) vs. mean speed compensated for the difference in Young's modulus caused by the change in temperature. Right plot: Calculated Stribeck parameter (λ) vs. mean speed *not* compensated for the difference in Young's modulus caused by the change in temperature.

SD 3: Theoretical calculation of μ in full-fluid film hydrodynamic regime of PDMS vs. PDMS contact.

A way to estimate the friction coefficient in hydrodynamic regime is to consider that the friction is generated solely from liquid shear between two solid surfaces.

The shear strength (σ) when shearing a (Newtonian) liquid is:

$$\sigma = \frac{du}{dy} = \frac{\frac{dx}{dt}}{dy} \cdot \eta \qquad (3)$$

where dx/dt is equal to the mean speed in the x direction, and dy is equal to the film thickness.

The shear strength (σ) is also equal to (where A is the area of contact/shear):

$$\sigma = \frac{F_{shear}}{A} \qquad (4)$$

Hence:

$$F_{shear} = \sigma \cdot A \qquad (5)$$

Substituting eq. (1) into (3) we get:

$$F_{shear} = \frac{\frac{dx}{dt}}{dy} \cdot \eta \cdot A \qquad (6)$$

And then COF is:

$$\mu = \frac{F_{shear}}{F_{load}} = \frac{\frac{\frac{dx}{dt}}{dy} \cdot \eta \cdot A}{F_{Load}} \qquad (7)$$

In eq. 5 we can insert the mean speed as dx/dt, and use the film thickness calculated by the Hamrock-Dowson equation for dy (dependent on speed). The viscosity of water is 1.75 mPas at 1 °C, and the area of contact for the PDMS-PDMS contact at 5 N load is $2.1*10^{-5}$ m^2. By using these parameters we can plot μ vs. mean speed for water at 1 °C:

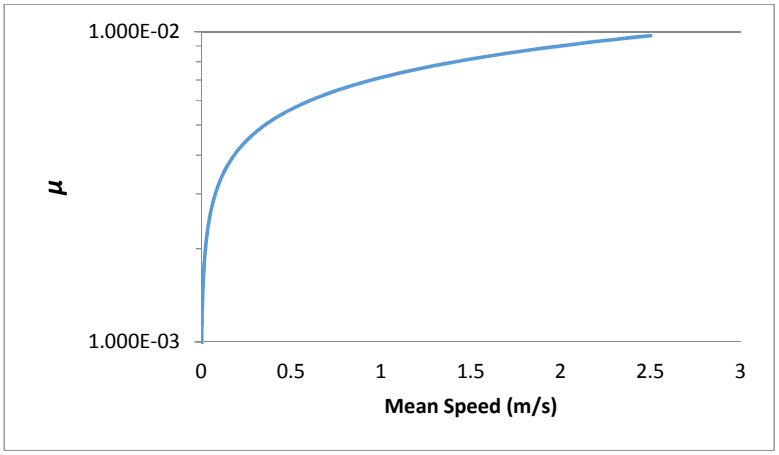

Figure SD3: Calculated μ from shearing of water layers between PDMS vs. PDMS surfaces at 1 °C.

As observed in Figure SD3, the friction coefficient is less than 0.008 even at 1.2 m/s (1,200 mm/s), hence the friction increase due the hydrodynamic shearing of water would not be observed in the operating speed range of 10-1200 mm/s even at 1 °C where the viscosity of water is largest.

REFERENCES in Supplementary Data

X1: Rubinstein, M.; Colby, R. H. Polymer Physics; Oxford University, Press, Inc.: Oxford, 2003, page 259.

X2: Wong, Eehern J., Modeling and control of rapid cure in polydimethylsiloxane (PDMS) for microfluidic device applications, Modeling and control of rapid cure in PDMS for microfluidic device applications, Ph.D. Thesis, MIT, 2010, page 58.

4.6 Lubrication of Soft and Hard Interfaces with Thermoresponsive F127 Hydrogel.

Article draft. See next pages.

Lubrication of Soft and Hard Interfaces with Thermo-responsive F127 Hydrogel

Troels Røn,[†] Ioannis S. Chronakis,[‡] and Seunghwan Lee[†]

[†] Department of Mechanical Engineering, and

[‡]DTU-Food, Technical University of Denmark, DK-2800, Kongens Lyngby, Denmark.

Abstract

In this study, we have investigated the lubricating properties of an aqueous fluid prepared with polyoxamer triblock copolymer in water, namely "F127-**20**" (F127 at the concentration of 20% w/vol). In coherent with its well-known thermo-responsive rheological properties, lubricating properties of F127 also displayed vary lubricating properties, both in the lubricating mechanism and efficacy, as a function of temperature, speed, and tribopairs. F127-**20** was most effective in lubricating a soft interface (PDMS-PDMS) based on its gel-forming properties in 22.5-60 °C and feasible formation of hydrodynamic lubricating films at all speeds. More importantly, enhanced shear thinning of F127-**20** and an optimum pressure opposed from the PDMS-PDMS tribological contact led to a substantial reduction in viscosity of the lubricant and smooth gliding of the interface while maintaining fluidic lubricating films. At temperatures lower or higher than temperature range 22.5-60 °C, F127-**20** behaved as a liquid, and boundary lubrication became the dominant lubrication mechanism.

1. Introduction

Hydrogels consisting of cross-linked hydrophilic polymer or aggregate networks in aqueous environment presents a potential as lubricant for biomedical applications due to their low friction, low toxicity, and often accompanied biocompatibility.[1,2] The applications of liquid hydrogels consisting of mixtures of water, glycerin and cellulose have been available as medical and sexual lubricants for decades.[3] Biomedical applications of permanent physical and chemical hydrogels based on chitosan, polyvinylalcohol (PVA), polyvinylpyrrolidone (PVP), polyhydroxyethylmethacrylate (PHEMA), and silicone etc. for contact lenses and tissue engineering have also been drawing increasing attentions in the last 10-15 years.[1,4,5,6] Researches on thermo-responsive hydrogels have also been active, but they have mostly been focused on drug-delivery and wound dressing healing to date.[7,8,9,10] Reversible and thermo-responsive hydrogels are interesting as lubricants too as their rheological properties can be tuned by change in temperature and that they do not degrade chemically due to mechanical stress as permanent gels do.[11] Researches on the lubricating properties of hydrogels are meaningful and interesting also in the context of broadening our understanding of fundamental lubrication mechanisms of biological systems, as they are generally lubricated by biological hydrogels such as saliva for oral and dental processing,[12] mucus for slugs[13] and for a variety of internal tissues, including colon, cervix, and gastrointestinal tract of humans and mammals.[14] Thus, hydrogels of hydrophilic synthetic polymers may be considered as substitute lubricants in biomedical applications or provide a comparison to studies on biological hydrogels at temperatures below or higher than room temperature.

In this study, we are particularly interested in polyoxamer triblock copolymer, poly(ethylene glycol)-*b*-poly(propylene oxide)-*b*-poly(ethylene glycol) (PEO-*b*-PPO-*b*-PEO) that are known to show thermo-responsive gelation in water. Among them, "F127" (PEO_{100}-b-PPO_{69}-b-PEO_{100}) has probably been most studied in terms of thermo-responsive rheological properties.[15,16,17] The conformation of F127 is dependent on both weight fraction and temperature; F127 aqueous solution transforms into a gel in the temperature range of 20-70 °C, but is a liquid with medium viscosity at temperatures below 20 °C, and finally becomes soft gel above ca. 70 °C.[17,18] The friction-reducing behavior of polyoxamers at low concentration (≤ ca. 0.5 wt.% in water) for hydrophobic PDMS interfaces has previously been studied,[19,20] but the lubricating effects in these cases were attributed to the formation of lubricious brushes based on the amphiphilic characteristics of the trilock copolymer, and they are limited to boundary lubrication. F127-based hydrogels with high viscosity that can be obtained with higher concentrations and elevated temperature have a potential to provide a broad range of

lubricating effects, from low-speed (boundary lubrication) to high-speed (hydrodynamic lubrication) regimes, due to more feasible formation of thicker lubricating films. The aim of this study is thus to investigate the lubricating properties of F127, in particular at the concentration of 20% (wt/vol), whose sol/gel state and viscosity can be tailored with the change of temperature. Unlike rheological properties, lubricating properties of fluids can be significantly different for different tribopairs. Thus, we have tested the lubricating capabilities of F127 fluid at three different tribopairs, varying in elasticity and surface hydrophilicty; soft-hydrophobic interface (*soft*-**HB**, self-mated poly(dimethylsiloxane (PDMS), hard-hydrophilic interface (*hard*-**HL**, steel-glass), and hard-hydrophobic interface (*hard*-**HB**, self-mated polyoxymethylene (POM)). The frictional properties of the same tribopairs in pure water were taken as a reference. The lubricity and predicted film thicknesses and viscosity in the tribocontact will be compared to the rheology measurement of the viscoelastic properties of F127 20% wt/vol. solutions.

2. MATERIALS & METHODS

2.1 Rheometry

Rheological measurements under low-amplitude linear viscoelastic oscillatory were performed on a controlled stress HAAKE MARS rheometer (Thermo Scientific Inc., Germany) using a parallel plate geometry (60 mm radius; 1.0 mm separation). The sample was loaded on the plate of the rheometer preset at 15 °C, and frequency sweeps (0.01 to 100 rad/sec) were carried out at different temperatures from 15 to 80 °C. The temperature sweep was performed from low to high and back to low temperature. The sample was temperature calibrated for 5 min prior to analysis. The rheological parameters of storage modulus (G'), the loss modulus (G'') were monitored as a function of temperature, and frequency of oscillation. The complex viscosity (η^*) was calculated by the following equation:

$$\eta^* = \left(\eta'^2 + \eta''^2\right)^{1/2} = \left[\left(\frac{G''}{\omega}\right)^2 + \left(\frac{G'}{\omega}\right)^2\right]^{1/2} \qquad \text{(eq. 1)}$$

2.2 Numerical model to predict the lubricating film thickness

A numerical model proposed by Hamrock and Dowson,[21] which was later revised by Esfahanian and Hamrock,[22] was employed to estimate the lubricant film thickness in tribological contact as a function of contact parameters, including tribopairs' elasticity moduli, lubricant's viscosity, as well as load and entrainment speed. In order to identify the EHL regime to which the tribological contacts in this study belong, i.e. among isoviscous-rigid (IR), piezoviscous-rigid (VR), isoviscous-elastic (IE), and piezoviscous-elastic (VE) regimes, dimensionless viscosity parameter, g_E, and dimensionless elasticity parameter, g_V, must be evaluated first.[21,22] The onset of fluid film EHL and thus low friction was evaluated by the Stribeck parameter (λ) parameter: λ = (film thickness)/(mean surface roughness), where λ parameter is defined as $\lambda = h/(\sigma_{ball}^2 + \sigma_{disc}^2)^{½}$, where σ_x are the root-mean-square roughness of ball and disc substrates. λ = 3 was applied as threshold value onset of fluid film EHL.[23] *soft*-**HB** contact lies within the IE regime for all viscosities. Transition from IE to IR regime could occur at smallest observed viscosity of 3.0 Pa·s as measured by rheometry in section 3.1, for *hard*-**HB** and *hard*-**HL** contacts, respectively. However, the estimated film thicknesses and Stribeck parameters are unrealistically high in IR regime (at 20 mm/s λ > 10 and λ > 100, for *hard*-**HB** and *hard*-**HL**, respectively). Furthermore, due to severe shear thinning of the lubricant with increasing shear rate, thus effective viscosities of the F127 fluids are most probably even less than 0.1 Pa·s at the tribological contact. Thus, IE regime was applied for all three contact types. The results of the calculations are shown in the Figure S1 (Supporting Information). Then, the lubricating film thickness for circular contacts in IE regime can be estimated according to the equation,

$$h = 3.28\left(w^{-0.21}E'^{-0.45}\eta_0^{0.66}u^{0.66}R_x^{0.76}\right) \qquad \text{(eq. 2)}$$

where η_0 is lubricant's viscosity at atmospheric pressure, u is mean speed, E' is reduced Young's modulus, w is applied load, R_x is radius in the x direction (direction of movement), which is equal to R_y in circular contact. It is noted that pressure coefficient of viscosity, the response of viscosity to pressure change, is not included as a parameter to influence the lubricating film thickness in IE regime. For the calculations of the film thickness by applying the theoretical model as described in Appendix A, the effective viscosity η_{eff} is used. In the tribobocontact we argue that $\eta_{eff} \cong \eta^*$ or that the effective viscosity consists of both viscous (η') and elastic (η'') parts. However, since the

calculated η_{eff} values in Results and Discussion section are very low and much closer to water than the F127 gel, we assess that the viscoelasticity behavior is mostly viscous not elastic.

2.3 MTM (Mini-traction Machine)

A mini-traction machine (MTM) (MTM2, PCS Instruments, London, UK) with software version 3.2.3.0 was employed to investigate the frictional properties of tribopairs lubricated with water. The principal setup of MTM consists of independently rotating ball and disc immersed in fluid lubricant with the possibility to control load and temperature (See Supporting Information for illustration). The friction forces are measured with a strain gauge connected to ball shaft arm. Coefficient of friction, μ, is defined from the relationship, $\mu = F_{friction}/F_{load}$. Independent control of disc and ball speeds allows for the variation of the degree of slide/roll ratio. The mean speed is defined as [$|speed_{ball} - speed_{disc}|/2$]. The slide/roll ratio, SRR(%), is defined as SRR(%) = ($|speed_{ball} - speed_{disc}|$)/[($speed_{ball} + speed_{disc}$)/2] × 100%, where 0% SRR represents pure rolling and 200% SRR represents pure sliding. The SRR in this study was 50% unless otherwise stated. The data points in Figure 4 and 7-11 are average values of three consecutive measurements from mean speed 5 mm/s to 1,200 mm/s at each temperature, and the error bars represent the standard deviation. The applied load was 2 N for hard contacts (POM-POM and steel-glass) and 5 N soft contact (PDMS-PDMS), respectively. Apparent contact pressures for each tribopair are shown in Table 2.

Since MTM operates with an enclosed pot inside which a lubricated tribocontact is formed, it is feasible to control the temperature. Higher temperatures than ambient were obtained by heating the pot with a built-in thermistor, whereas lower temperatures than ambient were obtained by circulating a coolant surrounding the pot. The lowest temperature at which the friction measurements were conducted was 1 °C. From 10 °C to 90 °C, the friction coefficients were measured at 10 °C increments. The temperature was automatically regulated by the MTM instrument with an accuracy of ± 1 °C, with thermocouple inside the pot. The order of measurements was from the lowest to highest temperature. There was ca. 5 min equilibration time between each temperature before measurement.

2.4 Tribopairs

3 different tribopairs have been employed (ball-disc): (a) poly(dimethylsiloxane)-poly(dimethylsiloxane) (PDMS-PDMS) to represent *soft*-**HB** interface, (b) steel-glass to represent *hard*-**HL** interface,. (c) polyoxymethylene-polyoxymethylene (POM-POM) to represent *hard*-**HB** interface, PDMS balls and discs were fabricated from a two-component kit (SYLGARD® 184, Dow Corning, Midland, MI) consisting of base PDMS and crosslinker. The PDMS base and crosslinker were mixed at 10:1 wt. ratio, and dispersed air bubbles formed during mixing were removed by a vacuum using an oil pump. For PDMS disc, the mixture fluid was poured on top of the steel disc in a plastic mold with nearly same diameter and cured overnight at 70 °C. PDMS-coated disc was obtained by removing the mold. The thickness of PDMS disc on top of the steel disc was 2 mm. PDMS balls with ¾ inch (19.05 mm) in diameter were cast in a home-machined aluminum mold. Commercially available bearing steel balls (AISI 52100) and glass discs were also employed (PCS Instruments, London, UK). POM discs were prepared by cutting from commercially available rods (Rias A/S, Roskilde, Denmark) and polished to smallest possible roughness. Commercially available POM balls (¾ inch (19.05 mm) in diameter) were used as received (Precision Plastic Ball Company, Franklin Park, IL).

Surface roughness of the discs and balls was characterized by acquiring root-mean-square roughness (Rq) from topographic images over a 100 μm × 100 μm area with tapping-mode AFM. Three different spots were characterized for statistical evaluation. In order to obtain the average asperity radius of the tribopairs, surface topographic images of 1 μm × 1 μm area were obtained. The full list of the surface roughness and asperity radii of the tribopairs is shown in Table 1. A Bruker AFM model Dimension® Edge™ and NanoScope 8.02 software were used for AFM imaging, with Nanoscope Analysis software (ver. 1.40) for calculating roughness and asperity radii.

2.5 20% wt. F127 polymer solution

Pluronics® F127 polymer (Sigma-Aldrich Denmark ApS, Brøndby, Denmark) was used as received without further purification. A solution of 20% wt./vol. (16.7% wt./wt. in water) F127 was prepared by dissolving 200 g of polymer to 1 L Millipore water and stirring the solution overnight. For the sake of simplicity, the 20% wt./vol. F127 is designated as F127-**20** and 1% wt./vol. F127 as F127-**1** hereafter.

2.6 Hydrophilization of substrates and wetting by F127

The static water contact angles on POM and PDMS surfaces were 84.8 ± 2.9° and 105.6 ± 2.2°, respectively. In order to hydrophilize PDMS balls and discs, steel, and glass, a plasma cleaner/sterilizer (Harrick Plasma, model PDC-002, New York, NY) was employed. Air plasma treatment for 3 minutes at 30 W lowered the water contact angles of the substrates significantly. See Table 1 for contact angle values of pristine and hydrophilized substrates. Table 1 also provides the relative wetting of the different surfaces by F127-**20**. Wetting tests were conducted by applying one drop of 5 °C F127-**20** (ca. 40 µL) and measure the static contact angle after 30 sec at room temperature (ca. 21 °C). The wetting is relative since the drop is increases its temperature when applied to the surface, and F127-**20** transforms into gel at room temperature.

3. Results & Discussion

*3.1 Rheological properties of F127-**20***

F127 forms viscoelastic gels at concentrations higher than 20% (wt/vol) and at temperatures higher than 20 °C, as shown in Figure 1**,** which is also in accordance with previous studies.[17,18,24]

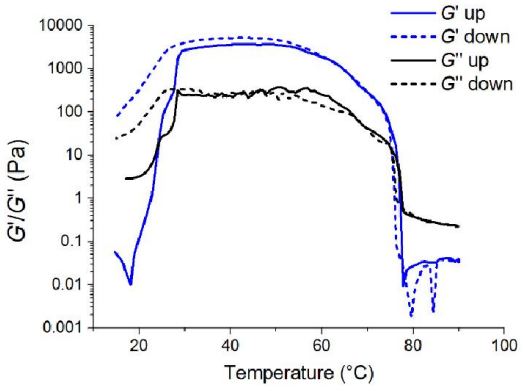

Figure 1: *G*' and *G*'' vs. temperature at 1 °C·min^{-1} heating rate and ω = 1 rad/s. 'up' corresponds to heating, whereas 'down' corresponds to cooling.

At temperature above 22.5 °C, there is a sharp increase of both elastic and loss modulus up to about 30 °C. Both *G*' and *G*'' remain constant at the temperature range 30-60 °C, whereas with further increase of temperature, both diminish and cross-over at 75 °C. This gelation is reversible. The tan δ (*G*''/ *G*') values of the sample are 0.731 at 30 °C, 0.111 at 60 °C, and 0.202 at 70 °C, denoting that the viscoelastic characteristics of the F127-**20** are temperature dependent. The gel-like rheological behavior is due to the formation of F127 micelles at above ~20 °C, spontaneously self-assembled into a face centered cubic structure.[24] Prud'homme et al. proposed that the ordered micelle structures were due to repulsive interactions among the close packed spherical micelles.[17,25]

At higher temperatures than ca. 70 °C, the volume fraction of the micelles of F127 increases but, a 'soft gel' is formed where micelles are still dominant, but their interaction is weaker.[26] At temperatures lower than 20 °C, unimer (free chain) state of F127 predominates in aqueous solution.

Figure 2 shows the complex viscosity of F127-**20** as a function of frequency of oscillation, shear rate, and temperature, respectively.

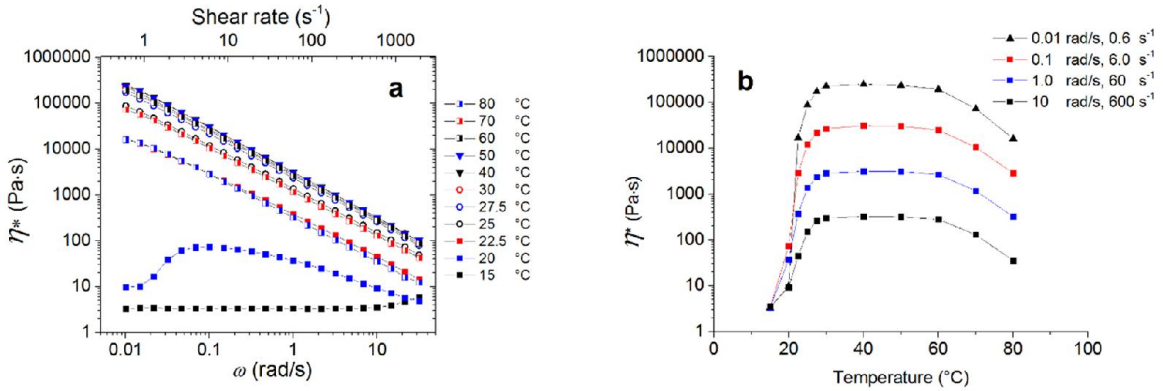

Figure 2: (a) Complex viscosity (η*) of F127-**20** vs angular frequency (ω) and shear rate. Plots of separate viscous (η') and elastic (η'') parts vs angular frequency (ω) are provided in Supporting Information. (b) Complex viscosity (η*) of F127-**20** vs temperature for angular frequency (rad/s) and shear rate (s^{-1}).

F127 micelle gels lack permanent physical or chemical cross-links, and thus sliding of the micelle layers can occur under shear, leading to shear thinning. Moreover, the slope of complex viscosity vs

frequency is close to -1, typical of gel-like systems (see section 3.2.1). The complex viscosity (η^*) of F127-**20** vs. temperature plot at different frequencies of oscillation (rad/s) or shear rate (s^{-1}) is displayed in Figure 3, and it clearly shows the lower viscosity regime for the temperatures < 20 °C and > 80 °C.

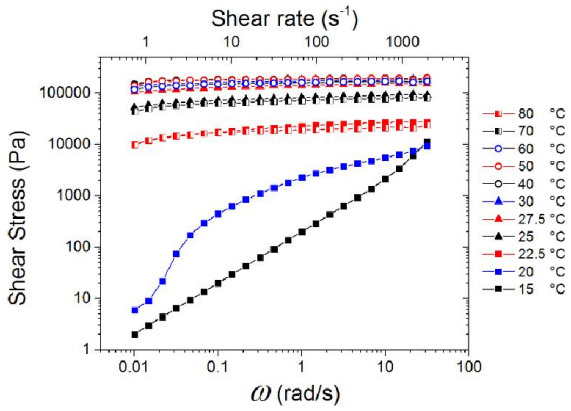

Figure 3: Shear stress of F127-**20** as a function of frequency of oscillation, shear rate at different temperatures.

Figure 3 shows the calculated shear stresses (τ) of F127-**20** from the relation $\tau = \dot{\gamma} \cdot \eta$ where shear rate ($\dot{\gamma}$) is x axis and τ is y axis. The shear stress is significantly increased due to the increase in viscosity in the gel state, ranging 20-60 °C in temperature. In the subsequent tribological studies, if sufficiently thick lubricating films are formed between the two contacting surfaces, i.e. in hydrodynamic lubrication regime, interfacial friction forces would emerge from shear stresses in shearing of F127-**20** gels.

3.2 *Lubricating properties of F127-**20***

*3.2.1 Soft-**HB** PDMS vs. PDMS contact – Comparison with Rheology Data*

As shown in Figure 4, F127-**20** lubricates *soft*-**HB** contact much more effectively (Figure 4(a)), e.g. $\mu < 0.02$ at all mean speeds and all temperatures than pure water (Figure 4(b)).

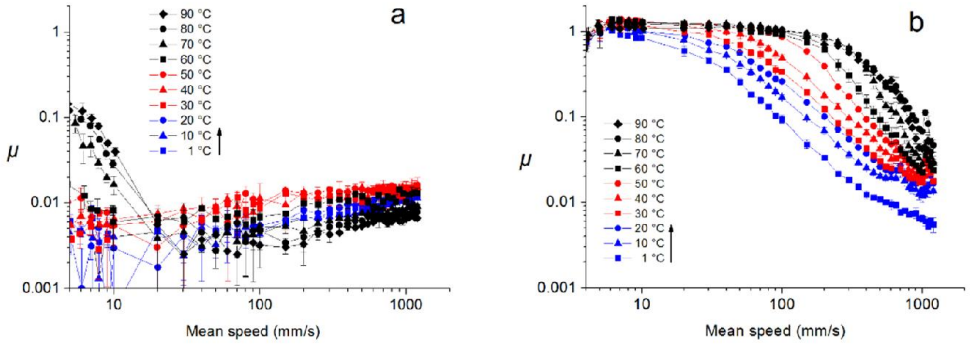

Figure 4: MTM friction experiment. (a) μ vs. mean speed for *soft*-**HB** (PDMS vs PDMS) contact in F127-**20** (b) Reference measurement of PDMS vs. PDMS contact in water. Load was 5 N and SRR = 50%.

The μ vs. mean speed plots of the F127-**20** at temperatures ≤ 60 °C (Figure 4(a)) showed the characteristics of hydrodynamic lubrication for almost the entire range of speeds where the friction increases linearly with increasing mean speed, starting from ca. 5-10 mm/s. This suggests that the film thickness is high enough to afford full separation even from low mean speeds. Furthermore, the friction forces are slightly higher at 30-60 °C than at other temperatures, which could be related to the higher viscosities at those temperatures as observed by rheometry in section 3.1; as well known, the friction force in the hydrodynamic lubrication regime is proportional to the viscosity of the lubricating films i.e. $\mu = F/w = A \cdot \dot{\gamma} \cdot \eta / w$, where A is the area of contact. In Figure 5, μ values at different speeds are plotted against temperature for visualization of the influence of temperature on the frictional properties of F127-**20**.

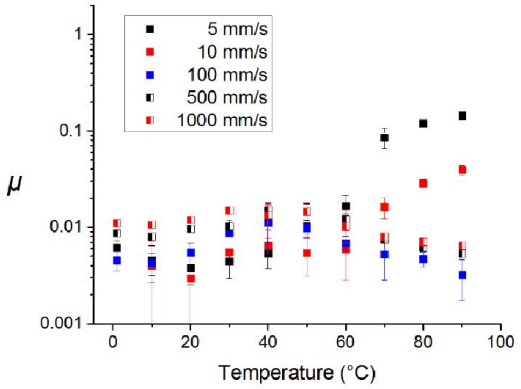

Figure 5: μ vs. temperature plot for *soft*-**HB** PDMS vs PDMS contact in F127-**20**.

In Figure 4, it is also notable that the friction forces of F127-**20** at 1-20 °C are slightly higher than those at 70-90 °C, despite the reversed relative order of viscosity according to the rheometry experiments (Figure 2(b)). This suggests that the viscosity of F127-**20** under tribological contacts does not scale with the viscosity of bulk state due to high strain.

As mentioned above, the rheological behavior of F127-**20** in section 3.1 clearly showed shear thinning behavior with increasing shear rate when the temperature is higher than ca. 22 °C (Figure 2). The shear-rate dependent viscosity is an important factor in theoretical calculation of the lubricating film thicknesses based on eq. 2 for the PDMS vs. PDMS contact in F127-**20**; the calculation results are plotted in Figure 6(a) along with the corresponding Stribeck parameter (λ) in Figure 6(b).

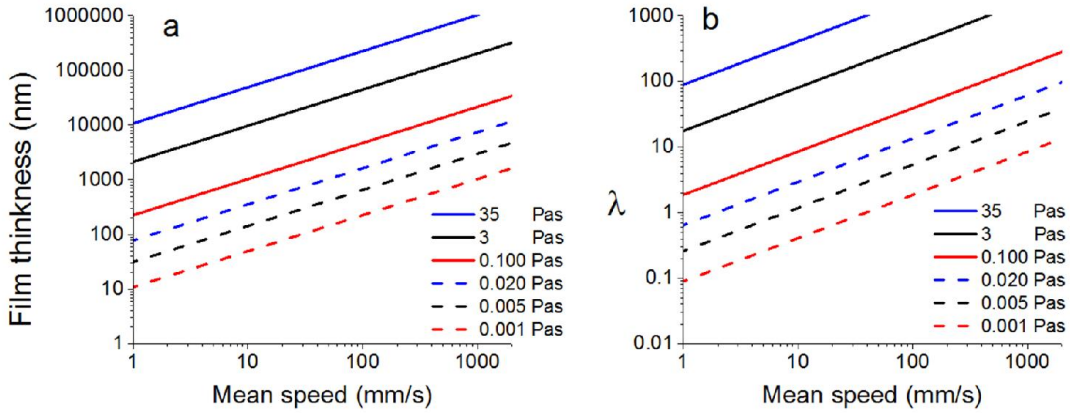

Figure 6: (a) Calculated film thickness and (b) Stribeck parameter (λ) for *soft*-**HB** PDMS vs. PDMS contact by applying eq. 2 and effective viscosities of 35, 3, 0.100, 0.020, 0.005, and 0.001 Pa·s.

The calculations show that even for the lowest viscosity of 3 Pa·s at 15 °C, where shear thinning behavior is not observed (Figure 2(a)), a film thickness of > 1 μm is expected, and consequently a Stribeck parameter larger than 20 at 5 mm/s is also expected. For the lowest viscosity of 35 Pa·s observed at 80 °C (at the highest shear rate, 600 s^{-1}), the expected film thickness is higher than 10 μm at 5 mm/s, giving λ > 100. Moreover, if the viscosities of 1000 Pa·s were applied, then it would afford film thickness of 45 μm at 10 mm/s and 2 mm at 100 mm/s (not plotted). Clearly, a direct incorporation of viscosities of F127-**20** obtained from rheometry experiments (Figure 2) into the lubricants' rheological properties under tribological contacts leads to a serious discrepancy between expected low $\mu \leq 0.01$ values in hydrodynamic regime (λ > 3) and experimentally observed values. Overall, the calculated Stribeck parameter values are unrealistically high even when the lowest viscosity is employed for the calculation of the film thickness, since the μ values in Figure 4 at 5 mm/s for the 70-90 °C ($\mu \approx 0.1$) and the corresponding estimated λ > 50 value in Figure 6(b) do not support each other.

3.2.2 Soft-**HB** *PDMS vs. PDMS contact – Theoretical μ Modeling*

In hydrodynamic lubrication regime, the two sliding surfaces are completely separated from each other, and friction forces originate entirely from shearing of the fluidic lubricant at the tribological interface and are proportional to the shear rate and the viscosity of the lubricant. Appendix A describes in detail a model for calculating the friction coefficient in a circular contact in hydrodynamic lubrication regime, where the shear rate $\dot{\gamma}$ = (mean speed)/(film thickness) and the friction/shear force $F_{shear} = A \cdot \tau = A \cdot \dot{\gamma} \cdot \eta$, resulting in $\mu \propto u^{0.34} \cdot \eta^{0.34}$. Thus, theoretically predicted μ values can be plotted as a function of speed (u) with different viscosities (η) of lubricants and can be compared with the experimentally determined μ vs speed plots, as shown in Figure 7(a).

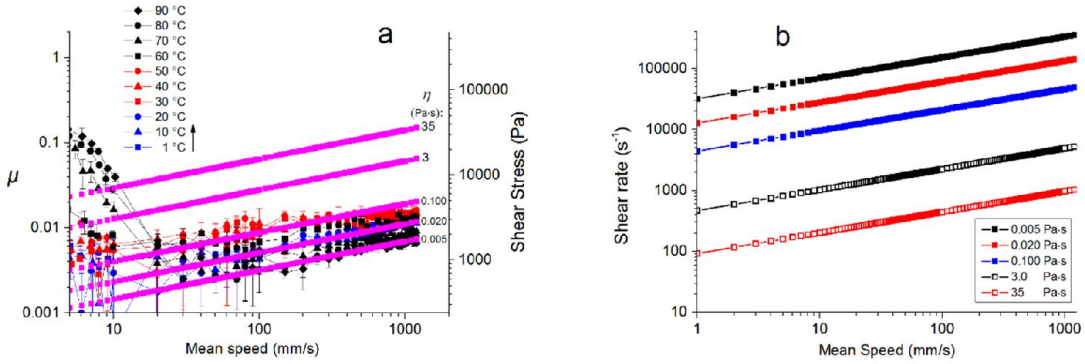

Figure 7: (a) μ and shear stress vs. mean speed plot as in Figure 4(a) with theoretically calculated μ due to hydrodynamic shearing of the lubricant at effective viscosities 0.005, 0.020, 0.100, 3 and 35 Pa·s. (b) Theoretically calculated shear rates. Both (a) and (b) for *soft*-**HB** PDMS vs. PDMS contact.

In the calculation of the theoretical μ values in Figure 7(a), the viscosity was assumed to be constant and fitted to the best average at all mean speeds. Likewise, shear rates of F127-**20** under the tribological contact Figure 7(a) can be plotted as a function of speed with varying viscosities, as shown in Figure 7(b). In Figure 7(a), the lubricants with the viscosities of 3.0 and 35 Pa·s display higher calculated μ values arising from hydrodynamic shearing at PDMS vs. PDMS interface than the experimental results. Instead, the experimentally measured μ values are better matched with calculated μ values when the viscosities of 0.005, 0.020 and 0.100 Pa·s are employed, in the temperature ranges of 70-90, 1-20 and 30-60 °C, respectively. These theoretically predicted viscosities – lower than those observed from rheometer experiments – also corroborate reasonably well with the calculated λ values in Figure 6(b); the threshold speed where λ reaches 3 (hence predicting the approximate onset of the hydrodynamic lubrication regime) is 2 mm/s for η = 0.100 Pa·s, 11 mm/s for η = 0.020 Pa·s, and 42 mm/s for η = 0.005 Pa·s. Thus, the effective viscosities at the tribological interfaces must be much smaller than those observed by rheometry experiments in section 3.1. If hydrodynamic lubrication mechanism is indeed prevailing at the tribological contacts, the μ values were expected to be proportional to the viscosities at varying temperature as seen in section 3.1, i.e. μ(30-60 °C) > μ(70-90 °C) > μ(1-20 °C). The data from Figure 4(a) shows, however, that the ranking of μ values is μ(30-60 °C) > μ(1-20 °C) > μ(70-90 °C), although the differences are very small. This indicates that, as mentioned above, friction forces in hydrodynamic regime may

be more complicated due to the complex relationship between shear rate, viscosity, and lubricating film thickness.

Figure 7(b) shows the calculated shear rates of F127-**20** with different viscosities applied in the calculation of the theoretical μ values (pink squares in Figure 7(a)). It is noted that the calculated shear rates are orders of magnitude higher than those employed in the rheometry experiments. The higher calculated shear rates are not related to high mean speeds, but rather very small surface separation, i.e. much lower lubricating film thickness compared to the 1 mm gap applied in rheology measurements in section 3.1 (note that shear rate $\dot{\gamma}$ = (mean speed)/(film thickness)). The experimentally obtained shear stresses (Figure 7(a)) of 1-4 kPa are much less than the limiting shear stresses of ca. 100-200 kPa (Figure 3) at temperatures higher than 20 °C where F127-**20** is a gel. The shear stress is derived from $\tau = \mu \cdot w/A$ where μ is the coefficient of friction and A is the Hertzian contact area. The lower shear stress and consequently lower μ values in the tribological contact further support that the effective viscosity at the PDMS vs. PDMS tribological interface must be much lower than the complex viscosities observed in section 3.1. For instance, if the viscosity of 1000 Pa·s as observed at 22.5 °C were applied (Figure 2(b)), it would afford much higher theoretical friction values, such as μ = 0.1 at 10 mm/s and μ = 0.4 at 1000 mm/s.

3.2.3 Soft-**HB** *PDMS vs. PDMS contact – Structural and Rheological Interpretation*

As mentioned above, the reason for the effectively much lower viscosities than those as measured by rheometry is enhanced shear thinning of F127-**20** at the PDMS vs PDMS tribological interface, and it is responsible for much higher shear rates, lower μ values, and lower shear stress. The gelation of F127 polymer solutions has been ascribed to the close packing of spherical micelles of F127 (as described in section 3.1), where the shear thinning is attributed to the sliding of stacked micelle layers in the flow direction[24] and occurs when the inverse of the shear rate exceeds the relaxation time of the sheared system/solution,[17] i.e. higher Deborah number. Applying a power law model[27] for the non-Newtonian liquid, one can fit the viscosity vs. shear rate to the following equation:

$$\eta^* = B \cdot \dot{\gamma} \qquad \text{(eq. 3)}$$

We approximate that the complex viscosity (η^*) equals to η_{eff}, where B is a proportionality coefficient. The model allows us to extrapolate the experimental complex viscosity vs. shear rate data, thus enabling prediction of the viscosity at higher shear rates. Fitting the power law to the temperatures 80 °C and 40 °C gave the generally lowest and highest complex viscosities with shear thinning behavior in the η^* vs. shear rate data in Figure 2. This gives $\eta^* = 13571 \cdot \dot{\gamma}^{-0.924}$ at 80 °C and $\eta^* = 171777 \cdot \dot{\gamma}^{-0.981}$ at 40 °C. If the highest estimated shear rate of ca. 200 000 s^{-1} from the lowest viscosity of 0.005 Pa·s and the highest mean speed in Figure 7(b) are used in the calculation, the η_{eff} values are 0.17 and 1.08 Pa·s, at 80 and 40 °C, respectively, i.e. within ca. one order of magnitude of the theoretically predicted viscosities in Figure 7(a). However, if medium value of ca. 10 000 s^{-1} of the predicted shear rates in Figure 7(b) is applied, then the obtained complex/effective viscosities are 2.7 and 20.5 Pa·s for 80 and 40 °C, respectively. Thus, fitting rheology data by eq. 3 and extrapolating even to very high shear rates still gives inaccurate effective viscosities for the tribocontact. The hydrodynamic radius of F127 micelles have been reported to be 8-11 nm,[17] hence when the film thickness approaches that value, the continuum approximation fails. At breakdown of the micelle layer structure at low separations, the effective viscosity may be close to that of the base lubricant/solvent (in this case water), or at least is not reflecting the viscosity of the aggregated structure. The shearing of the gel is most probably in non-linear viscoelastic regime, i.e. high Deborah number (high shear rate) and high strain,[26] which is probably the cause for false estimation of viscosities based on the eq. 3., along with Knudsen number close to one (small separation compared to the micelle size) caused by the load squeezing the contact together. Shear thinning of F127 due to non-linear viscoelastic behavior of F127 has been observed before at higher strains of $\gamma > 1000\%$;[28] in the present case, the strains could be even higher due to the small gap/film thickness in the tribocontact.

At low temperatures, such as 15 and 20 °C, the tribological shear stress in Figure 7(a) is close to that in Figure 3 for rheological behavior of F127-**20**. In this temperature range, the micelles are not aggregated into a gel structure nor is micellization pronounced, but the unimer state is predominant.[18] Hence, the lubricating effects observed at ≤ 20 °C could be ascribed primarily to the brush formation of the unimers at the *soft*-**HB** PDMS-vs-PDMS interface.[19] Since the hydrodynamic regime is not apparent for mean speeds < 10 mm/s at 70-90 °C, the lower friction of F127-**20** compared to pure water (Figure 4(a-b)) could also be attributed to the amphiphilic nature of F127 copolymers' ability to bind onto and lubricate PDMS sliding interfaces.[19] If the lubricating effects in the temperature range of 70-90 °C and mean speeds < 10 mm/s are primarily due to the boundary lubricating by

unimer F127 molecules, distinctively higher friction forces at 70-90 °C ($\mu \approx 0.1$) than 1-20 °C could be the lower availability of unimers at 70-90 °C. F127-**20** does still have a large degree of micellization at 70-90 °C but the fluid in this condition is a soft gel,[25] as compared to that at 1-20 °C where unimers are predominant.

As a comparison, the lubricating properties of F127-**1** at the *soft*-**HB** contact are displayed in Figure 8.

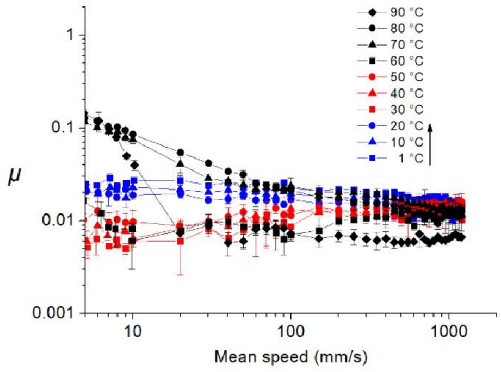

Figure 8: MTM friction data of PDMS vs. PDMS tribopair in F127-**1** in water. 5 N load, 50% SSR.

The μ vs speed plots in the lower mean speeds regime is quite similar to those obtained by lubrication with F127-**20**, although the μ values at 70-90 °C were somewhat higher. This means that in low-speed regime, the lubrication by F127-**20** is dominated by boundary lubrication mechanism, and there is no large difference between F127-**1** and F127-**20**. Unlike the case of F127-**20**, a clear drop, followed by a gradual increase of μ, the signature of onset of hydrodynamic lubrication, is missing in F127-**1**. This could be ascribed to low viscosity of F127-**1**, resulting in low film thickness or to that micelles in F127-**20** can supply more unimers to the sliding contact. Nevertheless, at other temperatures and mean speeds, the μ values of F127-**1** were higher than those of F127-**20** by ca. 0.015. Thus, F127-**20** provides enhanced lubrication compared to F127-**1** primarily by higher viscosity and more feasible formation of hydrodynamic lubricating films. For F127-**1**, only unimer state is present, thus the poor lubrication at the highest temperatures (70-90 °C) in low-speed regime could also be attributed to

more desorption of F127 as facilitated by the entropy gain and consequent deficit of unimers as described above.

3.2.2 *Hard contacts: Steel ball vs. glass disc and POM vs. POM*

As shown in Figure 9(a), the high μ values for the *hard*-**HL** steel ball vs. glass disc at the lowest mean speeds in F127-**20** are generally close to those from the reference measurements in water (Figure 9(b)).

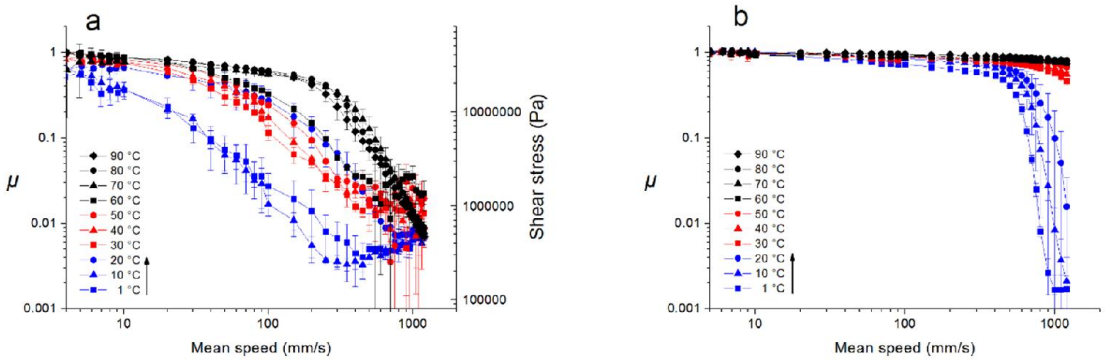

Figure 9: (a) μ and shear stress vs mean speed plot of *hard*-**HL** steel ball vs. glass disc in F127-**20** (b) Reference μ vs mean speed plot of steel ball vs. glass disc in water. 2 N load and SRR = 50%.

At all temperatures, the μ values in F127-**20** were observed to be < 0.02 when the mean speed reaches 1000 mm/s or higher. At 1-10 °C, μ < 0.01 was observed already at 500 mm/s. However, at 1-20 °C, μ values of < 0.02 were also observed in the reference water solution (Figure 9(b)), even though the viscosity of water is only ca. 1 mPa·s. However, no onset of hydrodynamic regime was observed in neat water. For F127-**20**, the lowest μ values are observed for temperatures 1-10 °C for mean speeds ≥ 500 mm/s where apparent onset of hydrodynamic regime is observed (Figure 9(a)). Interestingly, F127-**20** provides the lowest μ values at 1-10 °C for the entire span of mean speeds. As emphasized in previous sections, at < 20 °C unimers dominate F127-**20** and the viscosity is lower than at higher temperatures due to the lack of gel formation. For steel ball vs. glass disc tribopair, the apparent contact pressure is 160 MPa, hence the gel is probably easily squeezed out of the contact and/or

subjected to severe shear thinning and strain. Furthermore, the shear stresses in the contact are much higher (0.4-100 MPa) for most of the mean speeds compared to F127 gel (Figure 3) in bulk state, where the highest limiting shear stress is only ca. 0.2 MPa, thus the friction is probably caused by boundary tribostress between the steel ball and glass disc, not fluidic slip of F127 gel at the interface. The shear stress of F127-**20** in Figure 9 at temperatures 1 and 10 °C and mean speeds 500-1200 mm/s (Figure 9(a)) is close to the limiting shear stress of the F127 gel. However, as unimers dominate F127-**20** solution at < 20 °C, and the limiting shear stress in Figure 3 at 15 and 20 °C is less than that at the higher temperatures of gelation, slip of the gel at the interface at temperatures less than 20 °C is unlikely to occur. Rheological properties of F127-**20** could unfortunately not be characterized at temperatures below 15 °C.

Figure S2(a-b) in the Supporting Information display the calculated film thicknesses and Stribeck parameter (λ) for the steel ball vs. glass disc contact. The onset of the hydrodynamic lubrication regime (λ = 3) at 500 mm/s fits best with a viscosity of 0.050 Pa·s for F127-**20**. However, this viscosity value is too low compared to the viscosity needed to match the theoretically calculated μ values, i.e. 1-3 Pa·s (Figure 10(a)).

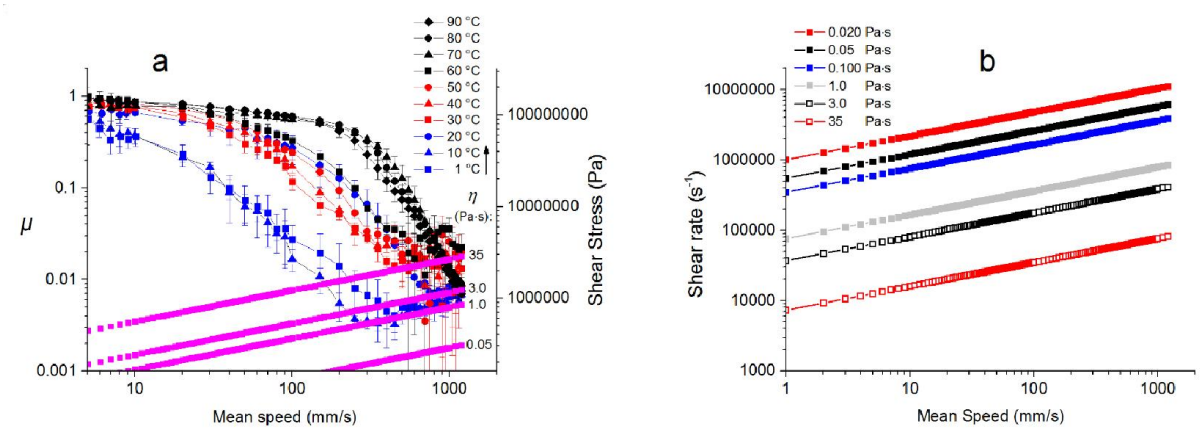

Figure 10: (a) μ vs mean speed plot as in Figure 9(a) with theoretical calculated μ due to hydrodynamic shearing of the lubricant at viscosities 0.05, 1, 3 and 35 Pa·s. (b) Theoretical calculated shear rates. Both (a) and (b) for *hard*-**HL** steel ball vs. glass disc contact.

Viscosities in that range would afford the onset of the hydrodynamic lubrication regime ($\lambda = 3$) from 5 and 15 mm/s, for 1 and 3 Pa·s, respectively. The tribological *hard*-**HL** contact at 1-10 °C in the mean speeds ≥ 500 mm/s is probably in mixed EHL lubrication regime where the asperities in contact are to some extent lubricated by boundary lubricant films of F127. At all temperatures, the μ values in F127-**20** were lower than those in the reference measurement in water (Figure 9(b)) in the 20-700 mm/s regime, which indicates that some extent of boundary lubrication mechanisms are active. Given the relative hydrophilic nature of the interface, hydrogen bonding between hydroxyl groups on both tribopairs and oxygen atoms in the ether bond of both PPO and PEO could retain some F127 polymers at the sliding/rolling contact interface, thus affording boundary lubricating effect at mean speeds < 700 mm/s. In turn, the activation of boundary lubrication mechanism by F127 means that its effect would be proportional to the availability of free unimers, which is the predominant state of F127 at ≤ 20 °C, and it can explain the observed lowest friction in that temperature regime.

Figure 11(a) shows the μ vs mean speed plots of the tribological contacts of *hard*-**HB** POM ball vs. POM disc in F127-**20**. Unlike the other tribopairs, the POM-POM pair was not effectively lubricated by F127-**20**. For instance, at ≤ 50 °C, μ values varied from 0.2 to 0.08 in F127-**20**, and they are only marginally lower than those in distilled water, namely, μ = from 0.4 to 0.2 over the entire speed range (Figure 11(b)).

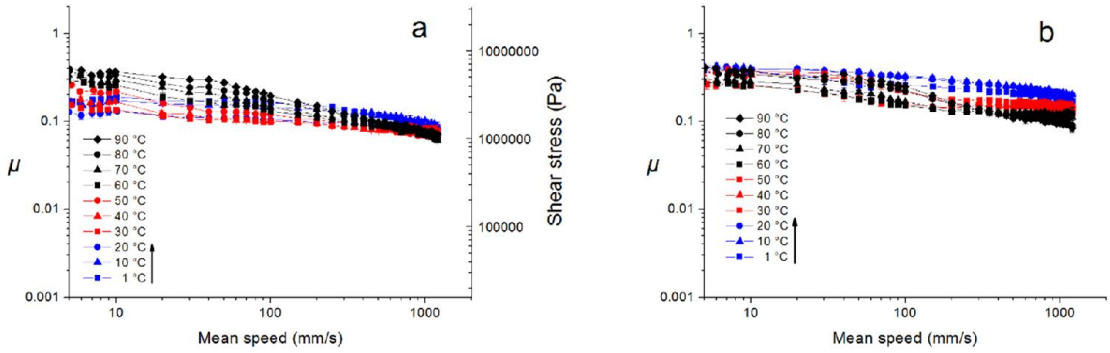

Figure 11: MTM friction data. (a) μ vs mean speed plot of POM ball vs. POM disc in F127-**20** (b) Reference μ vs mean speed plot of *hard*-**HB** POM ball vs. POM disc in water. 2 N load and SRR = 50%.

The calculated film thicknesses and Stribeck parameter for the POM-vs-POM tribopair are displayed in Figure S3 in the Supporting Information and show that a viscosity of 1 Pa·s is needed in order to

obtain $\lambda > 3$ for even relatively high mean speeds, such as 100 mm/s or higher. The F127-**20** appears to provide only negligible extent of lubricity at the POM vs. POM contact, which is in contrast to the case of steel ball vs. glass disc contact where the shear stresses are similar but the normal contact pressure is 10 times higher (For POM vs. POM contact pressure is 16 MPa). The poor lubricity for POM vs POM tribopair is attributed to severe shear thinning of F127-**20** solution at this tribocontact, leading to low viscosities and consequently too thin film thicknesses to separate the asperities of the contact. Additionally, the relative wettability of F-127 on the tribopairs seems to play a role; the relative wettability of the two hard contacts shown in Table 1 supports that F127-**20** wets plasma treated steel and glass surfaces better than the POM surface. The F127-**20** contact angles were 42.0 ± 1.4°, 33.9 ± 0.8° and 58.1 ± 1.7°, for steel, glass and POM surfaces, respectively. The better wettability of the hydrophilic steel vs glass contact by F127-**20** suggests better interaction and thus better retention of F127-**20** at contact, resulting in better lubrication. Even though unimers in the F127-**20** solution were expected to adsorb and lubricate the hydrophobic POM surfaces via their amphiphilic nature, as observed on hydrophobic PDMS, only very small magnitude of friction decrease was observed in the low temperature regime, (≤ 10 °C).

4.0 Conclusions:

We have studied the lubricating properties of F127-**20** (F127 20% w/vol. in water) as a function of temperature at 3 types of tribological contacts, soft-**HB** (PDMS vs PDMS), hard-**HL** (steel ball vs. glass disc), and hard-**HB** (POM ball vs. POM disc), and compared the lubrication performance with rheological data of F127-**20**. The lubricating properties of F127-**20** showed a complex dependence on temperature, primarily due to its temperature-dependent rheological properties and additionally complex shear thinning properties under tribological contacts. Among three different tribopairs, F127-**20** was most effective in lubricating the PDMS vs. PDMS contact in the temperature range of 1-60 °C at all speeds. The lubricating effects in temperature range 22.5-60 °C can be ascribed to F127-**20**'s activation of hydrodynamic lubrication mechanisms via sufficiently high viscosity to generate lubricating film. But, subsequent lowering of viscosity through enhanced shear thinning under tribological contacts, where the film thickness is much smaller than rheological measurements, leads to smooth gliding of the interface. The lubricating effects at low temperatures (1-20 °C) and low mean speeds (ca. 5-30 mm/s) could be ascribed to the brush formation following adsorption of unimers onto the tribopair surfaces due to the amphiphilic nature of F127. At all temperatures, i.e. whether gels are formed or not, hydrodynamic lubrication mechanism dominates at higher mean

speeds > 50 mm/s. However, in low-speed regime, good lubricity of F127-**20** fails when temperature reaches 70-90 °C. At temperatures lower or higher than temperature range 22.5-60 °C, F127-**20** behaved as a liquid with much lower viscosities compared to viscosities measured by rheometry. F127-**20** showed severe shear thinning behavior as a gel. This behavior was extensively pronounced in the tribocontact, where the estimated viscosities were many orders of magnitude lower than measured by rheometry probably due to non-linear behavior induced by very high strains and compression. F127-**20** lubricated the steel ball vs. glass disc contact moderately, and lubricating effect was negligible for POM vs. POM contact. The poor lubrication properties were ascribed to the severe shear thinning behavior of F127-**20** in the hard contacts, where the high contact pressure squeezes out the gel of F127 and/or induces high shear rates that the effective viscosities are close to that of the base lubricant of water, hence affording lower film thicknesses. Better lubricity of F127-**20** for the steel ball vs. glass contact compared to POM vs. POM was attributed to the better wettability of the former, despite the ten times higher contact pressure. Shear thinning behavior of F127-**20**, and further enhanced shear thinning under tribological contacts may be favorable for the lubrication of PDMS vs. PDMS as the dominant lubrication mechanism is hydrodynamic lubrication and lower viscosity can reduce the friction effectively.

5.0 References:

[1] Gong, J. P. *Soft Matter*, **2006**, *2*, 544-552.

[2]Ishikawa, Y.; Hiratsuka, K.; Sasada, T. *Wear*, **2006**, 500-504.

[3] (a) Patent: US 5208031 A. Sexual lubricants containing zinc as an anti-viral agent. (b) Mehta, H. K.; *British Journal of Ophthalmology*, **1984**, *68*, 765-767.

[4] Dunn, A. C; Urueña, J. M.; Hou, Y.; Perry, S. S.; Angelini, T. E.; Sawyer, W. G. *Tribol Lett*, **2013**, *49*, 371-378.

[5] Freeman, M. E.; Furey, M. J.; Love, B. J. Hampton, J. M. *Wear*, **2000**, *241*, 129-135.

[6] Berger, J., Reist, M.; Mayer, J.M.; Felt, O.; Gurny, R.; *Eur. J. Pharm. Biopharm.*, **2004**, *57*, 35-52.

[7] Gilbert, J. C.; Hadgraft, J.; Bye, A.; Brookes, L. G.; *International Journal of Pharmaceutics*, **1986**, *32*, 223-228.

[8] Bhattarai, N.; Gunn, J.; Zhang, M.; *Adv. Drug Deliv. Rev.*, **2010**, *62*, 83-99.

[9] Rimmer, S.; Biomedical Hydrogels, Woodhead Publishing Ltd., 2011, Cambridge, UK.

[10] Corkhill, P. H.; Hamilton, C. J.; Tighe, B. J.; *Biomaterials*, **1989**, *10*, 3-10.

[11] Gong, J. P., Katsuyama, Y.; Kurokawa, T.; Osada, Y., *Adv. Mater.*, **2003**, *15*, 1155-1158.

[12] (a) de Wijk, R. A.; Prinz, J. F., *Journal of Texture Studies*, **2006**, *37*, 413–427. (b) Sajewicz, E., *Tribol Int*, **2009**, *42*, 327-332.

[13] Zhou, Y.; Huitink, D.; Liang, H.; *Materials Performance and Characterization*, **2012**, *1*, 1-8.

[14] Lai, S. K.; Wang, Y-Y.; Hanes, J.; *Adv. Drug Deliv. Rev.*, **2009**, *61*, 158-171.

[15] Malmsten, M.; Lindman, B. *Macromolecules*, **1993**, *26*, 1282-1286.
[16] Chen-Chow, P.; Frank, S. G.; *International Journal of Pharmaceuticals*, **1981**, *8*, 89-99.

[17] Prud'homme, R. K.; Wu, G.; Scheider, D. K. *Langmuir*, **1996**, *12*, 4651-4659.

[18] Wanka, G.; Hoffmann, H; Ulbricht, W. *Macromolecules*, **1994**, *27*, 4145-4159.

[19] Lee, S.; Iten, R.; Müller, M.; Spencer, N. D.; *Macromolecules*, **2004**, *37*, 8349-8356.

[20] Lee, S.; Spencer, N. D.; *Tribol Int*, **2005**, *38*, 922-930.

[21] Hamrock BJ, Dowson D. Minimum film thickness in elliptical contacts for different regimes of fluid-film lubrication. Proceedings of the 5th Leeds-Lyon symposium on tribology. Bury St Edmunds, Suffolk: Mechanical Engineering Publication 1979; p. 22–27.

[22] Esfahanian M, Hamrock BJ. Fluid-film lubrication regimes revisited. Tribol Trans 1991;34(4): 628–632.

[23] Gohar, R.; Rahnejat, H., Fundamentals of Tribology, 2nd Edition. Imperial College Press, London, UK, 2012.

[24] Wu, C.; Liu, T; Chu, B.; Schneider, K. D.; Graziano, V. *Macromolecules* **1997**, *30*, 4574–4583.

[25] Jiang, J.; Burger, C; Li, C.; Li, J.; Lin, M. Y.; Colby, R. H.; Rafailovich, M. H.; Sokolov, J. C. *Macromolecules*, **2007**, *40*, 4016-4022.

[26] Chaibundit, C.; Ricardo, N. M. P. S.; Costa, F. d. M. L. L.; Yeates, S. G.; Booth, C. Langmuir, 2007, 23, 9229-9236.

[27] Macosko, C. W.; Rheology: Principles, Measurements and Applications, Wiley, NY, USA, 1994.

[28] Hyun, K.; Nam, J. G.; Wilhellm, M.; Ahn, K. H.; Lee, S. J.; *Rheol Acta*, **2006**, *45*, 239–249.

[29] Mark J. E. Polymer Data Handbook. Oxford University Press, Inc., New York;1999.

[30] The effective Young's modulus of composite layers in the antiparallel direction of the layers is calculated from the relation: $E = (f_1/E_1+f_2/E_2)^{-1}$, where f_x is volume fraction the material and E_x is the bulk Young's modulus. For the case of 2 mm PDMS layer on a 5 mm thick steel disc the effective Young's modulus is: $((0.2/0.7)/2 \text{ MPa} + (0.5/0.7)/207 \text{ GPa}))^{-1} = 7.0$ MPa.

[31] www.matweb.com.

[32] Callister WDJ. Material Science and Engineering, an Introduction. 7th ed. John Wiley & Sons, Inc., New York;2007.

[33] Mata A, Fleischman AJ, Roy S. Characterization of polydimethylsiloxane (PDMS) properties for biomedical micro/nanosystems. Biomedical Microdevices 2005;7(4):281-293.

Table 1. Bulk mechanical and surface properties of the tribopair materials.

Substrate	**Young's modulus (MPa)**	**Poisson's Ratio**	**Hardness (MPa)**	**Roughness, R_q, (nm)**		**Asperity diameter average (nm)**		**Static water contact angle (°)**
				Disc	Ball	Disc	Ball	
PDMS	2.0[32] (7.0)[a,33]	0.5 [32]	2.2[f]	1.6 ± 0.3	121.4 ± 36.4	No asperities	1448 ± 300	pristine: 105.6 ± 2.2[e] F127-**20**: 81.8 ± 0.3
POM	3100[34]	0.35[34]	354[34,h]	223 ± 51	659 ± 179	5086 ± 504	4743 ± 1419	pristine: 84.8 ± 2.9[c] F127-**20**: 58.1 ± 1.7
Steel (AISI E 52100)	210000[34]	0.3[34]	8319[34]	-	26.1 ± 5.5		116 ± 17	pristine: 57.5 ± 0.7[b] plasma tr.: < 2[b] F127-**20**: 33.9 ± 0.8[b]
Glass	73000[35]	0.17[35]	7848[34]	2.9 ± 0.3	-	73 ± 49		pristine: 32.9 ± 3.3 plasma tr.: < 2 F127-**20**: 42.0 ± 1.4

[a] 7.0 MPa represents the effective Young's modulus of a 2 mm PDMS layer on steel.

[b] Contact angle of water on 304 steel plate. F127-**20** wetting test were performed on plasma treated surface in the case of steel and glass.

[c] Hydrophobic surfaces with high roughness can have increased contact angle due to Wenzel effect.

[e] PDMS disc (smooth)

[f] Estimated from the (tensile strength)/3.45. 7.5 MPa/3.45 = 2.2 MPa. [35,36]

[h] Estimated from Rockwell M hardness

Table 2. Contact characteristics of the tribopairs: load, Hertzian contact pressure, reduced Young's modulus (*E'*), mean surface roughness (σ*), and plasticity index: ($\psi = (E'/H)\cdot(\sigma/R_{asp})^{.½}$

	HYDROPHILIC	**HYDROPHOBIC**
Soft	-	***PDMS-PDMS***
Load		5 newton
E'		2.07
Pressure		0.24 MPa
σ*		116.9 nm
ψ		0.27
Hard	***Steel*†*-glass*†**	***POM-POM***
Load	2 newton	2 newton
E'	56700 MPa	1766 MPa
Pressure	160 MPa	16 MPa
σ*	26.3 nm	695 nm
ψ	5.8	1.9

†Plasma-treated

Appendix A:

Theoretical calculation of μ in full-fluid film hydrodynamic regime of PDMS vs. PDMS contact.

A way to estimate the friction coefficient in hydrodynamic regime is to consider that the friction is generated solely from liquid shear between two solid surfaces.

The shear strength (τ) when shearing a (Newtonian) liquid is:

$$\tau = \dot{\gamma} \cdot \eta = \frac{du}{dy} \cdot \eta = \frac{dx/dt}{dy} \cdot \eta \qquad \text{(A1)}$$

where dx/dt is equal to the mean speed in the x direction, and dy is equal to the film thickness.

The shear strength (τ) is also equal to (where A is the area of contact/shear):

$$\tau = \frac{F_{shear}}{A} \qquad \text{(A2)}$$

Hence:

$$F_{shear} = \tau \cdot A \qquad \text{(A3)}$$

Substituting eq. (A3) into (A1) we get:

$$\tau = \frac{dx/dt}{dy} \cdot \eta \cdot A \qquad \text{(A4)}$$

And then the friction coefficient is:

$$\mu = \frac{F_{shear}}{F_{load}} = \frac{\frac{dx/dt}{dy} \cdot \eta \cdot A}{F_{load}} \qquad \text{(A5)}$$

In eq. 7 we can insert the mean speed as dx/dt, and use the film thickness calculated by the Hamrock-Dowson equation for dy (dependent on speed). The area of contact at 5 N load is $2.1*10^{-5}$ m^2 for PDMS vs. PDMS, $1.25*10^{-8}$ m^2 for steel ball vs. glass disc at 2 N load and $1.25*10^{-7}$ m^2 for POM vs. POM. When equation (A5) is combined with the Hamrock-Dowson equation the expression is:

$$\mu = \frac{u^{0.34} \cdot \eta^{0.34} \cdot E'^{0.45} \cdot A}{3.28 \cdot w^{0.79} \cdot R_x^{0.76}} \qquad \text{(A6)}$$

Thus in the theoretical μ values in the hydrodynamic regime scales to both mean speed and the viscosity to the 0.34^{th} power. The theoretical predicted μ values at different viscosities are presented in Figure X5(a) for PDMS vs. PDMS. The shear rates in Figure 7 and 10 are obtained by first fitting

eq. A6 to the experimental μ values by varying the viscosity. The viscosity which fit the data is then applied in eq. 2 to obtain the film thickness, and then the shear rate is calculated by the relation: Shear rate = (mean speed/film thickness).

6. Supporting Information.

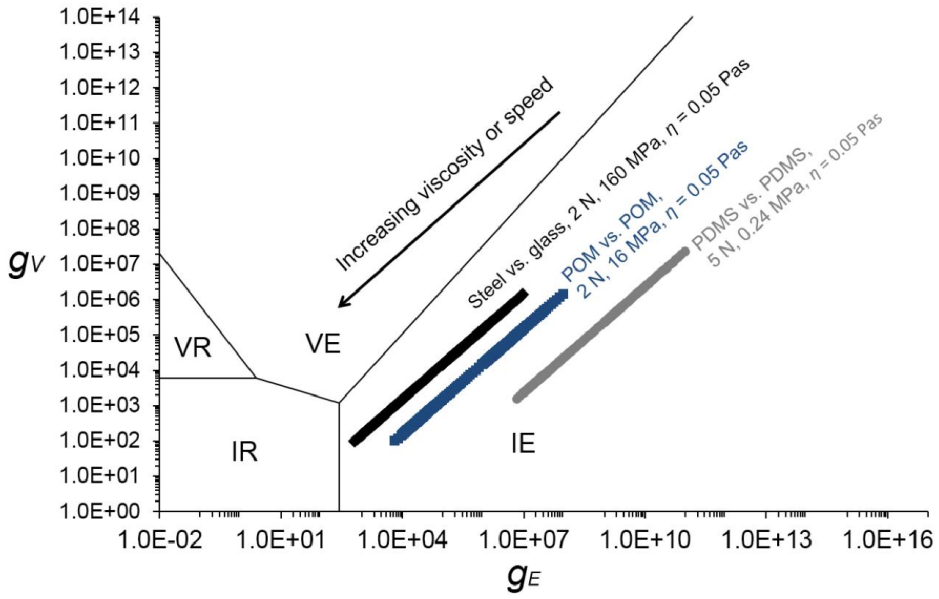

Figure S1: Lubrication regime map of the three types of contacts.

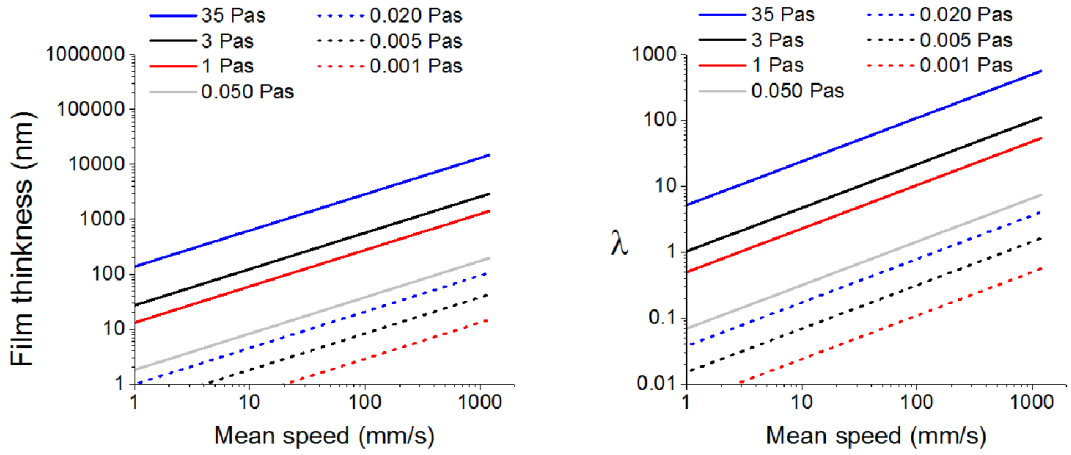

Figure S2: (a) Calculated film thickness and (b) stribeck parameter (λ) for *hard*-**HL** steel ball vs. glass disc contact by applying eq. 2 and viscosities of 35, 3, 0.100, 0.050, 0.020, 0.005, and 0.001 Pa·s.

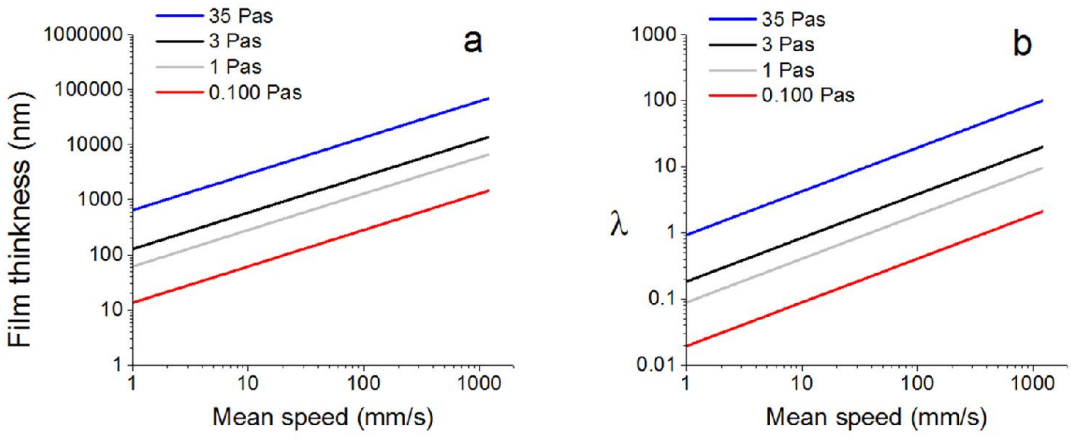

Figure S3: (a) Calculated film thickness and (b) Stribeck parameter (λ) for POM ball vs. POM disc contact by applying eq. 2 and viscosities of 35, 3, 1 and 0.100 Pa·s.

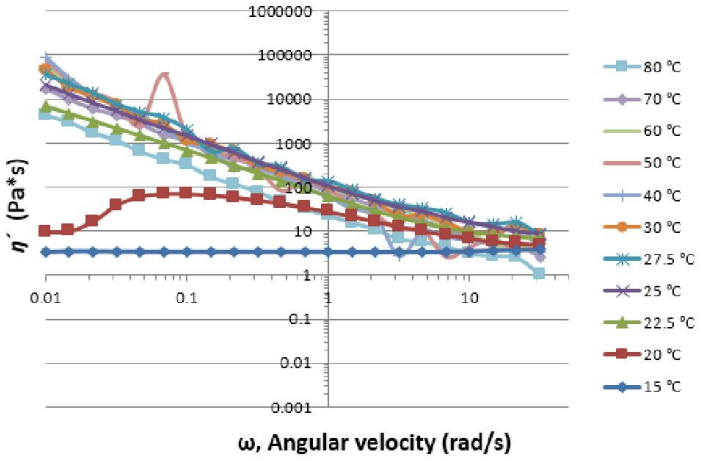

Figure S4: Viscous (η') part of complex viscosity vs. angular frequency (ω) of F127-**20**.

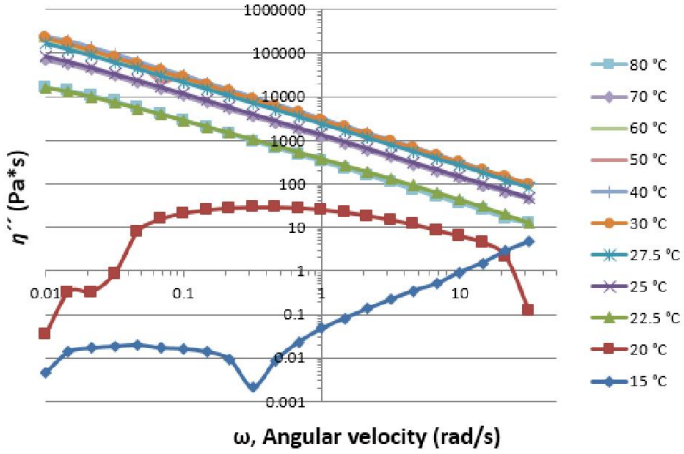

Figure S5: Elastic (η'') part of complex viscosity vs. angular frequency (ω) of F127-**20**.

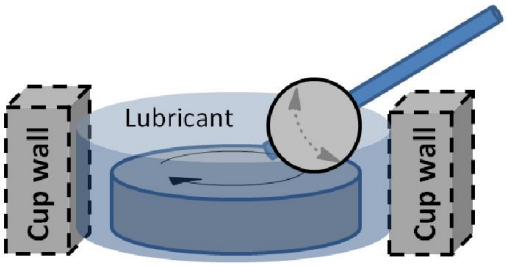

Figure S6: Schematic MTM setup with rotating ball on rotating disc submerged in lubricant.

4.7 Hydrophobins as aqueous lubricant additive for a soft sliding contact.

Article draft. See next pages.

Hydrophobins as aqueous lubricant additive for a soft sliding contact

Seunghwan Lee,[1*] Troels Røn,[1] Kirsi I. Pakkanen,[1] and Markus Linder[2,3]

[1]Department of Mechanical Engineering, Technical University of Denmark, DK-2800, Kgs. Lyngby, Denmark

[2]Technical Research Centre of Finland, VTT Biotechnology, FIN-02044 VTT, Finland
[3]Department of Biotechnology and Chemical Technology, Aalto University, 00076 Aalto, Finland

*Corresponding author: seele@mek.dtu.dk

Key words: hydrophobin, amphiphilic, FpHYD5, HFBI, lubrication

Abstract

Two type II fungi hydrophobins, HFBI and FpHYD5, have been studied as aqueous lubricant additive at a nonpolar, compliant sliding contact (self-mated poly(dimethylsiloxane) (PDMS) contact) at two different concentrations, 0.1 mg/mL and 1.0 mg/mL. The two hydrophobins are featured as non-glycosylated and lighter (HFBI, m.w. ca. 7 kDa) vs glycosylated and heavier (FpHYD5, m.w. ca. 10 kDa) proteins. Far UV CD spectra of the two hydrophobins were very similar, suggesting overall structural similarity, but showed a noticeable difference according to the concentration. This is proposed to be related to the formation of multimers at 1.0 mg/mL. Despite ten-fold difference in the bulk concentration, the adsorbed masses of the hydrophobins onto PDMS surface obtained from the two solutions (0.1 and 1.0 mg/mL) were nearly identical, suggesting that a monolayer of the hydrophobins are formed from 0.1 mg/mL solution. PDMS-PDMS sliding interface was effectively lubricated by the hydrophobin solutions, and showed a reduction in the coefficient of friction by as much as ca. two orders of magnitude. Higher concentration solution (1.0 mg/mL) provided a superior lubrication, particularly in low-speed regime, where boundary lubrication characteristic is dominant via ‘self-healing’ mechanism. FpHYD5 revealed a better lubrication than HFBI presumably due to the presence of glycans and improved hydration of the sliding interface. Two type II hydrophobins function more favorably compared to a synthetic amphiphilic copolymer, PEO-PPO-PEO, with a similar molecular weight. This is ascribed to higher amount of adsorption of the hydrophobins to hydrophobic surfaces from aqueous solution.

1. Introduction

Hydrophobins are small (m.w. 7-10 kDa) amphiphilic proteins originating from filamentous fungi displaying a variety of biological functions as in structural formulation, growth, and morphogenesis [1-7]. Based on the comparison of amino acid residue sequence, hydrophobins are classified into two groups, type I and type II [1-7]. Surface-active properties of hydrophobins have drawn particular interests in self-assembled adsorption behavior of hydrophobins at air/water [8-10], water/oil [11,12], and water/solid interfaces [13-21]. This, in turn, sparked intensive researches to utilize hydrophobins as coating materials for biomedical, technical, and personal care products [22-27].

Hydrophobins' surface-active properties have recently started to draw attention for tribological applications as well [28-30]. Nanotribological studies of a layer of *Sc3* from *schizophylum commune* on polymeric surfaces with atomic force microscopy (AFM) showed a reduction of friction forces in ambient condition [28]. More recent studies of type II hydrophobins, namely HFBI and FpHYD5, have shown a potential as boundary lubricant additive to lubricate stainless steel in aqueous environment [29,30]. Despite different environment and substrates, the efficacy of hydrophobins as lubricant additive in these studies is commonly based upon a strong adsorption onto material surfaces. In this study, we have investigated two type II hydrophobins, namely HFBI and FpHYD5, as boundary lubricant additive for a sliding contact of elastomeric, hydrophobic interface by employing a self-mated poly(dimethylsiloxane) (PDMS) pair in aqueous environment. Based on distinct amphiphilicity of hydrophobins, it is hypothesized that they are ideally suited to hydrate and lubricate hydrophobic interfaces in aqueous environment. While various synthetic [31-33] and biopolymeric [34-36] amphiphiles have shown facile lubricating effects for hydrophobic interfaces, comparative studies of the two hydrophobins in this study are particularly interesting in the following viewpoints. Firstly, the molecular weight of the hydrophobins in this study, ca. 7 − 10 kDa, is much smaller than those of other amphiphilic biomacromolecules that are related to biological lubrication, such as

lubricin (in the range of ca. 250 kDa [37,38]) or mucins (0.5 to 20 MDa [39]), and is rather comparable to those of synthetic amphiphilic polymers that have been used as aqueous lubricant additive [31]. Thus, it is of interest to study whether small biomolecules as hydrophobins can also display as effective lubricating capabilities as much larger ones. Secondly, in the same context, it is also of interest to compare the lubricating properties of hydrophobins with synthetic copolymers, especially those showing comparable molecular weights. Thirdly, despite the differences in the fungi of origin, structural and sequence homology of hydrophobins are very high [1-7]; both hydrophobins contain eight cystein residues, i.e. four disulfide bonds, one α-helix and two β strands, and a number of aliphatic hydrophobic residues. A major structural difference between the two hydrophobins is N-glycosylation (ca. 1.7 kDa) of FpHYD5 [30,40], and thus its influence on the lubricating properties can be studied. Lastly, it is well known that hydrophobins form multimers as a result of self-assembly in bulk aqueous solution [41-43], which may have an influence the surface adsorption and boundary lubricating properties too; for this reason, all the experiments were performed at two concentrations, namely at 0.1 and 1 mg/mL.

2. Materials and Methods

2.1 Hydrophobins and hydrophobin solutions

Two type II hydrophobins, namely HFBI from *T. reesei* [5-9] and FpHYD5 from *F. poae* [40], were employed. Details on culture, extraction, and purification processes of the two hydrophobins are found in literature [8,9,40]. Molecular weights of HFBI and FpHYD5 are 7.54 kDa [30] and 9.21 kDa [30,40], respectively. For FpHYD5, a molecular weight of ca. 1.7 kDa is indebted from N-glycosylation at N-37 site (2 N-acetyl glycosamines and 7 hexoses [40]). For comparison, a triblock copolymer, poly(ethylene oxide)-*block*-poly(propylene oxide)-*block*-poly(ethylene oxide) (PEO-PPO-PEO) with a similar molecular weight with HFBI, namely Synperonic® PE P105 (m.w. ca.

6.5kDa, abbreviated as “P105” hereafter, Sigma-Aldrich Denmark ApS, Broendby, Denmark), was employed.

Hydrophobin and P105 solutions were prepared by dissolving in sodium acetated buffer (pH 5) at 0.1 mg/mL and 1.0 mg/mL, respectively. A slightly acidic buffer solution was selected based on the previous studies, where an optimum adsorption [44] and lubrication [30] were observed in this buffer, especially for HFBI.

2.2 Circular Dichroism Spectroscopy

Far UV circular dichroism (CD) spectra of the hydrophobin solutions were acquired with a Chirascan spectrophotometer (Applied Photophysics Ltd., Surrey, UK) at room temperature (ca. 22 °C). A cylindrical quartz cuvette with 10 mm path length (Hellma GmbH & Co. KG, Müllheim, Germany) was used. The wavelength range was selected from 280 to 190 nm with step size of 2 nm and bandwidth of 1 nm. The far-UV CD signals of the buffer background were subtracted from the data. The presented data are average of three independent measurements, each averaged of three scans.

2.3 Optical Waveguide Lightmode Spectroscopy (OWLS)

OWLS (Microvacuum, OWLS model 210, BioSense software version 2.6.10, Hungary) is an optical, non-labeling technique to monitor the adsorption characteristics of macromolecules from liquid to interfacing solid surfaces. OWLS is based on the in-coupling of incident linear polarized laser light (He-Ne, 633 nm) with diffraction grating waveguides. Upon adsorption of macromolecules onto or at the vicinity of the waveguide surface, specific incidence angle, where total internal reflectance occurs, is changing due to the changes in refractive index at the interface. Adsorbed mass on the waveguide surface can be deduced using de Feijter equation [45]. Refractive index increment values, dn/dc, for the two hydrophobins and P105 were assumed to be 0.182 cm^3/g and 0.150 cm^3/g [46],

respectively. OWLS experiments started from exposing waveguides to the buffer solution until a stable baseline was obtained. Then, hydrophobin or P105 copolymer solution was injected into the flow cell by means of a programmable syringe pump. Upon initiation of adsorption, the pump was stopped and the adsorption was allowed to proceed under static condition for 1 h. Since the signal at this stage includes the contribution from not only adsorbed polymers but also from the change in refractive index at the vicinity of the surface, the adsorbed mass was assessed after rinsing the flow cell with buffer solution, presumably leaving only strongly bound polymers on the surface.

In order to emulate the tribopair surface (see the section 2.4), the waveguides for OWLS adsorption experiments were coated with a thin layer of PDMS. To this end, waveguides were ultrasonicated in EtOH for 10 minutes and spin-coated with a Sylgard® 184 PDMS kit mixture (base component and crosslinker 3:1 wt. ratio dissolved in heptane to give a spin coating solution of 0.5 wt. %) at 2 000 rpm for 60 s. After spin coating, the waveguides were cured overnight at 70 °C. The reference thickness of the spin-coated PDMS layer as measured on silicon wafers by ellipsometry was 16.4 ± 0.17 nm [33].

2.4 Pin-on-disk tribometry

The lubricating properties of hydrophobin or P105 solutions have been assessed by acquiring the coefficient of friction vs. speed plots with a pin-on-disk tribometer (CSM Instruments, software version 4.4 M, Switzerland). In this approach, a loaded pin is placed on disk surface, and the disk was allowed to rotate over a defined sliding track using a motor underneath the disk. Dead weights were employed to apply external load. The friction forces were detected by strain gauge on the arm holding the pin. Coefficient of friction, μ, is defined as F_f/L, where F_f is friction force and L is load, under a fixed load (5 N). This corresponds to the Hertzian contact pressure of 0.36 MPa. Variation of speed, from 0.25 mm/s to 100 mm/s, gives μ vs. speed plots.

PDMS discs and pins were prepared with the PDMS kit mentioned above. Base and crosslinker were mixed at 10:1 wt. ratio. Dispersed foams generated during mixing were removed by vacuum. The mixture was then poured into molds and cured overnight at 70 °C. Home-machined aluminum was used for disc mold (diameter; 30 mm, thickness; 5 mm), and Nunc™ U96 MicroWell™ plates (Thermo Scientific, Denmark) were used for pin (radius; 3.0 mm) mold. The roughness of the PDMS discs and pins was measured by AFM tapping mode. The root-mean-square roughness (R_q) was measured to be 1.34 nm and 4.62 nm for discs and pins, respectively, over a 2 μm × 2 μm area. Water contact angle on PDMS surfaces were 105.6 ± 2.2° (tested with Millipore water, standard deviation from 5 measurements).

3. Results & Discussion

3.1 Secondary structures of hydrophobins

The far UV CD spectra obtained from HFBI and FpHYD5 at 0.1 mg/mL and 1.0 mg/mL are presented in Figure 1.

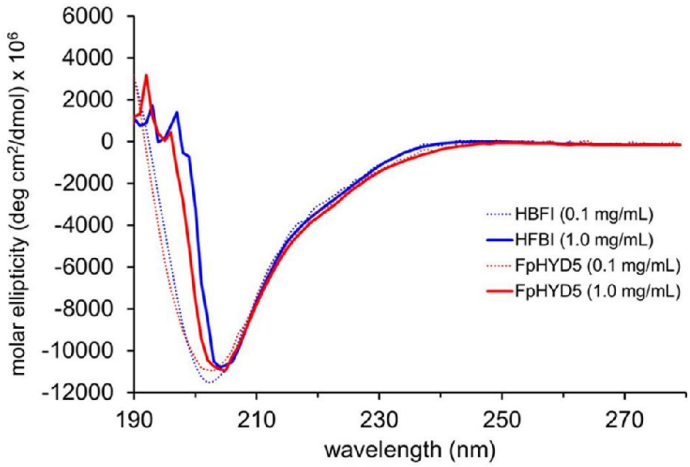

Figure 1. Far UV CD spectra of HFBI (blue lines) and FpHDY5 (red lines) at 0.1 mg/mL (dotted lines) and 1.0 mg/mL (solid lines) in Na-acetate buffer (50 mM), pH 5.

The overall features of the far UV CD spectra are very similar at both concentrations, supporting the structural similarities of the two hydrophobins. The far UV CD spectrum of HFBI at 0.1 mg/mL in Figure 1 is similar to that reported in a previous study in the same buffer [20]. This also suggests that a minor difference in amino acid residue composition and sequence as well as the presence of glycans for FpHYD5 do not induce significant differences in the structure of the two hydrophobins.

Nevertheless, un-ignorable differences between the two hydrophobins are also noticeable according to the type and concentration. For instance, while the far UV CD spectra of the two hydrophobins at both concentrations are generally similar to each other, the major negative peaks are clearly narrower for the spectra obtained from 1.0 mg/mL than 0.1 mg/mL, in particular in the region from 190 to 205 nm (Figure 1). It is also noted that the minima of the major negative peaks of the two hydrophobins shift to higher wavenumbers by ca. 2 nm. In the comparison of the far UV CD spectra of the two hydrophobins, somewhat weaker, yet similar difference is observed too; the far CD UV spectra of HFBI is slightly narrower compared to those of FpHYD5 in the region from 190 to 205 nm, and this contrast slightly stronger at higher concentration (1 mg/mL) than at lower concentration (0.1 mg/mL). In contrast, the far UV CD spectra in the wavelength region higher than ca. 203 nm are much closer to each other despite the variation of the type or concentration of hydrophobins.

We propose that the concentration-dependent changes of far UV CD spectra of the hydrophobins are related to the self-assembly to form multimers in high concentration [41-43]. Previous studies have shown that HFBI molecules tend to assemble at high concentration for its amphiphilicity in aqueous environment with a threshold of ca. 0.15 mg/mL [42]; dimers/tetramers are dominant in higher concentration, whereas monomer is dominant at low concentration than the threshold concentration [47]. Thus, in this study too, monomers are likely to be the dominant form of the hydrophobins at 0.1 mg/mL solutions, whereas multimers are more dominant species at 1.0

mg/mL solutions. As the formation of dimer/tetramer is essentially driven by the interaction between surface hydrophobic patches, major secondary structures, such as α-helix or β-strand, are expected to be preserved in this process. Thus, the fact that only minor changes occur in the far UV CD upon increasing the concentration by 10 times (Figure 1) is consistent with the scenario of multimerization without disturbing the major protein structural features of the hydrophobins. In the same context, a slight difference between the two hydrophobins shown at 1.0 mg/mL can also be related to bulkier structure of FpHYD5 than HFBI due to the presence of glycans, and consequent alteration in the conformation of the assembled multimers. Nevertheless, it is more important to emphasize that all these changes are minor in magnitude, and the far UV CD spectra shown in Figure 1 mainly support the structural resemblance of the two hydrophobins in this study.

3.2 Adsorption of hydrophobins onto surface

Upon exposure of the PDMS-coated waveguides to the solutions of hydrophobin or P105, a rapid surface adsorption, followed by saturation was observed; more than 90% of saturated adsorption signals were achieved within the first 5 min (representative adsorption profiles shown in Fig S1 in Supplementary Information). No meaningful difference was observed in the adsorption profiles according to the type or concentration of the hydrophobins. Adsorbed masses, as defined after rinsing the flow-cell with buffer solution, from three measurements of the hydrophobins and two concentrations, 0.1 mg/mL and 1.0 mg/mL, are presented in Figure 2.

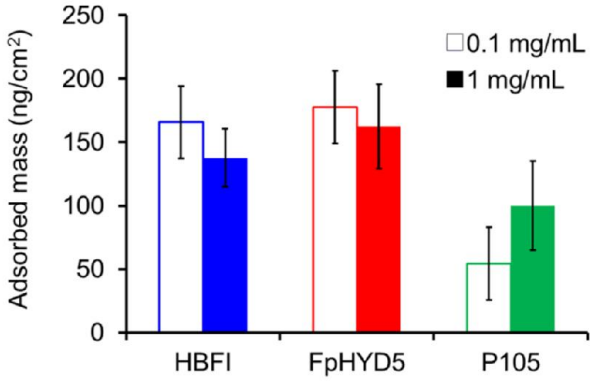

Figure 2. Adsorbed masses of HFBI, FpHYD5, and P105 onto PDMS-coated OWLS waveguides from 0.1 mg/mL and 1.0 mg/mL solutions in Na-acetate buffer (50 mM), pH 5.

Table 1. Adsorbed masses, surface density of the hydrophobin molecules, and are per molecule on PDMS surface, as characterized by OWLS.

	HFBI		FpHYD5	
	0.1 mg/mL	1.0 mg/mL	0.1 mg/mL	1.0 mg/mL
Adsorbed mass (ng/cm^2)	165.7 ± 5.7	137.7 ± 22.7	177.7 ± 16	162.3 ± 33.2
Surface density of the hydrophobin molecules (/nm^2)	0.132 ± 0.005	0.110 ± 0.018	0.116 ± 0.022	0.106 ± 0.010
Area per molecule (nm^2)	7.58 ± 0.29	8.62 ± 1.53	9.09 ± 1.37	9.43 ± 1.65

The average adsorbed masses of hydrophobins were 165.7 ± 5.7 ng/cm^2 for HFBI and 177.7 ± 16.0 ng/cm^2 for FpHYD5, respectively, from 0.1 mg/mL solutions, and 137.7 ± 22.7 ng/cm^2 for HFBI and 162.3 ± 33.2 ng/cm^2 for FpHYD5, respectively, from 1.0 mg/mL solution (Table 1). Despite the 10-fold difference in the concentration of bulk solution, the adsorbed masses of the hydrophobins from 0.1 mg/mL and 1.0 mg/mL solutions were statistically indistinguishable. This means that the hydrophobin solutions at 0.1 mg/mL provide a saturated monolayer on PDMS surface, and an increase of the concentration of bulk solution to 1.0 mg/mL does not contribute to further surface

adsorption, via e.g. multilayer formation. On the other hand, at even further lower concentration, e.g. at 0.01 mg/mL, the adsorbed masses of both HFBI and FpHYD5 were much smaller than those at 0.1 or 1 mg/mL (< 70 ng/cm^2, data not shown). Lastly, the adsorbed masses of P105 at 0.1 and 1 mg/mL concentration were obtained as 64.0 ± 35.3 ng/cm^2 and 100.0 ± 35.3 ng/cm^2, respectively. Based on the molecular weights of the hydrophobins and the adsorbed masses, the number of hydrophobin molecules per unit area (1 nm^2), and in turn, the area occupied per hydrophobin molecule can be estimated under the assumption of random close packing. The results are shown in Figure 3 and Table 1; 7.58 ± 0.29 nm^2 (0.1 mg/mL) and 8.62 ± 1.53 (1.0 mg/mL) for HFBI, and 9.09 ± 1.37 nm^2 (0.1 mg/mL) and 9.43 ± 1.65 nm^2 for FpHYD5 (1.0 mg/mL), respectively. Again, the area per molecule was statistically indistinguishable for the two hydrophobins at both concentrations.

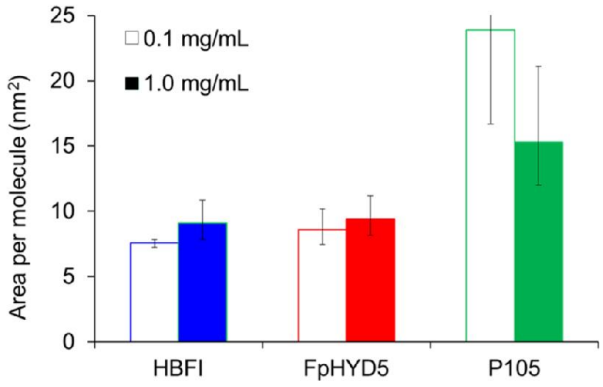

Figure 3. Estimated areas per hydrophobin molecule from the adsorbed masses (Figure 2) and the molecular weights of HFBI and FpHYD5 from 0.1 mg/mL and 1 mg/mL solutions.

Many previous experimental studies have shown facile adsorption of HFBI or HFBII onto a variety of hydrophobic substrates, including graphite [8], alkylated gold [21], polystyrene (PS) [14], and PDMS [16,18] from aqueous solution for its distinct amphiphilicity. An MD simulation study also confirmed that the binding of HFBI onto PDMS surface is energetically most favorable when the

adsorption occurs exclusively through the interaction of hydrophobic patches with PDMS substrate [13]. As FpHYD5 is relatively a new molecule, its surface adsorption has been studied to a much less extent to date. Based on structural homology though, a similar adsorption mechanism and conformation with HFBI, i.e. aliphatic hydrophobic patches on the protein surface acting as anchoring units, is expected in the adsorption onto PDMS surfaces. Additionally, one N-glycosylation (1695 Da) residing on the opposite side of hydrophobic patches [40] further improves the amphiphilicity of FpHYD5.

3.3 Aqueous lubricating properties

Figure 4 presents the speed-dependent lubricating properties, namely μ-vs-speed plots, of the two hydrophobins and P105 solutions, at the concentration of 0.1 mg/mL (Figure 4(a)) and 1.0 mg/mL (Figure 4(b)), respectively.

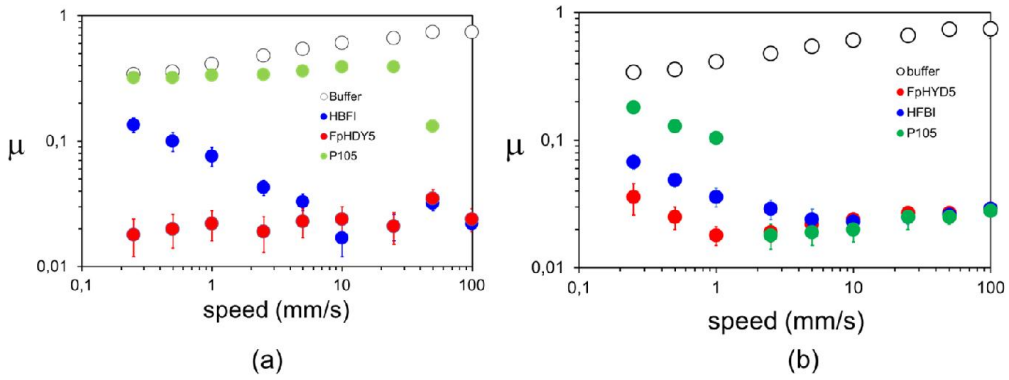

Figure 4. μ vs speed plots for HFBI, FpHYD5, and P105 from (a) 0.1 mg/mL and (b) 1.0 mg/mL, respectively.

The μ-vs-speed plots of additive-free acetate buffer solution are also presented as reference. The μ values of PDMS-PDMS sliding contacts lubricated either by the hydrophobins or P105 solutions were

lower than those of buffer solutions, yet to different extents depending on the type of additive, concentration, and speed range.

Between the two hydrophobins, FpHYD5 showed clearly superior lubricating capabilities, especially at low-speed (< 10 mm/s) and low-concentration (0.1 mg/mL) regime, where boundary lubrication mechanism is dominant. This can be firstly linked to the slightly higher adsorbed mass of FpHYD5 than HFBI (Figure 2). But, as this difference is very small, it cannot account for the large difference in the μ values between them. Instead, the superior lubricating properties of FpHYD5 in this regime can be related to the presence of glycosylated region in it and consequently more effective hydration, as confirmed by QCM-D study in a previous study [40]. Glycosylation is a common strategy for biomacromolecules, such as mucins [34,35] and lubricins [37,38], to enhance the hydrophilicity and entrainment of base lubricant, i.e. water, at the gliding interface. The present study with hydrophobins further confirms the significance of glycosylation for aqueous lubricating properties of biopolymeric additives. Judging from the μ vs speed plots obtained in this study, overall aqueous lubricating properties of FpHYD5 can be assessed fairly comparable to those by much larger biomacromolecules, such as mucins at the same tribopair [48,49]. Both hydrophobins showed superior lubricating behavior compared to P105 as aqueous lubricant additive for this tribopair. This is expected from that the adsorbed masses of the two hydrophobins are higher than that of P105 at the same concentrations (Figure 2). With increasing speed, however, the difference in μ values for the two hydrophobins, as well as with P105, started to disappear. This difference is much smaller in high-concentration regime (1.0 mg/mL, Figure 4(b)). This may be an indication that fluid-films started to form at the interface in this speed regime [31,32].

Direct comparison of each additive at different concentrations is not shown, as all of them showed clearly superior lubricating effects (i.e. lower μ values) at high concentration (1.0 mg/mL) than at low concentration (0.1 mg/mL), with the difference being larger in low-speed regime. A

superior lubricating effect of hydrophobins at 1 mg/mL concentration than at 0.1 mg/mL is not directly related to the surface adsorption properties (Figure 2), according to which the adsorbed masses from 1.0 mg/mL solutions are comparable to those from 0.1 mg/mL solutions. In other words, higher concentration of the hydrophobin molecules in 1.0 mg/mL solution contributes to lubrication, even though they do not contribute to higher surface adsorption. This is, however, not due to an increase in viscosity; proteins or glycoproteins at 1.0 mg/mL concentration are virtually identical with water in viscosity [35]. Furthermore, the improvement of lubricating properties at high concentration is evident in slow-speed regime, where boundary lubrication is most active, rather than in high-speed regime, where viscosity plays a significant role due to a higher likelihood of forming fluid-films. The improved lubrication at high concentration of hydrophobins can be related to the more effective *recovery* of the lubricating film under cyclic tribological stress in pin-on-disk tribometry [50]; hydrophobins on PDMS surface are easily rubbed away from the tribostress whereas excess proteins in bulk solution can readily reform the lubricating film as well due to non-covalent bonding characteristic, and this process is continuously repeating. In this context, higher concentration of the additives is advantageous for faster reformulation of the lubricating layer due to the steeper concentration gradient near the contact area. A control experiment involving a monolayer coating only, as prepared by replacing hydrophobin solution with buffer solution after the formation a monolayer showed that the degradation in lubricating properties started to occur immediately after the initial contacts (Figure S2, in Supplementary Information). Thus, excellent lubricating performance of the hydrophobins for the sliding contacts of PDMS-PDMS tribopair is mainly indebted from fast (re)adsorption kinetics on to the surface when excess hydrophobins are present in bulk solution, which is, in turn, indebted from the presence of distinct hydrophobic patches on the protein surface and enhanced amphiphilicity.

5. Conclusions

In this study, tribological properties of type II hydrophobins, HFBI and FpHYD5, as aqueous lubricant additive for a soft hydrophobic sliding interface, PDMS-PDMS, were studied at the concentration of 0.1 mg/mL and 1.0 mg/mL. Far UV CD spectra of the two hydrophobins were very similar, suggesting overall structural similarity of the two hydrophobins, yet showed somewhat different secondary structural features according to the concentration change from 0.1 to 1.0 mg/mL. This is suggested to be related to the dominance of monomoers and multimers and monomers at 0.1 mg/mL and 1.0 mg/mL, respectively. However, its influence on adsorption was insignificant due to the formation of monolayer already at lower concentration (0.1 mg/mL). The adsorption strength of the hydrophobins was not sufficient to withstand the tribostress under 5 N with a monolayer coating on the surface. But, the hydrophobins displayed very efficient aqueous lubricating capabilities as a solution based on “self-healing” mechanism. Despite its much smaller molecular weight (within the range of 7 to 10 kDa) compared to other biomolecular amphiphiles, such as mucins or lubricins, the two hydrophobins in this study, especially FpHYD5, showed comparable aqueous lubrication capabilities for PDMS-PDMS tribopair. This is mainly due to the presence of distinct hydrophobic patches on protein surface, rather than being entirely buried inside, and consequently enhanced amphiphilicity of the molecules. In low-speed regime, where boundary lubrication character is dominant, FpHYD5 showed relatively superior lubricity to HFBI, presumably related to the presence of glycans and consequently more efficient hydration. With increasing speed though, the difference in the lubricating properties of the two hydrophobins as well as with P105 started to disappear, due to more feasible entrainment of base lubricant, water, into the sliding interface.

6. Acknowledgements

The authors are grateful for the financial support from the Danish Council for Independent Research (DFF), Technology and Production Sciences (FTP) (10-082707), European Research Council (Funding scheme, ERC Starting Grant 2010, Project number 261152), and COST Action program (TD1003, Bioinspired Nanotechnologies). Riitta Suihkonen (VTT) is also acknowledged for her technical assistance in the purification of the hydrophobins in this study.

References

[1] Wösten, H.A.B., van Wetter, M. A., Lugones, L. G., van der Mei, H. C., Busscher, H. J., Wessels, J. G. How a fungus escapes the water to grow into the air. *Curr. Biol.* 1999. 9, 85 – 88.

[2] Wösten, H.A., Hydrophobins: Multipurpose proteins. *Ann. Rev. Microbiol.* 2001, 55, 625 – 646.

[3] Lumsdon, S., Green, J., Stieglitz, B., Adsorption of hydrophobin proteins at hydrophobic and hydrophilic interfaces. *Colloids and Surfaces B: Biointerfaces* 2005, 44, 172 – 178.

[4] Hektor, H., Scholtmeijer, K. Hydrophobins: proteins with potential. *Current Opinion in Biotechnology* 2005, 16, 434 – 439.

[5] Zampieri, F., Wösten, H.A.B., Scholtmeijer, K. Creating surface properties using a palette of hydrophobins. *Materials* 2010, 3, 4607 – 4625.

[6] Linder, M.B., Szilvay, G.R., Nakari-Setälä, Penttilä, M.E. Hydrophobins: the protein-amphiphiles of filamentous fungi. *FEMS Microbiology Reviews* 2005, 29, 877 – 896.

[7] Linder, M.B. Hydrophobins: Proteins that self-assemble at interfaces. *Current Opinion in Colloid & Interface Science* 2009, 14, 356 – 363.

[8] Szilvay, G.R., Paananen, A., Laurikainen, K., Vuorimaa, E., Lemmetyinen, H., Peltonen, J., Linder, M.B. Self-assembled hydrophobin protein films at the air-water interface: structural analysis and molecular engineering. *Biochemistry* 2007, 46, 235 – 2354.

[9] Kisko, K., Szilvay, G.R., Vuorimaa, E., Lemmetyienen, H., Linder M.B., Torkkeli, M., Serimaa, R. Self-assembled films of hydrophobin proteins HFBI and HFBII studied in situ at the air/water interface. *Langmuir* 2009, 25, 1612 – 1619.

[10] Zhang, X.L., Penfold, J., Thomas, R.K., Tucker, I.M., Petkov, J.T., Bent, J., Cox, A., Campbell, R.A., Adsorption behavior of hydrophobin and hydrophobin/surfactant mixtures at the air-water interface. *Langmuir* 2011, 27, 11316 – 11323.

[11] Cheung, D.L. Molecular simulation of hydrophobin adsorption at an oil–water interface. *Langmuir* 2012, 28(23), 8730 – 8736.

[12] Reger, M., Hoffmann, H. Hydrophobin coated boehmite nanoparticles stabilizing oil in water emulsions. *J. Coll. Interf. Sci.* 2012, 368, 378 – 386.

[13] Liu, Y., Wu, M., Feng, X., Shao, X., Cai, W. Adsorption behavior of hydrophobin proteins on polydimethylsiloxane substrates. *J. Phys. Chem. B* 2012, 116, 12227 – 12234.

[14] Wang, Z., Huang, Y., Li, S., Linder, M.B., Qiao, M. Hydrophilic modification of polystyrene with hydrophobin for time-resolved immunofluorometric assay. *Biosensors and Bioelectronics* 2010, 26, 1074 – 1079.

[15] Zhao, Z.-X., Wang, H.-C., Wang, X.-S., Qiao, M.-Q., Anzai, J.-I., Chen, Q. Self-assembled film of hydrophobins on gold surfaces and its application to electrochemical sensing. *Colloids & Surfaces B: Biointerfaces* 2009, 71, 102 – 106.

[16] Qin, M., Wang, L.-K., Feng, X.-Z., Yang, Y.-L., Wang, R., Wang, C., Yu, L., Shao, B., Qiao, M.-Q. Surface modification of mica and poly(dimethylsiloxane) with hydrophobins for protein immobilization. *Langmuir* 2007, 23, 4465 – 4471.

[17] Lumsdon, S.O., Green, J., Stieglitz, B. Adsorption of hydrophobin proteins at hydrophobic and hydrophilic surfaces. *Colloids and Surfaces B: Biointerfaces* 2005, 44, 172 – 178.

[18] Hou, S., Yang, K., Qin, M., Feng, X.-Z., Guan, L., Yang, Y., Wang, C. Patterning of cells on functionalized poly(dimethylsiloxane) surface prepared by hydrophobin and collagen modification. *Biosensors and Bioeletronics* 2008, 24, 912 – 916.

[19] de Vocht, M.L., Reviakine, I., Ulrich, W.-P., Bergsma-Schutter, W., Wösten, H.A.B., Vogel, H., Brisson, A., Wessels, J.G.H., Robillard, G.T. Self-assembly of the hydrophobin SC3 proceeds via two structural intermediates. *Protein Science* 2002, 11, 1199 – 1205.

[20] Askolin, S., Linder, M., Scholtmeijer, K., Tenkannen, M., Penttilä, de Vocht, M.L., Wösten, H.A.B. Interaction and comparison of a class I hydrophobin from *Schizophyllum commune* and class II hydrophobins from *Tichoderma reesei*. *Biomacromolecules 2006*, 7, 1295 – 1301.

[21] Linder, M., Szilvay, G.R., Nakari-setälä, T., Söderlund, H., Penttilä, M. Surface adhesion of fusion proteins containing the hydrophobins HFBI and HFBII from *Trichoderma reesei*. *Protein Science* 2002, 11, 2257 – 2266.

[22] Wösten, H.A.B., de Vocht, M.L. Hydrophobins, the fungal coat unravelled. *Biochim. Biophys. Acta* 2000, 1469, 79 – 68.

[23] Scholtmeijer, K., Wessels, J.G.H., Wösten, H.A.B. Fungal hydrophobins in medical and technical applications. *Appl. Microbiol. Biotechnol.* 2001, 56, 1 – 8.

[24] Scholtmeijer, K., Janssen, M.I., Van Leeuwen, M.B.M., Van Kooten, T.G., Hektor, H. Wösten, H.A.B. The use of hydrophobins to functionalize surfaces. *Bio-Med. Mater. Eng*. 2004, 14, 447 – 454.

[25] Scholtmeijer, K., Janssen, M.I., Gerssen, B., de Vocht, M.L., Van Leeuwen, M.B.M. Surface modifications created by using engineered hydrophobins. *Appl. Environ. Microbiol*. 2002, 68, 1367 – 1373.

[26] Janssen, M.I., Van Leeuwen, M.B.M., Scholtmeijer, K., Van Kooten, T.G., Dijkhuizen, L., Wösten, H.A.B. Coating with genetic engineered hydrophobin promotes growth of fibroblasts on a hydrophobic solid. *Biomaterials* 2002, 23, 4848 – 4854.

[27] von Vacano, B., Xu, R., Hirth, S., Herzenstiel, I., Rueckel, M., Subkowski, T., Baus, U. Hydrophobins can prevent secondary protein adsorption on hydrophobic substrates without exchange. *Anal. Bioanal. Chem.* 2011, 400, 2031 – 2040.

[28] Misra, R., Gordon, J.L., Morgan, S.E. Nanoscale reduction in surface friction of polymer surfaces modified with Sc3 hydrophobin from Schizophylum commune, *Biomacromolecules* 2006, *7(5)*, 1463 – 1470.

[29] Ahlroos, T., Hakala, T.J., Linder, M.B., Holmberg, K., Mahlberg, R., Laaksonen, P., Varjus, S. Biomimetic approach to water lubrication with biomolecular additives. *Proc. I. Mech. Eng. J.* 2011, *225*, 1013 – 1022.

[30] Hakala, T., Laaksonen, P., Saikko, V., Ahlroos, T., Helle, A., Mahlberg, R., Hähle, H., Jacobs, K., Kuosmanen, P., Linder, M.B., Holmberg, K. *RSC Advances* 2012, 2, 9867 – 9872.

[31] Lee, S., Iten, R., Müller, M., Spencer, N.D. Influence of molecular architechture on the adsorption of poly(ethylene oxide)-poly(propylene oxide)-poly(ethylene oxide) on PDMS surfaces and implications for aqueous lubrication. *Macromolecules* 2004, 37, 8349 – 8365.

[32] Lee, S., Spencer, N.D. Aqueous lubrication of polymers: Influence of surface modification. *Tribol. Int*. 2005, 38, 922 – 930.

[33] Røn, T., Javakhishvili, I., Jankova, K., Hvilsted, S., Lee, S. Adsorption and aqueous lubricating properties of charged and netural amphiphilic diblock copolymers at a compliant, hydrophobic interface. *Langmuir* 2013, 29, 7782 – 7792.

[34] Cassin, G., Heinrich, E., Spikes, H.A. The Influence of surface roughness on the lubrication properties of adsorbing and non-adsorbing biopolymers. *Tribol. Lett*. 2001, 11, 95 – 102.

[35] Lee, S., Müller, M., Rezwan, K., Spencer, N.D. Porcine gastric mucin (PGM) at the water/poly(dimethylsiloxane) (PDMS) interface: Influence of pH and ionic strength on its conformation, adsorption, and aqueous lubrication properties. *Langmuir* 2005, 21, 8344 – 8353.

[36] Garrec, D.A., Norton, I.T. The influence of hydrocolloid hydrodynamics on lubrication. *Food Hydrocolloids* 2012, 26, 389 – 397.

[37] Zappone, B., Ruths, M., Greene, G.W., Jay, G.D., Israelachvili, J.N. Adsorption, lubrication, and wear of lubricin on model surfaces: polymer brush-like behavior of a glycoprotein. *Biophys J.* 2007, 92, 1693 – 708.

[38] Chang, D.P., Abu-Lail, N.I., Coles, J.M., Guilak, F., Jay, G.D., Zauscher, S. Friction force microscopy of lubricin and hyaluronic acid between hydrophobic and Hydrophilic Surfaces. *Soft Matter* 2009, 5, 3438 – 3445.

[39] Hattrup, C.L., Gendler, S.J. Structure and function of the cell surface (tethered) mucins. *Annual Review of Physiology* 2008, 70, 431 – 457.

[40] Sarlin, T., Kivioja, T., Kalkkinen, N., Linder, M.B., Nakari-Setälä, T. Identification and characterization of gushing-active hydrophobins from *Fusarium graminearum* and related species *J. Basic Microbiology* 2012, 52, 184 – 194.

[41] Hakanpa, J., Paananen, A., Askolin, S., Nakari-Seta, T., Parkkinen, T, Penttila, M., Linder, M.B., Rouvinen, J. Atomic resolution structure of the HFBII hydrophobin, a self-assembling amphiphile. *J. Biol. Chem* 2004, 279(1), 534 – 539.

[42] Szilvay, G.R., Nakari-Seta, T., Linder, M.B. Behavior of *Trichoderma reesei* hydrophobins in solution: Interactions, dynamics, and multimer formation. *Biochemistry* 2006, 45, 8590-8598

[43] Hakanpa, J., Szilvay, G.R, Kaljunen, H., Maksimainen,M., Linder, M.B., Ruvinen, J. Two crystal structures of *Trichoderma reesei* hydrophobin HFBI - The structure of a protein amphiphile with and without detergent interaction. *Protein Science* 2006, 15, 2129 – 2140.

[44] Wang, Z., Lienenmann, M., Qiau, M., Linder, M.B. Mechanism of protein adhesion on surface films of hydrophobin. *Langmuir* 2010, 26(11), 8491 – 8496.

[45] de Feijter, J. A., Benjamins, J., Veer, F.A. Ellipsometry as a tool to study the ad-sorption of synthetic and biopolymers at the air-water interface. *Biopolymers* 1978, 17, 1759 – 1772.

[46] Malmsten, M., Linse, P., Cosgrove, T. Adsorption of PEO-PPO-PEO block copolymers at silica. *Macromolecules* 1992, 25, 2474 – 2481.

[47] Torkkeli, M., Serimaa, R., Ikkala, O., Linder, M. Aggregation and self-assembly of hydrophobins from *Trichoderma reesei*: Low-resolution structural models. *Biophys. J.* 2002, 83, 2240 – 2247.

[48] Lee, S., Müller, M., Rezwan, K., Spencer, N.D. Porcine gastric mucin (PGM) at the water/ poly(dimethylsiloxane) (PDMS) interface: Influence of pH and ionic strength on its conformation, adsorption, and aqueous lubrication properties. *Langmuir*, 2005, 21, 8344 – 8353.

[49] Yakubov, G.E., McColl, J., Bongaerts, J.H.H., Ramsden, J.J. Viscous boundary lubrication of hydrophobic surfaces by mucin. *Langmuir*, 2009, 25, 2313 – 2321.

[50] Lee, S., Müller, M., Heeb, R., Zürcher, S., Tosatti, S., Heinrich, M., Amstad, F., Pechman, S., Spencer, N. D. Self-healing behavior of a polyeletrolyte-based lubricant additive for aqueous lubrication of oxide materials. *Tribol. Lett.*, 2006, 24, 217– 223.

Supplementary Information

Hydrophobins as aqueous lubricant additive for a soft sliding contact

Seunghwan Lee,1 Troels Røn,1 Kirsi I. Pakkanen,1 and Markus Linder2,3

1Department of Mechanical Engineering, Technical University of Denmark, DK-2800, Kgs. Lyngby, Denmark

2Technical Research Centre of Finland, VTT Biotechnology, FIN-02044 VTT, Finland
3Department of Biotechnology and Chemical Technology, Aalto University, 00076 Aalto, Finland

Figure S1.

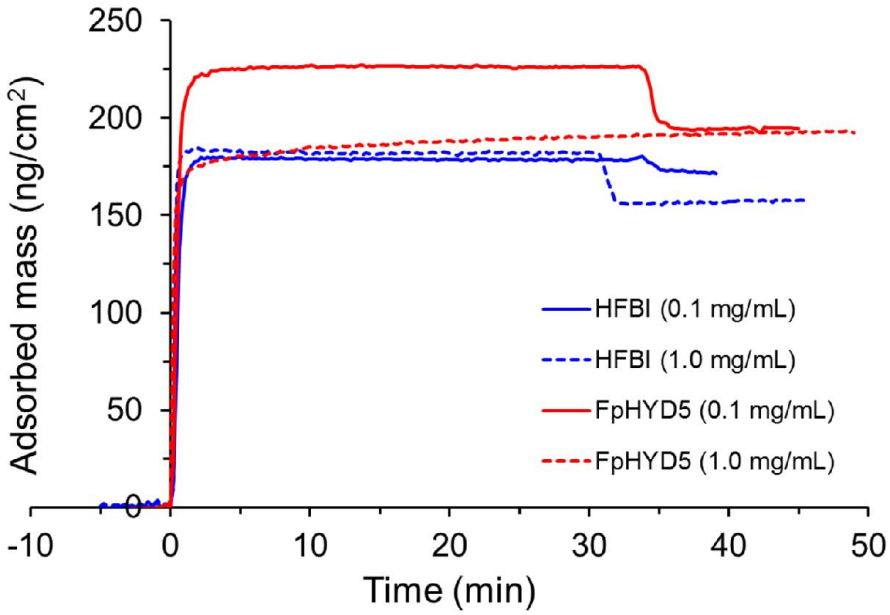

Figure S2.

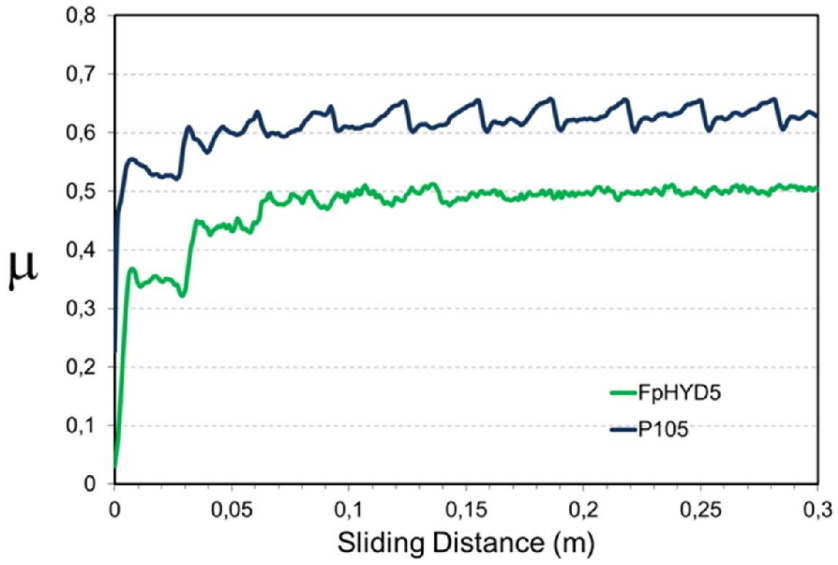
0,8
0,7
0,6
0,5
0,4
0,3
0,2
0,1
0
μ
0
0,05
0,1
0,15
0,2
0,25
0,3
Sliding Distance (m)
FpHYD5
P105

5.0 Summary

The first primary objective of investigating different synthetic amphiphilic copolymers – which adsorb and form polymer brushes on hydrophobic surfaces – as aqueous boundary lubricant additives was successfully conducted. The study reveals that applying polyelectrolyte brushes formed on hydrophobic surfaces by means of adsorbed diblock copolymer from ample polymer solution at pH 7.0 and low salt conditions is not a feasible way to obtain good lubricity under cyclic tribostress. Charged polyelectrolyte diblock copolymers PAA-*b*-PS and PAA-*b*-PMEA were inferior in lubricity to their neutral PEG-*b*-PS and PEG-*b*-PMEA counterparts, despite the sizeable adsorbed amount of PAA-*b*-PMEA at the PDMS-water interface. PEG-*b*-PS and PEG-*b*-PMEA maintained good lubricity over longer periods of time, displaying the 'self-healing' behavior. PAA-*b*-PS did not adsorb at the PDMS-water interface, and thus showed no lubricity. The poor lubricating capabilities of PAA-*b*-PMEA was attributed to the electrostatic repulsion induced during tribostress at the interface. When salt was added or pH was lowered to either screen the charge repulsion or remove the charges some improvement in lubricity was observed for the polyelectrolyte diblock copolymer.

When amphiphilic graft copolymers with dilution of the charges in the hydrophilic graft chains were applied as aqueous lubricant additives, the lubricity was also poor at neutral conditions. However, in 150 mM NaCl the lubricity of the amphiphilic graft copolymers was far better than the charged diblock copolymers, affording low coefficients of friction even at low sliding speeds.

Dilution of charges with PEG blocks on the surface by applying triblocks copolymers of the type PEG-*b*-PMEA-*b*-PMAA turned out to be a viable way to obtain lubricious polyelectrolyte brushes, however, the PEG-*b*-PMEA-*b*-PMAA was not more lubricious than its entirely neutral counterpart.

Overall, in terms of the first objective, it has been elucidated that applying fully charged blocks is not possible to obtain good lubricity of adsorbed polyelectrolyte brushes. Charge screening by salt or structural dilution of charges is necessary to obtain good lubricity of the polyelectrolyte even when adsorbed from excess polymer in aquoeus solution.

The second main objective was also carried out successfully. The friction behavior in neat water of four different contacts, hand and soft, hydrophobic and hydrophilic was evaluated at the temperature range 1-90 °C. The hydrophobic contacts behaved closely to what was theoretically predicted according to the Stribeck parameter. However, the hydrophilic contacts displayed much better lubricity than expected. This was

ascribed to the surface affinity of water to the hydrophilic contacts, hence retaining water and affording lubricity. The study also revealed significant temperatures dependency, due to water's change in viscosity.

The investigations on hydrogel showed good potential for F127 to lubricate soft contact. However, the F127 hydrogel failed to lubricate the hard POM-POM and steel-glass contacts due to shear thinning. The high viscosity at gelation did not participate in the lubricity as expected due to the severe shear thining in the tribocontact. Nevertheless, shear thining was assessed to be compelling in the soft PDMS-PDMS contact thus lowering the viscous shear force in the hydrodynamic regime.

Application of hydrophobins as boundary lubricant additive in water at sliding PDMS-PDMS hydrophobic interface was successful and showed significant lubrication and adsorption.

6.0 Outlook

Biomimetic aqueous lubrication by means of polymer brushes formed from adsorbed amphiphilic copolymers in solution is an attractive method of affording low friction sliding interface. However, as shown in this thesis it was not possible to supersede the neutral PEG amphihilic copolymers. Biolubricants of nature such as lubricin and mucins have charges which are believed to assist lubrication, but their charge density is not high. One may speculate if a 'golden ratio' between charge density to anchoring efficacy could be obtained, as it has been outlined in this thesis that too many charges do not gives desirable lubrication properties of amphiphilic macromolecules/polymers.

Another future challenge of applying the 'self-healing' lubrication approach is the diminishing of the polymer additive lubricants when the excess polymer solution is gone. In order to have good lubricity excess polymer in solution must be present. If polymer brushes could be incorporated into the material surface itself, not by slow grafting-to or grafting-from techniques, but spontaneously form when exposed to water, then long term lubricity of the material itself could be achieved.

Applying F127 hydrogel at aqueous lubricant displays a potential as lubricant for soft contact, nevertheless, due to its severe shear thinning behavior giving a viscosity close to that of neat water, it is not possible to lubricate hard contact. However, some hydrophilic polymer solutions display shear *thickening*, and thus could be candidates for lubricanting hard sliding contact in water.

7.0 List of Publications and Article Submissions

Title:	Status
Adsorption and Aqueous Lubricating Properties of Charged and Neutral Amphiphilic Diblock Copolymers at a Compliant, Hydrophobic Interface.	Published article in Langmuir, 2013.
Synthesis, Characterization, and Aqueous Lubricating Properties of Amphiphilic Graft Copolymers Comprising 2‑Methoxyethyl Acrylate.	Published article in Macromolecules, 2014.
Aqueous Lubricating Properties of Charged (ABC) and Neutral (ABA) Triblock Copolymer Chains.	Submitted article to the journal 'Polymer', 2014.
Influence of temperature on the frictional properties of water-lubricated surfaces.	Submitted article to the journal 'Lubricants', 2014.

8.0 List of Activities

Year	Activity
2011	Biotribology conference in London, UK (poster presenter)
2012	Gordon Research Conference (GRC), Ventura, California. (poster presenter)
2012	Nordic Polymer Days conferen, Copenhagen (Oral presenter)
2012	External stay for 3 months in at ETH Zürich
2013	World Tribology Conference, Torino, Italy (WTC) (oral presenter)
2014	International nanotribology forum, conference, Kochi, India, (Poster presenter)
2014	Bio-inspired materials, conference, Berlin, Germany, (oral presenter)